UNIVERSITY OF LIVERPOOL

Maximising Resource Efficiency for the Manufacture of Lamellar Based Consumer Products

by

Isaac Taiwo Pirisola

A Thesis submitted to The University of Liverpool for the degree of

Doctor of Philosophy

In the Faculty of Science and Engineering

August 2014

Declaration

I declare that no portion of the work referred to in the Thesis has been submitted in support of an application for another degree or qualification of this or any other University or other institute of learning

Abstract

The work disseminated within this Thesis pertain to an industrially funded study whose primary aims were to enhance the understanding of the effect of a range of process variables on the underlying microstructure of a rinse-off Hair Conditioner. The study utilised a range of analytical techniques namely; rheology, microscopy, SAXS and thermal transition.

Findings herein have demonstrated that through process optimisation, more resource efficient processes are achievable which offer the possibility to significantly reduce raw materials use whilst maintaining a desired viscosity.

In some cases a significant raw material reduction of 40 % could be realised (calculated on the amount of FA, CS & QUAT in the formulation) if the following steps are applied;

i. Initial formation of the FA, CS & QUAT lamellar system such that the morphological makeup is predominantly a QUAT/CS rich L_{β} microstructure - this is primarily a function of process temperature whilst ensuring fine state of dispersion of this product intermediate.
ii. Followed by a dispersive and distributive mixing step to reduce QUATS rich L_{β} microstructure domain size via a low temperature, high shear post processing operation – a function of increasing deformation rates within mixing equipment.

In addition to this, the Controlled Deformation Dynamic Mixing technology was found to be an efficient device at delivering the required deformation rates to the hair conditioner product, compared to the other mixing technologies tested. Deformation rates have been characterised with respect to [1] extensional (a function of process flow-rate), [2] rotational shear rates (a function of mixer rotational speed) and more importantly [3] Mixer design (a function of equipment geometry). The trio determines the deformation rates available to process fluids during an operation, and likewise vital to any scale-up operation for geometrically similar CDDM devices.

The main commercial outputs for this work therefore can be estimated using Euromonitor figures, which state that the total UK market for hair conditioner alone is £324.4 million per annum. Thus if we assume even a fraction of the raw material costs can be realised in the supply chain, saving of several million per annum are conceivable.

Dedication

I dedicate this Thesis to my immediate family.

Everyone holds his fortune in his own hands, like a sculptor the raw material he will fashion into a figure. But it's the same with that type of artistic activity as with all others: We are merely born with the capability to do it. The skill to mould the material into what we want must be learned and attentively cultivated.

—JOHANN WOLFGANG VON GOETHE

Do not think that what is hard for you to master is humanly impossible; and if it is humanly possible, consider it to be within your reach.

—MARCUS AURELIUS

Don't think about why you question, simply don't stop questioning. Don't worry about what you can't answer, and don't try to explain what you can't know. Curiosity is its own reason. Aren't you in awe when you contemplate the mysteries of eternity, of life, of the marvellous structure behind reality? And this is the miracle of the human mind—to use its constructions, concepts, and formulas as tools to explain what man sees, feels and touches. Try to comprehend a little more each day. Have holy curiosity.

—ALBERT EINSTEIN

Acknowledgements

First and foremost I would like to thank the Almighty God, who in his mercies decided to keep me alive and in good health from the start of the project till today.

James 4 verse 13 - 15

> "Go to now, ye that say, To day or to morrow we will go into such a city, and continue there a year, and buy and sell, and get gain: [verse 14] Whereas ye know not what *shall be* on the morrow. For what is your life? It is even a vapour, that appeareth for a little time, and then vanisheth away [verse 15] For that ye *ought* to say, If the Lord will, we shall live, and do this, or that".

I could never have done this without the Almighty God by my side constantly showering me with blessings, I know I do not deserve.

I would also like to thank my supervisors sincerely; [1] Dr Peter Bongers[1], [2] Dr Neil Irving[2] [3] Dr Michael Egan[3], and [4] Professor Adam Kowalski[4] for giving me the opportunity to work with them on such an exciting industrial project. I would like to especially thank Professor Adam Kowalski for his insightful advice and constructive feedbacks on my work during the entire period I was under him. Likewise Dr Neil Irving and Dr Michael Egan for their guidance – Academia aside, I have learnt a lot from them, which I know will be useful to me at different stages in my life. I have been very fortunate to have Dr Michael Egan as a supervisor - I offer gratitude for his investment in me in ensuring this Thesis is completed.

Inconceivable is the unconditional love, support and constant encouragement showered on me by my family (nuclear and extended[5]) – I am grateful to my parents – most especially my mother, who practically does everything I would rather not do. My father, who is my biggest well-wisher and all my siblings (all three of them) – they have been selfless in ensuring I was comfortable throughout the duration of the project, I express my never ending appreciation, respect and love to them for being the blessings that they are . My family is everything, I am lost without them. I appreciate Mr. Ajibola Makinde for his constant calls, which I always miss and his numerous

[1] God rest his soul (1961 – 2012) - Unilever Research and Development Vlaardingen [Netherlands]
[2] Unilever Research and Development Port Sunlight, Liverpool [United Kingdom]
[3] University of Liverpool
[4] Unilever Research and Development Port Sunlight, Liverpool (UR&D Port Sunlight) [United Kingdom]
[5] In the united kingdom and abroad

encouraging voice mails and many more individuals from my extended family for their constant words of encouragement.

I know I will never be able to find the words to express the support I received from all the staffs at Unilever Port Sunlight under whom I felt as an apprentice learning anything and everything about the subject matter; [1] Mr Michael Cooke[6], [2] Mrs Cha Coloma-Casugbo, [3] Mr John Naughton, [4] Mrs. Anne-Laure Ferry, [5] Cesar Mendoza, [6] Mr. Harvey Brimelow, [7] Mr Mark Flanagan, [8] Mr David Littlewood[7], [9] Mr Geraint Roberts[8], [10] Dr Sally Wood, [11] Mr Patrick Maguire, [12] Mr Lee Brennan, and [13] Miss Busayo Onasile – all of whom I have developed a mentor-protégé relationship with. I have learned several skills, know-how and acquired intelligence – they have all inspired me and taught me a lot about my subject matter. The knowledge I have gained from these individual have helped me improve rapidly as I worked towards the goals of my work.

I would like especially thank Mr Michael Cooke and Mr Mark Flanagan – great individuals, who always take time out of their very busy schedule to have short noticed meeting in which I am able to present my ideas/theories and receive a reaction – I am really grateful, they were always around in the lab.

I would like to thank the [1] Mr Hans Hoogland and [2] Dr Jo Janssen who took care of me during my internship at Unilever Vlaardingen. I would also like to extend my gratitude to Dr Michael Henson of University and the University of Massachusetts for his support during collaborative work carried out between me, his student[9] and Mr Arend Dubbelboer[10] of the Eindhoven University of Technology.

I am thankful to Mr Richard Feetham[11] for all his assistance during my time at the University of Liverpool. I appreciate the support of my many friends – too many to list, a few of whom include [1] Mr Segun Shodamola, [2] Mr Adetayo Otubisin, [3] Mr John Ogundele, [4] Miss Bolanle Andre[12], [5] Miss Zena Ehdego[13], [6] Mr Mayowa Obeisun, [7] Mr Dolapo Akisanya, [8]

[6] Great individual, selfless and always creates time for me at extremely short notice
[7] Thank God for him, he ensured I didn't get in trouble with regards to safety – always cautioning me with love when breaking safety laws unconsciously.
[8] Great individual, his calmed approach to everything inspires me
[9] Mr Shashank Maindarkar
[10] Supervisors – Mr Hans Hoogland and Dr Jo Janssen
[11] Ultra Mixing and Processing Facility (Lab Technician)
[12] Favourite Cousin
[13] 'Favourite female medic'

Miss Uduak Williams, [9] Mr Charles Falodun, [10] Miss Namubo Syatwinda, [11] Miss Tomi Yussuf [12] Miss Amara Inusa, [13] Mr Bankole Oluwajana, [14] Mr Ibrahim Idowu, [15] Miss Nyinishu Marison [16] Miss Kike Odekunle [17] Lanre Okeya etc. Likewise all my library buddies Ahmed Musa, Oyedeji Afolabi, Jamal Ali, Sarah Aribo, Wori Steven, Tunde Ogidan, Yemi Jegede, Ade Sotayo etc. finally many unsung heroes i.e. church members/unnamed friends for all the uplifting and continuous encouragement. God has used a lot of people in diverse ways to help in accomplish this Thesis that much more easier - thank you everyone, I am forever grateful and God bless the work of your hands.

Table of Content

List of Figures

List of Tables

Chapter 1

1 Introduction

1.1 Background and Context

The issue of environmental sustainability makes up the seventh of the United Nation's eight Millennium Development Goals (UN 2013) time-bound and measurable goals to be reached by 2015 – these goals are to be achieved via several documented objectives.

The most important objective relevant to this Thesis is "integrate the principles of sustainable development into country policies and programmes and reverse the loss of environmental resources". According to a document published by the Technology Strategy Board (TSB 2009), to date, some progress has been made in addressing straight forward environmental issues such as "close monitoring of ozone-depleting substances" in the fight against climate change yet problems such as the inefficient use of resources still pose a persistent threat to sustainable development. To ensure a sustainable future amidst increasing world population/resource consumption, radical changes must be made to the use of resources.

Unilever as a multinational Fast Moving Consumer Goods (FMCG) company manufactures personal care[14], foods[15], refreshment[16] and home care[17] products. Unilever's largest product segment is its personal care business which in 2013 turned over €18.0bn in revenue – this amount is over a third of Unilever Group's total turnover (Unilever 2013). This Sector is responsible for skin cleansing[18], hair care[19] skin care and deodorants[20] and oral care products. Key raw materials such as surfactants, vegetable oils, fatty alcohols etc. are vital in the formulation of such products - with increasing population and the expansion of the Unilever personal care business[21], the demand for such raw materials is expected to increase - efficient use

[14] 36 % of total turnover in 2013
[15] 27 % of total turnover in 2013
[16] 19 % of total turnover in 2013
[17] 18 % of total turnover in 2013
[18] I.e. shower gel
[19] I.e. shampoo, Hair Conditioner
[20] I.e. body spray, after shave
[21] Underlying sales growth of 7.3% across the hair care, skin cleansing and skin care, deodorants and oral care growing more than 5% in 2013 (Unilever 2013).

of these material is therefore important from both a cost and sustainability perspective. One of such key raw material relevant to this project is surfactant.

Surfactants also referred to as SURFace ACTive AgenTS are amphiphilic molecules[22] that exhibit interesting behaviours at interfaces by absorbing on surfaces or interfaces thus altering the thermodynamic properties of such surfaces (Clint 1992). Surfactants are used in many chemical industries as discussed in Section 2.1. They are also present in biological systems (i.e. cell membrane structure) and are referred to as lipids - more introductory text on surfactants can be found in (Demus et al. 1997; Figueiredo Neto & Salinas 2005; Gary 1962).

Historically, the manufacture of surfactants dates back to around 2800 B.C. when a soap-like material was found in clay cylinders during the excavation of ancient Babylon - inscriptions on the cylinders say that fats were boiled with ashes, which is a method of making soap, but do not refer to the purpose of the "soap." (CleaningInstitute 2005)

Today in 2014, the global surfactant industry is a multi-billion pound business with markets everywhere from household detergents, industrial cleaning, personal care, oil field, emulsion polymerisation, food, pulp and paper, explosives etc. it is expected to be worth an estimated £22 billion by 2017 (Rohan 2013). Surfactants are rarely used on their own i.e. in the area of personal care, food and home care products - they are often blended with a range of other ingredients such as edible oils, other surfactants, chelating agents etc. Its manufacture is one of the largest in the process industry due to the fact that its usage occurs in a variety of formulated products.

High demands by consumers for such formulated products at a very low cost as well as consideration of the effect of the industry on the environment is swaying the major industry players in the formulated product sectors such as Unilever, Procter & Gamble, Colgate Palmolive etc. to reassess their business strategies to ensure it accounts for industry changes[23] - whilst ensuring they remain competitive. These demands pose challenges for manufacturers in ensuring they deliver good quality products at effective prices. To ensure this, a good knowledge of raw materials (surfactant) as well as the manufacturing process is required. Good knowledge of surfactants behaviour under different processing conditions is vital in developing a competitive strategy with respect to production for a company such as Unilever. More information on surfactants can be found in Chapter 2

[22] Possessing both polar (hydrophilic head) and non-polar (hydrophobic tail) regions are materials
[23] Such as new environmental legislations, changes in consumer behaviour etc.

1.2 Approach

A decision was made to focus this thesis on a formulated product (rinse-off Hair Conditioner) within the Unilever personal care brand – this is down to the size of the Sector as introduced earlier as well as the fact that Unilever Research and Development Port Sunlight, Liverpool[24] was in close proximity to the University of Liverpool - any findings can be directly taken advantage of by the Unilever business. More importantly data published in (Bongers, Egan & Irving 2013) highlighted the opportunities[25] that exist with respect to processing of similar lamellar systems to the one utilised in this text.

This selected formulation is spread across a range of brands in the Unilever portfolio i.e. Sunsilk, Dove, Clear and Sedal.

Addressing the efficient use of resources would require the consideration of product lifecycle (Figure 1-1) with a focus on understanding - product (formulation) interaction (processing) with current manufacturing technology (equipment) as schematically illustrated in Figure 1-2.

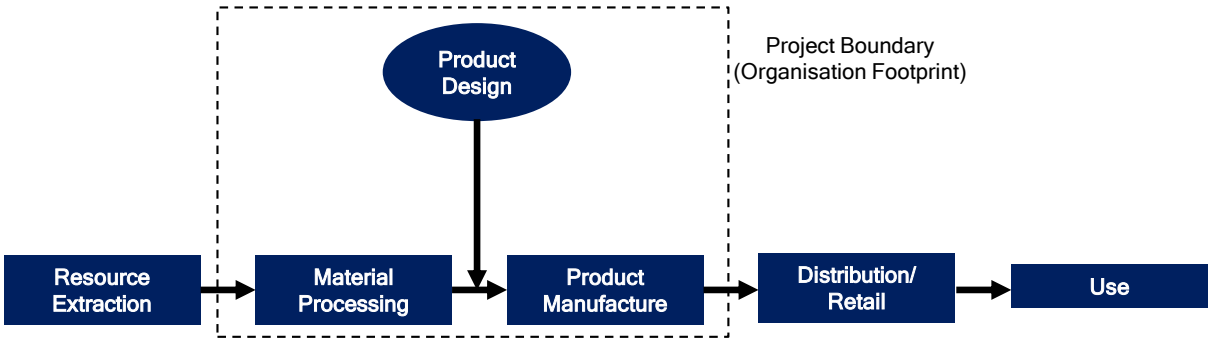

Figure 1-1: Schematic of a simplified resource (product) lifecycle (adapted from TSB 2009).

The dematerialisation (TSB 2009) approach is used to address the challenge of resource efficiency in this text which in a nutshell is using less material to manufacture products without compromising on performance benefit for consumers.

[24] Centre is at the heart of the business strategy with major R&D programmes for Hair, Laundry, Deo and Household Care being run from the site etc.
[25] I.e. commercial advantage, raw material efficiencies etc.

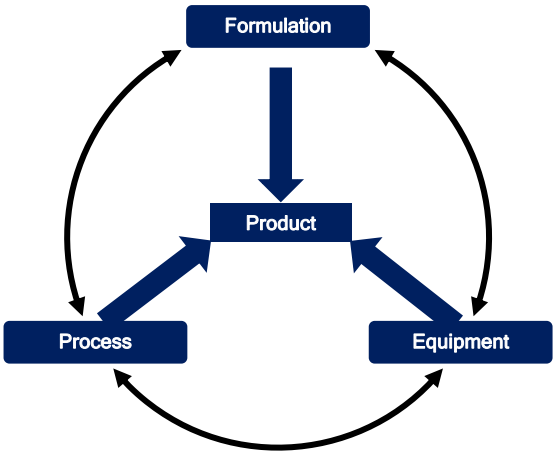

Figure 1-2: Schematic illustrating Thesis approach to addressing the resource efficiency challenge.

Alongside the Hair Conditioners – simple oil in water food emulsion is also used to help achieve Thesis aims.

The upcoming Section presents a brief introduction to the nature of the formulation, equipment, process and products considered in reference to the schematic in Figure 1-2 as well as the technical approach taken to achieving Thesis aims.

Product/Formulation: Formulated Products (Structured Liquids)

Structured liquids are materials possessing multiple phases i.e. particles dispersed in liquid - whose rheological properties are dictated by the interaction of the constituents (Franck 2004a). These liquids, are often classified as colloidal solutions, aggregates, polymers and surfactants liquid crystals (Pincus & Witten 2004). They possess ordered connected polyatomic structures causing them to exhibit a wide range of behaviour. Few structured liquids encountered from daily experiences in foods (mayonnaise, margarine), cosmetics, paints, pharmaceuticals (syrup), personal care products (lotion, cream etc. Hair Conditioner is a structured liquid.

The focus of this project is lyotropic liquid crystals with application in the hair industry (Hair Conditioner), this is a surfactant liquid crystal – more on surfactant liquid crystal is discussed in Chapter 2. More importantly the project's focal point is one class of such surfactant liquid crystals termed the lamellar liquid crystal.

Process/Equipment: Fluid Processing (Mixing Operation)

Liquids, gases and some solids (i.e. powders and particulate materials) are termed fluids and can flow without disintegration when kinetic energy in form of (vibration, rotation and translation) is applied to them (Fellows 2000). The practical application of this science in industry is associated with the term 'processing', a branch of manufacturing associated with manufacture of products from set recipes (formulation).

The production of structured liquid; personal care products (i.e. deodorants, toothpaste, soap, body lotion, hair care products etc.), food products (i.e. dressings, spreads, ice creams etc.) and homecare products such as household cleaning products, laundry are just some of the few applications involving fluid processing.

Fluid processing is a branch of manufacturing involving product development from a set formulation and more often than not, it involves mixing as a unit operation in which a uniform mixture is obtained from two or more components by dispersing one within the other (Fellows 2000). The processing of dispersed liquid systems (i.e. colloidal and surfactants solutions), is a multi-phase operation (Harnby, Edwards & Nienow 1997), and could either be a single phase operation (i.e. blending together miscible fluids), a two-phase operation (i.e. solid-liquid mixing, gas-liquid mixing, liquid-liquid mixing) or a three phase contacting operation involving a two phase operation coupled with another phase (i.e. gas: liquid: solid) or the use of catalyst.

Devices such as static mixers, agitated vessel, rotor-stator mixers, valve homogenizers and Ultrasonics etc. are used to achieve mixing in such industry (Atiemo-Obeng & Calabrese 2004; Davies 1987). Mixing can be described as either distributive or dispersive (Figure 1-3) – for multi-phase operation, each phase comprises of discrete domains – distributive mixing aims to change relative spatial positions of the domains of each phase while dispersive mixing seeks to overcome cohesive forces thereby altering the size and size distribution of each phase (Bongers, Egan & Irving 2013). Commercially available mixing devices could be either dispersive alone, distributive alone or both – often selection of mixer by experts is usually dependent on the nature of the process in consideration.

The process of dispersing and/or distributing one phase (the dispersed phase) in a second phase (the continuous phase) using mechanical energy (Tanguy, Fradette & Khopkar 2009) is vital to several mixing applications in the fluid processing industry.

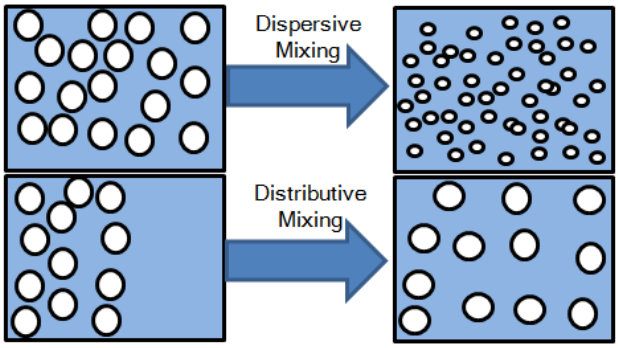

Figure 1-3: Schematic representations of dispersive and distributive mixing

This project considers mixing in a class of mixers referred to as high shear rotor-stator mixer for liquid – liquid operations. It is worth mentioning that some materials could be solid (flakes or powder) at ambient temperature and would require heating above melting temperature. Others might need to be dissolved in solvents.

1.2.1 Technical Approach

Having decided on the formulated product[26], a range of analytical techniques is used to assess the impact of a range of process variables on the underlying microstructure/rheology of formulated product and/or its intermediate[27] – process variables reviewed are related to the manufacturing of the formulated product in question as summarised in Figure 1-2.

Analytical techniques such as Brookfield viscosity measurements[28] presented bulk viscosity measurements in relation to microstructure, optical (light) microscopy[29] presented a more detailed representation on the qualitative nature of the microstructure thus aiding the identification of the various components of the underlying microstructure thereby complimenting all rheological (viscometry[30] and rheometry[31]) measurements.

Microscopic techniques such as bright field/cross polarised illumination as well as hot stage microscopy were used to visualise the microstructural characteristics. Differential scanning calorimetry (DSC) and small angle x-ray Scattering (SAXS) analysis further complimented all analysis performed in helping identify transition temperatures and detect/assess changes to the underlying microstructure on a molecular scale respectively.

[26] Rinse-off Hair Conditioner based on the H-C formulation
[27] AA % QUAT/CS/FA/Water
[28] Controlled Strain Shear Viscometer
[29] Polarising Microscopy
[30] Brookfield T-bar B viscosity measurements
[31] Controlled Strain Shear Rheometer (Oscillatory Shear Measurement)

A second aspect to the work is the study of existing technology[32] and the development of a new mixing technology referred to as the 'Controlled Deformation Dynamic Mixer (CDDM)' –

The CDDM technology; a novel equipment which has a very low ratio of physical size/manufacturing is currently installed at the Ultra Mixing and Processing Facility (UMPF)[33] – the CDDM/UMPF technology allowed the optimisation of the CDDM design using two process fluids relevant to the Unilever business [1] Hair Conditioner and [2] sunflower oil emulsion[34] relevant to its personal care and food business respectively.

The Thesis reviewed an experimental program within the realms of the CDDM/UMPF capability for the optimisation of the confronting surfaces (rotor and stator) of the CDDM technology with respect to cavity configuration and relative positions of the rotor-stator surfaces during operation i.e. relative axial position, radial separation and relative angular.

Finally new formulated products produced are also subjected to consumer performance tests to confirm consumer liking - tests consist of experts in the Unilever salon applying products on consumers and selected panellists (consumers) self-style their own hair by applying products in respective homes for which feedback is obtained.

[32] Silverson high shear mixer and Sonolator
[33] See Section 3.3.1
[34] In this study emulsion droplet analysis was conducted using laser light scattering technique in the Malvern Mastersizer 2000

1.3 Thesis Layout

Chapter 1: it begins by putting the Thesis in the context of environmental sustainability which is in line with Unilever's greenhouse gas strategy - which is to double the size of its business while reducing its environmental footprint. It also gives a brief introduction to the surfactant industry. The Chapter concludes by presenting an overview of the approach taken to solving the Thesis question.

Chapter 2: a comprehensive literature review concerning all aspects related to the Thesis work. – these include surfactant structure, surfactant self-assembly process, micellisation, lyotropic liquid crystals, various types of liquid crystals and the factors affecting their formation and response of lamellar crystalline phase to shear. A review of various papers considering a mixed emulsifier system is performed – for this Section, particular attention is paid to the manufacturing process. The nature of the formulation of Hair Conditioners is presented alongside the nature/functionality of its raw materials. A review of the CDDM technology is presented – this is followed by the concept of rheology with relevance to the processing of structured liquid. Finally the various method to which high shear rotor-stator device are characterised is presented

Chapter 3: the process ingredients, process equipment and methods used in this research are discussed. The Chapter begins by introducing the process ingredients – this is followed by a detailed review of the experimental facilities[35]/components used to effect all experimental trials reported within the Thesis. Finally, the underlying theory behind the analytical techniques is reviewed – this is followed by the experimental protocols utilised within the research.

Chapter 4: the work disseminated in this Chapter is performed against the back drop of a batch bench mark process used in the manufacture of Hair Conditioners based on the mixture of QUAT/CS and fatty alcohol. Using a range of analytical techniques[36], the effect of a range of process variables[37] on the underlying microstructure of the formulated product intermediate[38] is elucidated. Learnings from the work conducted in the Chapter are then applied to the batch benchmark process.

[35] [1] University of Liverpool – UMPF and [2] Unilever Research and Development Port Sunlight, Liverpool
[36] Rheology (viscometry and rheometry), optical microscopy (bright field/cross polarised illumination and hot stage), DSC and SAXS
[37] Process temperature, high shear post processing operation (hot vs. cold)
[38] AA % QUAT/CS/FA/Water

Chapter 5: this work is an extension of the work discussed in Chapter 4 – it utilises two sets of analytical techniques[39] to examine the effect of a range of process variables[40] concerned with the continuous manufacturing of Hair Conditioners based on the complex mixture of QUAT/CS/FA/Minor ingredients[41]/Water using the static variant of the CDDM technology. The impact of a range of variables[42] affecting the concept of dematerialisation is investigated using two sets of analytical techniques[43].

Chapter 6: the chapter focuses on using two analytical techniques[44] to aid the optimisation of the CDDM using two systems - [1] rinse off Hair Conditioners based on the QUAT/CS/FA/Water system and [2] a simple O/W[45] emulsion stabilised by a non-ionic surfactant[46] - the novel equipment was optimised for the production of resource efficient Hair Conditioner.

Chapter 7: the main conclusions are presented in this Chapter – likewise future work is discussed

[39] Rheology (viscometry) and optical microscopy (bright field/cross polarised illumination)
[40] Equipment set-up, process temperature and process flow-rate (pressure drop)
[41] I.e. preservatives, electrolyte, perfume etc.
[42] Raw material efficiency, equipment deformation rate, Hair Conditioner age and mixing technology.
[43] Rheology (viscometry) and optical microscopy (bright field/cross polarised illumination)
[44] Rheology (viscometry) and laser scattering respectively
[45] Oil in Water
[46] Pluronic F-68

1.4 References

- Atiemo-Obeng, V.A. & Calabrese, R.V. (2004) Rotor-Stator Mixing Devices, in E.L. Paul, V.A. Atiemo-Obeng & S.M. Kresta (eds), *Handbook of Industrial Mixing*, John Wiley & Sons, Inc., New York, pp. 479 - 505.
- Bongers, P.M.M., Egan, M.J. & Irving, G.N. (2013) *Method For Production Of Structured Liquid And Structured Liquid*, Great Britain.
- CleaningInstitute (2005) *Soap & Detergents History* [Online], Cleaning Institute, Available from: http://www.cleaninginstitute.org/clean_living/soaps__detergent_history.aspx (Accessed).
- Clint, J.H. (1992) *Surfactant Aggregation*, Blackie, Glasgow.
- Davies, J.T. (1987) 'A physical interpretation of drop sizes in homogenizers and agitated tanks, including the dispersion of viscous oils', *Chemical Engineering Science*, vol. 42, no. 7, pp. 1671-1676
- Demus, D., Goodby, J.W., Gray, G.W., Spiess, H.-W. & Vill, V. (1997) *Handbook of Liquid Crystals*, Wiley, New York.
- Fellows, P. (2000) Theory of Liquid Mixing, in, *Food Processing Technology*, Woodhead Publishing Limited, Cambridge England.
- Figueiredo Neto, A.M. & Salinas, S.R.A. (2005) *The Physics of Lyotropic Liquid Crystals: Phase Transitions and Structural Properties*, Oxford University Press.
- Franck, A.J. (2004) *Understanding Rheology of Structured Fluids*, TA Instruments,
- Gary, G.W. (1962) *Molecular Structure and The Properties of Liquid Crystals*, Academic Press, New York.
- Harnby, N., Edwards, M.F. & Nienow, A.W. (1997) Introduction to Mixing Problems, in J.W. Mullin (ed.), *Mixing In the Process Industries*, Butterworth Heinemann.
- Pincus, P. & Witten, T. (2004) *Structured Fluids: Polymers, Colloids, Surfactants*, Oxford University Press, New York.
- Rohan (2013) *Global Surfactant Market worth $36.5 Billion by 2017* [Online], Markets And Markets, Available from: http://www.marketsandmarkets.com/PressReleases/surfactants.asp (Accessed).
- Tanguy, P.A., Fradette, L. & Khopkar, A.R. (2009) 'Emulsification capability of a dual shaft mixer', vol. 87, no. 1631-1639.

- TSB (2009) *Resource Efficiency Strategy 2009 - 2012*, Technology Strategy Board, United Kingdom
- UN (2013) *Millenium Development Goals And Beyond 2015* [Online], UN Department of Public Information, Available from: (Accessed: 2010-12-12).
- Unilever (2013) *Making Sustainable Living Commonplace: Annual Report And Accounts 2013*, United States

Chapter 2

2 Literature Review

2.1 Surfactants

Surfactants play a crucial role in many industries involved with surface science chemistry; industries such as the pharmaceutical (Malmsten 2001), food (Bergenstahl 2001), detergency (Rybinski 2001), agricultural (Tadros 2001), photography (Texter 2001), paints (Holmberg 2001), paper (Tiberg, Daicic & Froberg 2001), polymerisation (Tauer 2001), ceramics (Bergstrom 2001), dispersion (Moudgil, Singh & Adler 2001) and petroleum (Kanicky et al. 2001). They[47] are surface-active[48] chemical compounds that absorb on surfaces or interfaces[49] thus altering the thermodynamic properties of such surfaces. Surfactants (Figure 2-1) are also referred to as amphiphilic molecules - possessing both polar (hydrophilic head) and non-polar (hydrophobic tail) regions - this characteristic forms the basis of their activity as one part readily dissolves in water and the other in oil furthermore, they can also form aggregates when dissolved in a solvent[50] under certain conditions.

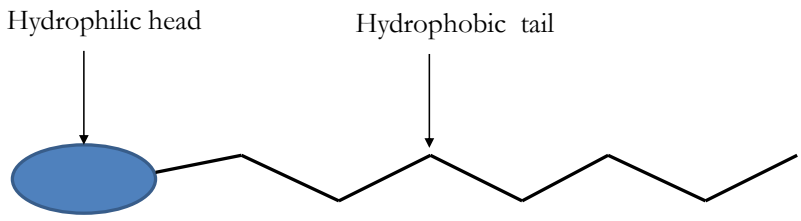

Figure 2-1: Schematic representation of a surfactant molecule highlighting its amphiphilic features.

The amphiphilic nature of surfactants, amongst many properties is responsible for their relevance in the aforementioned industries i.e. in dilute aqueous solutions, surfactants molecules self-assemble to form aggregates thus leading to the formation of liquid crystals (lyotropic phases[51]) as their concentration is increased - depending on the type of surfactant and the solution conditions, aggregates formed may be spherical, globular, rodlike, a spherical bilayer structure, closed aggregates with hydrophobic interiors called micelles or spherical bilayers

[47] Surfactants
[48] as introduced in Section 1.1
[49] i.e. liquid/liquid, liquid/gas or liquid/solid interface systems
[50] in the case of this Thesis (water)
[51] More on lyotropic phases in Section 2.3

containing an encapsulated aqueous phase called vesicles (Nagarajan & Ruckenstein 1991) – the formation of aggregates/lyotropic phases results in changes in the solution properties i.e. increase in the viscosity of the medium[52], stability of solutions etc. Formation of aggregates/lyotropic phases results in the formation of a template microstructure which forms the foundation of several products i.e. detergent, hair conditioner[53], shampoo, fabric softeners etc.

2.1.1 Surfactant Classification

The chemical structure of surfactants compound can be constructed in a number of different ways as found in literature; [1] Perfluorinated tailed surfactants (La Mesa & Sesta 1987) , [2] Bile salts, which possesses a unique molecular structure when compared to typical detergent molecules (Carey & Small 1972), [3] surfactants possessing multiple tails attached to a single head group for which tails can be branched (Warr et al. 1988), and [4] surfactants with two head groups attached to either end of the hydrocarbon chain termed Bolaform surfactants and dimeric surfactants which are two conventional surfactant molecules as shown in Figure 2-1 joined at the head with a spacer.

More simply - since the hydrophilic part normally achieves its solubility either by ionic interactions or by hydrogen bonding, the simplest classification is based on surfactant head group type (Eastoe 2002c), - they can be classified based on charge (or lack of it) on the polar head group thus giving the common classes which include non-ionic, anionic, cationic, and zwitterionic (Rosen 2004) - a summary of the schematic of these major classifications can be seen in Figure 2-2.

Cationic[54] - The surface active portion of cationic surfactants bears a positive charge; examples include alkyltrimethylammonium and alkylpyridinium halides (Edlund et al. 1994; Laughlin 1990)

Anionic - A surfactant is classed as anionic if the charge on the surface active portion on the molecule possesses a negative charge; examples include soap, alkyl sulfonate (alkyl sulphates, alkyl phosphates and fatty acid salts (Ekwall, Mandell & Fontell 1969a; Jeon et al. 1996; Wrigth & Tartar 1939)

[52] Solvent
[53] Relevant to this project
[54] This thesis utilised surfactants within this classification

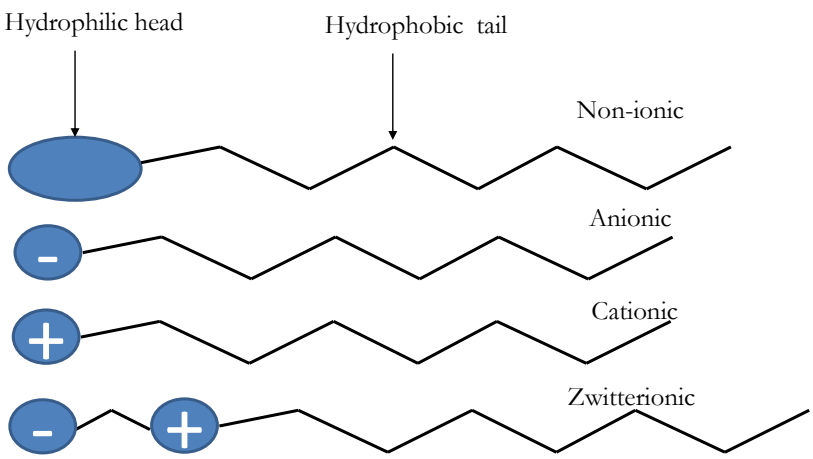

Figure 2-2: Schematic classification of common surfactant according to hydrophilic head group composition.

Zwitterionic - These surfactant possess both positive and negative charges on the surface active portion - examples include long-chain amino acid and sulfobetaine

Non-ionic - These class of surfactants bears no ionic charge that can be easily ionised; examples include monoglyceride of long-chain fatty acid, polyoxyethylenenated alcohol or polyoxyethylenated alkyl phenol (Clunie, Goodman & Symons 1969; Nilsson, Soderman & Johansson 1996)

2.2 Surfactant Micellisation (Aggregation)

2.2.1 Micelle Formation

Solute (surfactants) dissolved in a solvent (water) will self-assemble – a spontaneous cooperative process that results in aggregation stabilised by weak van der Waals, hydrophobic interactions, hydrogen-bonding, and screened electrostatic interactions. The different aggregates formed by surfactants can be seen in Figure 2-3 (Israelachvili 1991; Pincus & Witten 2004).

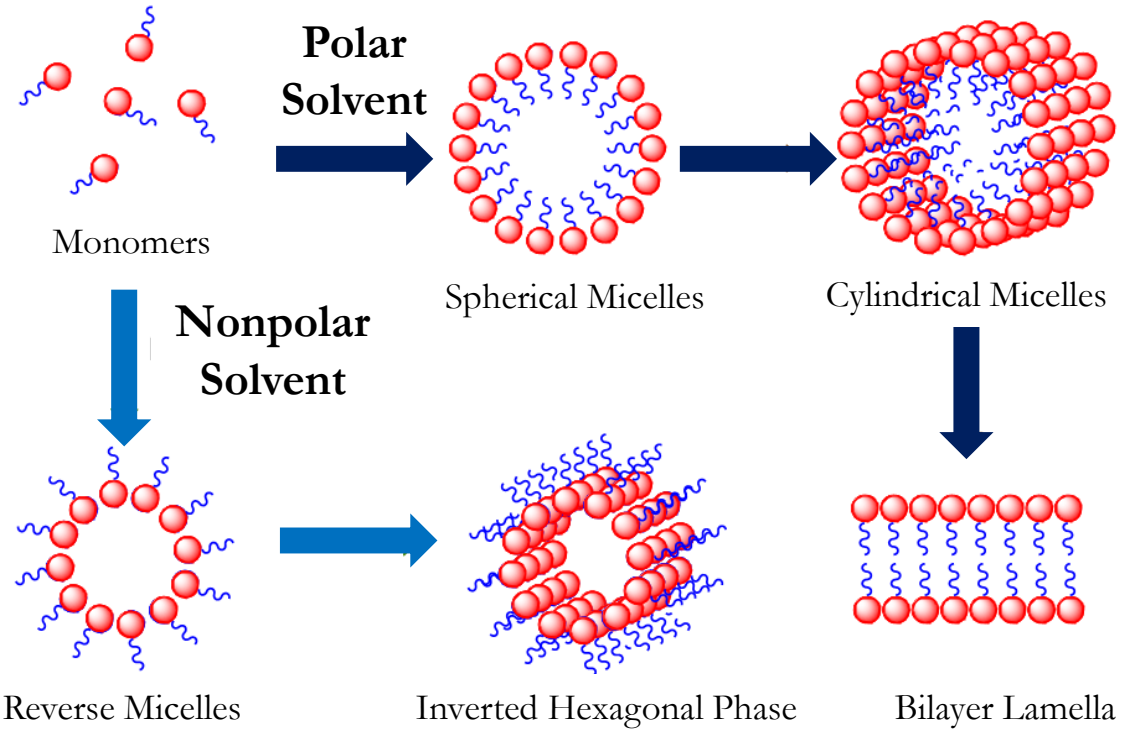

Figure 2-3: Schematic of various types of surfactant aggregate structures formed in aqueous solution (Clint 1992; Israelachvili 1991).

For self-assembled aggregates and micelles to form, Critical Micelle Concentration (CMC) must be exceeded - if the concentration of the surfactant is above CMC, surfactant molecules will aggregate to form micelles. - changes to solution conditions[55] will also affect the interaction between aggregates, effectively modifying the size and the shape of the structures (Israelachvili 1991) as shown in Figure 2-3 .The number of molecules in an aggregate is referred to as the aggregation number and is dependent on the type of surfactant.

[55] I.e. pH, electrolyte concentration, concentration of surfactant molecules and temperature

2.2.2 Aggregation

2.2.2.1 Critical Micelle Concentration (CMC)

Surfactant molecules cannot exist in isolation in water (except at low concentrations); instead they assemble themselves forming extended structures called micelle (Pincus & Witten 2004) - for self-assembled aggregates and micelles to form, CMC must be exceeded. If the concentration of the surfactant is increased above CMC, surfactant molecules will aggregate to form micelles. Literature consists of well-defined changes in some of the physico-chemical properties of aqueous surfactant solutions above CMC (Hassan, Verma & Ganguly 2012) a few of which are shown in Figure 2-4.

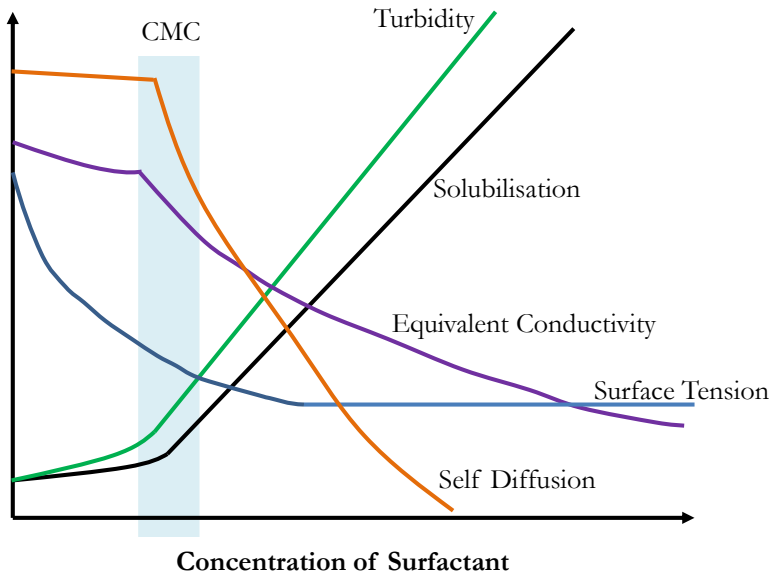

Figure 2-4: Schematic representation showing the variation of some of the physical properties of a solution with the concentration of surfactants (Eastoe 2002a; Hassan, Verma & Ganguly 2012).

It is worth mentioning that the change described in Figure 2-4[56] occurs over a narrow concentration as opposed to a precise point as is illustrated by some authors, and the magnitude of the CMC obtained depends on the property being measured (Ekwall 1975). For surfactant mixtures (i.e. a combination of more than one surfactant), the formation of micelle will be more complex due to components specific CMCs (Clint 1992).

Micellisation is an entropy-driven process; when surfactants are dissolved in water, the hydrophobic group disrupts the structure of water thus increasing the free energy of the system

[56] CMC

– surfactant molecules therefore concentrate at interfaces, so that their hydrophobic groups are directed away from the water and the free energy of the solution is minimized – distortion of the water structure can also be decreased by the aggregation into clusters (micelles) with the hydrophobic groups directed towards the interior of the cluster and their hydrophilic groups directed towards the water (Patist 2001) - a schematic of the process in is shown in Figure 2-5.

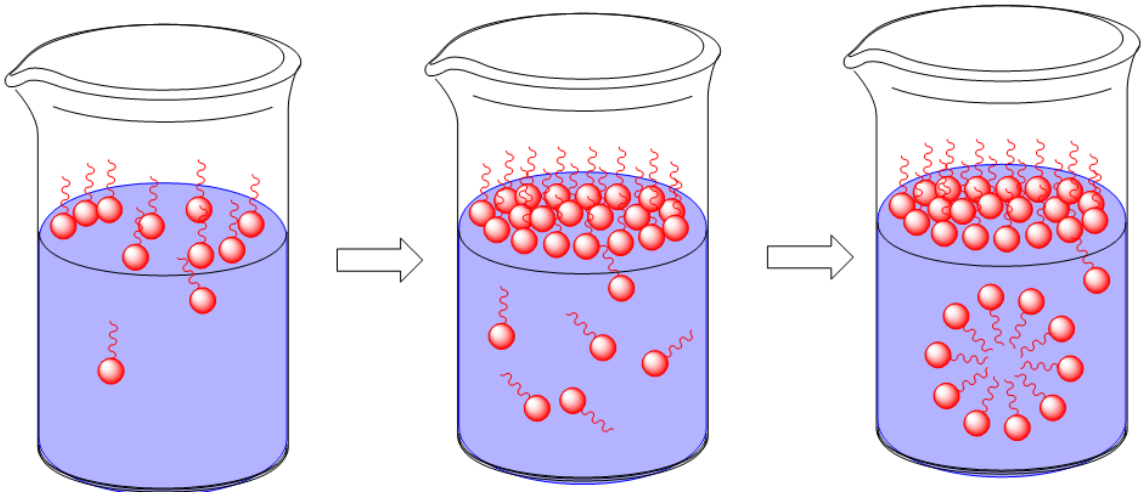

Figure 2-5: Schematic representation showing micelle formation; monomers absorbed at the air/water interface – monomers in the bulk solution and micelles (Hunter 2000; Patist 2001)

Measurement of aqueous solution parameters[57] i.e. surface tension, electrical conductivity, static and dynamic light scattering, refractive index, molecular absorption and diffusion coefficient can be employed to determine the CMC of surfactant systems. These involve measuring the changes in physicochemical properties of the aqueous solution – some of which have been shown in Figure 2-4.

Extensive work on the determination of the CMC's of surfactants in aqueous and non-aqueous media can be found in (Mukerjee & Mysels 1971; Rosen 2004; Van Os, Haak & Rupert 1993) - determining the value of CMC is an important parameter in a variety of industrial applications as it gives information relating to the effectiveness of surfactant for i.e. emusification, solubilisation etc.

2.2.2.2 Krafft Temperature

In addtion to micelles forming at CMC, they can also only form above a particular temperature reffered to as Krafft temperature (T_K) – this is the temperature at which surfactant solubility

[57] Figure 2-4

becomes equal to CMC (Jonsson et al. 2002; Krafft & Berichte 1899; Patist 2001) – at this point the solubility of surfactant increases dramatically and below this point surfactant solubility increases slowly. As shown in Figure 2-6, the Krafft temperature is the point of intersection of both the solubility and CMC curve – below the T_K surfactant exsist as monomers in equilibrium with hydrated crystalline phase, and above the T_K, micelles are formed and thus solubility is increased (Jonsson et al. 2002).

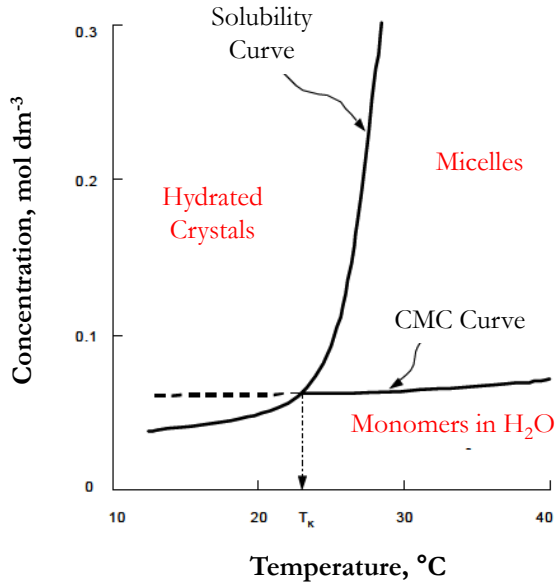

Figure 2-6: Schematic illustrating the point at which surfactant solubility equals CMC; Krafft temperature (Eastoe 2002a; Jonsson et al. 2002) .

The Krafft point may vary dramatically with changes to the chemical structure of the surfactant – below are a few comments on alkyl chain surfactants and Krafft point (Hato, Tahara & Suda 1979). The Krafft point is dependent on the head group, alkyl chain length and chain structure – the Krafft point increases strongly as the alkyl chain length increases due to the dependence of the CMC on alkyl chain length. Salt addition typically raises the Krafft point, introduction of a methyl group, a double bond, or some other chain branching in the alkyl group, and introducing a polar segment between the alkyl chain and the ionic group would influence the packing conditions (Jonsson et al. 2002) hence the packing efficiency of the lyotropic phase. The development of surfactants with adjusted Krafft points i.e. lower without compromising on its effectiveness i.e. lowering surface tension presents several processing benefits for the industry at

large. Information on the formulation space[58] for the material[59] utilised/manufactured in this Thesis is discussed in Appendix D.

2.2.2.3 Hydrophobic Effect

Surfactant molecules have a high affinity for different interfaces – they migrate to these interfaces (Claesson & Rutland 2001) thereby modifying the properties of such surfaces i.e. the polar head group dissolves in the polar medium and the non-polar head group dissolves in the hydrophobic medium – this allows the different mediums to be held together as the surface tension is reduced.

The hydrophilic polar head group present strong interactions with solvent molecules (water) due to the uneven distribution of electrical charge in the molecule from the bonding of atoms thus presenting water solubility or adsorption - on the other hand, according to (Tanford 1980) the non-polar hydrophobic tail possesses a uniform distribution of the electrical charge in the molecule, thereby offering neither attraction nor repulsion towards the solvent however the hydrophobic tails drives the formation of self-assembled aggregate structures such as micelles, bilayers, liquid crystals due to strong interactions when placed in a water environment (Jonsson et al. 2002).

Models reported by (Mittal 1977; Tanford 1974, 1980) have helped explain the physicochemical features of surfactant assembly by examining the free energy change associated with micellisation (Nagarajan & Ruckenstein 1991). Tanford demonstrated that the hydrophobic effect is responsible for the cooperative growth of micelles – while the interactions between the polar head groups of surfactant provide the anti-cooperativity that constrains the aggregates to remain of finite sizes (Nagarajan & Ruckenstein 1991).

Surfactant molecules aggregation arises from the interplay of two opposing forces – the first is the 'hydrophobic effect' of the hydrocarbon tails which tends to bring the molecules closer together, the other the 'solvation' of the head groups which will tend to keep the hydrophilic parts away from each other (Hassan, Verma & Ganguly 2012; Tanford 1980). In addition to the interaction between the hydrocarbon chains, the origin for the hydrophobic effects are the strong attractive forces occurring between the water molecules by the introduction of non-polar molecule into the water. For polar or ionic solutes, strong bonds can be formed with the water

[58] With respect to Figure 2-6 i.e. concentration of the surfactant in solution
[59] Hair Conditioner product

molecules also if the solute is non-polar dissolution in water is resisted (Tiddy, Hassan & Rowe 2001).

A thermodynamic analysis of the micellisation process shows that the introduction of a hydrocarbon into water at ambient temperature is always associated with a decrease in entropy within the system, and an enthalpy of about zero which results in a large positive free energy (Costa, Kronberg & Silveston 1994; Kronberg, Castas & Silvestonti 1994; Shinoda & Fujihara 1968) suggesting that micellisation is an entropy driven process attributed to the structuring of water molecules around hydrocarbon chain (Glew 1962).

Other authors who have discussed the issue in detail are (Costa, Kronberg & Silveston 1994; Kronberg, Castas & Silvestonti 1994) - these authors view the hydrophobic effect as a combination of two effects with one arising from the ordering of water molecules around the solute and the second from the energy required to make a cavity in water large enough to accommodate the non polar solute (Tiddy, Hassan & Rowe 2001). The first is associated with negative entropy associated with the water moleules next to a non-polar solute which have fewer conformations available than "free" water resulting in decrease in entropy and the second and opposite contribution arises from the large amount of energy required to form a cavity to accommodate the non-polar solute. This is large due to both the high cohesion in water arising from strong hydrogen-bonding connectivity, and the small size of water molecules compared to the hydrocarbon (e.g alkanes).

An important conclusion from this mechanism is that it allows the the prediction of the CMC for almost any surfactant as the magnitude of the hydrophobic effect is proportional to the surface area of hydrophobic contact (cavity) between water and the solute.

2.2.2.4 Factors Influencing CMC

There are many factors known to affect the value of CMC – most important is the structure of the surfactant as well as other parameters such as the counterion nature, presence of additives as well as change in temperature (Eastoe 2002a)

The hydrophobic group: the 'tail'

CMC are shown to depend on hydrocarbon chain length by (Klevens 1953) as discussed earlier. For a homologous series of linear single-chain surfactants, the CMC decreases logarithmically with the linear alkyl chain length of a surfactant, n_c (number of carbon atoms in the chain), based

on the well-known Klevens equation shown below (Huibers 1999; Klevens 1953) where A and B are constants that vary according to the charge and type of the head group and contribution of the CH_2 group respectively (Alexander et al. 2014).

$$\mathrm{Log_{10}(CMC)} = \mathrm{A} + \mathrm{Bn_C} \qquad [2.1]$$

The CMC decreases strongly with increasing alkyl chain length of surfactant – as a general rule, the CMC decreases by a factor of ca. 2 for ionic surfactant and by a factor of ca. 3 for non-ionic surfactants on adding one methylene group to the alkyl chain (Lindman 2001).

The CMCs of non-ionic surfactants are much lower than those of ionic surfactants – the effects of the head-groups are moderates. Cationic surfactants have slightly higher CMCs than anionic surfactant. Alkyl chain branching and double bonds, aromatic groups or some other polar character in the hydrophobic part produce noticeable changes in CMC (Eastoe 2002a; Rosen 2004). In hydrocarbon surfactants, chain branching gives a higher CMC than a comparable straight chain surfactant (Rosen 2004).

The hydrophilic group

For surfactants with similar alkyl chain, variation in the hydrophobic part (i.e., from ionic to non-ionic) has a direct impact on the CMC value i.e. the CMC of a C_{12} hydrocarbon with an ionic group head lies in the range of 1×10^{-3} mol dm^{-3}, while the same with a non-ionic head group is much lower (1×10^{-4} mol dm^{-3}) (Eastoe 2002a). The exact nature of the ionic group has no dramatic effect on the CMC values since a major driving force for micellisation is entropy as discussed earlier.

Effect of added salt

A vital issue is the effect of added electrolyte on the CMC of ionic surfactants according to (Lindman 2001) who listed a few features of this action in his text on "Physico-Chemical Properties of Surfactants" – a few of which includes salt addition dramatically lowers the CMC, the effect is moderate for short-chain surfactants and much larger for long-chain surfactant, for non-ionic surfactant simple salts produce only small variations in the CMC with both increases and decreases possible etc.

According to (Eastoe 2002a), the presence of an indifferent electrolyte can cause a decrease in the CMC of most surfactant with the greatest effects found for ionic surfactants. The main effect

of the salt is to partially screen the electrostatic repulsion between the head groups thus lowering CMC. Non-ionic and zwitterionic surfactants display a much smaller effect.

Several authors (Hayase & Hayano 1978; Stead & Taylor 1969) have also investigated the effects of added salt on the value of CMC and have come up with similar conclusions as those mentioned above – 'electrolytes have a dramatic effect on the CMC values'. According to (Gunnarsson, Joensson & Wennerstroem 1980) the addition of an electrolyte (sodium chloride) to solution of sodium alkyl sulfate surfactant solutions reduces the the CMC dramatically due to a reduction in electrostatic repulsion present between the head groups thus enabling micellisation at lower concentration.

For mixed surfactants systems in which CMC varies according to system components/composition – CMC values will be dependent on interations between head groups as investigated by (Jonsson et al. 2002).

Effect of temperature

The dependence of temperature on the value of CMC is a weak one but complex – testing for such would need to account for factors such as subtle changes in bonding, heat capacity etc. associated with heating up the solvent (water) (Eastoe 2002a). (Kresheck 1975) in his book show that the CMC of most ionic surfactants passes through a minimum as the temperature is increased from 0 – 70 °C. Other studies on ionic surfactant have also shown similar trend (Akhter & Al-Alawi 2000; Flockhart 1961; Stead & Taylor 1969). For non-ionic surfactants (Jonsson et al. 2002) mentioned that the CMC decreases with increasing temperature however the effect is small. As discussed earlier the major effect of temperature on micellisation is the Krafft temperature.

2.2.2.5 Micellisation, Structure and Shape

In the micellisation process, molecular geometry is vital to understanding how surfactants pack (Eastoe 2002a) - main structures encountered are micelles, vesicles, bilayer or inverted micelles as shown in Figure 2-3. In the micellisation process, the various geometry formed are dependent on the structure of the surfactant as well as solution conditions (e.g. concentration, temperature, pH, electrolyte content) as reported by (Hartley 1936; McBain 1913; Reychler 1913).

As discussed earlier, two opposing forces control the self-association process. This basic idea was reviewed and quantified by (Israelachvili 1991; Israelachvili, Mitchell & Ninham 1976;

Mitchell & Ninham 1981) resulting in the concept that aggregation of surfactant is controlled by a balanced molecular geometry.

In brief the geometric treatment separates the overall free energy of aggregation to three critical geometric terms as shown in Figure 2-7.

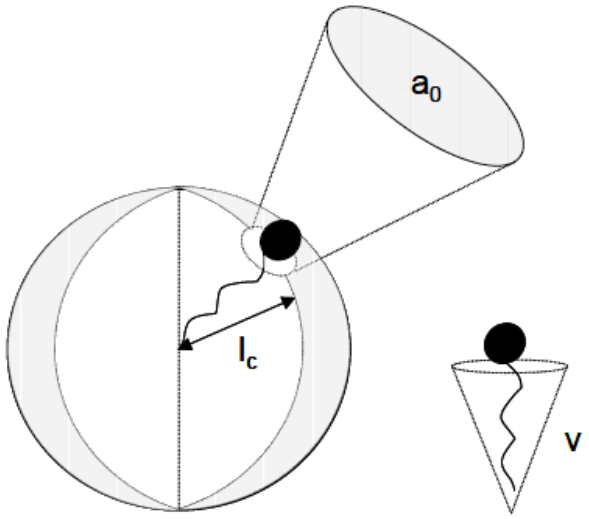

Figure 2-7: Schematic of a surfactant molecule indicating the parameters for packing (Eastoe 2002a)

These three critical parameters are the minimum interfacial area occupied by the head group (a_o), the volume of the hydrophobic tail(s), (v) and the maximum extended chain length of the tail in the micelle core (l_c).

These parameters can be combined into a dimensionless function referred to as the critical packing parameter ($v/a_o l_c$). The concept[60] helps describe the relationship between surfactant molecular shape, micelle shape and consequently liquid crystalline phase structure (Israelachvili, Mitchell & Ninham 1976; Tanford 1980). Liquid crystalline phase structure is considered further down in this text.

Since the micelles are present in solution above the CMC, the most important consideration for liquid crystal phases is the micelle shape (Tiddy, Hassan & Rowe 2001). There are three major types namely; spheres, rods and discs (Table 2-1) which can be described using the packing constraint concept (Israelachvili, Mitchell & Ninham 1976; Tanford 1980). This give a simple description for the relationship between the micelle shape and the molecular shape - in accessing

[60] Critical packing parameter

this concept, the micelles are assumed to be smooth, with only the hydrophobic volume in the micelle interior. Main molecular parameters are those shown in Figure 2-7.

For a spherical micelle, having a hydrophobic volume (V) with radius (r), a total surface (A) and aggregation number (q), the relationship for the volume of the core of micelle and its surface area is;

$$V = q \times v = \frac{4}{3} \pi r^2 \quad [2.2]$$

$$A = q \times a_o = 4 \pi r^2 \quad [2.3]$$

Solving for r,

$$a = 3 \frac{v}{r} \quad [2.4]$$

Ignoring end and edge effects for rod and disc shapes the resulting relationship for rod micelle (radius r) and bilayer/disc (thickness 2r) are

$$a = 2 \frac{v}{r} \text{ (rod)} \quad [2.5]$$

$$a = \frac{v}{r} \text{ (disc)} \quad [2.6]$$

respectively.

The value of 'r' cannot be larger than 'l_t' ($r \leq l_c$) as the length of the tail can fold over one another and hence there are limitations on the lowest value of 'a' for a given shape

$$a \geq 3 \frac{v}{l_c} \text{ (sphere)}; \; a \geq 2 \frac{v}{l_c} \text{ (rod)}; \; a \geq \frac{v}{l_c} \text{ (disc)} \quad [2.7]$$

Table 2-1 shows the major micelle (sphere, rod and disc) encountered alongside packing constraints.

Table 2-1: Summary of the major micelle shape classification with packing constraints

Class	**Micelle size and aggregation (q)**	**Limitations on size of the head group (a)**
Sphere	Largest head group, smallest alkyl chain length. Low aggregation number, q < 60	$P \leq \frac{1}{3}$ $a \geq 3\,\frac{\mathrm{v}}{l_c}$
Rod	Small head group, large alkyl chain length. Large aggregation number, q > 60	$\frac{1}{3} \leq \mathrm{P} \leq \frac{1}{2}$ $a \geq 2\,\frac{\mathrm{v}}{l_c}$
Disc	Smallest head group, largest alkyl chain length. Low aggregation number, q < 300	$\frac{1}{2} \leq \mathrm{P} \leq 1$ $a \geq 3\,\frac{\mathrm{v}}{l_c}$
The relative size of the polar and the non-polar groups determines what kind of micelles produced.		

A surfactant with a given chain length can pack into spheres, rods or disc, according to the size of the head group, with all three shapes being possible for the largest 'a' values and only disc micelles for small 'a' values (Tiddy, Hassan & Rowe 2001).

Thus far, the literature review has shown that the geometric packing properties of surfactants can be expressed in terms of packing parameter ($v/a_o l_c$) in a given solvent conditions – the value of which determines the type of aggregate formed. Table 2-2 illustrates the structures formed by some common surfactants (Israelachvili 1991).

Changes in critical packing parameters of a surfactant molecules gives rise to different aggregate structures – it is also possible to determine the size and shape of liquid crystal structures into which surfactants can assemble (Table 2-2). This can be determined by using the surfactant packing parameter which is the ratio of the hydrophobic group area to the hydrophilic head area.

For an unbranched and saturated hydrocarbon chain with n carbon atoms, the v (volume) and the l_c (length of the hydrophobic tail) can be obtained using the equations below (Tanford 1980);

$$v = (27.4 + 26.9n)\ X\ 10^3\ (nm^3) \quad [2.8]$$

$$l_c \leq l_{max} \approx 0.154 + 0.1265n\ (nm) \quad [2.9]$$

Where l_{max} is the fully extended molecular length of the chains.

Table 2-2: Table showing schematic representation of the mean molecular packing shapes alongside aggregate structures formed by common surfactants (Israelachvili 1991).

Typical Surfactant Type	**Critical Packing Parameter ($P = v/a_o l_c$)**	**Critical Packing Shape**	**Aggregate Structures Formed**
Single-tailed surfactants with large head group area	<1/3	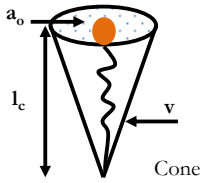	Spherical micelles 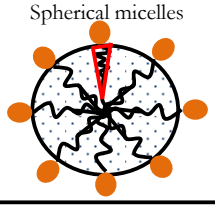
Single-tailed surfactants with small head group area	1/3 – 1/2	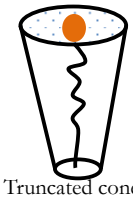	Cylindrical micelles 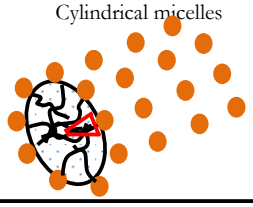
Double-tailed surfactants with large headgroup areas, tails in liquid-like conformation	1/2 - 1	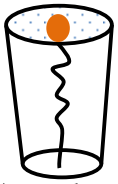	Flexible bilayers vesicles 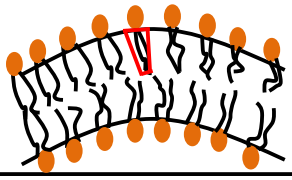
Double-tailed surfactants with small headgroup areas, tails in solid-like conformation	Approx. 1	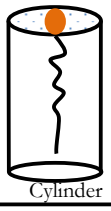	Planar bilayers 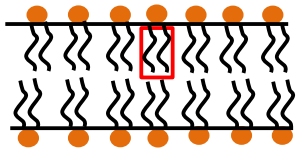
Double-tailed surfactants with small headgroup areas, high temperature	> 1	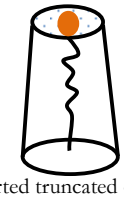	Inverted micelles 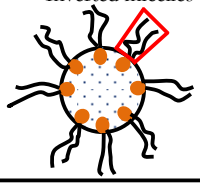

According to (Israelachvili 1991), a number of other factors such as ionic environment, temperature, chain unsaturation etc. affect the shape of the miceller aggregates as has been summarised below

Factors affecting headgroup area; surfactants with smaller headgroups areas (high $v/a_o l_c$) form larger vesicles, less-curved bulayers, or inverted micellar phase. In the case of anionic surfactants, increasing salt concentration or decreasing pH results in head group repulsions and thus the head group area.

Factors affecting chain packing; introducing chain branching and unsaturation reduces l_c this increases $v/a_o l_c$ thus leaading to larger vesicles and ultimately a change in aggregate structure such as inverted micelles.

Effect of temperature; the areas of more hydrophilic head groups usually increase with temperature due to the increased steric repulsion between them, thus decreasing $v/a_o l_c$. For cationics, increasing temperature causes them to shrink (Missel et al. 1980) – spherical micelles of non-ionics grow and become more cylindrical and zwitterioncs appear to behave somewhere in between, and their aggregation numbers hardly change with temperature (Malliaris et al. 1985) .

Effect of surfactant mixtures; as long as the different molecules are mixed ideally, for aggregates composed of mixture of surfactants , the properties of the aggregates may be treated in a first approximation - in terms of some mean packing parameter intermediate between the individual components (Carnie, Israelachvili & Pailthorpe 1979). The sizes of vesicles may be increased or decreased by adding an appropriate amount of another component whose packing parameter is larger or smaller than that of the host surfactant. More on this is discussed in (Carnie, Israelachvili & Pailthorpe 1979; Kaler et al. 1992; Murphy 1982; Yuet & Blankschtein 1996).

Increasing the concentration of surfactants in a micellar solution, results in the formation of a series of lyotropic liquid crystalline phases (mesophase). In summary, surfactants molecules initially aggregate to form micelles – as surfactant concentration is increased, the different surfactant aggregates (Table 2-2) pack in a variety of ways thus resulting in the formation of a variety of liquid crystalline structures (Eastoe 2002a). Upcoming section discusses the main classes of such structures

2.3 Lyotropic Liquid Crystalline Phases

The liquid crystal state (often referred to as mesophase) is an intermediate state of matter observed between the crystalline (solid) and isotropic (liquid) states. The molecules of such crystals are arranged at regular points in space and usually form under suitable conditions i.e. temperature, concentration and pressure. They can be based on colloidal solutions, aggregates, polymers and surfactants liquid crystals and are made up of two or more components (Brown, Doane & Neff 1971; Ekwall, Mandell & Fontell 1969a; Luzzati & Tardieu 1974) - usually, one of the components is an amphiphile containing a polar head group attached to one or more long hydrocarbon chain and the other is water.

There are six main well characterised liquid crystal structures – these are lamellar, gel, hexagonal, cubic, nematic and intermediate phases. Each of these structures can exist in both water or oil continuous as either a 'normal' or a 'reverse' configuration which is denoted by subscripts 1 and 2 respectively (Leigh et al. 1981; Seddon 1990) . In this text four of these classes of surfactant liquid crystals namely lamellar, hexagonal, cubic and gel phases are reviewed.

2.3.1 Lamellar Phase (L_α)

The lamellar phase is the most commonly processed liquid crystal mesophase in concentrated surfactant systems (Berni, Lawrence & Machin 2002; Ekwall 1975; Luzzati 1968a; Mitchell et al. 1983). In this phase, surfactant molecule are arranged into stacks of bilayers extending over large distances (a micron or more), which are separated by water layers (Mitchell et al. 1983).

Figure 2-8: Schematic representation of surfactant molecules (lamellar phase) arranged in bilayer (Eastoe 2002a; Mitchell et al. 1983).

Despite the fact that this phase does not usually flow under gravity, its viscosity is fairly low with the material being easily shaken into a container – it can also be identified from its characteristic optical textures (Tiddy, Hassan & Rowe 2001) - The alkyl chains are in a liquid like state thereby allowing each flat layer to slide past each other – this account for the low viscosity.

Lamellar phases[61] are known to exist in two configurations; either as planar lamellar phase ordered in sheets (Bleasdale & Tiddy 1991) and/or bilayers ordered in closed concentric shells often referred to as multilamellar vesicles (onions) (Hoffmann et al. 1994b; Jurgens 1989; Van de Pas 1991). Vesicles are a type of aggregate; they consist of bilayers self-closed into spherical aggregates enclosing a water core. Vesicles can form inside each other; such a particle is called an onion or a multilamellar vesicle (Persson 2003). They are usually very large bilayer structures (> 100 nm) and are more related to the lamellar phase than to micelles and can often be formed by agitating a lamellar phase (Evans & Wennerstrom 1994).

X-ray diffraction analysis present features which are characteristics of this phase. The first is the hydrocarbon chains in the bilayer which are more mobile (i.e. fluid like) and are identified via a diffuse wide-angle X-ray scattering (WAXS) corresponding to a Bragg reflection (d) of 4.5Å (Luzzati 1968a; Mills et al. 2008). The second is the repeat bilayer d-spacing where d is the sum of the water and alkyl chain layer dimensions (Bragg's Law) displaying sharp reflections in the ratio *d:d/2:d/3*,....etc. (Figueiredo Neto & Salinas 2005; Tiddy, Hassan & Rowe 2001). The water layer thickness varies over a much larger range i.e. > 8 to > 200 μÅ and is the same throughout the sample, except at very high water contents where low energy fluctuations can occur (Tiddy 1980)

2.3.2 Gel Phase (L_β)

The gel phase (L_β) closely resembles the lamellar phase in that it consists of surfactant bilayers (Figure 2-9), but differs as it possesses a very high viscosity thus the term 'gel' which originates from industry where systems were observed to have a gel-like rheology (Tiddy, Hassan & Rowe 2001).

Within the gel phase, the bilayers have rigid mostly all-trans alkyl chains as displayed by a sharp, wide-angle X-ray spacing of about 4.2 Å (Mills et al. 2008) and a large transition heat on melting, typically 25 – 27 % of the crystalline surfactant melting transition – indicative of a restricted chain motions, mostly limited to rotation about the long axis only – perpendicular to the plane of the lamellar. Both states (L_α & L_β) can be interchanged via heating and cooling respectively (Tiddy, Hassan & Rowe 2001).

[61] Section 3.4.2 discusses optical microscopy techniques employed in the analysis of the lamellar phase

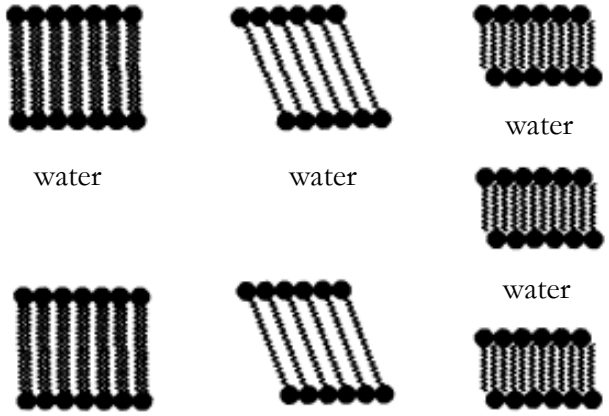

Figure 2-9: Schematic representations of gel phases: (left) normal; (middle) tilted; (right) inter-digitated (Tiddy, Hassan & Rowe 2001) .

There are three commonly reported gel phase according to (Tiddy, Hassan & Rowe 2001) as shown in Figure 2-9; the first is the normal gel phase in which the bilayer is normal to the liquid crystal axis and is most commonly found in dialkyl lipid systems (Chapman, Williams & Ladbrooke 1967) - here the alkyl layer thickness is found to be approximately twice the all trans alkyl chain length of the surfactant, the second structure is the tilted bilayer found in systems where the polar head group is larger than the width of the alkyl chain such as reported for monoglyceride systems (Larsson 1967) and the third is the inter-digitated form observed with long chain monoalkyl systems such as potassium stearate (Vincent & Skoulios 1966).

The stability of the gel phase is determined by the packing of the alkyl chains, and the formation of the various gel phase structures is dependent on the size of the head group

2.3.3 Hexagonal Phase (H_1, H_2)

The second most common mesophase type is the hexagonal phase (Ekwall 1975; Luzzatti 1968; Mitchell et al. 1983). This phase sits between the extremely viscous cubic phase[62] and the less viscous lamellar phase. There are two distinct classes of the hexagonal phase namely; the normal hexagonal H_1 phase and the inverse hexagonal H_2 phase (Figure 2-10).

[62] Discussed in the next section

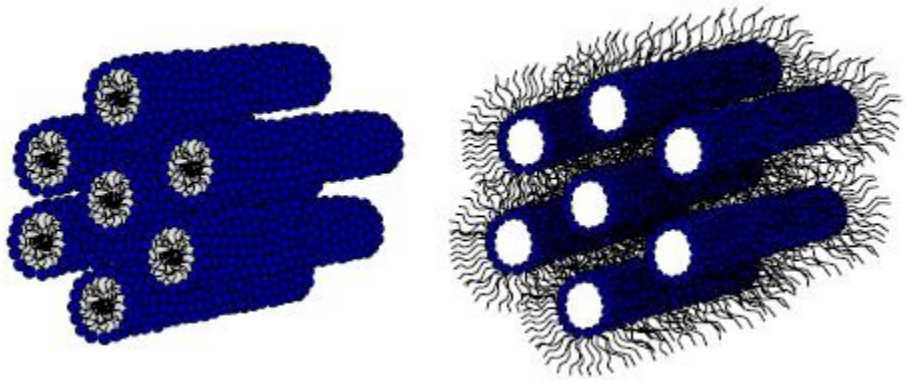

Figure 2-10: Schematic representation of (left) normal hexagonal phase (H_1)and (right) inversed hexagonal phases (H_2) (Eastoe 2002a; Tiddy, Hassan & Rowe 2001) .

The normal micelles have a diameter of 1.3 – 2.0 times the all-trans alkyl chain length (l_c), with typical inter-micellar separation being in the region of 8 – 50 Å – for the inverse micelles diameter is in the order of (1 – 1.5 l_c) in thickness and the inter-micellar separation is similar to that mentioned for the normal micelles (8 – 50 Å) (Tiddy, Hassan & Rowe 2001). X-ray diffraction studies of both phases show Bragg reflections in the ratio 1:1/√3: 1/√4: 1/√7: 1/√12 ….etc. with a diffuse reflection at 4.5 Å.

The H_1 phase is water–continuous while the H_2 is alkyl-chain-continuous (i.e. surfactant molecules dispersed in a non-polar medium). The phases are also identifiable as they exhibit 'fan like' and 'non geometric' textures when observed under polarised light – optical textures are similar for both types of structure (Tiddy, Hassan & Rowe 2001).

2.3.4 Cubic Phase I_1, I_2, V_1, V_2

The cubic phases are also referred (Tiddy, Hassan & Rowe 2001) to as viscous isotropic phases due to their very high viscosity (μ cubic phase < μ hexagonal phase < μ lamellar phase) – and as the name implies, the structure of these phases are formed based on several possible cubic lattices, namely the primitive, face-centred and body-centred. Two very distinct aggregate structures are known (Figure 2-11) where one is comprised of small micelles, normal or reversed, and the other is based on three-dimensional bicontinuous aggregates.

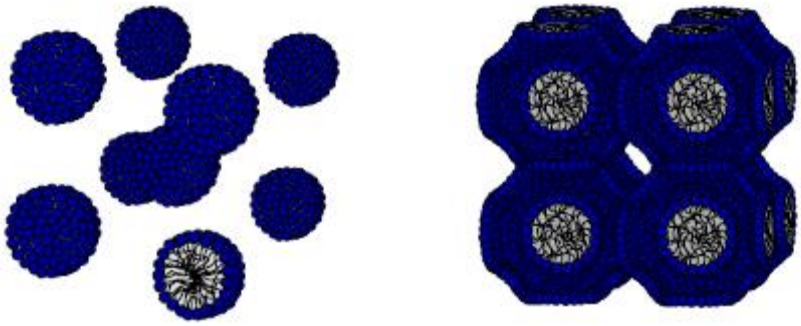

Figure 2-11: Schematic representation of (left) cubic and (right) bicontinuous cubic phases (Eastoe 2002a).

The "normal" and "reverse" structures that occur for both make up a total of four classes.

The two classes of the cubic phases (I and V) are distinguished from each other by their location in the phase diagram. The I phases occur at compositions between micellar solutions and hexagonal phases, while the V phases occur between hexagonal and lamellar phases. Both phases are isotropic and thus appear black under cross polarised light. More on these phases and the systems in which these phases occur can be found in (Ekwall 1975; Luzzati 1968b; Mitchell et al. 1983).

2.3.5 The Formation of Water Continuous - Surfactant Liquid Crystals

Thus far - surfactant molecules aggregate to form micelles as concentration is increased and these aggregates form liquid crystalline phases, likewise illustrations from literature has help established that the I_1, H_1 and L_α (liquid crystal phases) have structures based on ordered spherical, rod and disc (bilayer) micelles – hence the mesophases formed and their sequences can be described simply in terms of micelle shape at the CMC and the effective volume fraction of micelles which governs the behaviour of micelle packing at high concentrations (Mitchell et al. 1983).

The effective volume fraction accounts for the volume occupied by the tails, head groups and bound water as well as soft-core inter-micellar interactions[63] according to (Evans & Wennerstrom 1994; Israelachvili 1991) – such interations[64] also alters the concentration ranges of the mesophases but not its sequence (Tiddy, Hassan & Rowe 2001).

[63] I.e. inter/intra aggregate interaction

[64] Head group interactions and alkyl chain packing constraints) have been discussed previously (Section 2.2.2) specifically the section that considers 'Micellisation, Structure and Shape'.

Micelle shape as alluded earlier is determined/predicted by the surfactant molecular structure and packing constraints – at a critical volume fraction (concentration) as the concentration of the surfactant molecule is increased, aggregate (spheres, rods and discs (bilayer) concentration increases thereby compelling them to come together (closer). An ordered state (liquid crystal) is then formed at some higher concentrations if the surfactant is sufficiently soluble due aggregate interaction – Table 2-3 shows the general scheme.

Table 2-3: Table showing the effect of increasing surfactant concentration on the formation of liquid crystals from aggregates (Tiddy, Hassan & Rowe 2001).

INCREASING CONCENTRATION		
MICELLAR SOLUTION	→	**LIQUID CRYSTALS**
Spheres	→	CUBIC liquid crystals (I_1)
Rods (cylindrical)	→	HEXAGONAL liquid crystals (H_1)
Discs (bilayer)	→	LAMELLAR liquid crystals (L_α)

From this - spherical micelles form cubic liquid crystal phase, rods and discs form the hexagonal and the lamellar liquid crystal phase respectively.

When the available volume is occupied for a given shape, more surfactant can only dissolve with a reduction in aggregate curvature to a shape with a higher packing limit - hence a phase transition occurs to aggregates of smaller head group area. Therefore the sequence of mesophase with increasing concentration is shown in Table 2-4.

Table 2-4: Sequence of mesophase formation with increasing concentration; also showing the relationship between the area of the head group and micelle shape (Tiddy, Hassan & Rowe 2001).

→ **INCREASING CONCENTRATION**					
AREA OF HEAD GROUP	**MICELLE SHAPE**	**LIQUID CRYSTAL SHAPE**			
Small polar group	Disc (ruler shaped)	Lamellar			
Medium polar group	Rod	Hexagonal	Intermediate (V1)		Lamellar
Large polar group	Spherical	Cubic	Hexagonal	Intermediate (V1)	Lamellar
INCREASING SURFACTANT CONCENTRATION →					

The intermediate and V_1 cubic phases possess more complex shapes (unusual micelle curvature) and thus do not easily lend themselves to the easy treatment described above however because the micellar curvature is between that of H_1 and L_α phases, they are expected to occur at these concentrations according to the sequence and they do (Tiddy, Hassan & Rowe 2001).

The sequence in which reversed phases occur is more complicated than that of normal phases and is not yet understood in terms of surfactant structure – the main reason for this according to (Tiddy, Hassan & Rowe 2001) is probably because there is no limitation on the radius of the inverse micelles such as that imposed by the length of the paraffin chain on normal micelles - water could swell the micelles indefinitely (this does not happen because the size and shape of inverse micelles is controlled by limits on surfactant packing on a curved surface).

Figure 2-12 is often employed to describe the general pattern of mesophase behaviour as a function of surfactant (water) concentration.

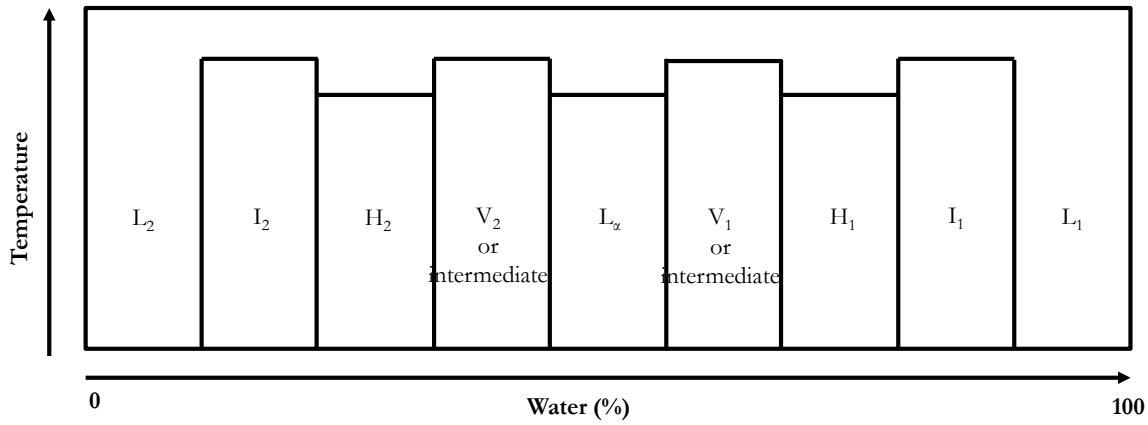

Figure 2-12: Schematic representation of the mesophase sequence with increasing water concentration as a function of temperature (Seddon & Templer 1995).

From Figure 2-12, - the figure does not take into consideration the role of the head-group size – more on the deficiencies of this schematic representation can be found in (Tiddy, Hassan & Rowe 2001).

2.3.6 Lamellar Phase under Shear

Lyotropic liquid crystals present complicated rheological response when subjected to shear flow (Franco, Munoz & Gallegos 1995; Matsumoto, Heiuchi & Horie 1989; McKeown, Mackley & Moggridge 2003; Oswald & Allain 1988; Singh et al. 2004) – when liquid crystalline sample is

sheared, its rheological response is dependent on the rearrangement of the structure during the flow (Barnes 1997; Laughlin 1994; Mortensen 2001; Viola & Baird 1986).

The effects of shear on such systems have been investigated using a combination of several analytical techniques (i.e. light scattering and/or rheometry) - Optical microscopy, small angle light scattering (SALS), small-angle neutron scattering (SANS), small-angle X-ray scattering (SAXS), Rheo-SALS[65], Rheo-optics, deuterium nuclear magnetic resonance (HNMR) spectroscopy etc. (Lauger et al. 1996; Laughlin 1994).

Shear flow is known to have a strong influence on the structure of complex fluid (Berghausen et al. 1998) i.e. aqueous surfactant solutions and block polymer melt - these materials though possessing different molecular structure and composition, they exhibit similar effects of shear orientation. For both materials, a shear-induced alignment of the lamellae characterised by comparing the orientation of the layer normal with the direction of flow, the direction of the velocity gradient and the vorticity direction (Safinya et al. 1993).

Work performed by (Berghausen et al. 1998) investigated the influence of shear on sodium dodecyl sulfate/decanol/D_2O using SANS, SALS, rheology and birefringence. They concluded that shear flow can lead to different states of lamellae orientation – i.e. from perpendicular lamellae (with layer normal along the vorticity direction) to parallel lamellae (with the layer normal along the velocity gradient direction) as the shear rates is increased. The reorientation process was also accompanied by a decrease in viscosity.

Experiments with higher decanol content were considered – three different states (Figure 2-13) were found in the sample when the SANS patterns were considered as opposed to two from the lower concentration experiments.

[65]Rheometry combined with SALS

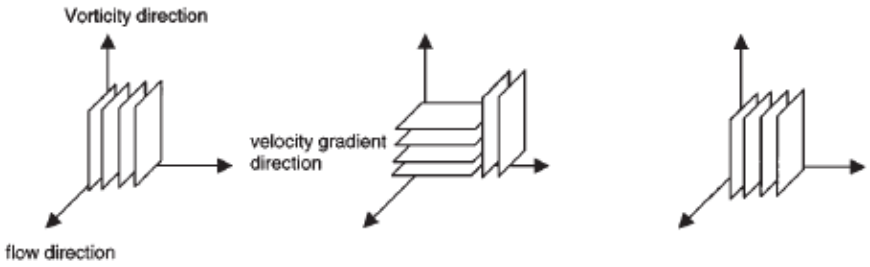

Figure 2-13: Schematic illustrating the orientation of lamellar layers with increasing shear rates (left – right) (Berghausen et al. 1998)

This behaviour is similar to the observations (Diat, Roux & Nallet 1993a) who found the parallel orientation at low and high shear rates as well – however at intermediate shear rates, they observed multilamellar vesicles ('MLV [onions]') - Figure 2-14. The layering effects described in Figure 2-13 has also been perceived by several authors (Berghausen et al. 2000; Berghausen et al. 1998; Diat, Roux & Nallet 1993a; Penfold et al. 1997a; Roux, Nallet & Diat 1993; Safinya et al. 1993; Zipfel et al. 1999).

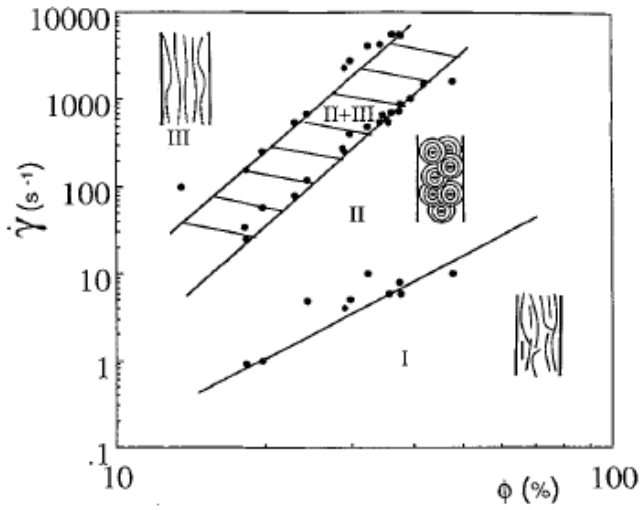

Figure 2-14: Orientation diagram defining three pure orientation states for the lamellar phase where is the shear rate (ẏ) and the volume fraction (ϕ) of membrane for quaternary mixture of water/Sodium Dodecyl Sulfate /pentanol/dodecane (Diat, Roux & Nallet 1993c)

Further work performed by (Zipfel et al. 1999) shows that - as decanol concentration was increased by replacing SDS, a transition from a defective lamellar phase, characterised by a ribbon like structure and then by a pore like structure to a classical lamellar phase was observed. At low decanol content, two reorientations were observed – from a parallel (at low shear rates)

to a perpendicular alignment of the lamellae and then to a parallel alignment again at the highest shear rates. At intermediate decanol content, the formation of multilamellar vesicles (MLV) was observed at certain shear rate region. However at high decanol content samples exhibited no shear induced vesicle formation.

In the work performed by (Diat, Roux & Nallet 1993c) on quaternary mixture of water/SDS/pentanol/dodecane - similar analytical techniques as above were used which helped identify the different stationary orientation states of lamellar phase as illustrated in Figure 2-14. They investigated the effects of shear on a defective lamellar phase thus detecting three different microstructure regime for this system. The straight line represents the limits between these different zones. Region I corresponds to a state for which the lamellar phase is oriented with the membranes parallel to the surface of the cylinders, with a lot of defects moving in the flow. Region II corresponds to a liquid of close contact spherulites. There are some spherical multilayer vesicles which can roll over each other in the flow. Region III corresponds to the same orientation as Region I but with no more defects in the flow direction and hence a better/uniform/ordered oriented lamellar phase. The crossed region called II + III correspond to a coexistence zone with two orientations (II and III).

According to (Mortensen 2001), MLVs are formed by applying a controlled (fixed) shear rate to lamellar phase dispersion – the lamellar organisation undergoes an evolution in which the lamellar phase rolls into a cylindrical morphology aligned along the flow direction at certain composition (Fritz, Wagner & Kaler 2003). Other factors such as strain and frequency are believed to also affect the formation of vesicles as recorded by (Fritz, Wagner & Kaler 2003), who considered the formation of MLVs from the lamellar phase of sodium bis(2-ethylhexyl) sulfosuccinate (AOT) in brine. They concluded that the formation of MLVs can be controlled by steady, oscillatory shearing and that increasing stress amplitude or decreasing frequency leads to more rapid onion formation. Vesicles are formed because at a critical shear rate (as shear rate increases), the lamellar buckles into a harmonic shape modulation thereby inducing buckling (undulation) instability and ultimately the formation of vesicles and that below the critical shear rates, shear stress induced within the structure is balanced by the elastic restoring forces of the lamella (Auernhammer, Brand & Harald 2000; Zilman & Granek 1999).

MLV formation is dependent on the nature of the system of study, its concentration, composition as well as shear rates (Le et al. 2001; Weigel et al. 1996).

Studies on the effect of concentrations (i.e. high surfactant concentration) have shown that the formation of MLVs (onions) is shifted to higher shear rates (Diat, Roux & Nallet 1993b, 1995; Roux, Nallet & Diat 1993).

The effect of shear on systems forming MLVs has also been extensively researched - MLVs changes size with the shear rate increasing in size, indicating that the vesicle size decreases with the shear rate (Diat, Roux & Nallet 1993a, 1993b; Sierro & Roux 1997). According to Panizza, Roux et al. 1996, a characteristic of this intermediate state (MLVs) is that the multilamellar vesicles formed under shear flow all have the same size and can be tuned down from a few micrometers to a tenth of this by increasing the shear rate of formation and that the size varies as the inverse of the square root of the shear rate (Diat 1992; Diat, Roux & Nallet 1993a).

Another feature of the MLVs is that after shear is stopped, the onion structure relaxes very slowly over a few days to several months depending particularly upon the lamellar composition (Panizza et al. 1996) also the lamellar phase d-spacing is not affected by MLVs formation (Diat, Roux & Nallet 1993a).

Introduced earlier is the lamellar phase, a periodic arrangement of stacked amphiphilic bilayers separated by water layers (Figure 2-8) – however the lamellae makeup up are not as simple as described (i.e. smooth and infinite) as it is generally assumed (Oswald & Allain 1988). Various systems exhibit various structural defects - example of a system with defects is the lamellar phase of hexaethylene glycol dodecyl ether in aqueous solution as observed by (Oswald & Allain 1988) possessing stable thermodynamically structural defects with a highly curved bilayer and dislocation loops. Other studies conducted by the aforementioned author has also shown the different forms of dislocation loops defects i.e. screw, edge dislocations, pores, contractions etc. that could exist in lamellar system. (Allain 1986). The presence of such defects (Oswald & Allain 1988; Penfold et al. 1997b; Riise et al. 1995) as well as other factors such as elastic properties (Berghausen et al. 1998; Colin et al. 2001; Goulian & Milner 1995; Maring & Wiesner 1997; Roux, Nallet & Diat 1993) can influence the shear induced transformations in lamellar phases due to their influence on flow (Dhez, Nallet & Diat 2001).

The study on the influence of shear on lamellar system of sodium dodecyl sulphate (SDS)/decanol/water by (Zipfel et al. 1999) reported that the decanol molar content affected nature of defects observed in the system however all systems displayed similar to those observed by (Diat, Roux & Nallet 1993a).

2.4 A Review of Mixed Emulsifier/Water Systems (Multiple-Phase Oil in Water O/W Emulsion)

Colloids are generally described as systems consisting of one substance often referred to as the dispersed phase of characteristic sizes, finely dispersed in another (the continuous phase) which can be a solid, a liquid, or a gas – combinations that give rise to systems of varying practical applications (Eastoe 2002c). Colloids can be classified based on the nature of the interaction between the dispersed phase and dispersion medium.

A popular example of such system is lyophobic (solvent-hating) colloids (Eastoe 2002c; Seager & Slabaugh 2011) formulated as a mixture of immiscible components i.e. solid particles in a solvent often water (Faraday 1857). Examples of such colloids include milk (liquid fat dispersed as fine droplets in an aqueous phase), smoke (solid particles dispersed in air), paints (small solid particles dispersed in liquid), jelly (large protein molecules dispersed in water) etc. (Eastoe 2002c).

A second example is the lyophilic (solvent-loving) colloids (Eastoe 2002c; Seager & Slabaugh 2011) which are solutions that form spontaneously and are thermodynamically stable. Such systems consist of solute molecules that are polymer of much larger size than that of the solvent molecules. Examples of such systems include gelatine, starch, proteins and certain polymers in organic solvents.

Emulsion stabilised by lyotropic liquid crystals have been reported by (Friberg, Mandell & Larson 1969) – these emulsions contain a third phase or multi-molecular layers of lyotropic liquid crystals and are often found in the cosmetic product industry – they add specific properties such as viscosity, consistency, storage stability or application convenience (Eccleston 1990; Engels & Ryabinski 1988). Cosmetic oil-in-water emulsions are complex multiple phase systems – in there preparation, combinations of fatty amphiphiles (glyceryl monoesters of fatty alcohols) and ionic and non-ionic surfactants are widely used (Eccleston 1990) – these mixed emulsifier combinations interact often at high temperatures in the aqueous continuous phases to form lamellar or liquid crystalline structures which converts to gel phases when the emulsion cools, so that the property of this phase dominate the emulsion.

A short review of mixed emulsifier/water system i.e. ternary system is given here as it is central to this project - particular attention is paid to method of production, as manufacturing of such systems is core to this Thesis.

Ternary mixtures of cationic surfactant/fatty alcohol/water form liquid crystalline microemulsions or multilamellar vesicles depending on composition (Eccleston & Beattie 1989; Ekwall 1975; Fontell et al. 1991; Hoffmann 1984; Hoffmann et al. 1994a; Imae et al. 1994; Montalvo, Valiente & Rodenas 1995; Neto & Salinas 2005; Winsor 1968) and temperature (Kazanci & Yildiz 2008; Yamaguchi & Noda 1987, 1989) - phase transition by heating is observed as well (Imae & Trend 1991).

They are often prepared by adding molten fatty alcohol to a surfactant aqueous solution at the same temperature while mixing and stirring (Barry & Saunders 1970; Rowe & McMahon 1987). Such systems often form highly viscoelastic gel networks when cooled from elevated temperatures (typically a lamellar phase) to temperatures below their chain melting point (Barry 1975; Barry & Shotton 1967). The structures (mesophase) formed by these systems are also sensitive to physical external influences (Nesrullajev, Kazanci & Yildiz 2003), such as mechanical deformation as discussed earlier – mechanical deformation is capable of changing their morphology (Masalci & Kazanci 2009)

As was reviewed by (Muller-Goymann 2004), a number of techniques are used to determine the structural characteristics formed by such systems[66]; polarized light microscopy (Zhang et al. 2008), transmission electron microscopy (Mondain-Monval 2005), small-angle X-ray scattering (SAXS) (Zhuang et al. 2008), differential scanning calorimetry (DSC) (Feher et al. 2005) and rheological measurements (Berni, Lawrence & Machin 2002; Nemeth et al. 1998; Youssry et al. 2008).

Structural changes occurring in a cetrimide/cetostearyl alcohol/water system prepared at low temperature (4 °C) was conducted using freeze-etch transmission electron microscopy, differential interference contrast microscopy, conductivity measurements and viscosity measurements using a rheometer (Patel et al. 1985b). The ternary mixture was prepared by dispersing cetostearyl alcohol at 80 °C in an aqueous solution of cetrimide and propyl hydroxybenzoate at similar temperatures and stirred gently with a paddle stirrer for 1 hour before being allowed to cool to approximately 60 °C. The dispersion was then homogenised using a Silverson multipurpose high speed mixer until the setting point of the gel was reached. The gel was then allowed to cool to room temperature and samples stored at both 25 °C and 4 °C. The system was found to change from an opaque smooth gel of high viscosity, low conductivity and

[66] Mixed Emulsifier/Water Systems

low free water, to a pearlescent milky lotion of low viscosity, high conductivity and high free water – over 48 hours at room temperature an opaque granular gel of similar consistency, but slightly higher conductivity. Examination using the various analytical techniques showed the system changed from one consisting of a liquid crystalline network localised around cetostearyl alcohol particles, to a system consisting of large waxy plates coexisting with some residual liquid crystalline network.

The change in viscoelastic behaviour due to phase transition of the assembly of a cetyltrimethylammonium chloride/cetyl alcohol/water system was studied using an electron microscope and oscillatory rheological shear measurements (Yamagata & Senna 1999a). The mixture was added to deionised water and heated to 75 °C for 2 hours in a water bath. After being mixed and stirred by a rod with four paddles for 20 minutes, the mixture was cooled to 35 °C at 2 K/min while stirring. The product was defoamed in a bell jar by an aspirator and aged at 25 °C up to 60 days it was found out that the molecular assembly prepared at 75 °C showed onion like multilamellar vesicles (0.2 – 5 μm in diameter) immediately after preparation but transformed on aging into a rosary network of vesicles and finally fused into lamellae as it aged. Dynamic modulus (G') of the assembly monotonically increased with frequency, while the loss modulus (G") showed 2 peaks – Cole – Cole analysis conducted on the system suggested the underlying microstructure contained a network of coagulated vesicles and lamellae.

The mechanical properties, thermal behaviour, physical states, and colloidal structure of metastable gel formed from the mixture of different ratios of sodium dodecyl sulphate polyacrylamide (SDS)/cety/stearyl fatty alcohol (FA)/water was conducted using methods such as rheology (stress sweeps), DSC, SAXS, and proton-NMR (Awad et al. 2011). The fatty alcohol mixture of cetyl/stearyl was added to preheated water at 75 – 80 °C and the mixture was thoroughly mixed for a few minutes on a hot plate until the fatty alcohol was fully melted – required amount of SDS was then added to the hydrated FA melt and the mixture was agitated slowly until all the SDS had dissolved and was evenly distributed in the mixture. The sample temperature was then cooled gradually to room temperature while agitation was continued – sample increased in viscosity on reaching room temperature and solidifies into a homogeneous gel network. This work elucidated the physical nature of the gel network associated with the system used.

Semitranslucent gel formed by cetyltrimethylammonium chloride/cetyl alcohol/water system spontaneously formed at room temperature via the addition of cetyltrimethylammonium chloride

to a saturated solution including an excess of solid globules of cetyl alcohol without mixing – it was found out that this mixture contains anisotropic lamellae (Yamagata & Senna 1999b) – this was the compared by morphology and thermal properties to a ternary mixture system (Yamagata & Senna 1998) of similar composition prepared by mixing and stirring at 75 °C, it was found out that this comprised of dispersed particles of multilamellar vesicles. It could be said that this work considered the effect of processing temperature i.e. 25 and 75 °C alongside route to manufacture. Thermal data show that primary endothermic peaks observed at about 69 and 67 °C can be attributed to the melting points of vesicles and lamellae respectively due to their interlamellar water content.

The structural properties of the mesophases of tetradecyltrimethyl ammonium bromide/octanol/water system was studied using polarizing microscopy – the mixture was prepared by measuring the required amount of the raw materials – this was periodically mixed by a vortex shaker and kept in thermostat at a temperature of 308[67] ± 0.1 K for homogenisation (Masalci & Kazanci 2009; Yavuz, Masalci & Kazanci). The system formed different anisotropic mesophases namely; isotropic phase (L_1), and nematic calamitic (N_C), nematic discotic (N_D), hexagonal E and lamellar D all of which were determined using polarising microscopy. Application of mechanical deformation to the mesophases changed the structural properties of the mesophases (Yavuz, Masalci & Kazanci)

A pharmaceutical gel made-up of a mixture of cetrimide/cetostearyl alcohol/water was analysed using SAXS by (Barry & Rowe 1989) – the mixture had been prepared by heating both the alcohol and aqueous phases to 80 °C, mixing them and stirring gently with a paddle stirrer for 1 hour before homogenisation and cooling. Gel examination confirmed the network formed was in direct agreement with similar structures published in literature (Patel et al. 1985d) i.e. a series of cetostearyl alcohol bilayers separated by water indicating a water layer thickness of the order of 34 nm. Water layer thickness was also estimated to be of the order of ± 1 nm.

The structure of gels and emulsions containing the mixed emulsifier system of cetrimide and cetostearyl alcohol was studied by (Patel et al. 1985d) using differential interference contrast microscopy and freeze-etch microscopy. Cetostearyl alcohol at 80 °C was dispersed in aqueous cetrimide solution at the same temperature and stirred gently with a paddle stirrer for a period of 1 hour before being allowed to cool to approximately 60 °C. The mixture was then homogenized

[67] 35 °C

using a Silverson multipurpose high speed mixer until the setting point of the get was reached or for a period of not more than 15 minutes. The gel was then allowed to cool to room temperature. Other experiments were performed by dissolving the cetostearyl alcohol in liquid paraffin at 80 °C before it was added to the aqueous cetrimide solution at the same temperature – all systems were allowed to stand for at least 2 weeks before being tested. It was found out that increasing the cetostearyl alcohol concentration results in a gradual change from a vesicular structure to one consisting of a liquid crystalline phase largely localized around particles of cetostearyl alcohol.

The phase behaviour of isothermal ternary system of hexadecyltrimethylammonium bromide/alcohol/water system was investigated by (Fontell et al. 1991) - when the alcohol chain length is varied. This methods of investigation used included; optical inspection, polarizing microscopy, SAX, WAX and, centrifugation. The authors found out the phase behaviour of the system was in line with other anionic surfactant system of potassium decanoate/octanol/water system (Ekwall, Mandell & Fontell 1969b; Neeson & Tiddy 1982) albeit with very little differences.

Changes to the rheological behaviour during aging was conducted by (Yamagata & Senna 1998) on a ternary mixture of cetyltrimethylammonium chloride/cetyl alcohol/water system using cyclic shearing tests – the cetyltrimethylammonium chloride and cetyl alcohol were added to deionized water and heated to 75 °C for 2 hours in a water bath. After mixing and stirring by a rod with four paddles for 20 minutes, the mixture was cooled to 35 °C at 2 K/min while stirring. The product was closed into a bell jar and defoamed by an aspirator and aged at 25 °C up to 60 days before analysis was performed. Cyclic shearing test determined that the internal structure of the mixture is formed in two steps – the first steps occurs immediately after the preparation, and is related to elastic properties such as apparent value and yield value. The second step in contrast seems to be associated with the gradual penetration of the surfactant, resulting in the swelling of crystalline alcohol

Many more studies on emulsifier/water systems can be found in (Adam et al. 1984; Alam, Ushiyama & Aramaki 2009; Berni, Lawrence & Machin 2002; Bonacucina et al. 2012; De Vringer, Jooster & Junginger 1984; Eccleston 1985; Eccleston & Beattie 1988, 1989; Eccleston et al. 2000; Eccleston 1976; Feher et al. 2005; Fukushima, Yamaguchi & Harusawa 1977; Garti 2000; Goldszal et al. 1996; Gonzalez-Gaitano et al. 1999; Harms, Mackeben & Muller-Goymann 2005; Hoffmann et al. 1994a; Huang et al. 1997; Larsson & Krog 1973; Mackeben, Muller &

Muller-Goymann 2001; Masalci & Kazanci 2009; Montalvo, Valiente & Rodenas 1995; Nakarapanich et al. 2001; Nemeth et al. 1998; Partial et al. 2001; Patel et al. 1985a, 1985c, 1985d; Reis, Akpinar & Neto 2013; Rydhag & Gabran 1982; Savic et al. 2011; Sharma & Warr 2012; Wang et al. 2006; Yildiz & Kazanci 2008; Zhang et al. 2008; Zhuang et al. 2008).

From the review of literature, it is evident that the various route taken in manufacturing these systems, all affect the characteristics that the product exhibit – the process steps (process variables) such as nature of mixing (low/high shear), heating (process temperature), ageing, nature of cooling, process time, method in which process ingredients are brought together, the order of addition of process ingredients etc. all have an impact on the manufactured product.

2.5 Hair Conditioner: Formulation, Process History and Microstructure

The microstructure of a conditioner or any structured fluid (personal products, foods and detergent) is determined by its formulation and process history conversely its microstructure and rheology. Application of such liquids is highly dependent on these thus prompting the need to understand the links between process history – rheology and product performance. In such structured liquids, microstructure is the nature of the assembly of its surfactant aggregates. Typical microstructure (micelle aggregate structures/liquid crystals) found in structured fluids could be one or a combination of the structures - formed as a result of different process histories, temperature and concentration.

Generally two classes of Hair Conditioners are available namely; rinse-off or leave-on with a wide range of viscosities due to composition. These conditioners are presented to have a wide range of claimed benefits by various manufacturers and are often dispersions of cationic surfactants and fatty alcohols alongside other minor ingredients (such as polymers, silicones, preservatives etc.) in water. They contain varying combination of a wide range of ingredients (conditioning agents) in varying concentrations, for which patents are often filed. Most products usually contain similar sets of conditioning agents however the distinguishing characteristics are usually the concentrations, number of different agents and the particular members of conditioning class employed (Kuo-Yann 2006).

2.5.1 Formulation/composition

Hair conditioner's basic formulation often include surfactant - classed as [1] conditioning agents and [2] minor ingredients that often range from preservatives, polymers and silicones combined at different compositions and/or temperature dispersed in solvent (Kuo-Yann 2006).

Important factors that determine product formulation are consumer satisfaction (i.e. provide required benefits), fast acting product during use, physio-chemical stable products (i.e. under storage), products exhibiting low toxicity and irritation and of suitable rheology amongst many other factors.

2.5.2 Conditioning Agents

Cationic surfactants such as quaternary ammonium compounds (QUAT) are the primary components of commercially available Hair Conditioner formulation (Gerstein 1979; Hunting 1987) as they are readily available, cheap and effective. Few examples are steralkonium chloride, cetrimonium chloride, dicetyldimonium chloride, behenyltrimethylammonium chloride (BTAC), cetyltrimethylammonium chloride (CTAC) and stearamidopropyldimethylamine (TAS). QUATS possess a positive charge which binds to negatives sites on the surface of hair resulting in hydrophobic coating of hair fibres making it softer and easier to comb (Foerster & Schwuger 1990) as well as reducing static charge build-up on hair surface (Jachowicz, Wis-Surel & Garcia 1985) which often results in flyaway.

Lipophilic conditioners such as long chain fatty alcohols (FA) (i.e. cetyl alcohol, stearyl alcohol and behenyl alcohol) are often used alongside QUATS to boost their conditioning properties(Gerstein 1979; Polovsky 1991). The addition of fatty alcohol to cationic surfactants under the right conditions results in the formation of gel networks (Eccleston & Florence 1985; Eccleston 1976; Saunders, Barry & Howard 1972) that can increase emulsion viscosity/stability.

The combination of anionic surfactants with cationic polymers (i.e. Polyquaternium-10, -7, -11, -16 and Polyquaternium- 6) also improves wet combing and reduces static charge (Barel, Paye & Howard 2009; Kuo-Yann 2006).

Silicones such as dimethicone, dimethiconecopolyol, dimethiconol, amodimethiconedimethicone and cyclomethicone are used in Hair Conditioners as conditioning agents (Luoma & Kara 1998) as they possess a range of unique properties i.e. low surface tension, water insolubility and low intermolecular forces that allow then form hydrophobic film easily on hair surface aiding conditioning (Barel, Paye & Howard 2009). Most silicones are insoluble in water and require emulsification before addition to Hair Conditioners. More information on conditioning agents can be found in (Barel, Paye & Howard 2009).

2.5.3 Minor Ingredients

In Hair Conditioner formulation, there exist a number of minor ingredients such as dyes, emulsifying agents, preservatives, rheological modifiers, opacifying agents, antioxidants, fragrances, humectants and vitamins which play functional, esthetic and marketing roles(Hoshowski 1997). A single preservative or a combination are often used to ensure the

microbiological integrity of a product; rheological modifiers (i.e. thickening agents) may be required to provide increased viscosity to pre-existing liquid crystal formed as a result of QUATS, FA and cationic polymers and humectants are often added to products for the sole purpose of attracting ambient moisture.

Blends of fatty alcohol/QUATS are emulsions that would overtime destabilise; emulsifiers are often added to formulation if necessary to improve stability. Opacifying agents are added to surfactant solutions to produce pearlescent appearance. The degree of opacity is strongly dependent on the size distribution, shape and reflectance of the precipitated crystals (Kuo-Yann 2006). Fragrances are added to mask undesirable odour which are likely to put consumers off the product. More information on minor ingredients can be found in (Hunting 1987; Leung 1980; Lochhead 1988; McCutcheon 1991; Wenninger & McEwen 1995).

2.6 Controlled Deformation Dynamic Mixer (CDDM)

The Controlled Deformation Dynamic Mixer (CDDM) is a high shear rotor and stator type mixer - a novel technology currently installed at the University of Liverpool for research and development purposes within the fluid mixing industry (Brown, Irving & Kowalski 2010a; Maelstrom 2010). The innovative mixer utilises a range of mixing mechanisms namely; shear and extension with (Brown, Irving & Kowalski 2010c) in promoting a high level of dispersive/distributive mixing.

The confronting surfaces[68] has cavities machined on as illustrated in Figure 2-15 for which the relative axial position of these two surfaces enables mixer to function as a Cavity Transfer Mixer (CTM) which provide efficient low shear distributive mixing or as Controlled Deformation Dynamic Mixer (CDDM) which has zones of intense shear (Brown, Irving & Kowalski 2010b) as illustrated in schematic displayed in Figure 2-15.

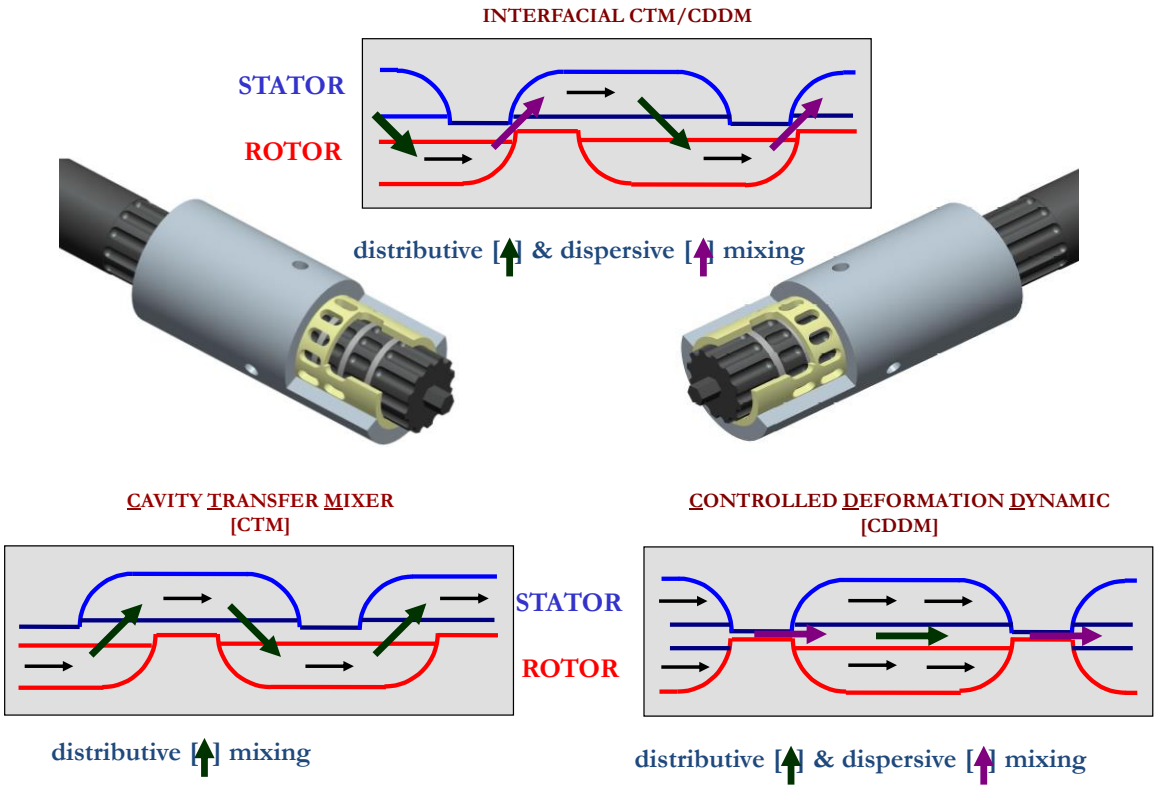

Figure 2-15: Image of a cut out section of the CDDM technology (CDDM-1) and schematic representing dominant mixing actions when mixer is operated in different modes; full CDDM (left), full CTM (right) and Interfacial CTM/CDDM (top).

[68] Inner surface of a stator and the outer surface of a rotor

In either mode[69], process fluid is subjected to low/high deformation rates (extensional and/or shear) in different ratios at strategic locations within the mixer as it progresses[70] through the mixer effecting dispersive and distributive mixing actions. Deformation rates can be closely controlled, and are as a result of both flow-rates and mixing speeds accessible from the installed components i.e. pumps and motors installed at Ultra Mixing and Processing Facility (UMPF) set up[71].

The background and/or information in regards to the technology is detailed in several patents – a few of which are EP194812A2; WO96/20270; EP 0799303; GB 2118058 WO2010/089320A1; WO2010/089322A1; WO2010/091983A1.

EP 194 812 A2 introduces the use of a Cavity Transfer Mixer (CTM) a highly distributive mixer for performing chemical reactions in which the reactants are subjected to shear by passing the streams through a shear zone formed within the bulk of the material (Irving & Edwards 1986). This is achieved by relative movement of surfaces between which the material passes aiding/driving the reaction towards completion. Likewise WO96/20270 describes a novel apparatus (CTM) for use in the production of liquid composition. The device comprises of two confronting surfaces with series of cavities - surfaces move relative to each other. Process fluid flows along a pathway successively passing through cavities in each surface - generally, the cross sectional area for flow varies by a factor of less than 3 through the apparatuses described.

WO 96/20270 also describes the CDDM, with similar characteristics to afore-described CTMs however it is distinguished from the CTM in that material is also subjected to extensional deformation effecting high dispersive mixing operation. Here the cross sectional area for process fluid flow increases and decreases by a factor of at least 5 through the apparatus (Akay et al. 1995).

WO2010/089320A1(Brown, Irving & Kowalski 2010c);WO2010/089322A (Brown, Irving & Kowalski 2010d); WO2010/091983A1 (Brown, Irving & Kowalski 2010a) all disclose variants of a distributive and dispersive mixing device of the CDDM/CTM type comprising two confronting surfaces having cavities.

[69] CTM or CDDM
[70] Under the action of a pump - in this text, two types of pumps are used [1] progressive cavity pump and [2] positive displacement pump
[71] More on UMPF in Section 3.3.1

This project considers how such a new and enabling technology could be moved from the laboratory/pilot plant scale into full industrial scale. This work considers design optimisation and also provides insights on the topic of scale-up.

2.7 Processing Structured Liquids

Introduced earlier[72] is the topic of multiphase fluid processing and the concept of structured liquid – in that regard structured liquids are materials possessing multiple phases i.e. a dispersed phase in a liquid medium whose rheological properties are dictated by the interaction of the constituents (Franck 2004a). The phases are usually a combination of Newtonian and/or non-Newtonian fluids. The processing of such fluids would require an understanding of process fluid behaviour when subjected to a wide range of process conditions (i.e. flow rate, pressure, shear rates, temperature etc.). In essence a good prediction of process fluid behaviour gives a user a degree of control thus ensuring the output of a specific process is well understood.

A good grasp of such knowledge would also extend and aid good/accurate equipment selection, specification and design (i.e. pumps, vessel design, mixers etc.) as well as process design and scale up - as discussed later on in this text non-Newtonian fluids are shear sensitive (Figure 2-17) in terms of rheology and since the topic of rheology is central to this text and industry, it is without a doubt that a good grasp of the factors influencing it is needed to be understood.

In designing process equipment i.e. mechanically stirred vessels used in mixing, appropriate size, type of wall baffles and impeller type must be selected to create an effective flow pattern – impellers have be classified based on flow patterns (axial or radial flow), nature of shear (i.e. high or low shear), applications etc. (Calabrese & Leng 2004). It could also be a combination of the above (flow pattern and shear rates) alongside other factors such as residence time, pressure drop etc. hence understanding how these can be estimated within a process equipment is vital for product performance control.

This section reviews a few of the approaches found in Literature that help characterise rheological processes and process equipment for process fluids (Newtonian and non-Newtonian) as well as an introduction to the scale up of a specific mixing technology (rotor-stator) as it is central to this text.

2.7.1 Shear Dependent Viscosity of Process Fluids

Fluids can be classified in two different ways; either according to their response to externally applied pressure, or their response to the action of a shear stress. The first classification gives rise to the terms ‘compressible’ and ‘incompressible’ fluids in that the volume of an element of fluid

[72] Chapter 1

is dependent on its pressure – while the other classification considers flow characteristics of the fluid in the absence of turbulent eddies (Chhabra & Richardson 2008) – giving rise to the terms 'Newtonian' and non-Newtonian fluid. This text utilises the latter classification.

Consider a fluid at rest between two parallel plates (Figure 2-16) of area A [m^2] separated by a distance h [m]. A force F [N] at a speed v [m/s] is applied to the upper plate which is initially at rest. The particles of the material will flow (undergo continuous deformation) between the plates as long as the force is applied.

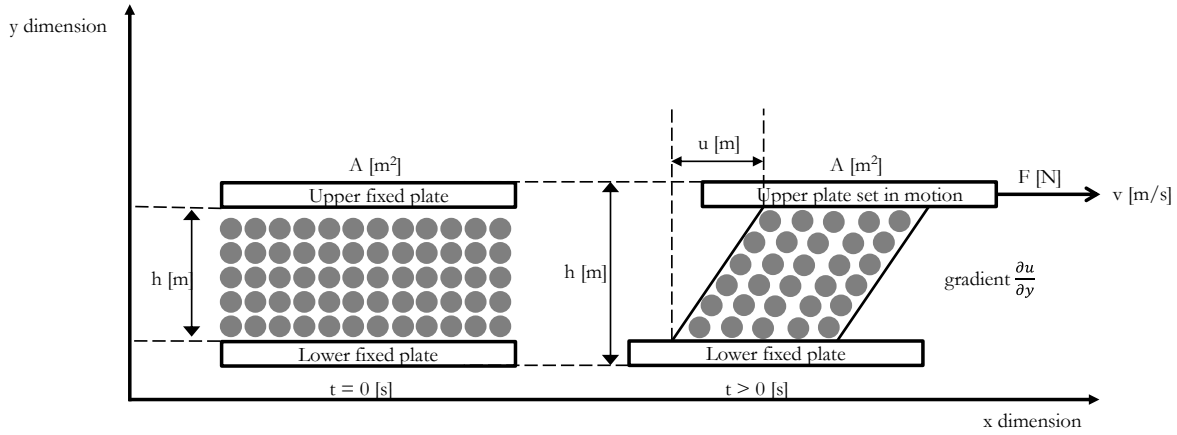

Figure 2-16: Fluid deformation under the action of a shear stress - simple shear flow Adapted from (Barnes, Hutton & Walters 1993).

The force applied is directly proportional to the area of the plate - the shear stress is

$$\tau = \frac{F}{A} \qquad [2.11]$$

where

τ	shear stress	Pa (kg/ m.s^2)
F	force	N (kg.m/s^2)
A	area	m^2

Within the fluid, the linear velocity profile u = Uy/h is established (no slip conditions) under these boundary conditions (Navier-Stokes). Fluid constrained to the lower plate has zero velocity while those constrained to the upper plate moves at plate velocity (U) - the velocity gradient is referred to as the shear rate ($\dot{\gamma} = du/dy$) for this flow (Bourgoyne Jr. et al. 1986; Perry & Green 1999).

According to Newton's Law of Viscosity (Newtonian fluid), the ratio of shear stress (τ) to shear rate ($\dot{\gamma}$) is the viscosity (η) also synonymous to absolute/shear viscosity as shown below.

$$\eta = \frac{\tau}{\dot{\gamma}} \qquad [2.12]$$

where

τ	shear stress	Pa (kg/ m.s^2)
η	viscosity	Pa.s (kg/m.s)
$\dot{\gamma}$	shear rate	s^{-1}

On occasion, we read of kinematic viscosity (v) – this type of viscosity is the ratio of viscosity (η) to density (ρ)

For laminar flow of Newtonian fluid (i.e. water, oil, gases), the Newton's Law of Viscosity gives a constant value (for η) for which viscosity is independent of stress. Such fluids seldom occur in the processing industry dealing with food, home-care and personal-care products – they are usually one part of a multiphase non-Newtonian fluid. These multiphase non-Newtonian fluids exhibit complex behaviour under the application of shear.

Several authors (Barnes, Hutton & Walters 1993; Bourgoyne Jr. et al. 1986; Cross 1965; Perry & Green 1999; Sisko 1958) have published equations to predict these complex behaviours of non-Newtonian fluids however most of such empirical models are limiting - in essence they are accurate up to an extent. According to (Barnes, Hutton & Walters 1993), equations that predict the shape of a geneal flow curve, requires at least four parameters – one of such equations is the Cross model (Cross 1965) given by

$$\frac{\eta - \eta_\infty}{\eta_0 - \eta_\infty} = \frac{1}{(1 + (K\dot{\gamma})^n)} \qquad [2.13]$$

or,

$$\frac{\eta - \eta_\infty}{\eta_0 - \eta_\infty} = (K\dot{\gamma})^n \quad [2.14]$$

where

η_0	viscosity at very low shear rate	Pa.s (kg/s.m)
η_∞	viscosity at very high shear rate	Pa.s (kg/s.m)
K	consistency index for the fluid (constant parameter)	s
n	power law index	-
$\dot{\gamma}$	Shear rate	s^{-1}

An alternative to the Cross model was derived by Carreau (Carreau 1972)

$$\frac{\eta - \eta_\infty}{\eta_0 - \eta_\infty} = \frac{1}{(1 + (K_1\dot{\gamma})^2)^{n/2}} \quad [2.15]$$

Where K and n, have a similar significance to the ones mentioned for the Cross model. The Cross model is also able to predict a general flow curve albeit limiting; it is not accurate for all values of shear rate.

Making certain approximations such as "$\eta << \eta_0$ and $\eta >> \eta_\infty$" to the cross model, reduces it to another very popular and widely used model which is the Power law

$$\eta = \frac{\eta_0}{(K\dot{\gamma})^n} \quad [2.16]$$

Above equation can be re-written as

$$\eta = K\dot{\gamma}^{n-1} \quad [2.17]$$

Otherwise known as the power law model; where

where

η	viscosity	Pa.s (kg/s.m)
K	consistency index for the fluid (constant parameter)	$Pa.s^n$
n	power law index (flow behaviour)	-
$\dot{\gamma}$	Shear rate	s^{-1}

The power law model is used to represent non-Newtonian fluid flow behaviour for a range of flow curves - when a log/log plot of viscosity as a function of shear rate is plotted – deviations from Newtonian behaviour can be seen (Figure 2-17).

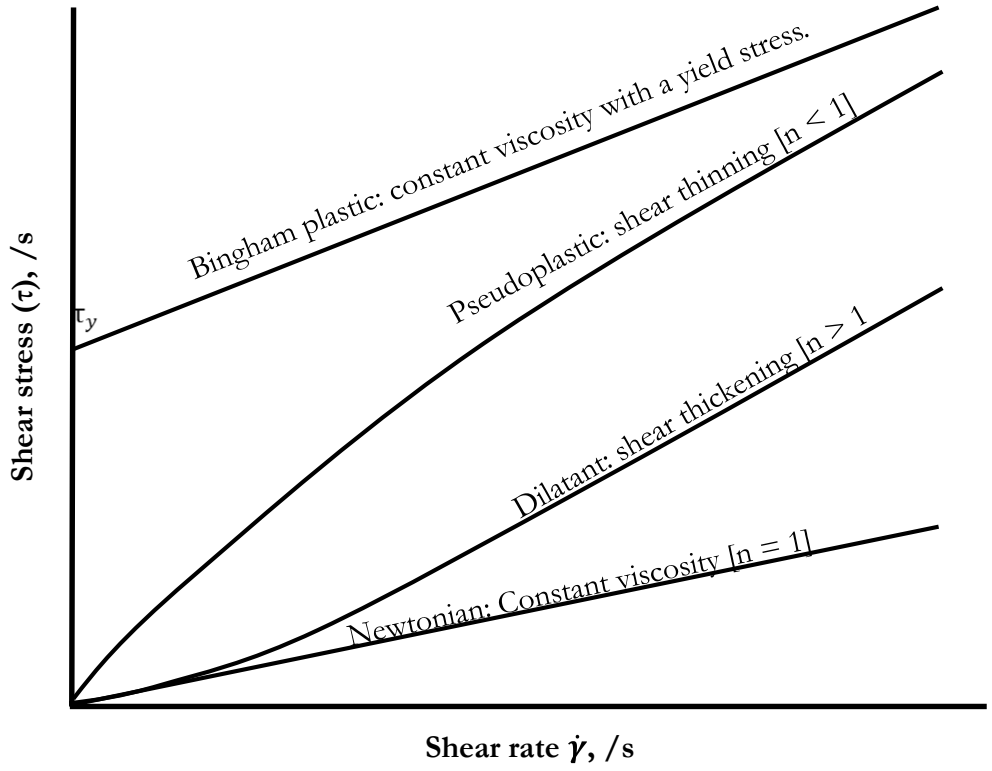

Figure 2-17: Shear diagram illustrating the fluid behaviour of non-Newtonian fluids adapted from (Perry & Green 1999)

From the plot of log η/log $\dot{\gamma}$ from Equation 2.17, values of K and n can then be obtained from intercept and gradient respectively as shear thinning and shear thickening fluids are represented as straight lines.

This method is also limiting in obtaining viscosity at very high and very low shear rates as some non-Newtonian fluids exhibit Newtonian characteristics. In this regions the Sisko model (Sisko 1958) can be employed.

For some shear thinning fluids - at very high shear rates (i.e. > 10^5 /s), viscosity will begin to approach a constant value and the value of 'n' towards '1' the Sisko model can be used to solve such flow curve problems by inserting the assumption ($\eta << \eta_0$) into the Power law equation

$$\eta = \eta_\infty + \frac{\eta_0}{(K\dot{\gamma})^n} \qquad [2.18]$$

which can be rewritten as

$$\eta = \eta_\infty + K\dot{\gamma}^{\,n-1} \qquad [2.19]$$

This is the Sisko model – if 'n' = 0, we obtain

$$\eta = \eta_{\infty} + \frac{K}{\dot{\gamma}} \qquad [2.20]$$

which forms the basis of the Bingham model equation with a simple redefinition of parameters (Barnes, Hutton & Walters 1993). The Bingham equation can be used to describe the shear stress/shear rate behaviour of many shear thinning fluids at low shear rates.

2.7.2 High Shear Rotor Stator Mixers: An Introduction to Characterisation

High shear rotor-stator (HSRS) devices are commonly used in several process industries; (e.g. food, cosmetics, fine chemicals and pharmaceutical) to manufacture structured emulsified products and packaged goods. These products are by their nature a mixture of immiscible liquids, stabilised by a surface active agent or surfactant to obtain a stable homogeneous blend via an emulsification process. Engineers in such industries are often tasked with getting more out of their processes i.e. in terms of increased production rates, better handle on product quality especially in a continuous processes thereby increasing the need for high shear blending (Myers et al. 1999).

High-shear mixers have proven effective in process performance optimisation by providing a focused delivery of energy to accelerate and combine a number of operations such as mixing, dispersion, dissolution, emulsification and de-agglomeration (Atiemo-Obeng & Calabrese 2004).

> "Despite the growing application for such high-shear rotor stator devices; the current understanding of them has almost no fundamental basis. There are few theories by which to predict, or systematic experimental protocols by which to assess, the performance of these mixers. In fact there are few archival publications on high shear rotor-stator processing (Atiemo-Obeng & Calabrese 2004)".

Currently process development at increasing scales in HSRS devices are based on trial and error leading to high development costs, start-up problems, lost time to market, considerable wastage due to high amounts of trials as well as the inability to maintain desired product attributes at ascending scales from laboratory – pilot plant – plant scale (Hall et al. 2011b).

The use of adequate correlations (i.e. to effect scale up) for such devices is necessary to avoid these problems thereby enabling industries to meet new processing challenges and performance

goals. Such correlations would require adequate understanding of the relationship that exists between process variables (rotor speed & flow rate, pressure drop etc.); design (size and geometry) relative to desired product attributes (Hall et al. 2011b). A key message, process scientist often recommend when a scale-up and/or scale-down operation is being performed is the need to maintain geometric similarity as it simplifies design calculations.

For liquid-liquid dispersions, a key parameter often used as a descriptor for the effect of process on the physical properties in an emulsification process is the surface area weighted mean droplet diameter ($d_{3,2}$), also referred to as the Sauter mean diameter (Hall et al. 2011b). Sauter mean diameter (SMD) presents an estimate of the mean size of a given particle distribution; defined as the diameter of the sphere possessing similar volume/surface area ratio as the particle of interest (Filippa, Trento & Alvarez 2012). Mathematically it is defined after Equation 2.21 (Pacek, Man & Nienow 1998).

$$\mathrm{SMD} = d_{3,2} = \frac{\int_{d_{min}}^{d_{max}} d^3 p(d) dd}{\int_{d_{min}}^{d_{max}} d^2 p(d) dd} \qquad [2.21]$$

Where d is the particle diameter, d_{max} and d_{min} indicates the maximum and minimum diameters of the particle distribution, p(d) indicates the probability density function of d size.

The first step in assessing a HSRS mixers performance for the purpose of scale up is to determine the energy required to accomplish a degree of emulsification; batch rotor-stator mixers are characterise by a single power number (P_O) and power draw is calculated in the same way as for stirred tanks Equation 2.22

$$P = P_O \rho_C N^3 D^5 \qquad [2.22]$$

where

P_O	power number	-
ρ_C	density of the continuous phase	kg m^3
N	rotor speed	s^{-1}
D	rotor diameter	m

P_O is dependent on type of mixer and flow regime. (Padron 2001) and (Utomo, Baker & Pacek 2009) obtained a value for this dimensionless constant for turbulent flow in batch Ross and Silverson rotor–stator mixers. While (Hall et al. 2011a; Hall et al. 2011b) and (Kowalski, Cooke

& Hall 2011) have done likewise for inline Silverson rotor-stator devices. Power draw of an inline rotor stator mixer in the turbulent regime was obtained via;

$$P = P_O \rho N^3 D^5 + k_1 Q_M N^2 D^2 + P_L \quad [2.23]$$

where

k_1	proportionality constant in power equation	-
Q_M	mass flow rate	kg s^1
P_L	losses power term	W

The first term on RHS of Equation 2.23 corresponds to power required to rotate the rotor to overcome the fluid resistance which is comparable to power consumption in a stirred vessel, the second term is a result of the flow accounting for the pumping action of the mixer accelerating and pumping fluid away, while the third term, accounts for energy losses and can be neglected. P_O is essentially constant at Reynolds numbers greater than 10^4 in a baffled stirred vessel - a few studies have highlighted some uncertainty as to whether the regime was in the laminar or turbulent region (Doucet, Ascanio & Tanguy 2005)

A mixture of just pure oil and water does not form an emulsion spontaneously when in contact; introduction of energy in the form of mixing is required to disperse oil droplets within the water continuous phase - emulsification is a combination of two processes occurring simultaneously; break-up of large droplets into several smaller drops and the coalescing of several smaller droplets to form larger drops (Razzaque et al. 2003). At very high surfactant concentration, droplet coalescence is negligible and the evolution of droplet size distribution in the emulsification process is solely dependent on droplet breakup (Vankova et al. 2007)

This study considers the mean and maximum droplet sizes obtained as a result of droplet breakup in turbulent flow in an emulsification process to aid equipment characterisation

Kolmogorov (Kolmogorov 1949) and Hinze (Hinze 1955) studies of emulsification process in turbulent flow indicates the existence of two different regimes namely; "turbulent inertia" and "turbulent viscous" regimes. The transition between these regimes of emulsification, is dependent on the size of the smallest eddies in the turbulent flow (η) - determined mainly by the rate of energy dissipation (ε) and the viscosity of the aqueous phase (μ_c), density of the continuous phase (ϱ_C) and the maximum drop size of the emulsion formed. The size of the smallest eddies (η) is obtained via Kolmogorov length scale equation defined as;

$$\eta = \varepsilon^{-1/4}\mu_c{}^{3/4}\rho_C{}^{-3/4} \quad [2.24]$$

Equation 2.24 illustrates that for a typical emulsions with $\varrho_C \approx 1000$ kg/m^3, the size of the smallest eddies is dependent on the continuous phase viscosity as well as stirring intensity.

Using the model described above, maximum stable equilibrium drop size (d_{max}), can be related to the maximum local energy dissipation rate (ε_{max}), interfacial tension (σ) and density of the continuous phase (ϱ_c)(Calabrese & Leng 2004)

$$d_{max} = C_1 \left(\frac{\sigma}{\rho_c}\right)^{3/5} \varepsilon_{max}^{-2/5} \quad [2.25]$$

Constant C_1 is of the order of one (Davies 1985) for turbulent flow conditions using geometrically similar systems. Equation 2.25 can be rearranged to a dimensionless form by replacing d_{max} with $d_{3,2}$ and simplified by using Weber number (We); ratio of disruptive forces to cohesive forces.

$$\frac{d_{3,2}}{D} = C_2 We^{-3/5} \quad [2.26]$$

The dimensionless group "Weber number" (Hall et al. 2011a); is obtained via;

$$We = \frac{\rho_c N^2 D^3}{\sigma} \quad [2.27]$$

Another commonly used correlation used to characterise emulsification in stirred vessels is tip speed of the rotor or impeller for which b = 1.2 (Kowalski, Cooke & Hall 2011).

$$d_{3,2} = C_3(\pi ND)^{-b} \quad [2.28]$$

The concept of $d_{3,2}$ as a function of energy density can be adopted to evaluate droplet disruption for continuous emulsification process after (Karbstein & Schubert 1995) who proposed;

$$d_{3,2} = C_4 E_V{}^b = \left(\frac{P}{Q}\right)^{-b} \quad [2.29]$$

Energy density describes the effect of process parameters applied to a certain emulsion volume; it accounts for the mean residence time acting on the drop assuming no re-coalescence.

This work utilises the concept equilibrium droplet sizes (SMD) – which in essence is the point at which an emulsion has achieved its target properties (droplet or particle-size distribution) at a

specified process condition. At the aforementioned point, droplet or particle size distribution will no longer change significantly regardless how long an emulsification operation is continued for.

2.8 References

- Adam, C.D., Durrant, J.A., Lowry, M.R. & Tiddy, G.J.T. (1984) 'Gel and Liquid Crystal Phase Structures of The Trioxyethylene Glycol Monohexadecyl ether/Water System', *Journal of the Chemical Society, Faraday Transactions*, vol. 80, pp. 789 - 801.
- Akay, G.R., Irving , G.N., Kowalski, A.J. & Machin, D. (1995) *Process For The Production Of Liquid Composition*, Great Britain.
- Akhter, M.S. & Al-Alawi, S.M. (2000) 'Influence of Alcohols on The Critical Micelle Concentration of Non-Aqueous Micellar Solutions', *Colloids and Surfaces A: Physicochemical and Engineering Aspects*, vol. 164, no. 2 - 3, pp. 247- 255.
- Alam, M.M., Ushiyama, K. & Aramaki, K. (2009) 'Phase Behaviour, Formation, and Rheology of Cubic Phase and Related Gel Emulsion In Tween 80/Water/Oil Systems', *Journal of Oleo Science*, vol. 58, no. 7, pp. 361 - 367.
- Alexander, S., Smith, G.N., James, C., Rogers, S.E., Guittard, F., Sagisaka, M. & Eastoe, J. (2014) 'Low-Surface Energy Surfactants with Branched Hydrocarbon Architectures', *Langmuir*.
- Allain, M. (1986) 'Possible Defect-Mediated Phase Trans tion in a Lyotropic Liquid Crystal. Electron Microscopy Observations.', *Europhysics Letters*, vol. 2, no. 8, pp. 597 - 602.
- Atiemo-Obeng, V.A. & Calabrese, R.V. (2004) Rotor-Stator Mixing Devices, in E.L. Paul, V.A. Atiemo-Obeng & S.M. Kresta (eds), *Handbook of Industrial Mixing*, John Wiley & Sons, Inc., New York, pp. 479 - 505.
- Auernhammer, G.K., Brand, H.R. & Harald, P. (2000) 'The Undulation Instability In Layered Systems Under Shear Flow - A Simple Model', *Rheologica Acta*, vol. 39, pp. 215 - 222.
- Awad, T.S., Johnson, E.S., Bureiko, A. & Olsson, U. (2011) 'Colloidal Structure and Physical Properties of Gel Networks Containing Anionic Surfactant and Fatty Alcohol Mixture', *Journal of Dispersion Science and Technology*, vol. 32, pp. 807 - 815.
- Barel, A.O., Paye, M. & Howard, I.M. (2009) *Handbook of Cosmetic Science and Technology*, Informa Healthcare, Newyork.
- Barnes, H.A. (1997) 'Thixotropy - A Review', *Journal of Non-Newtonian Fluid Mechanics*, vol. 70, pp. 1 - 33.

- Barnes, H.A., Hutton, J.F. & Walters, K. (1993) *An Introduction To Rheology*, Elsevier Science Publishers B.V., The Netherlands.
- Barry, B.W. (1975) 'Viscoelastic Properties of Concentrated Emulsions', *Advances in Colloid and Interface Science*, vol. 5, pp. 37 - 75.
- Barry, B.W. & Saunders, G.M. (1970) 'The Self-Bodying Action Of The Mixed Emulsifier Cetrimide/ Cetostearyl Alcohol', *Journal Of Colloid And Interface Science*, vol. 34, no. 2, pp. 300 - 315.
- Barry, B.W. & Shotton, E. (1967), *Journal of Pharmacy and Pharmacology*, vol. 19(Suppl.), no. 110 - 120.
- Barry, M.D. & Rowe, R.C. (1989) 'The Characterisation By Small Angle X-Ray Scattering of A Pharmaceutical Gel With A Lamellar Structure', *International Journal of Pharmaceutics*, vol. 53, pp. 139 - 143.
- Bergenstahl, B. (2001) Surface Chemistry in Food and Feed, in K. Holmberg, D.O. Shah & M.J. Schwuger (eds), *Handbook of Applied Surface and Colloid Chemistry Volumes 1 - 2: Part I. Surface Chemistry in Important Technologies*, John Wiley & Sons, Ltd, England, pp. 40 - 52.
- Berghausen, J., Zipfel, J., Diat, O., Narayanan, T. & Richtering, W. (2000) 'Lamellar Phases Under Shear : Variation of The Layer Orientation Across The Couette Gap', *Physical Chemistry Chemical Physics*, vol. 2, pp. 2623 - 3626.
- Berghausen, J., Zipfel, J., Lindner, P. & Richtering, W. (1998) 'Shear-induced Orientations In A Lyotropic Defective Lamellar Phase', *Europhysics Letters*, vol. 43, no. 6, pp. 683 - 689.
- Bergstrom, L. (2001) Colloidal Processing of Ceramics, in K. Holmberg, D.O. Shah & M.J. Schwuger (eds), *Handbook of Applied Surface and Colloid Chemistry Volumes 1 - 2: Part I. Surface Chemistry in Important Technologies*, John Wiley & Sons, Ltd, England, pp. 201 - 218.
- Berni, M.G., Lawrence, C.J. & Machin, D. (2002) 'A Review of the Rheology of the Lamellar Phase in Surfactant Systems', *Advances in Colloid and Interface Science*, vol. 98, no. 2, pp. 217-243.
- Bleasdale, T.A. & Tiddy, G.J.T. (1991) Surfactant Liquid Crystals, in D.M. Bloor & E. Wyn-Jones (eds), *The Structure, Dynamics and Equilibrium Properties of Colloidal Systems*, Springer, Netherlands, pp. 397-414.

- Bonacucina, G., Cespi, M., Mencarelli, G. & Palmieri, G.F. (2012) 'Characterization of Ternary Phase Diagrams By Means of Thermal and Rheological Analyses', *Drug Development and Industrial Pharmacy*, pp. 1 - 8.
- Bourgoyne Jr., A.T., Millheim, K.K., Chenevert, M.E. & Young Jr., F.S. (1986) *Applied Drilling Engineering*, Society of Petroleum Engineers, Texas.
- Brown, C.J., Irving, G.N. & Kowalski, A.J. (2010a) *Apparatus of the CDDM-and/or CTM-TYPE, and its use*, Great Britain.
- Brown, C.J., Irving, G.N. & Kowalski, A.J. (2010b) 'Apparatus of the CDDM-and/or CTM-TYPE, and its use', vol. G.B. Pat. Wo 2010/091983 A1.
- Brown, C.J., Irving, G.N. & Kowalski, A.J. (2010c) *Distributive And Dispersive Mixing Apparatus Of The CDDM Type, And Its Use*, Great Britain.
- Brown, C.J., Irving, G.N. & Kowalski, A.J. (2010d) *Mixing Apparatus of The CDDM- Or CTM-Type, And Its Use*, Great Britain.
- Brown, G.H., Doane, J.W. & Neff, V.D. (1971) *A Review of the Structure and Physical Properties of Liquid Crystals*, Butterworths, London.
- Calabrese, R.A. & Leng, D.E. (2004) Immiscible Liquid-Liquid Dispersions, in V.A. Atiemo-Obeng, E.L. Paul & S.M. Kresta (eds), *Handbook of Industrial Mixing*, John Wiley & Sons, Inc, USA, pp. 639 - 753.
- Carey, M.C. & Small, D.M. (1972) 'Micelle Formation by Bile Salts: Physical - Chemical and Thermodynamic Considerations', *Archives of Internal Medicine*, vol. 130, no. 4, pp. 506 - 527.
- Carnie, S., Israelachvili, J.N. & Pailthorpe, B.A. (1979) 'Lipid Packing and Transbilayer Asymmetries of Mixed Lipid Vesicles', *Biochimica et Biophysica Acta*, vol. 554, no. 2, pp. 340 - 357.
- Carreau, P.J. (1972) 'Rheological Equations From Molecular Network Theories', *Transaction Of The Society of Rheology*, vol. 16, pp. 99 - 127.
- Chapman, D., Williams, R.M. & Ladbrooke, B.D. (1967) 'Physical Studies of Phospholipds. VI. Thermotropic and Lyotropic Mesomorphism of Some 1,2-diacylphosphatidycholines (Lecithins).', *Chemistry and Physics of Lipids*, vol. 5, no. 1, pp. 445 - 475.
- Chhabra, R.P. & Richardson, J.F. (2008) *Non-Newtonian Flow and Applied Rheology: Engineering Applications*, Butterworth-Heinemann, Hungary.

- Claesson, P.M. & Rutland, M.W. (2001) Measuring Interactions Between Surfaces, in K. Holmberg, D.O. Shah & M.J. Schwuger (eds), *Handbook of Applied Surface and Colloid Chemistry Volumes 1 - 2: Part I. Surface Chemistry in Important Technologies*, John Wiley & Sons, Ltd, England.
- Clint, J.H. (1992) *Surfactant Aggregation*, Blackie, Glasgow.
- Clunie, J.S., Goodman, J.F. & Symons, P.C. (1969), *Transactions of the Faraday Society*, no. 65, p. 287.
- Colin, A., Leng, J., Arneodo, A. & Roux, D. (2001), *Physical Review Letters*, vol. 86, p. 1374.
- Costa, M., Kronberg, B. & Silveston, R. (1994) 'General Thermodynamic Analysis of The Dissolution of Non-polar Molecules into Water. Origin of Hydrophobicity', *Journal of The Chemical Society, Faraday Transactions*, vol. 90, pp. 1513 - 1522.
- Cross, M. (1965) 'Rheology of non-Newtonian fluids: A New Flow Equation For Pseudo-Plastic Systems', *Journal Of Colloid Science*, vol. 20, pp. 417 - 437.
- Davies, J.T. (1985) 'Drop Sizes of Emulsions Related to Turbulent Energy Dissipation Rates', *Chemical Engineering Science*, vol. 40, no. 5, pp. 839 - 842.
- De Vringer, T., Jooster, J.G.H. & Junginger, H.J. (1984) 'Characterisation of The Gel Structure In A Nonionic Ointment By Small Angle X-Ray Diffraction.', *Colloid and Polymer Science*, vol. 262, pp. 56 - 60.
- Dhez, O., Nallet, F. & Diat, O. (2001) 'Influence of Screw Dislocations on The Orientation of a Sheared Lamellar Phase', *Europhysics Letters*, vol. 55, no. 6, pp. 821 - 826.
- Diat, O. (1992) *Effets du Cisaillement Sur Les Phases Lyotropes: Phase Lamellaire et Phase Eponge*, Universite de Bordeaux I,, Bordeaux France.
- Diat, O., Roux, D. & Nallet, F. (1993a) 'Effect Of Shear On A Lyotropic Lamellar Phase', *Journal de Physique. II*, vol. 3, no. 9, pp. 1427 - 1452.
- Diat, O., Roux, D. & Nallet, F. (1993b) 'Effects of Shear on a Lyotropic Lamellar Phase', *Journal de Physique II*, vol. 3, no. 9, pp. 1427 - 1452.
- Diat, O., Roux, D. & Nallet, F. (1993c) 'Lamellar Phase Under Shear - SANS Measurements', *Journal de Physique. IV*, vol. 3, no. C8, pp. 193 - 204.
- Diat, O., Roux, D. & Nallet, F. (1995) '"Layering" Effect In a Sheared Lyotropic Lamellar Phase', *Physical Review E*, vol. 51, no. 4, pp. 3296 - 3299.

- Doucet, I., Ascanio, G. & Tanguy, P.A. (2005) 'Hydrodynamics Characterisation of Rotor-stator Mixer with Viscous Fluids', *Chemical Engineering Research and Design* vol. 85, no. 1186 - 1195.
- Eastoe, J. (2002a) Aggregation and Adsorption at Interfaces, in T. Cosgrove (ed.), *Colloid Science: Principles, Methods and Applications*, Blackwell Publishing, England.
- Eastoe, J. (2002b) Surfactant Chemistry and General Phase Behaviour, in T. Cosgrove (ed.), *Colloid Science: Principles, Methods and Applications*, Blackwell Publishing, England.
- Eccleston, G.M. (1985) 'Phase Transition In Ternary Systems and Oil-In-Water Emulsions Containing Cetrimide and Fatty Alcohols', *International Journal of Pharmaceutics*, vol. 27, pp. 311 - 323.
- Eccleston, G.M. (1990) 'Multiple-Phase Oil-In-Water Emulsions', *Journal of the Society of Cosmetic Chemists*, vol. 41, pp. 1 - 22.
- Eccleston, G.M. & Beattie, L. (1988) 'Microstructural Changes During The Storage of Systems Containing Cetostearyl alcohol/Polyoxyethylene Alkyl Ether Surfactants', *Drug Development and Industrial Pharmacy*, vol. 14, no. 15 - 17, pp. 2499 - 2518.
- Eccleston, G.M. & Beattie, L. (1989) 'The Influence of Emulsifier Composition In The Microstructure of Nonionic Semisolids', *Journal of Pharmacy and Pharmacology*, vol. 12, pp. 1 - 77.
- Eccleston, G.M., Behan-Martin, M.K., Jones, G.R. & Towns-Andrews, E. (2000) 'Synchronton X-Ray Investigations Into The Lamellar Gel Phase Formed In Pharmaceutical Creams Prepared With Cetrimide and Fatty Alcohols', *International Journal of Pharmaceutics*, vol. 203, pp. 127 - 139.
- Eccleston, G.M. & Florence, A.T. (1985) 'Application of Emulsion Theory to Complex and Real Systems', *International Jounal of Cosmetic Chemistry*, vol. 7, pp. 195-212.
- Eccleston, G.M.J. (1976) 'The Structure and Rheology of Pharmaceutical and Cosmetic Creams', *Journal of Colloid Interface Science*, vol. 57, pp. 66-74.
- Edlund, H., Lindholm, A., Carlsson, I., Lindström, B., Hedenström, A. & Khan, E. (1994) 'Phase Equilibria in Dodecyl Pyridinium Bromide - Water Surfactant Systems', *Progress in Colloid and Polymer Science*, no. 97, p. 134.
- Ekwall, P. (1975) *Advances In Liquid Crystal*, vol. 1, Academic Press, New York.
- Ekwall, P., Mandell, L. & Fontell, K. (1969a), *Molecular Crystals and Liquid Crystals*, vol. 8, p. 157.

- Ekwall, P., Mandell, L. & Fontell, K. (1969b), *Journal Of Colloid And Interface Science*, vol. 31, pp. 508 - 530.
- Engels, T. & Ryabinski, W. (1988) 'Liquid Crystalline Surfactant Phases In Chemical Applications', *Journal of Materials Chemistry*, vol. 8, pp. 1313 - 1320.
- Evans, D.F. & Wennerstrom, H. (1994) *The Colloidal Domain: Where Physics, Chemistry, Biology and Technology Meet*, Wiley-VCH, New York.
- Faraday, M. (1857), *Philosophical Transaction of The Royal Society*, vol. 147, p. 145.
- Feher, A., Csanyo, E., Csoka, I., Kovacs, A. & Eros, I. (2005) 'Thermoanalytical Investigation of Lyotropic Liquid Crystals And Microemulsions For Pharmaceutical Use', *Journal of Thermal Analysis and Caloriemetry*, vol. 82, pp. 507 - 512.
- Figueiredo Neto, A.M. & Salinas, S.R.A. (2005) *The Physics of Lyotropic Liquid Crystals: Phase Transitions and Structural Properties*, Oxford University Press.
- Filippa, L., Trento, A. & Alvarez, A.M. (2012) 'Sauter Mean Diameter Determination For The Fine Fraction Of Suspended Sediments Using A LISST-25X Diffractometer', *Measurement*, vol. 45, no. 3, pp. 364 - 368.
- Flockhart, B.D. (1961) 'The Effect of Temperature on The Critical Micelle Concentration of Some Parafin-chain salts', *Journal of Colloid Science*, vol. 16, pp. 484 - 492.
- Foerster, T. & Schwuger, M.J. (1990) 'Correlation between Adsorption and The Effects od Surfactants and Polymers on Hair', *Progress in Colloid and Polymer Science*, vol. 83, pp. 104-109.
- Fontell, K., Khan, A., Lindström, B., Maciejewska, S. & Puang-Ngem, S. (1991) 'Phase Equilibria And Structures In Ternary Systems Of A Cationic Surfactant (C16 Tabr Or (C16TA)2SO4), Alcohol, And Water', *Colloid and Polymer Science*, vol. 269, no. 7, pp. 727 - 742.
- Franck, A.J. (2004) *Understanding Rheology of Structured Fluids*, TA Instruments,
- Franco, J.M., Munoz, J. & Gallegos, C. (1995) 'Transient and Steady Flow of a Lamellar Liquid-Crystalline Surfactant/Water System', *Langmuir*, vol. 11, no. 2, pp. 669 - 673.
- Friberg, S., Mandell, L. & Larson, M. (1969) 'Mesomorphous Phases, A Factor of Importance For The Properties of Emulsions', *Journal Of Colloid And Interface Science*, vol. 29, pp. 155 - 156.
- Fritz, G., Wagner, N.J. & Kaler, E.W. (2003) 'Formation of Multilamellar Vesicles by Oscillatory Shear', *Langmuir*, vol. 19, pp. 8709 - 8714.

- Fukushima, S., Yamaguchi, M. & Harusawa, F.J. (1977) 'Effect of Cetostearyl Alcohol on Stabilization of Oil-In-Water Emulsion', *Journal Of Colloid And Interface Science*, vol. 59, pp. 159 - 165.
- Garti, N. (2000) *Thermal Behaviour of Dispersed Systems*, Marcel Dekker Inc, New York.
- Gerstein, T. (1979) 'An Introduction to Quaternary Ammonium Compounds', *Cosmetic & Toiletries Science Applied*, vol. 94, pp. 32-41.
- Glew, D.N. (1962) 'Aqueous Solubility and The Gas-Hydrates. The Methane-Water System', *The Journal of Physical Chemistry*, vol. 66, no. 4, pp. 605 - 609.
- Goldszal, A., Jamieson, A.M., Mann, J.A., Polak, J. & Rosenblatt, C. (1996) 'Rheology, Optical Microscopy, and Electron Microscopy of Cationic Surfactant Gels', *Journal Of Colloid And Interface Science*, vol. 180, pp. 261 - 268.
- Gonzalez-Gaitano, G., Valiente, M., Tardajos, G., Montalvo, G. & Rodenas, E. (1999) 'Ultrasonic Study of The L Phase of The CTAB/Benzyl Alcohol/Water System', *Journal Of Colloid And Interface Science*, vol. 211, pp. 104 - 109.
- Goulian, M. & Milner, S. (1995), *Physical Review Letters*, vol. 74, p. 1775.
- Gunnarsson, G., Joensson, B. & Wennerstroem, H. (1980) 'Surfactant Association Into Micelles. An Electrostatic Approach', *1980*, vol. 83, no. 23, pp. 3114 - 3121.
- Hall, S., Cooke, M., Kowalski, A.J. & El-Hamouz, A. (2011a) 'Droplet Break-Up By In-Line Silverson Rotor – Stator Mixer', *Chemical Engineering Science*, vol. 66, pp. 2068 - 2079.
- Hall, S., Cooke, M., Pacek, A.W., Kowalski, A.J. & Rothman, D. (2011b) 'Scaling Up of Silverson Rotor-Stator Mixers', *The Canadian Journal of Chemical Engineering*, no. 9999, pp. 1 - 11.
- Harms, M., Mackeben, S. & Muller-Goymann, C.C. (2005) 'Thermotropic Transition Structures In The Ternary System Lecithin/Isopropyl Myristate/Water ', *Colloids and Surfaces A: Physicochemical and Engineering Aspects*, vol. 259, pp. 81 - 87.
- Hartley, G.S. (1936) *Aqueous Solutins of Parafin Chain Salts*, Hermann & Cie, Paris.
- Hassan, P.A., Verma, G. & Ganguly, R. (2012) Soft Materials - Properties and Application, in S. Banerjee & A.K. Tyagi (eds), *Functional Materials - Preparation, Processing and Applications* Elsevier, London.
- Hato, M., Tahara, M. & Suda, Y. (1979), *Journal Of Colloid And Interface Science*, vol. 72, p. 458.

- Hayase, K. & Hayano, S. (1978) 'Effect of Alcohols on The Critical Micelle Concentration Decrease In The Aqueous Sodium Dodecy Sulfate Solution', *Journal Of Colloid And Interface Science*, vol. 63, no. 3, pp. 446 - 451.
- Hinze, J.O. (1955) 'Fundamentals Of The Hydrodynamic Mechanism Of Splitting Dispersion Process', *AIChE Journal*, vol. 1, pp. 289 - 295.
- Hoffmann, H. (1984) 'From Micellar Solutions To Liquid-Crystalline Phasess', *Berichte der Bunsengesellschaft für physikalische Chemie*, vol. 88, pp. 1078 - 1093.
- Hoffmann, H., Munkert, U., Thunig, C. & Valiente, M. (1994a) 'The Lyotropic Mesophases in Dilute Surfactant Mixtures of Tetradecyldimethylaminoxide, Tetradecyltrimethylammonium Bromide, and Hexanol: The Influence of Ionic Charge on the Mesophases', *Journal Of Colloid And Interface Science*, vol. 163, no. 1, pp. 217 - 228.
- Hoffmann, H., Thunig, C., Schmiedel, P. & Munkert, U. (1994b) 'Surfactant Systems with Charged Multilamellar Vesicles and Their Rheological Properties', *Langmuir*, no. 10, pp. 3972-3981.
- Holmberg, K. (2001) Surface Chemistry In Paints, in K. Holmberg, D.O. Shah & M.J. Schwuger (eds), *Handbook of Applied Surface and Colloid Chemistry Volumes 1 - 2: Part I. Surface Chemistry in Important Technologies*, John Wiley & Sons, Ltd, England, pp. 105 - 122.
- Hoshowski, M.A. (1997) Conditioning of Hair, in, *Johnson DH, ed. Hair and Hair Care Cosmetic Science Technology Series*, Marcel Dekker, New York, pp. 65-104.
- Huang, J.B., Zhu, B.Y., Zhao, G.X. & Zhang, Z.Y. (1997) 'Vesicle Formation of a 1:1 Catanionic Surfactant Mixture In Ethanol Solution', *Langmuir*, vol. 13, pp. 5759 - 5761.
- Huibers, P.D.T. (1999) 'Quantum-Chemical Calculations of The Charge Distribution In Ionic Surfactants', *Langmuir*, vol. 15, pp. 7546 - 7550.
- Hunter, R.J. (2000) *Foundations of Colloid Science*, Oxford University Press, Great Britain.
- Hunting, A.L.L. (1987) *Encyclopaedia of Conditioning Rinse Ingredients* Micelle Press, Cranford, NJ.
- Imae, T., Iwamoto, T., Platz, G. & Thunig, C. (1994) 'Electron Microscopic And Light Scattering Observation On A System With Two Iridescent Phases', *Colloid and Polymer Science*, vol. 272, no. 5, pp. 604 - 611.
- Imae, T. & Trend, B. (1991) 'VEM Observation of Molecular Assemblies In Iridescent Surfactant Solutions', *Journal Of Colloid And Interface Science*, vol. 145, no. 1, pp. 207 - 218.
- Irving, G.N. & Edwards, R.B. (1986) *Chemical Reactions*, Great Britain.

- Israelachvili, J. (1991) *Intermolecular and Surface Forces*, Academic Press, London.
- Israelachvili, J.N., Mitchell, D.J. & Ninham, B.W. (1976) 'Theory of Self-Assembly of Hydrocarbon Amphiphiles Into Micelles and Bilayers', *Journal of the Chemical Society, Faraday Transactions 2: Molecular and Chemical Physics*, vol. 72, pp. 1525 - 1568.
- Jachowicz, J., Wis-Surel, G. & Garcia, M.L. (1985) 'Relationship Between Triboelectric Charging and Surface Modifications of Human Hair', *Journal of The Society of Cosmetic Chemists*, no. 36, pp. 189-212.
- Jeon, J.S., Sperline, R.P., Raghavan, S. & Hiskey, J.B. (1996), *Colloids and Surfaces A*, no. 111, p. 29.
- Jonsson, B., Lindman, B., Kronberg, B. & Holmberg, K. (2002) *Surfactants and Polymers In Aqueous Solution*, 2nd edn, John Wiley & Sons, Ltd, Great Britain.
- Jurgens, A. (1989) 'Microstruture and Viscosity of Liquid Detergent.', *Tenside Surfactants Detergent*, no. 26, p. 222.
- Kaler, E.W., Herrington, K.L., Murthy, A.K. & Zasandzinski, J.A.N. (1992) 'Phase Behaviour and Structures of Mixtures of Anionic and Cationic Surfactants', *Journal of Physical Chemistry*, vol. 96, no. 16, pp. 6698 - 6707.
- Kanicky, J.R., Lopez-Montilla, J., Pandey, S. & Shah, D.O. (2001) Surface Chemistry in the Petroleum Industry, in K. Holmberg, D.O. Shah & M.J. Schwuger (eds), *Handbook of Applied Surface and Colloid Chemistry Volumes 1 - 2: Part I. Surface Chemistry in Important Technologies*, John Wiley & Sons, Ltd, England, pp. 251 - 267.
- Karbstein, H. & Schubert, H. (1995) 'Developments In The Continuous Mechanical Production of Oil-In-Water Macro-Emulsions', *Chemical Engineering and Processing*, vol. 34, pp. 205 - 211.
- Kazanci, N. & Yildiz, T. (2008) 'Investigation of Temperature Dependence of Mesomorphism and Refracting Index of Sodium Dodecysulphate+Water+Decanol Lyotropic System', *Journal of Molecular Structure*, vol. 886, pp. 158 - 165.
- Klevens, H.B. (1953) 'Structure and Aggregation In Dilate Solution of Surface Active Agents', *Journal of the American Oil Chemists' Society*, vol. 30, pp. 74 - 80.
- Kolmogorov, A.M. (1949) 'Breakup Of Droplets In Turbulent Flow', *Dokaldy Akademii Nauk Uzbekskoi SSr*, vol. 66, pp. 825 - 828.

- Kowalski, A.J., Cooke, M. & Hall, S. (2011) 'Expression For Turbulent Power Draw of An In-line Silverson High Shear Mixer', *Chemical Engineering Science*, vol. 66, no. 3, pp. 241 - 249.
- Krafft, F. & Berichte, D.B.G. (1899), *Berichte der deutschen chemischen Gesellschaft - Physical Chemistry Chemical Physics*, vol. 32, p. 1596.
- Kresheck, G.C. (1975) Water - A Comprehensive Treatise, in F. Franks (ed.)Plenum Press, New York.
- Kronberg, B., Castas, N. & Silvestonti, R. (1994) 'Understanding The Hydrophobic Effect.', *Journal Of Colloid And Interface Science*, vol. 15, no. 3, pp. 333 - 351.
- Kuo-Yann, L. (2006) *Liquid Detergents. Surfactant Science Series, Volume 129*, CRC, US.
- La Mesa, C. & Sesta, B. (1987) 'Micelles In Perfluorinated Surfactant Solutions', *The Journal of Physical Chemical*, no. 91, pp. 1450 - 1454.
- Larsson, K. (1967), *Zeitschrift für Physikalische Chemie*, vol. 56, p. 173.
- Larsson, K. & Krog, N. (1973) 'Structural Properties of The Lipid-Water Gel Phase', *Chemistry and Physics of Lipids*, vol. 10, pp. 177 - 180.
- Lauger, J., Weigel, R., Berger, K., Hiltrop, K. & Richtering, W. (1996) 'Rheo-small-angle-light-scattering Investigation of Shear-Induced Structural Changes In A Lyotropic Lamellar Phase', *Journal of Colloid and Interface Science*, vol. 181, no. 2, pp. 521 - 529.
- Laughlin, R.G. (1990) *Cationic Surfactants*, Marcel Decker, New York.
- Laughlin, R.G. (1994) *The Aqueous Phase Behaviour Of Surfactants*, Academic Press.
- Le, T.D., Olsson, U., Mortensen, K., Zipfel, J. & Richtering, W. (2001) 'Nonionic Amphiphilic Bilayer Structures Under Shear', *Langmuir*, vol. 17, pp. 999 - 1008.
- Leigh, I.D., McDonald, M.P., Wood, R.M., Tiddy, G.J.T. & Trevethan, M.A. (1981) 'Structure of Liquid-Crystalline Phases Formed by Sodium Dodecyl Sulphate and Water As Determined By Optical Microscopy, X-ray Diffraction and Nuclear Magnetic Resonance Spectroscopy', *Journal of The Chemical Society, Faraday Transactions 1: Physical Chemistry In Condensed*, vol. 12, no. 77, pp. 2867 - 2876.
- Leung, A.Y. (1980) *Encyclopedia of Common Natural Ingredients Used in Food, Drugs, and Cosmetics*, John Wiley, New York.
- Lindman, B. (2001) Physico-Chemical Properties of Surfactants, in K. Holmberg, D.O. Shah & M.J. Schwuger (eds), *Handbook of Applied Surface and Colloid Chemistry*, vol. 1 - 2, John Wiley & Sons Ltd, Chichester.

- Lochhead, R. (1988) 'Encyclopedia of Polymers and Thickeners for Cosmetics', *Cosmetic & Toiletries Science Applied*, vol. 103, no. 12, pp. 99-129.
- Luoma, A. & Kara, R. (1998) Silicones and the Perm Question, Society of Cosmetic Chemists. 1988 Spring Conference on Hair Care April 21-23, London, UK.
- Luzzati, V. (1968a) *Biological Membranes; Physical Fact and Function*, Chapman Academic Press, London.
- Luzzati, V. (1968b) *In Biological Membranes*, Chapman, Academic Press, New York.
- Luzzati, V. & Tardieu, A. (1974), *Annual Review of Physical Chemistry*, vol. 25, p. 79.
- Luzzatti, V. (1968) *Biological Membrances. Physical Fact and Function*, Academic Press, New York.
- Mackeben, S., Muller, M. & Muller-Goymann, C.C. (2001) 'The Influence of Water on Phase Transition of A Drug-Loaded Reverse Micellar Solution Into Lamellar Liquid Crystal', *Colloids and Surfaces A: Physicochemical and Engineering Aspects*, vol. 183 - 185, pp. 699 - 713.
- Maelstrom, A. (2010) *Innovation in fluid mixing*, Maelstrom APT Ltd, England
- Malliaris, A., Le Moigne, J., Sturm, J. & Zana, R. (1985) 'Temperature-Dependence of The Micelle Aggregation Number and Rate of Intramicellar Excimer Formation In Aqueous Surfactant Solutions', *Journal of Physical Chemistry*, vol. 89, no. 12, pp. 2709 - 2713.
- Malmsten, M. (2001) Surface Chemistry in Pharmacy, in K. Holmberg, D.O. Shah & M.J. Schwuger (eds), *Handbook of Applied Surface and Colloid Chemistry Volumes 1 - 2: Part I. Surface Chemistry in Important Technologies*, John Wiley & Sons, Ltd, England, pp. 4 - 23.
- Maring, D. & Wiesner, U. (1997), *Macromolecules*, vol. 660.
- Masalci, O. & Kazanci, N. (2009) 'Compared Properties of Textures of Lyotropic Mesophases of Binary and Ternary Systems Based on Tetradecyltrimethyl ammonium bromide', *Journal of Molecular Structure*, vol. 919, pp. 1 - 6.
- Matsumoto, T., Heiuchi, T. & Horie, K. (1989) 'Morphology and Viscoelasticity of Bilayer Aqueous Colloids of Low-molecular and Macromolecular Amphiphiles', *Colloid and Polymer Science*, vol. 267, no. 1, pp. 71 - 79.
- McBain, J.W. (1913) 'Colloids And Their Viscosity', *Transactions of the Faraday Society*, vol. 9, pp. 93 - 107.
- McCutcheon (1991) *Emulsifiers and Detergents*, MC Publishing Co, Glen Rock, NJ.

- McKeown, S.A., Mackley, M.R. & Moggridge, G.D. (2003) 'Shear-Induced Structural Changes In A Commercial Surfactant-Based System', *Chemical Engineering Research and Design*, no. 81, pp. 649 - 664.
- Mills, T.T., Tristram-Nagle, T.N., Heberle , F.A., Morales, N.F., Zhao, J., Wu, J., Toombes, G.E., Nagle, J.F. & Feigenson, G.W. (2008) 'Liquid-Liquid Domains in Bilayers Detected by Wide Angle X-Ray Scattering', *Biophysical Journal*, vol. 95, no. 2, pp. 682 - 690.
- Missel, P.J., Mazer, N.A., Benedek, G.B., Young, C.Y. & Carey, M.C. (1980) 'Thermodynamic Analysis of The Growth of Sodium Dodecyl Sulfate Micelles', *Journal of Physical Chemistry*, vol. 84, no. 9, pp. 1044 - 1057.
- Mitchell, D.J. & Ninham, B.W. (1981) 'Micelles, Vesicles and Microemulsion', *Journal of the Chemical Society, Faraday Transactions 2: Molecular and Chemical Physics*, vol. 77, pp. 601 - 629.
- Mitchell, D.J., Tiddy, G.J.T., Waring, L., Bostock, T. & McDonald, M.P. (1983) 'Phase Behaviour of Polyoxyethylene Surfactants With Water. Mesophase Structures and Partial Miscibility (Cloud Points)', *Journal of the Chemical Society, Faraday Transactions*, vol. 79, no. 975 - 1000.
- Mittal, K.L. (1977) *Micellization, Solubilization and Microemulsions*, Plenum Press, New York.
- Mondain-Monval, O. (2005) 'Freeze Fracture TEM Investigations In Liquid Crystals', *Current Opinion in Colloid & Interface Science*, vol. 10, pp. 250 - 255.
- Montalvo, G., Valiente, M. & Rodenas, E. (1995) 'Study of the Phase Diagram of the CTAB/Benzyl Alcohol/Water System', *Journal Of Colloid And Interface Science*, vol. 172, no. 2, pp. 494 - 501.
- Mortensen, K. (2001) 'Structural Studies of Lamellar Surfactant Systems Under Shear', *Current Opinion In Colloids and Interface Science*, vol. 6, no. 2, pp. 140 - 145.
- Moudgil, B.M., Singh, P.K. & Adler, J.J. (2001) Surface Chemistry in Dispersion, Flocculation and Flotation, in K. Holmberg, D.O. Shah & M.J. Schwuger (eds), *Handbook of Applied Surface and Colloid Chemistry Volumes 1 - 2: Part I. Surface Chemistry in Important Technologies*, John Wiley & Sons, Ltd, England, pp. 219 - 232.
- Mukerjee, P. & Mysels, K.J. (1971) *Critical Micelle Concentrations of Aqueous Surfactant Systems*, NSRDS-NBS 36, US Department of Commerce, Washington DC.

- Muller-Goymann, C.C. (2004) 'Physicochemical Characterization of Colloid Drug Delivery Systems Such As Reverse As Reverse Micelles Vesicles, Liquid Crystals And Nanoparticles For Topical Administration', *European Journal of Pharmaceutics and Biopharmaceutics*, vol. 58, pp. 343 - 356.
- Murphy, D.J. (1982) 'The Importance of Non-Planar Bilayer Regions In Photosynthetic Membranes and Their Stabilisation By Galactolipids', *FEBS Letters*, vol. 150, no. 1, pp. 19 - 26.
- Myers, K.J., Reeder, M.F., Ryan, D. & Daly, D. (1999) 'Get a Fix on High Shear Mixing', *Chemical Engineering Progress*, vol. 11, no. 95, pp. 33 - 42.
- Nagarajan, R. & Ruckenstein, E. (1991) ' Theory of Surfactant Self-Assembly: A Predictive Molecular Thermodynamic Approach.', *Langmuir*, vol. 7, pp. 2934 - 2969.
- Nakarapanich, J., Barameesangpet, T., Suksamranchit, S., Sirivat, A. & Jamieson, A.M. (2001) 'Rheological Properties and Structures of Cationic Surfactants and Fatty Alcohol Emulsions: Effect of Surfactant Chain Length and Concentration', *Colloid and Polymer Science*, vol. 279, pp. 671 - 677.
- Neeson, P.G. & Tiddy, G.J.T. (1982), *Journal of The Chemical Society, Faraday Transactions*, vol. 1, no. 78, p. 147.
- Nemeth, Z., Halasz, L., Palinkas, J., Bota, A. & Horanyi, T. (1998) 'Rheological Behaviour of A Lamellar Liquid Crystalline Surfactant-Water System', *Colloids and Surfaces A: Physicochemical and Engineering Aspects*, vol. 145, pp. 107 - 119.
- Nesrullajev, A., Kazanci, N. & Yildiz, T. (2003) 'Hexagonal Lyotropic Liquid Crystalline Mesophase: Change of Rod-Like Micelle Sizes With Changes In Concentrations', *Materials Chemistry and Physics* pp. 710 - 713.
- Neto, A.M.F. & Salinas, S.R.A. (2005) *The Physics of Lyotropic Liquid Crystals: Phase Transitions and Structural Properties*, Oxford University, New York.
- Nilsson, F., Soderman, O. & Johansson, I. (1996), *Langmuir*, no. 12, p. 902.
- Oswald, P. & Allain, M. (1988) 'Rheology and Structural Defects In a Lyotropic Lamellar Phase', *Journal of Colloid and Interface Science*, vol. 126, no. 1, pp. 45 - 53.
- Pacek, A.W., Man, C.C. & Nienow, A.W. (1998) 'On The Sauter Mean Diameter And Size Distribution In Turbulent Liquid/Liquid Dispersions In A Stirred Vessel', *Chemical Engineering Science*, vol. 53, no. 11, pp. 2005 - 2011.

- Padron, G.A. (2001) *Measurement and Comparison of Power Draw in Batch Rotor-Stator Mixers*, MSc Thesis, University of Maryland, College Park, MD., USA
- Panizza, P., Roux, D., Vuillaume, V., Lu, C.Y.D. & Cates, M.E. (1996) 'Viscoelasticity of The Onion Phase', *Langmuir*, vol. 12, pp. 248 - 252.
- Partial, P., Kowalski, A.J., Machin, D., Kiratzis, N., Berni, M.G. & Lawrence, C.J. (2001) 'Rheology and Microstructural Transitions in the Lamellar Phase of a Cationic Surfactant', *Langmuir*, vol. 17, pp. 1131 - 1337.
- Patel, H.K., Rowe, R.C., McMahon, J. & Stewart, R.F. (1985a) 'A Comparison of The Structure And Properties of Ternary Gels Containing Cetrimide and Cetostearyl Alcohol Obtained From Both Normal and Synthetic Sources', *Acta Pharmaceutica Technology*, vol. 31, pp. 243 - 247.
- Patel, H.K., Rowe, R.C., McMahon, J. & Stewart, R.F. (1985b) 'An Investigation of The Structural Changes Occuring In A Cetostearyl Alcohol/Cetrimide/Water Gel After Prolonged Low Temperature (4 °C) Storage', *Journal of Pharmacy and Pharmacology*, vol. 37, pp. 899 - 902.
- Patel, H.K., Rowe, R.C., McMahon, J. & Stewart, R.F. (1985c) 'Properties of Cetrimide/Cetostearyl Alcohol Ternary Gels; Preparation Effects', *International Journal of Pharmaceutics*, vol. 25, pp. 237 - 242.
- Patel, H.K., Rowe, R.C., McMahon, J. & Stewart, R.F. (1985d) 'A Systematic Microsopical Examination of Gels and Emulsions Containing Cetrimide and Cetostearyl Alcohol', *International Journal of Pharmaceutics*, vol. 25, pp. 13 - 25.
- Patist, A. (2001) Determining Critical Micelle Concentration, in K. Holmberg, D.O. Shah & M.J. Schwuger (eds), *Handbook of Applied Surface and Colloid Chemistry Volumes 1 - 2: Part I. Surface Chemistry in Important Technologies*, John Wiley & Sons, Ltd, England, pp. 239 - 248.
- Penfold, J., Staples, E., Khan Lodhi, A., Tucker, L. & Tiddy, G.J.T. (1997a) 'Shear-Induced Transformations in the Lamellar Phase of Hexaethylene Glycol Monohexadecyl Ether', *Journal of Physical Chemistry B*, vol. 101, pp. 66 - 72.
- Penfold, J., Staples, E., Lodhi Khan, A., Tucker, I. & Tiddy, G.J.T. (1997b), *Journal of Physical Chemistry B*, vol. 101, p. 66.
- Perry, R.H. & Green, D.W. (1999) Fluid and Particle Dynamics, in N.J. Tilton (ed.), *Perry's Chemical Engineers' Handbook*, 7th Edition edn, McGraw-Hill

- New York' Francisco, Washington, D.C. Auckland, Bogotá,Caracas, Lisbon, London, Madrid, Mexico City, Milan, Montreal, New Delhi, San Juan, Singapore, Sydney, Tokyo, Toronto.
- Persson, G. (2003) *Amphiphilic Molecules in Aqueous Solution: Effects of Some Different Counterions Then Monoolein/Octyglucoside/Water System*, Umea & Mid Sweden University, Sweden.
- Pincus, P. & Witten, T. (2004) *Structured Fluids: Polymers, Colloids, Surfactants*, Oxford University Press, New York.
- Polovsky, S.B. (1991) 'An Alkoxylated Methyl Glucoside Quaternary', *Cosmetic & Toiletries Science Applied*, vol. 106, pp. 59-65.
- Razzaque, M.M., Afacan, A., Liu, S., Nandakumar, J.H., Masliyah, J.H. & Sanders, R.S. (2003) 'International Journal of Multiphase Flow', *Bubble Size And Coalescence Dominant Regime Of Turbulent Air-Water Flow Through Horizontal Pipes*, vol. 29, pp. 1451 - 1471.
- Reis, D., Akpinar, E. & Neto, A.M.F. (2013) 'Effect Of Alkyl Chain Length Of Alcohols On Cholesteric Uniaxial To Cholesteric Biaxial Phase Transitions In A Potassium Laurate/Alcohol/Potassium Sulfate/Water/Brucine Lyotropic Mixture: Evidence Of A First-Order Phase Transition', *The Journal of Physical Chemistry B*, vol. 117, pp. 942 - 948.
- Reychler (1913), *Kolloid-Z*, vol. 12, p. 283.
- Riise, B.L., Frederickson, G.H., Larson, R.G. & Pearson, D.S. (1995), *Macromelecules*, vol. 28, p. 7653.
- Rosen, M.J. (2004) *Surfactants and Interfacial Phenomena*, John Wiley & Sons, Inc, New Jersey.
- Roux, D., Nallet, F. & Diat, O. (1993) 'Rheology of Lyotropic Lamellar Phases', *Europhysics Letters*, vol. 24, no. 1, pp. 53 - 58.
- Rowe, W. & McMahon, J. (1987) 'The Characterisation Of The Microstructure Of Gels And Emulsions Containing Cetostearyl Alcohol And Cetrimide Using Electron Microscopy — A Comparison Of Techniques', *Colloids and Surfaces*, vol. 27, no. 4, pp. 367 - 373.
- Rybinski, W.V. (2001) Surface Chemistry in Detergency, in K. Holmberg, D.O. Shah & M.J. Schwuger (eds), *Handbook of Applied Surface and Colloid Chemistry Volumes 1 - 2: Part I. Surface Chemistry in Important Technologies*, John Wiley & Sons, Ltd, England, pp. 53 - 72.

- Rydhag, L. & Gabran, T. (1982) 'Phase Equilibria In The System Dimyristoyl Phosphatidyl Choline/Hexadecyl Trimethylammonium Bromide/Water at 30 °C. Swelling Behaviour of The Lamellar Phase With Different Electrolyte Solutions', *Chemistry and Physics of Lipids*, vol. 30, pp. 309 - 324.
- Safinya, C.R., Sirota, E.B., Bruinsma, R.F., Jeppesen, C., Plano, R.J. & Wenzel, L.J. (1993) 'Structure of Membrane Surfactant and Liquid Crystalline Smetic Lamellar Phases Under Flow', *Science*, vol. 5121, pp. 588 - 591.
- Saunders, G.M., Barry, B.W. & Howard, I.M. (1972) 'Kinetics od Structure Build-up in Self Bodied Emulsions Stabilized by Mixed Emusifiers', *Journal of Colloid Interface Science*, vol. 41, pp. 331-342.
- Savic, S., Lukic, M., Jaksic, I., Reichl, S., Tamburic, S. & Muller-Goymann, C.C. (2011) 'An Alkyl Polyglucoside-Mixed Emulsifier As Stabilizer of Emulsion System: The Influence of Colloidal Structure on Emulsion Skin Hydrated Potential', *Journal Of Colloid And Interface Science*, vol. 358, pp. 182 - 191.
- Seager, S.L. & Slabaugh, M.R. (2011) *Introductory Chemistry for Today*, 7th edn, Brooks/Cole, United States.
- Seddon, J.M. (1990) 'Structure of The Inverted Hexagonal (H2) Phase, and Non-Lamellar Phase Transitions of Lipids', *Biochimica et Biophysica Acta*, vol. 1, no. 1031, pp. 1 - 69
- Seddon, J.M. & Templer, R.H. (1995) *Structure and Dynamic of Membrane: From Cells To Vesicles*, Elsevier Science, Amsterdam.
- Sharma, S.C. & Warr, G.G. (2012) 'Phase Behaviour, Self Assembly, and Emulsification of Tween 80/Water Mixtures With Limonene and Perfluoromethyldecalin', *Langmuir*, vol. 28, pp. 11707 - 11713.
- Shinoda, K. & Fujihara, M. (1968) 'Analysis of The Solubility of Hydrocarbons In Water', *Bulletin of The Chemical Society of Japan*, vol. 41, p. 2612.
- Sierro, P. & Roux, D. (1997) 'Structure of a Lyotropic Lamellar Phase Under Shear', *Physical Review Letters*, vol. 78, no. 8, pp. 1496 - 1499.
- Singh, M., Agarwal, V., De Kee, D., McPherson, G., John, V. & Bose, A. (2004) 'Shear-Induced Orientation of a Rigid Surfactant Mesophase', *Langmuir*, vol. 20, no. 14, pp. 5693 - 5702.

- Sisko, A.W. (1958) 'The Flow of Lubricating Greases', *Industrial And Engineering Chemistry*, vol. 50, no. 12, pp. 1789 - 1792.
- Stead, J.A. & Taylor, H. (1969) 'Some Solution Properties of Certain Surface-Active N-alkylpyridinium Halides: I. Effects of Temperature on The Critical Micelle Concentrations', *Journal Of Colloid And Interface Science*, vol. 30, no. 4, pp. 482 - 488.
- Tadros, T.F. (2001) Surface Chemistry in Agriculture, in K. Holmberg, D.O. Shah & M.J. Schwuger (eds), *Handbook of Applied Surface and Colloid Chemistry Volumes 1 - 2: Part I. Surface Chemistry in Important Technologies*, John Wiley & Sons, Ltd, England, pp. 73 - 83.
- Tanford, C. (1974), *The Journal of Physical Chemistry*, vol. 78, p. 2469.
- Tanford, C. (1980) *The Hydrophobic Effect: Formation of Micelles and Biological Membranes*, Wiley-Interscience, New York.
- Tauer, K. (2001) Surface Chemistry in the Polymerization of Emulsion, in K. Holmberg, D.O. Shah & M.J. Schwuger (eds), *Handbook of Applied Surface and Colloid Chemistry Volumes 1 - 2: Part I. Surface Chemistry in Important Technologies*, John Wiley & Sons, Ltd, England, pp. 175 - 190.
- Texter , J. (2001) Surface and Colloid Chemistry in Photographic Technology, in K. Holmberg, D.O. Shah & M.J. Schwuger (eds), *Handbook of Applied Surface and Colloid Chemistry Volumes 1 - 2: Part I. Surface Chemistry in Important Technologies*, John Wiley & Sons, Ltd, England, pp. 85 - 104.
- Tiberg, F., Daicic, J. & Froberg, J. (2001) Surface Chemistry of Paper, in K. Holmberg, D.O. Shah & M.J. Schwuger (eds), *Handbook of Applied Surface and Colloid Chemistry Volumes 1 - 2: Part I. Surface Chemistry in Important Technologies*, John Wiley & Sons, Ltd, England, pp. 123 - 138.
- Tiddy, G.J.T. (1980), *Physics Report*, vol. 57.
- Tiddy, G.J.T., Hassan, S. & Rowe, W. (2001) Surfactant Liquid Crystals and Surfactant Chemical Structure, in K. Holmberg, D.O. Shah & M.J. Schwuger (eds), *Handbook of Applied Surface and Colloid Chemistry*, vol. 1 - 2, John Wiley & Sons Ltd, Chichester.
- Utomo, A.T., Baker, M. & Pacek, A.W. (2009) 'The Effect of Stator Geometry on the Flow Pattern and Energy Dissipation Rate in a Rotor-Stator Mixer', *Chemical Engineering Research and Design* vol. 84, pp. 533 - 542.
- Van de Pas, J.C. (1991) 'Liquid Detergents', *Tenside Surfactants Detergents*, no. 28, p. 158.

- Van Os, N.M., Haak, J.R. & Rupert, L.A.M. (1993) *Physico-Chemical Properties of Selected Anionic, Cationic and Nonionic Surfactants*, Elsevier, Amsterdam.
- Vankova, N., Tcholakova, S., Denkov, N.D., Ivanov, I.B., Vulchev, V.D. & Danner, T. (2007) 'Emulsification In Turbulent Flow: 1. Mean And Maximum Drop Diameters In Inertial And Viscous Regimes', *Journal Of Colloid And Interface Science*, vol. 312, no. 2, pp. 363 - 380.
- Vincent, J.M. & Skoulios, A. (1966) '`Gel' et `coagel'. I. Indentification. Localisation Dans Un Diagramme de Phases et Détermination de La Structure du `Gel' dans Le Cas Du Stéarate de Potassium.', *Acta Crystallographica*, vol. 20, pp. 432 - 440.
- Viola, G.G. & Baird, D.G. (1986), *Journal Of Rheology*, vol. 30, p. 601.
- Wang, Z., Diao, Z., Liu, F., Li, G. & Zhang, G. (2006) 'Microstructure and Rheological Properties of Liquid Crystallines Formed in Brij 97/Water/IPM System', *Journal Of Colloid And Interface Science*, vol. 297, pp. 813 - 818.
- Warr, G.G., Sen, R., Evans, D.F. & Trend, J.E. (1988) "Microemulsion Formation and Phase Behaviour of Dialkyldimethylammonium Bromide Surfactants', *The Journal of Physical Chemistry*, no. 92, p. 774.
- Weigel, R., Lauger, J., Richtering, W. & Linder, P. (1996) 'Anisotropic Small Angle Light and Neutron Scattering from a Lyotropic Lamellar Phase under Shear', *Journal de Physique II*, vol. 6, no. 4, pp. 592 - 542.
- Wenninger, J.A. & McEwen, G.N. (1995) CTFA Cosmetic Ingredients Handbook 3rd Ed, in Cosmetic Toiletry and Fragrance Association, Washington DC.
- Winsor, P.A. (1968) 'Binary and Multicomponent Solutions of Amphiphilic Compounds, Solubilizatios and The Formation, Structure, and Theoretical Significance of Liquid Crystalline Solution', *Chemical Reviews*, vol. 6, no. 8, pp. 2 - 40.
- Wrigth, K.A.J. & Tartar, H.V. (1939), *Journal of the American Chemical Society*, no. 61, p. 539.
- Yamagata, Y. & Senna, M. (1998) 'Change In The Two-Step Flow Behavior On Aging The Ternary Mixture Comprising Monoalkyl Cationic Surfactant, Long-Chain Alcohol And Water I. Viscous Flow Preceded By Incipient Elastic Deformation', *Colloids and Surfaces A: Physicochemical and Engineering Aspects*, vol. 132, no. 2 - 3, pp. 251 - 256.
- Yamagata, Y. & Senna, M. (1999a) 'The Change In Viscoelastic Behaviour Due To Phase Transition Of The Assembly Of A Cetyltrimethylammonium Chloride/Cetyl Alcohol/Water System', *Langmuir*, vol. 15, pp. 4388 - 4391.

- Yamagata, Y. & Senna, M. (1999b) 'Effects of Temperature on the Development of The Internal Structure of the Cetyltrimethylammonium Chloride/Cetyl Alcohol/Water System', *Langmuir*, vol. 15, pp. 7461 - 7463.
- Yamaguchi, M. & Noda, A. (1987), *Nihon Kagaku Kaishi*, p. 1632.
- Yamaguchi, M. & Noda, A. (1989), *Nihon Kagaku Kaishi*, p. 26.
- Yavuz, A.Y., Masalci, Ö. & Kazanci, N. 'Phase Diagram of Tetradecyltrimethylammonium Bromide (TTAB) + Water + Octanol System With Application of Mechanical Deformation', *Applied Surface Science*, no. 0.
- Yildiz, T. & Kazanci, N. (2008) 'Investigation of Temperature Dependence of Mesomorphism and Refracting Index of Sodium Dodecylsulphate + Water + Decanol Lyotropic System', *Journal of Molecular Structure*, vol. 886, pp. 158 - 165.
- Youssry, M., Coppola, L., Nicotera, I. & Moran, C. (2008) 'Swollen and Collapsed Lyotropic Lamellar Rheology', *Journal of Colloid Interface Science*, vol. 321, pp. 459 - 467.
- Yuet, P.K. & Blankschtein, D. (1996) 'Effect of Surfactant Tail-Length Asymmetry On The Formation of Mixed Surfactant Vesicles', *Langmuir*, vol. 12, no. 16, pp. 3819 - 3827.
- Zhang, J., Dong, B., Zheng, L., Li, N. & Li, X. (2008) 'Lyotropic Liquid Crystalline Phase Formed In Ternary Mixtures of 1-cetyl-3-methylimidazolium bromide/p-xylene/Water: A SAX, POM, and Rheology Study', *Journal Of Colloid And Interface Science*, vol. 321, pp. 159 - 165.
- Zhuang, W., Chen, X., Cai, J., Zhang, G. & Qui, H. (2008) 'Characterisation of Lamellar Phases Fabricated From Brij-30/Water/1-butyl-3-methylimidazolium Salts Ternary Systems By Small-Angle X-Ray Scattering.', *Colloids and Surfaces A: Physicochemical and Engineering Aspects*, vol. 318, pp. 175 - 183.
- Zilman, A.G. & Granek, R. (1999) 'Undulation Instability of Lamellar Phases Under Shear:A Mechanism For Onion Formation?', *The European Physical Journal B*, vol. 11, pp. 593 - 608.
- Zipfel, J., Berghausen, J., Lindner, P. & Richtering, W. (1999) 'Influence of Shear on Lyotropic Lamellar Phases with Different Membrane Defects', *Journal of Physical Chemistry B*, vol. 103, pp. 2841 - 2849.

Chapter 3

3 Process Ingredients, Process Equipment, and Characterisation

3.1 Introduction

This Section details the raw materials, the various process equipment setup as well as the characterisation techniques[73] employed in this work.

In this project two systems have been studied - the first based on a model Hair Conditioner formulation and the second based on a 50 % w/w SFO/water emulsion premix.

3.2 Raw Materials

SYSTEM 1 - HAIR CONDITIONER [HC]

Typical cationic hair conditioner formulations can be found in (Bongers, Egan & Irving 2013). Typical ingredients may be understood as follows:

Fatty Alcohols [FA], Cationic Surfactants [CS] & Quaternary Ammonium Salts (QUAT)

FA, CS & QUAT are the materials which are combined with water during manufacture to form the lamellar gel phase which provides the hair conditioner with its viscosity (Bongers, Egan & Irving 2013).

Physically these materials are solid at room temperature and have to be melted prior to manufacture. Thus hair conditioners are manufactured at a temperature above the melt temperatures.

Preservative

A combination of preservatives is added at very small concentrations. They serve as anti-fungal and bactericide ingredients. Physically they may be liquid or solid at room temperature.

[73] Is displayed alongside experimental protocol utilised

Perfume

The perfume is used to mask odours arising from the ingredients and to provide consumer appeal. Physically perfumes are low viscosity liquids at room temperature.

Silicone Emulsion

Silicones are supplied as preformed emulsions of particular size. They possess relatively low viscosity and are included in the formulation to enhance conditioning performance. Physically the product is supplied as a colourless liquid.

SYSTEM 2 – SUN FLOWER OIL / WATER EMULSION

The thermodynamically unstable o/w emulsion investigated here was chosen as this element of the project was undertaken as part of a multi-national collaboration [University of Massachusetts, Technical University of Eindhoven and University of Liverpool] on emulsification [sponsored by Unilever] for which that emulsion provided a model system. The ingredients may be understood as follows:

Sun Flower Oil

SFO is a low viscosity [~50cP] vegetable oil at room temperature which is widely available.

Pluronic F68

Pluronic F68 is a non-ionic surfactant.

3.3 Process Equipment

In this section, all process equipment utilised in this text are described: Table 3-1 presents an overview of these equipment with respect to its location – upcoming sections elaborates on the nature of the equipment set up alongside process flow diagrams.

Table 3-1: Overview of process equipment employed in this study.

LOCATION	LOCATION	MIXERS
University of Liverpool	U.M.P.F[74]	CDDM-1 (Figure 3-2)
		CDDM-2 (Figure 3-3 & Figure 3-4)
	Laboratory	Bench Top CDDM (Figure 3-6 & Figure 3-7)
		Fluid Division Mixer [FDM] (Figure 3-9)
UR&D Port Sunlight	Pilot Plant	CDSM-1 (Figure 3-12)
		CDSM-2 (Figure 3-13)
		Mixer-1 (Figure 3-14)
		Mixer-2 (Figure 3-15)
	Laboratory	Mixer-3 [4 L processing rig] (Figure 3-16 &Figure 3-17

As shown above – experiments have been conducted at different locations. Details of the experimental apparatus are discussed within this Chapter – details of the experimental trials conducted with these experimental apparatus are discussed in the result Chapters.

3.3.1 University of Liverpool - Ultra Mixing and Process Facility

The UMPF facility (Figure 3-1) set-up is configured to mimic a small footprint factory in which up to five streams can be delivered by positive displacement pumps (LIP[75] and MIP[76]) into any installed[77] CDDM technology. The CDDM technologies used in the UMPF set-up include [1] CDDM-1 and [2] CDDM-2.

[74] Figure 3-1
[75] Large Intensifier Point (LIP) – pump volume as a function of plunger displacement is 0.75 L
[76] Medium Intensifier Point (MIP) – pump volume as a function of plunger displacement is 0.20 L
[77] I.e. CDDM-1 and CDDM-2

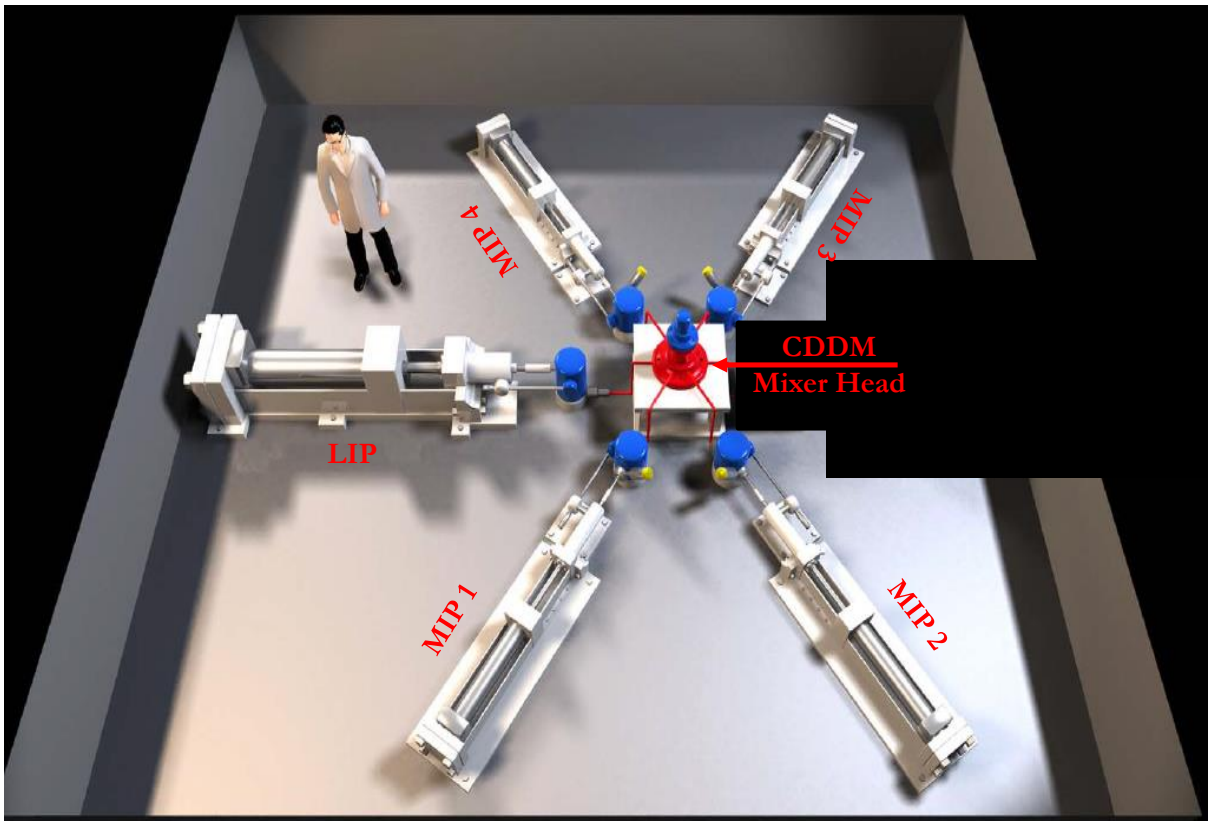

Figure 3-1: Schematic of the plan view of the UMPF facility showing the arrangement of components - central mixer is surrounded by five pumps (image courtesy Maelstrom APT Ltd, England).

The setup performance space includes - [1] batch or semi-continuous operation, [2] process flow-rates of up to 250 X 10^{-6} m^3/s [78], [3] maximum operating pressure of up to 5000 bar_g, [4] temperatures of up to 200 °C, and [5] mixing speeds of up to 50000 rpm.

For all experiments conducted in the UMPF, approximately 10 litres worth of process material is transferred into holding hopper i.e. individual hoppers connected to each positive displacement pumps (LIP and/or MIP) prior to the start of an experimental matrix (see Figure 3-5). Feed hoppers are sealed (air tight) and kept under static head pressure of approximately 2 bar_g throughout experiments - this ensured actuation of check valve "CV-1" (see Figure 3-5) enabling material flow into the pumps (LIP and/or MIP).

[78] 0.25 kg/s

For each trial, the pump is primed with fresh process material from the feed hopper to be delivered into the mixer via pipe work at set processing conditions. Samples are processed through mixer at a set position (mixer position corresponds to a 'nip position') dictated by the displacement of the rotor relative to the stator for which could either be a displacement in a positive (+ve) direction or negative (-ve) direction.

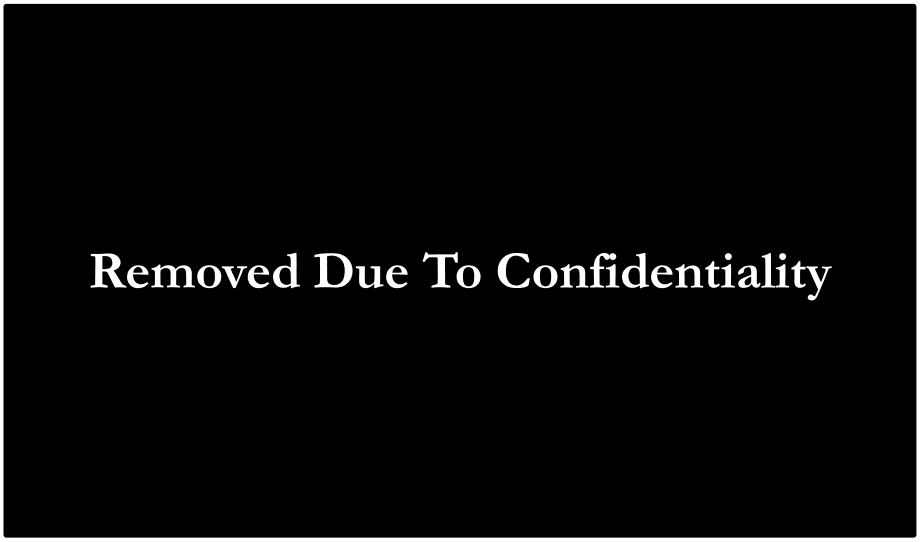

Figure 3-2: Image of the CDDM-1 rotor and stator highlighting its features.

The CDDM-2 has a dynamic[79] section at the top and a static[80] only section at the bottom.

Figure 3-3: Images of the CDDM-2 rotor and stator highlighting its features.

[79] Able to operate under both static i.e. 0 rpm and dynamic conditions i.e. 5000 – 10000 rpm
[80] Able to operate at 0 rpm only

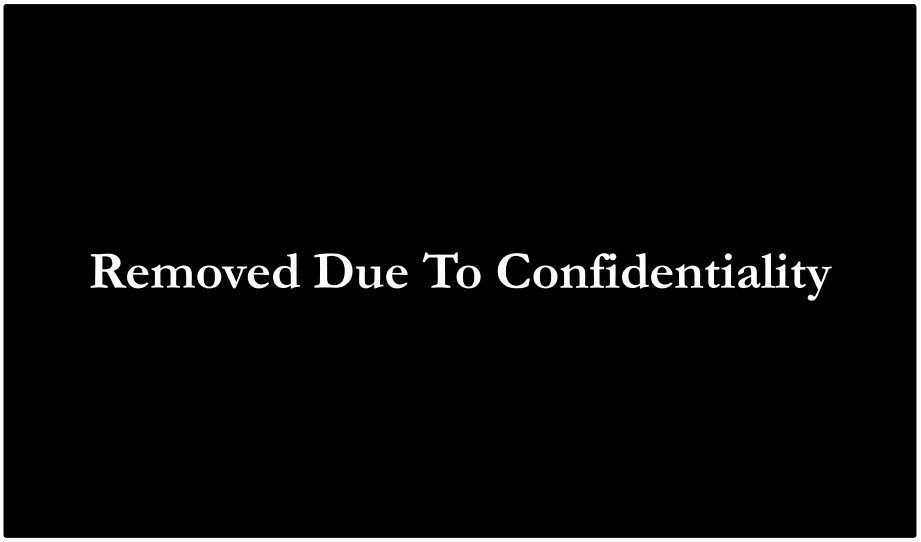

Figure 3-4: Schematic showing the CDDM-2 (static section) approximate angular displacement alongside angular position index.

A change in angular geometry (Figure 3-3) in the CDDM-2 mixer set up is accessible via a simple angular adjustment mechanism (Figure 3-3) and is only possible for the static section of the CDDM-2. Eight different angular positions are accessible as shown Figure 3-4 – coupled to this angular adjustment, the axial position of the mixer can also be adjusted for any set angular position.

UMPF Setup Experimental Methodology

The UMPF process matrix (Table 3-2) accessible in the UMPF experimental set-up can be operated in one of two modes; single shots (batch process), which is the operation of the syringe pumps or in multi-shot mode which is the continuous operation of the syringe pumps (pseudo continuous process) for static and dynamic operation – static operation as used here refers to when the rotor spindle is not operational while dynamic operation refers to when rotor spindle is operational i.e. rotating at 5000 rpm etc.

Table 3-2: Table showing the UMPF experimental matrix - the various mixer rotational speeds alongside process flow-rates available.

UMPF/CDDM Experimental Matrix		Rotational Speed, rpm		
		0 ⟷	5000 ⟷	10000
Flow-rate, kg/s	0.01			
	0.02			
	0.04			
	0.08			

For each single shot run (i.e. denoted by LIP[81] delivering shots into the mixer) about 150 ml of the initial material exiting the mixer is allowed to run to waste. Then the oncoming middle sample is collected in a 190 ml sample pot. Once this was full the rest of the material was allowed to run again as waste. This method ensured that the samples collected were fresh and had gone through the set processing conditions. However at higher flow-rate, the amount of sample allowed to run as waste were adjusted accordingly to ensure enough sample was collected in the sample pots.

Actual flow rate values are captured via sensors and relayed to a data logger instrumentation connected to LIP pumps. In-line pressure readings are recorded at pressure sensor (PS); location of sensors is seen in PFD diagram (Figure 3-5).

[81] Operation described for Large Intensifier Pump (LIP); other pumps shown in Figure 3-1 function in similar fashion.

Process Flow Diagram Setup For The MIPs Is Similar To The LIP Shown Below

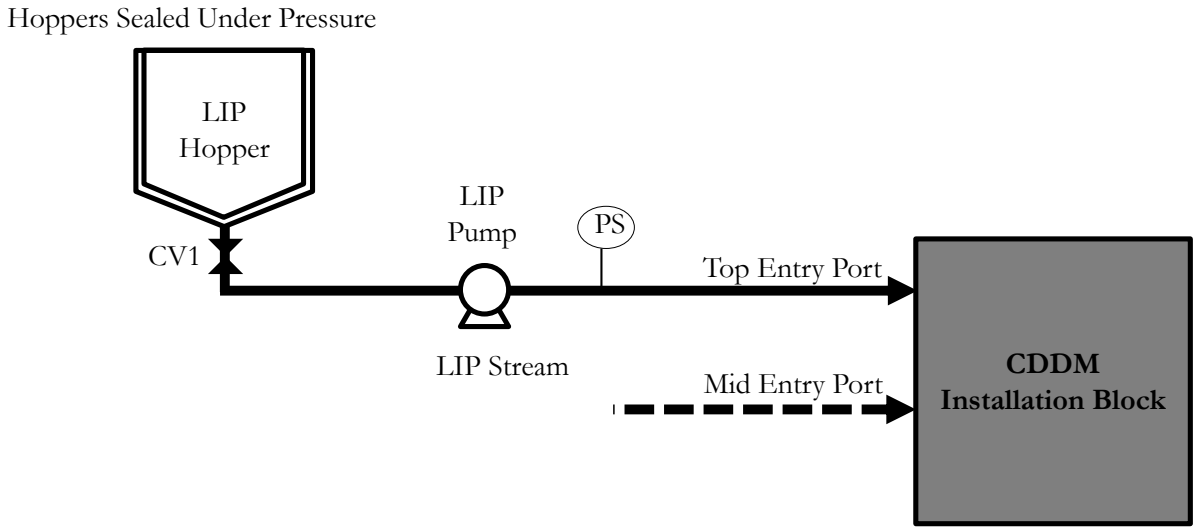

Figure 3-5: Schematic process flow diagram of the UMPF/CDDM Facility set up – process flow diagram shown only for the LIP line; process flow set-up is similar for MIP 1, MIP 2, MIP 3 and MIP 4.

For multi shot operation, similar steps described above are followed however the syringe pumps are operated in a continuous mode (i.e. syringe pumps shuttles back and forth delivering multiple shots). In this mode only static operation of the mixer is possible.

Bench Top CDDM Mixer

The Bench Top CDDM set up (Figure 3-6) is similar to the UMPF set-up described above albeit on a smaller scale – the set-up includes two [1] feed vessels and [2] two progressive cavity pumps drawing materials from this feed vessel and a gear pump to aid pumping of viscous fluids – described as pump 1, 2 and 3 respectively (see PFD diagram in Figure 3-8). Maximum operating pressure of up to 200 bar_g,, temperatures of up to 120 °C, and [4] mixing speeds of up to 15000 rpm. Experimental Protocol is similar to that of the UMPF as described above - process matrix accessible in the Bench Top CDDM experimental set-up can be seen in Table 3-3.

Inline pressure readings are recorded at pressure sensor (PS); location of sensors is seen in PFD diagram shown in Figure 3-8.

Figure 3-6: Image of the Bench Top CDDM Experimental set-up showing feed vessels, progressive cavity pumps, gear pump and data logging desktop computer.

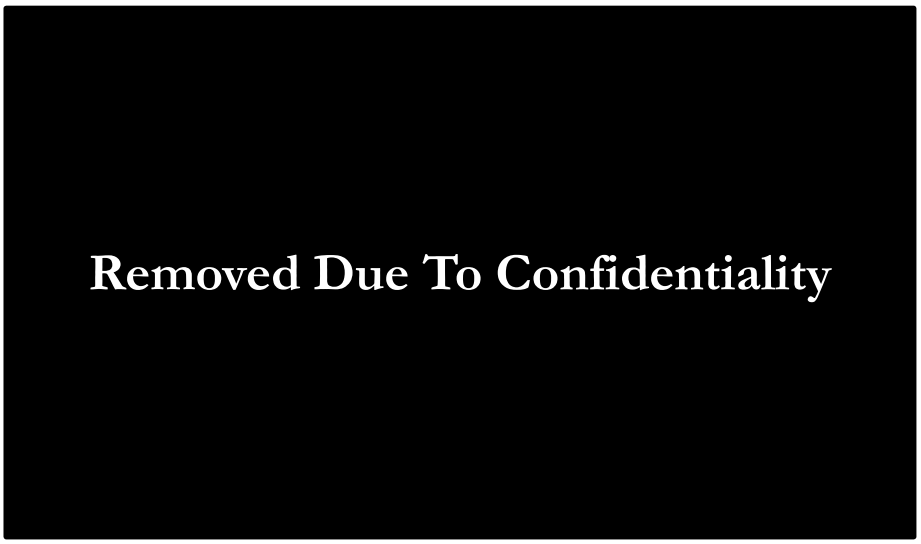

Figure 3-7: Images of the Bench Top CDDM the rotor and stator (right)

Table 3-3: Table showing the UMPF experimental matrix - the various mixer rotational speeds alongside process flow-rates available.

Bench Top CDDM Experimental Matrix		**Rotational Speed, rpm**		
		0 ⟷	5000 ⟷	10000
Flow-rate, kg/s	0.002			
	0.005			
	0.010			
	0.015			
	0.020			

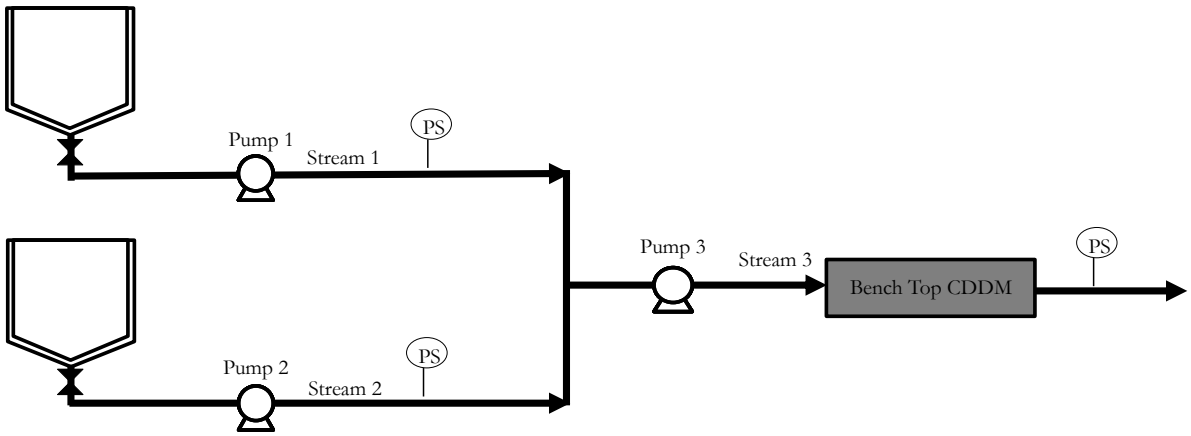

Figure 3-8: Schematic process flow diagram of the Bench Top CDDM set-up.

High Shear Batch Dip-In Rotor-Stator Mixers – Fluid Division Mixer (FDM)

The FDM (Maelstrom Advanced Process Technology, GB) is a batch mixer – mixer rotational speeds available are up to 6000 rpm. Process vessel has operating capacity of approx. 10 litres.

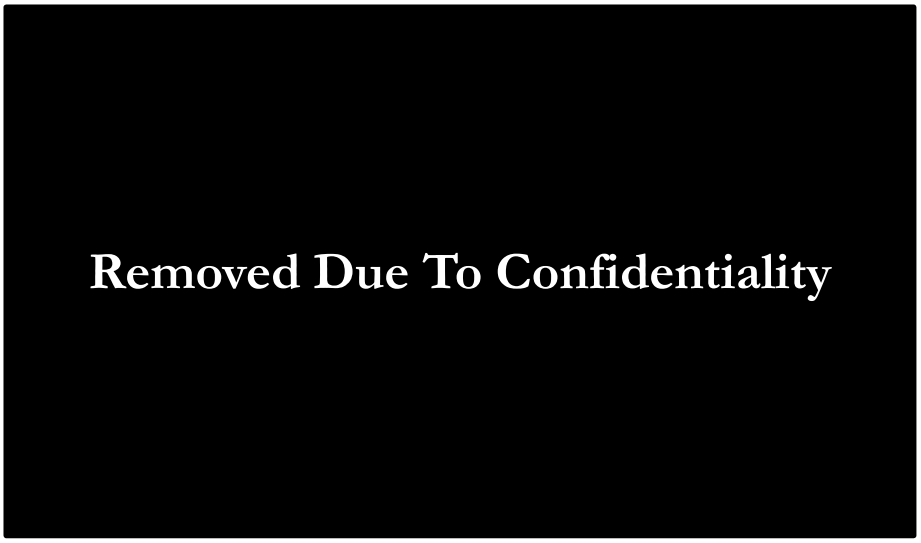

Figure 3-9: Images of the high shear batch rotor stator mixer - Fluid Division Mixer.

3.3.2 Unilever Research and Development Port Sunlight, Liverpool

The process equipment used in manufacturing lamellar dispersion based products from formulation 1.0H-C is shown in Figure 3-10 – schematic (PFD) shown in Figure 3-11 –

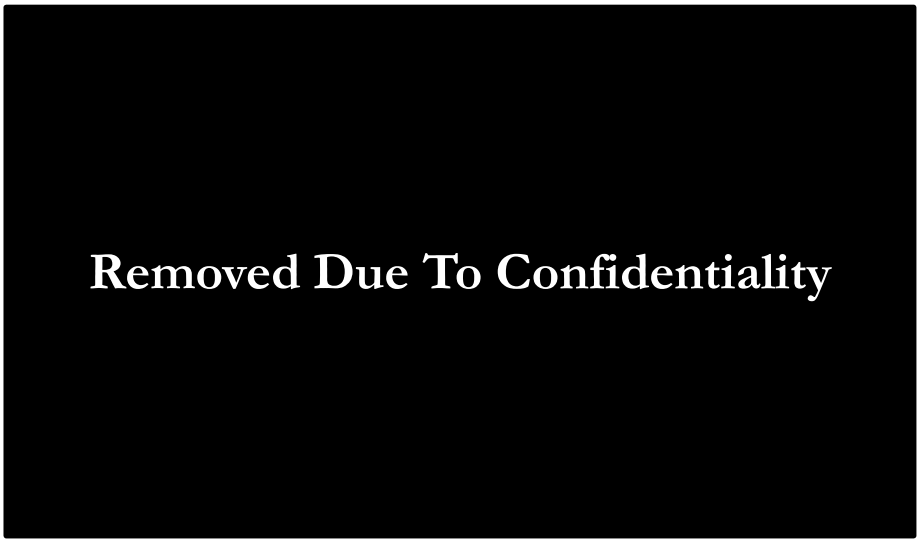

Figure 3-10: Image of the equipment platform used in experimental trials at the Unilever Research and Development Port Sunlight.

The platforms serves as a support for premix and single stream components holding vessels Pumps 1 – 4 draw process fluids from these vessels at set flow rates to be delivered to mixer set up.

In manufacturing - premixes are prepared according to the capacity of the plant vessels and are kept under agitation to ensure homogeneous mass. Premixes/single ingredients with set heating requirements are maintained at temperature via heated.

Vessel outlets are connected to flexible hoses (electrical trace heaters are wrapped around heated lines to maintain line temperature) which are connected to the inlet of the appropriate pump.

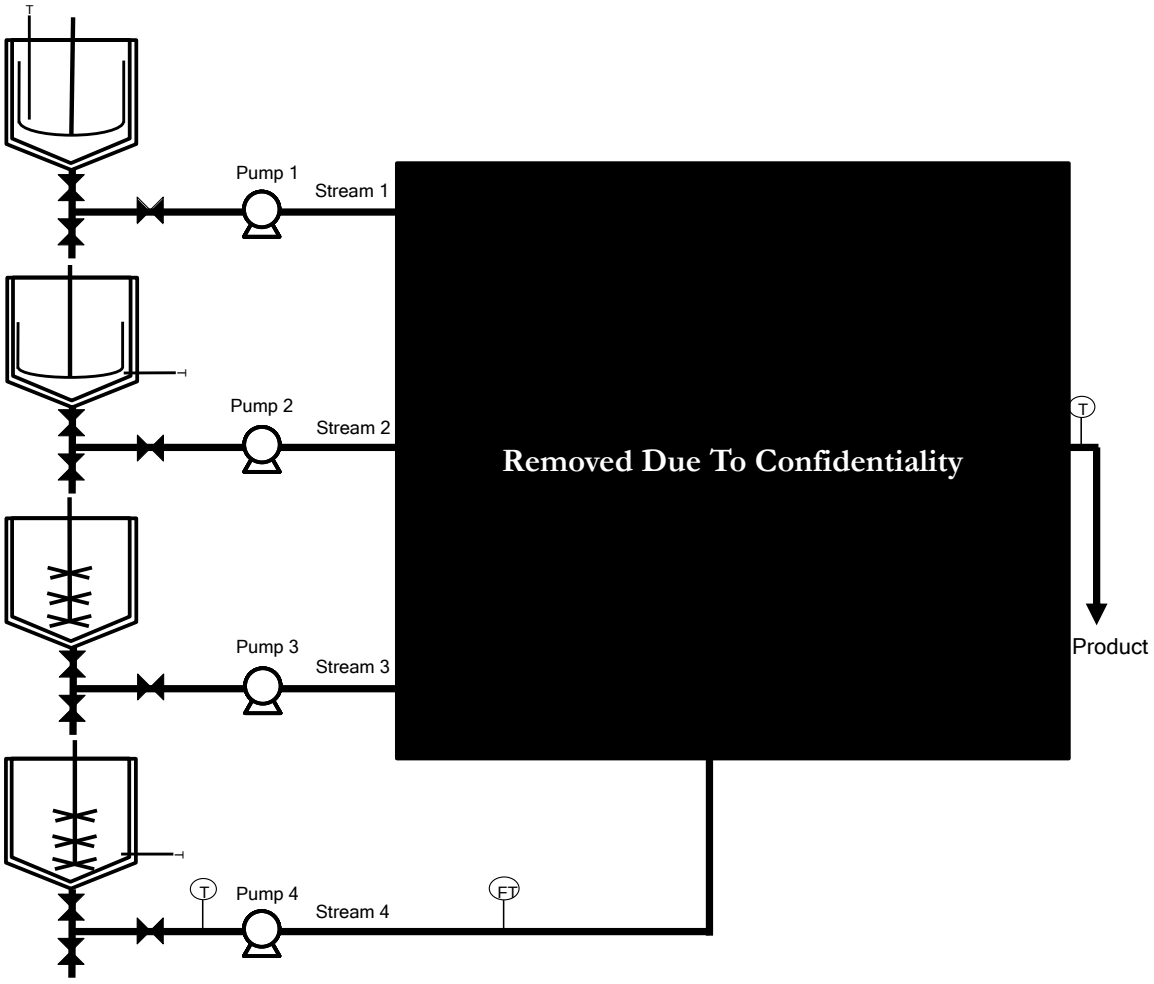

Figure 3-11: Schematic process flow diagram of the UR&D Port Sunlight set-up.

As alluded earlier, series of mixing technologies could be installable onto this rig namely [1] CDSM-1[82], [2] CDSM-2[83] [3] Mixer-1[84] and [4] Mixer-2[85] – subsequent section discusses these

[82] Figure 3-12

devices. They can be connected either singly or in series (two at a time). Set-ups reviewed are presented as a process flow diagram (PFD) in the result Chapters.

CDSM-1

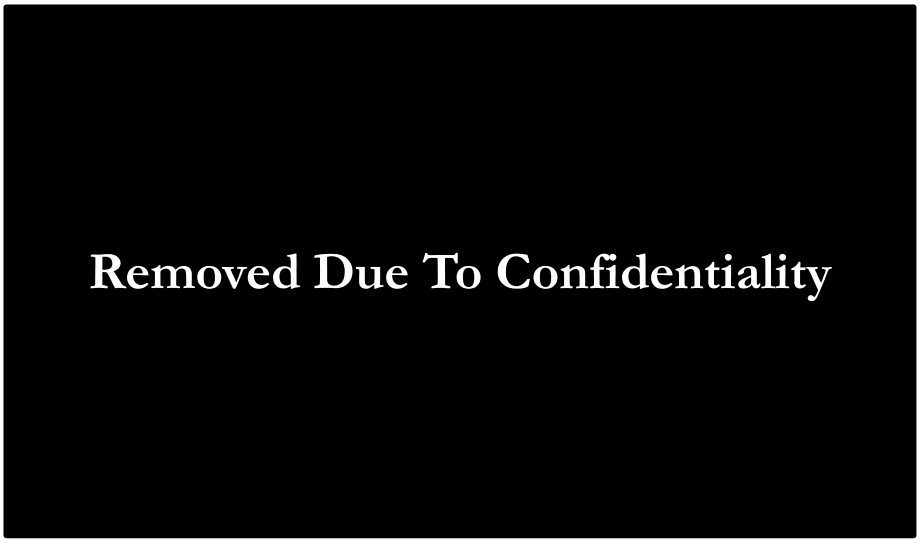

Figure 3-12: Section through CDSM-1 device.

CDSM-2

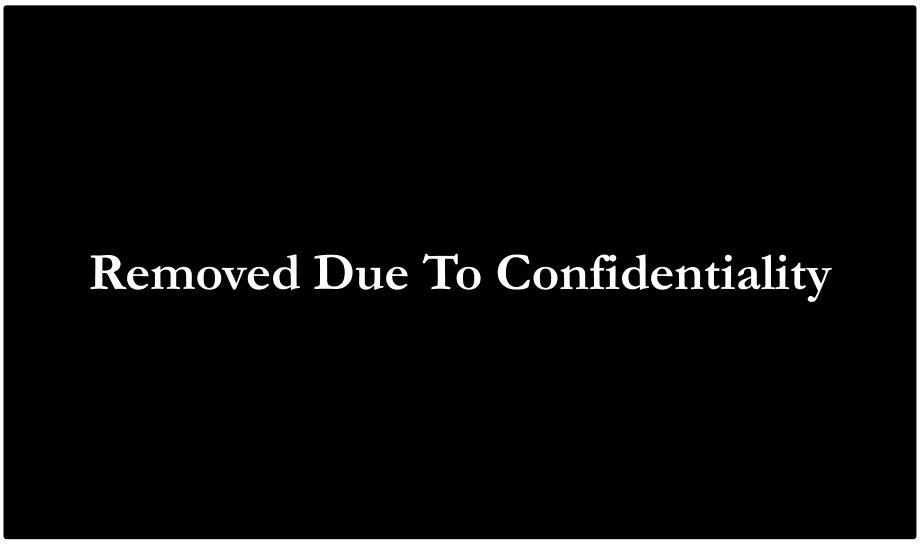

Figure 3-13: Section through CDSM-2 device.

[83] Figure 3-13
[84] Figure 3-14
[85] Figure 3-15

Mixer-1

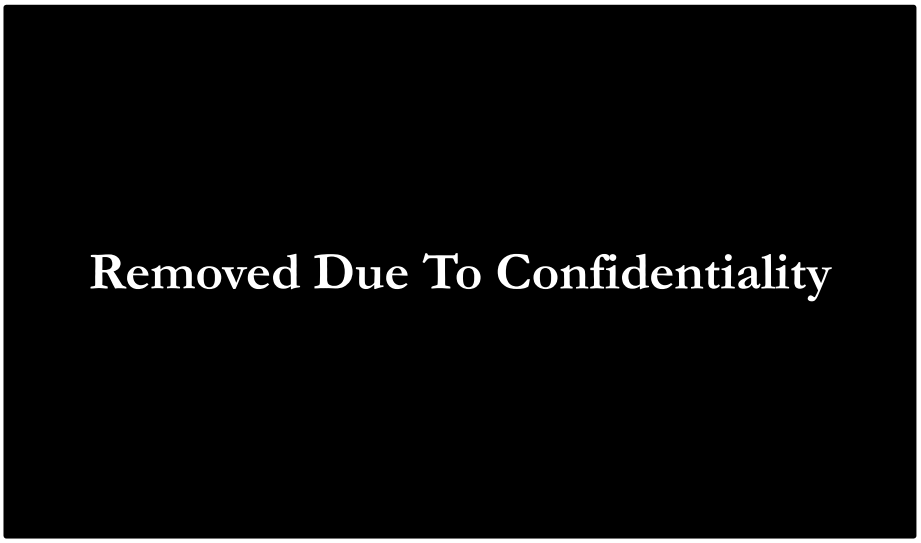

Figure 3-14: Dismantled Mixer-1 orifice.

Mixer-2

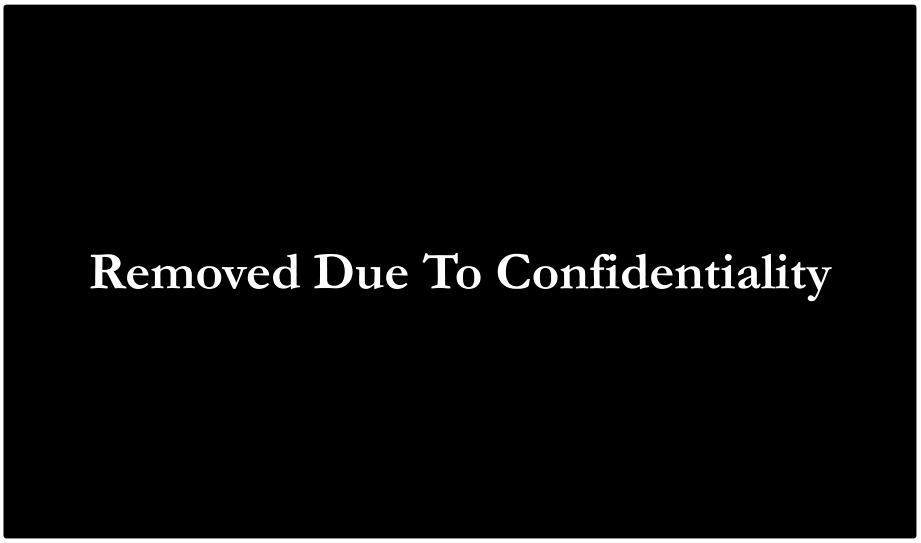

Figure 3-15: Dismantled Mixer-2

Mixer-3

Mixer-3 (Figure 3-16) is a batch processing vessel set-up containing a 4 litre batch vessel with an overhead low shear mixer, a peristaltic pump and an inline high shear rotor-stator mixer - a process flow diagram of the set-up is shown in Figure 3-17

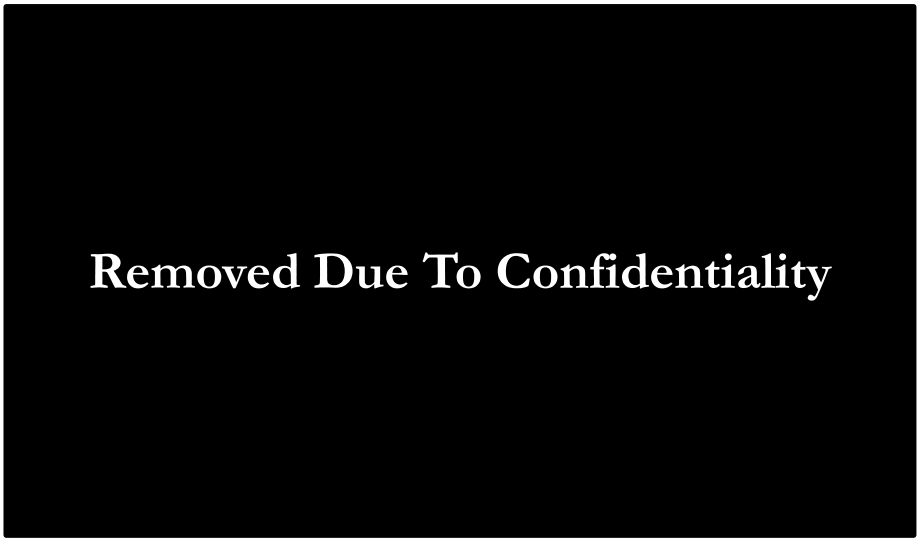

Figure 3-16: Image of Mixer-3 (4L processing rig).

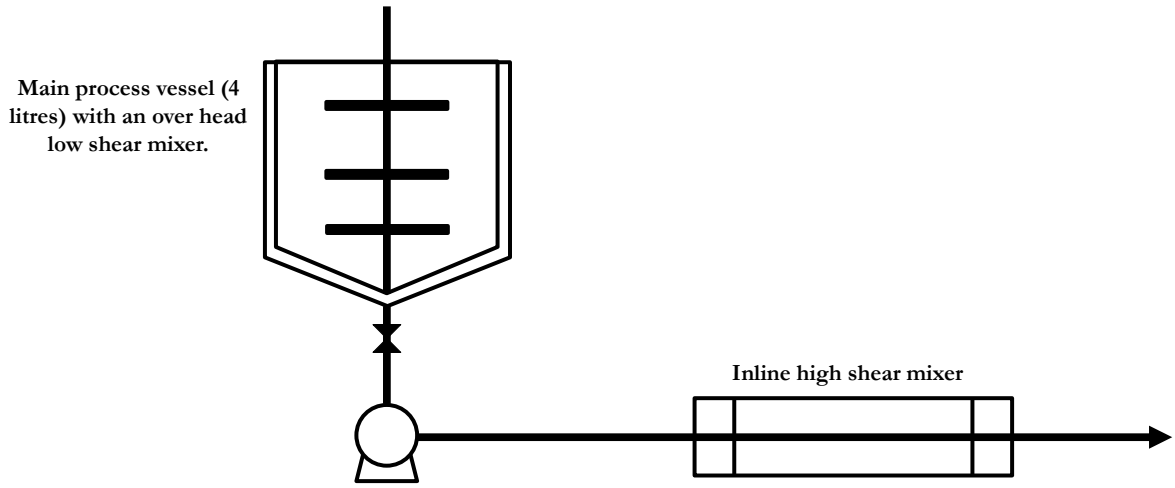

Figure 3-17: Schematic process flow diagram of Mixer-3 (4 L processing rig)

3.4 Characterisation Techniques (Theory)

This Section describes the various scientific analysis employed in characterising all the samples produced within this text; two classes of experiments were conducted; [1] lamella system experiments and [2] emulsification experiments – both of which are based on the raw materials discussed above

For the lamellar system experiments, several analytical methods have been employed to evaluate the underlying microstructure of the samples manufactured. Samples are subjected to two categories of analysis namely; [1] sample characterisation[86] and [2] product evaluation[87] tests.

For [1] sample characterisation - samples were subjected [a] rheology[88], [b] microscopy[89] [c] scattering[90] and [d] thermal transition[91] tests. On the other hand, product evaluation tests involved [a] salon and [b] consumer tests - these tests, although termed 'soft science' are however nonetheless important in obtaining a marketable and competitive product.

For [2] emulsification experiments conducted, only laser (light) scattering[92] technique has been used to assess the particle size distribution of the emulsions.

Subsequent Sections begin by presenting basic introduction to each technique described above - this is then followed by the analytical protocols used for analysis in Section 3.5.

3.4.1 Rheology

Rheology is the study of the fluid response of materials to an imposed stress (Balzer, Varwig & Weihrauch 1995; Barnes 2000; McCabe, Smith & Harriot 1993). The application of an external stress on a body causes displacement of the material's particles relative to each other. This displacement of particles is termed strain; type and extent of such strain elucidate the characteristics of such material rheology.

[86] [1] Samples based on AA % QUAT/CS/FA/Water system and [2] samples based on the fully formulated 1.0H-C rinse-off Hair Conditioner.
[87] Fully formulated 1.0H-C rinse-off Hair Conditioner
[88] Section 3.4.1
[89] Section 3.4.2
[90] Section 3.4.3
[91] Section 3.4.4
[92] Section 3.4.5

In defining strain, consider the Hookean response (Figure 3-18) of a cube material with its base fixed to a surface – the application of a constant pushing force (F) to the upper part of the cube[93], would result in elastic deformation (shear deformation) as shown in Figure 3-18 (right).

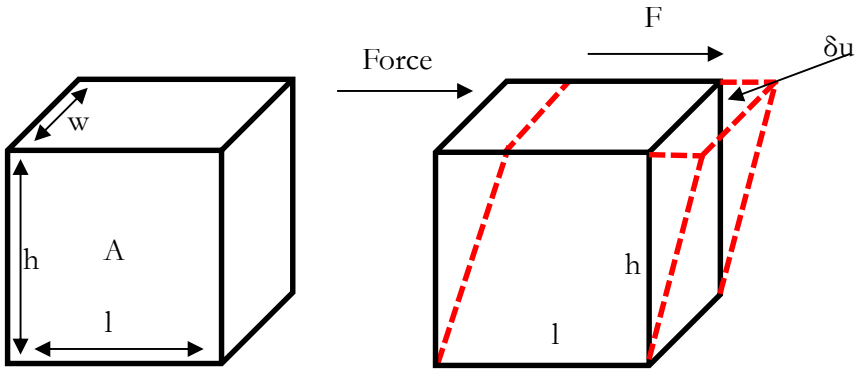

Figure 3-18: Simple deformation under an applied constant force - Hookean response (Bohlin 1994)

[ε] Shear strain (dimensionless) is therefore defined as;

$$\varepsilon = \frac{\delta u}{h} \qquad [3.1]$$

For pure elastic materials, Hooke's law states that stress is proportional to strain hence a linear response (strain) is expected when stress is i.e. doubled and the strain should return to zero when stress is withdrawn[94]. Secondly, consider a cube of material but in this case the material behaves as a Newtonian fluid. The application of a force (shear stress) will initiate a deformation which will continue to increase at a constant rate as shown in Figure 3-19.

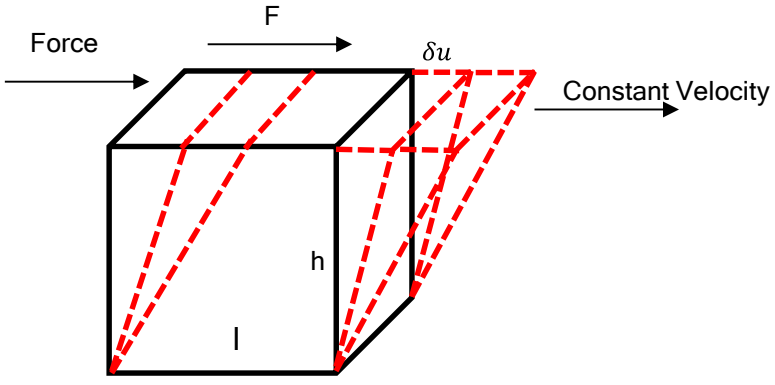

Figure 3-19: Laminar flow of a Newtonian fluid under constant shear stress.

[93] Assuming the material behave as an ideal solid
[94] Fully recoverable deformation

The rate of change of strain[95] commonly referred to shear rate (s^{-1}) can be obtained via computing the rate of change of strain (_) as a function of time (s) as shown below.

$$\dot{\gamma} = \frac{\delta u}{h} \times \frac{1}{s} \qquad [3.2]$$

The shear rate is therefore a function of shear stress and viscosity as shown in Equation 3.3 similar to the one derived in Section 2.7 - an equation representative of a Newtonian fluid where viscosity is independent of shear stress.

$$\eta = \frac{\tau}{\dot{\gamma}} \qquad [3.3]$$

Equations discussed thus far in this section are based on the application of a stress and measuring its resultant shear rate for which viscosity is the ratio of one to the other. However if the reverse is opposite i.e. applying shear rate and measuring shear stress Newton's law of viscosity still holds - this fundamental theory forms the basis of the operation of rheological instruments (viscometer or rheometer) which are often classified as either controlled shear rate or controlled shear stress equipment. In this text, a viscometry[96] is used for viscosity measurement and oscillatory rheology[97] is used to determine elastic stress and viscous modulus of samples.

Controlled Strain Shear Rheometer - Oscillatory Shear Measurement

Structured fluids i.e. liquid crystalline samples, exhibit viscoelastic properties (Barnes 2000) In this text, a controlled-strain rheometer is employed to elucidate the viscoelastic properties of liquid crystalline samples.

The application of sinusoidal varying stress to a sample would induce sinusoidally varying strain response (Figure 3-20 and Figure 3-21).

[95] Shear strain rate
[96] Rotational deformations
[97] Oscillatory deformations

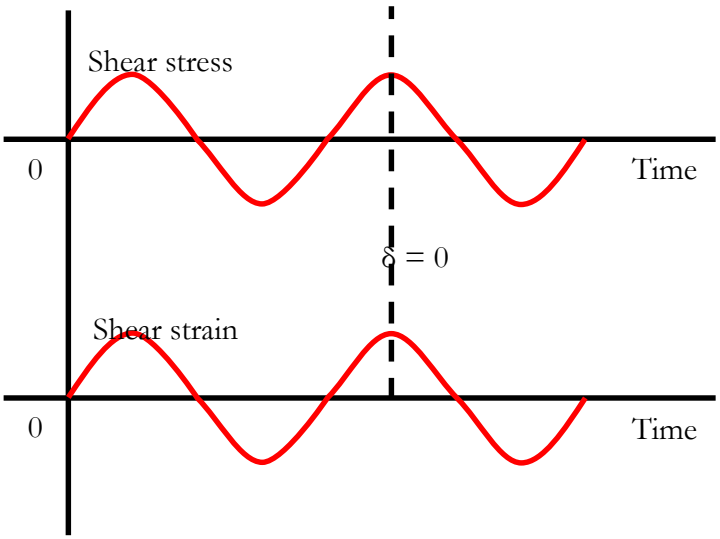

Figure 3-20: Schematic (sinusoidal wave) representation of the strain response of a solid subjected to stress

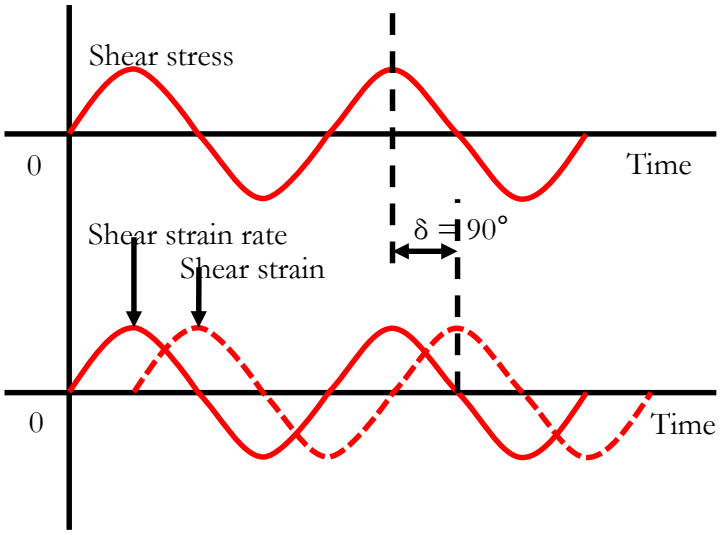

Figure 3-21: Schematic (sinusoidal wave) representation of the strain response of a liquid subjected to stress

For a Hookean solid (Figure 3-18), Shear Stress = Shear Strain × G[98] hence for a pure solid, the strain is controlled by the shear stress absolutely - therefore a consideration of such sine wave[99] would indicate strain response to be in phase with the applied stress (phase angle = 0°) as shown in Figure 3-20 - for this, strain will be at a maximum/zero when stress is at a maximum/zero respectively.

In the case of a Newtonian fluid (Figure 3-19), Shear Stress = Shear Strain Rate × Viscosity[100]. For this liquid the strain rate is proportional to the applied stress while the strain is out of phase

[98] Material constant [modulus]
[99] 360°
[100] A constant at a certain temperature and pressure

(phase angle = 90°) as illustrated in Figure 3-21. When the strain rate is at a maximum/zero, the rate of change of strain will be at zero/maximum respectively – resultant strain is totally out of phase to the applied stress.

Stated earlier is the fact that Hooke's law relates strain to stress via a constant 'G' (modulus). In oscillatory experiments, the stress and strain are constantly changing hence any number of instantaneous values can be considered to obtain a value for viscoelastic modulus (G*) also referred to as the complex modulus - obtained from the ratio of the stress amplitude to the strain amplitude.

This modulus is the sum of the elastic component modulus (G' – storage modulus)[101] and the viscous component (G" – loss modulus)[102]. Complex modulus is therefore defined as;

$$G^* = G' + iG'' \qquad [3.4]$$

By measuring the ratio of the stress to the strain (G*) as well as the phase difference between the two (delta,δ) – G' and G" can be defined in terms of sine and cosine functions as shown below;

$$G' = G^* Cos\delta \qquad [3.5]$$

$$G' = G^* Sin\ \delta \qquad [3.6]$$

Worth mentioning at this stage is that although elastic modulus has been discussed above – no elastic modulus data is shown in this work – only viscous modulus data is discussed. Literature review on elastic modulus has been included because equipment used records this data alongside the viscous modulus.

Controlled Strain Shear Viscometer – Brookfield Viscosity Measurements

Brookfield rotational viscometer measurement method provides a quick, reproducible qualitative means of assessing composite viscosity i.e. with respect to quality control of a batch of liquids etc. It is used in this text to assess the bulk viscosity of liquid crystalline samples.

The technique measures composite viscosity by using a spindle T-bar geometry driven by a motor through a calibrated spring (Figure 3-22) - the deflection of the spring represents a measure of the samples viscosity. The resistance to flow (indicated by the degree to which the

[101] Signifying elastic storage of energy since strain is recoverable in an elastic solid
[102] Describe viscous dissipation which is the loss of energy through permanent deformation in flow

spring winds up) is proportional to the spindle's rotational speed and is related to the spindle's geometry (Brookfield 2000).

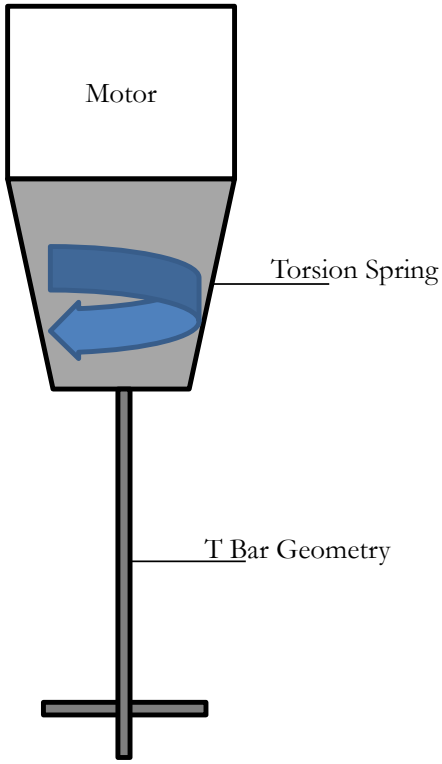

Figure 3-22: Schematic diagram of a Brookfield-type viscometer fitted with a T-bar geometry.

It is worth mentioning at this stage that the viscosity rotational speed is occasionally referred to as "shear rate" when T-bar geometry are used – this is incorrect as mathematical models are not available for obtaining viscosity functions using T-bar spindles (Brookfield 2000). This technique is used as a qualitative measure of liquid crystalline samples response to process variables relative to samples apparent viscosity

3.4.2 Microscopy

Liquid crystals are anisotropic in nature hence they demonstrate birefringent (possessing two indices) of refraction properties. The refractive index is a dimensionless number describing the speed of light in the medium. It is defined as;

$$n = \frac{c}{v} \qquad [3.7]$$

where

n	refractive index	_
c	speed of light in a vacuum	m/s
v	speed of light in the substance	m/s

Interaction of plane-polarised light with such birefringent (double refracting) specimen produces two individual rays termed the ordinary and extraordinary ray which travels with different velocities and in different directions hence different refractive (Robinson & Bradbury 1992; Stoiber & Morse 1994; Wood 1977). The distance of separation between both the ordinary and extraordinary ray increases with increasing crystal thickness (Davidson & Abramowitz 2002).

The two independent refractive indices are thus quantified in terms of their birefringence (B) which is a measure of the difference in refractive index and is defined as (Davidson & Abramowitz 2002);

$$B = \left| n_{high} - n_{low} \right| \qquad [3.8]$$

where

B	birefringence	_
n_{high}	largest refractive index	_
n_{low}	smallest refractive index	_

Optical (Light) Microscopy - Polarising Microscopy

Polarising light microscopy (Figure 3-23) is used extensively in identification of mesophases liquid crystals – it exploits anisotropy properties of liquid crystals specimens to reveal information in regards to its structure and composition (Demus et al. 1997; Gary & Goodby 1984; Gennes de & Prost 1974; Hartshorne 1974a, 1974b).

Like all anisotropic phases, lamellar mesophases display distinct optical textures when viewed under an optical microscope. Typically, the texture is "streaky" or mosaic like and resembles the marbling in freshly cut steak - also they can fold into vesicles (spherical globules) typically MLV (liposomes), exhibiting characteristic "Maltese cross" textures (Holberg, Shah & Schwuger 2002). Such textures are as a result of anisotropic specimen's ability to rotate plane polarised light.

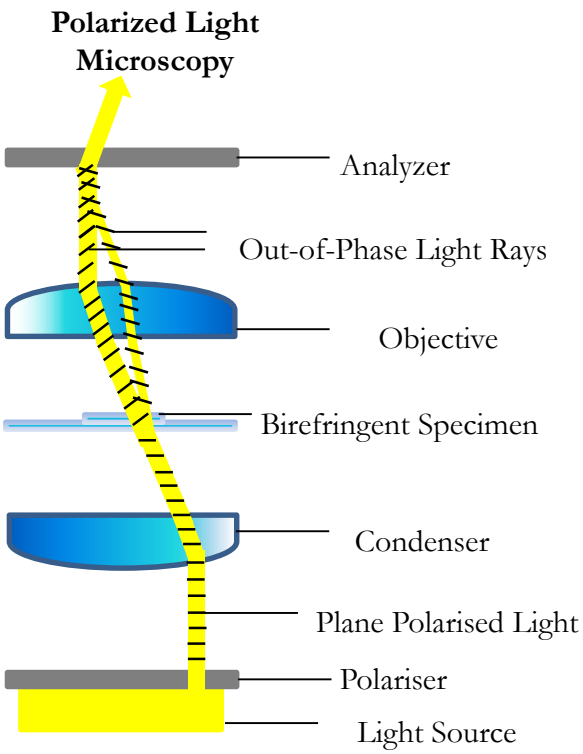

Figure 3-23: Schematic illustration of microscope configuration for birefringent specimen observation under cross polarised illumination redrawn from(Davidson & Abramowitz 2002)

In a polarised light microscope (Figure 3-23); white light through the polariser is planed polarised and concentrated onto the birefringent specimen by the condenser - emergent rays from the specimen interfere when they are recombined in the analyser, subtracting some of the wavelengths of white light, thus producing a myriad of tones and colour (Davidson & Abramowitz 2002).

3.4.3 Scattering I

X-Ray Scattering

X-ray diffraction has been used extensively (Figueiredo Neto & Salinas 2005; Kumar 2001b; Luzzati 1968b; Luzzati et al. 1957, 1960) to study liquid crystalline phases structures (i.e. molecular arrangement) due to their definite level of order and because the wavelength (λ) of X-rays is comparable to their atomic size. The planes are oriented at an angle that satisfy Braggs law (Figure 3-24) – which states that x-ray reflected from adjacent atomic planes separated by a distance (d) of a crystal interfere constructively when the path difference between them is an integer multiple of the wavelength (λ) i.e. $2d \sin\theta = n\lambda$ where n, an integer is the order of the

reflection – the reflected rays makes an angle of 2θ with the direction of the incident beam (Kumar 2001b).

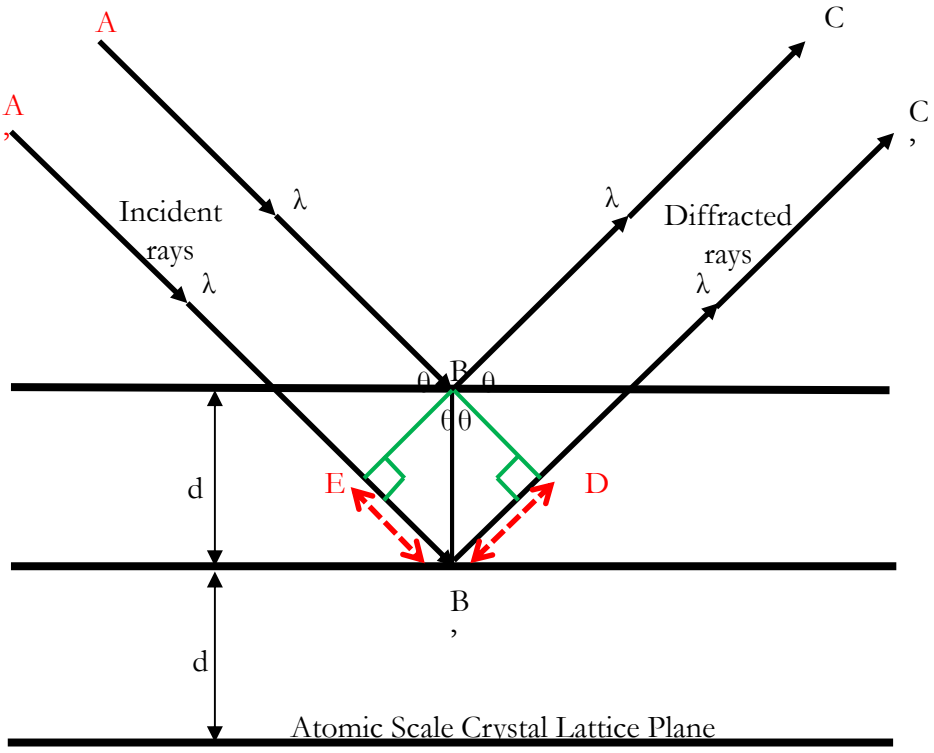

Figure 3-24: Schematic diagram outlining the principles of Bragg's law reflection redrawn from - (Meiser & Laidler 1982)

X-rays are electro-magnetic waves just like "ordinary" visible light. But the wavelength is much shorter (< 0.3 nm) than that of visible light (approx. 500 nm) which when interacted with matter (i.e. crystalline samples) are either absorbed and transferred to other forms of energy i.e. heat or scattered thus possessing a different wavelength than the incident radiation (Hubbell & Overbo 1979; Hubbell et al. 1975; Schnablegger & Singh 2011). The scattering pattern is detected and thus provides information about the materials molecular structure – the interference patterns detected can be constructive (in phase), destructive (out of phase) or somewhere in between depending on the observation angle 2θ, the orientation and the distance r of the light emitting atoms from each other (Schnablegger & Singh 2011).

Bragg's (Cruickshank, Juretschke & Kato 1992) work shows X-rays are diffracted at certain angles - dependent on the wavelength and the interplanar spacing of crystalline structure as shown in Figure 3-24: incoming incident ray at an angle θ and wavelength λ are reflected by

atomic crystal lattice plane in the same way a mirror reflects light (hence θ incident = θ reflection).

In explaining the interference pattern between X-ray scattering by crystalline samples – If reflected beams are not absorbed by the crystal i.e. if it is reflected from the surface atom (i.e. at point B) at each atomic plane, Bragg's law states that when reflected rays are in phase with each other they add to give diffracted beams through constructive interference (mirror analogy – hence the incident and reflected rays travels the same distance with similar reflecting angles).

To explain this, consider two x-rays (A & A') incident on two different atomic lattice planes of a substance as shown in Figure 3-24. The reflected rays forms an angle θ with the lattice plane – secondly X-ray A' travels an extra distance EB' + B'D with respect to X-ray A. For constructive interference of the reflected rays, the measure of the extra distance EB' + B'D should be equal to the whole number of wavelengths according to;

$$EB' + B'D = n_1 \lambda \qquad [3.9]$$

Where λ is the wave length of the incident light

$$EB' = B'D \qquad [3.10]$$

$$\therefore 2 \times E B' = n_1 \lambda \qquad [3.11]$$

In order to relate the interplanar spacing between atomic planes, d with the wavelength λ, and the application of trigonometry to triangle BEB' (sin θ = opposite/hypotenuse).

$$\sin\theta = E B'/d \qquad [3.12]$$

Combining equations 3.11 and 3.12,

$$2 \sin\theta = n_1 \lambda \qquad [3.13]$$

Hence,

$$n_1 \lambda = 2d \sin\theta \qquad [3.14]$$

Which is Bragg's law – where n is the order of diffraction, λ is the wave length of the ray used, d interplanar spacing between identical crystal planes and θ is half the diffraction angle of the Bragg's reflection.

The d spacing can then be related to the position of maxima intensities with respect to the crystal (Figure 3-25) – considering the incident and reflected rays on the atomic plane as wave vectors of K and K_O as shown in Figure 3-25, the detector captures the intensities of the diffracted waves therefore the magnitude of these vectors can be taken as (Birkholz 2005);

$$|K| = |K_O| = |2\pi/\lambda| \quad [3.15]$$

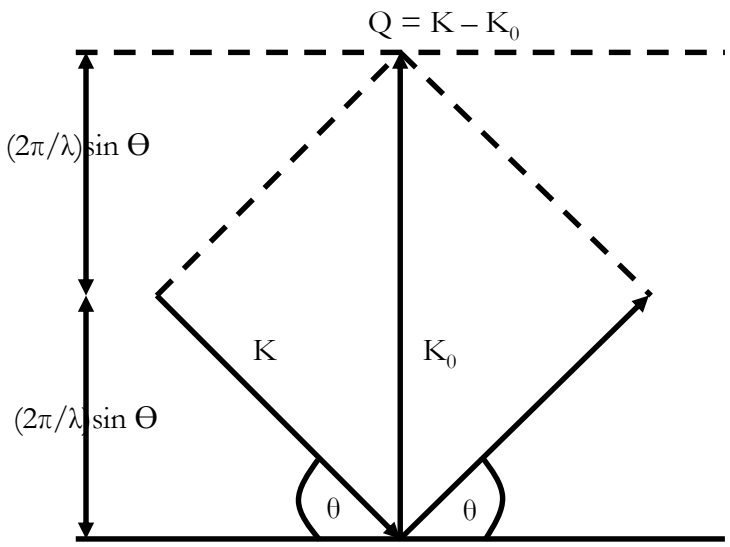

Figure 3-25: Geometry of scattering vector construction (Birkholz 2005)

A scattering vector Q related to K and K_O is thus defined as displayed in Figure 3-25 – with the scattering possessing the dimensionality of an inverse length, while its direction points along the bisection of incident and reflected beam. Q can then be related to K and K_O as

$$Q = K - K_O \quad [3.16]$$

Hence

$$Q = 4\frac{\pi \sin\theta}{\lambda} \quad [3.17]$$

The d spacing of a sample can then be obtained from the intensities and Braggs law using Equation below

$$Q = 2\pi/d \quad [3.18]$$

3.4.4 Thermal Transition

Differential Scanning Calorimetry (DSC)

DSC: a thermo-analytical tool used to access thermal (phase) transitions of substances i.e. polymers, liquid crystals (Arnold 1966; Barrall & Johnson 1974; Brown & Shaw 1957; Herbert 1967; Kumar 2001a), proteins, gels, peptides (Hohne, Hemminger & Flammersheim 2003). It works by measuring the temperatures and heat flows associated with phase transitions due to changes in physical and chemical properties in materials as a function of time and temperature in a controlled atmosphere. A range of thermodynamic parameters (Figure 3-27) can be obtained from such measurements i.e. glass transition temperature (T_g), crystallisation temperature (T_C), melting temperature (T_M).

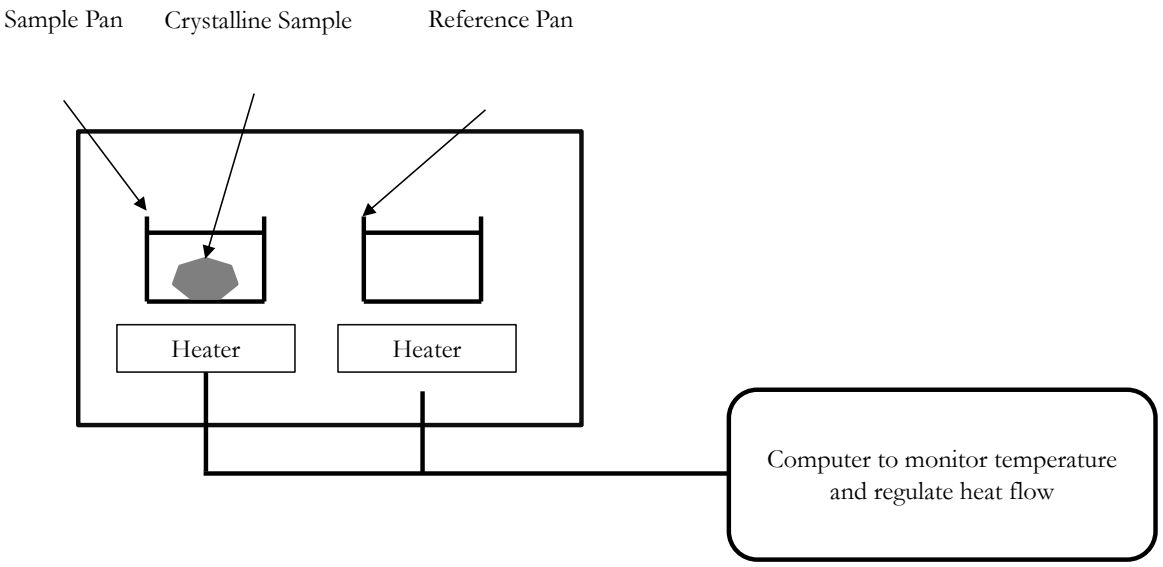

Figure 3-26: A schematic diagram of a typical DSC setup

Principle of operation of the device is schematically shown in Figure 3-26 two identical hermetically sealed steel pans are sited on a stage connected to a furnace via a common heat flow path. The sample to be tested is place in one of the two pans while the second is left empty as a reference pan. The pans are then heated at a desired rate based on a set protocol written by the user. For the duration of the experiment both samples are maintained at the same temperature.

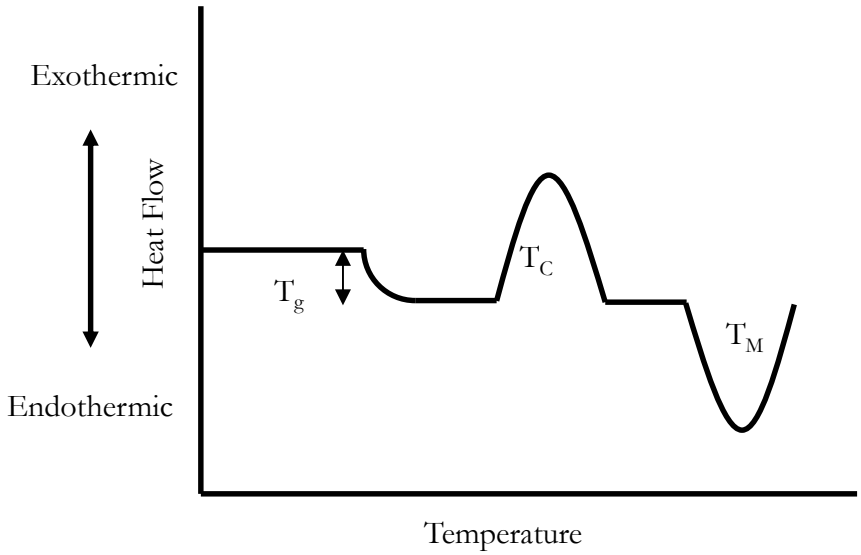

Figure 3-27: A schematic showing the features of a DSC curve

The underlying principle of DSC technique is thus; when a sample undergoes physical transformation i.e. phase transition, there is a change in heat flow to it (more or less) when compared to a reference which is dependent on whether the process is exothermic or endothermic i.e. as a solid sample melts to a liquid it will require more heat flowing to the sample to increase its temperature at the same rate as the reference due to an endothermic phase transition from a solid to liquid likewise, as a sample undergoes an exothermic processes (i.e. crystallization) less heat is required to raise the sample temperature. Transitions are identified via the plot of heat flow as a function of temperature (Figure 3-28).

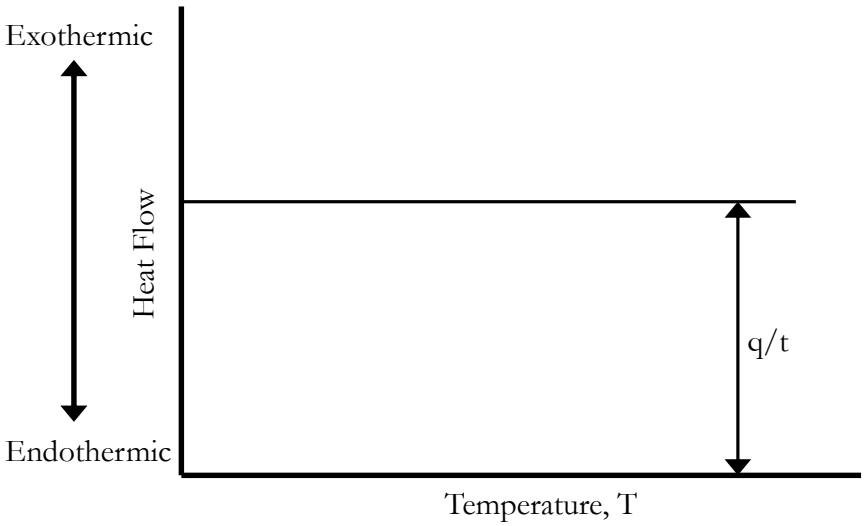

Figure 3-28: A schematic DSC curve showing heat flow q/t as a function of temperature, T.

By observing the difference in heat flow between the sample and reference, differential scanning calorimeters are able to measure the amount of heat absorbed or released during phase transition.

Heat flow, is the heat supplied per unit time t (q/t) and the heating rate is the change in temperature per unit time t (ΔT/t). The heat supplied per unit increase in temperature is obtained by dividing the heat flow by the heating rate;

$$\text{heat flow} = q/t \quad [3.19]$$

$$\text{heating rate} = \Delta T/t \quad [3.20]$$

$$\text{heat capacity} = \frac{q/t}{\Delta T/t} = \frac{q}{\Delta T} = C_p \quad [3.21]$$

Therefore $q = C_p \Delta T$ or in a differential form

where

C_p	specific heat	J/g °C
T	temperature	°C
q	Heat	J
q/t	heat flow	heat flow (J/min)mW (mJ/sec)
T/t	heating rate	(°C/min).

Surfactant liquid crystals and polymers melt at specific temperature. Melting is a consequence of loss of order within a system as a result of heat absorption resulting in a quantity termed latent heat of melting. When melting temperature is reached, the sample temperature will not rise until all the system has melted. This ensures that increased amount of heat is supplied to the sample to raise the temperature (at similar rate to the reference pan). This extra heat flow required during melting shows up as a dip in the DSC curve (Figure 3-27). The area under the curve gives the latent heat of melting and the apex of the dip is consequently the samples melting temperature.

3.4.5 Scattering II

Laser Light Scattering

Scattering techniques provide the most obvious methods for obtaining quantitative information on size, shape and structure of colloidal particles, since they are based on interactions between

incident radiations[103] and particles (Eastoe 2002b). Information on the size ranges colloidal dispersions (i.e. 10 Å – 10000 Å)[104] can therefore be obtained if the incident wavelength falls within this range.

Laser (light) diffraction technique/equipment[105] relies on the fact that diffraction angle is inversely proportional to particle size. Such instrument consists of a source laser and a means of passing the samples through the laser beam[106] - the detector is usually a slice of photosensitive silicon with a number of discrete detectors (Rawle 2002).

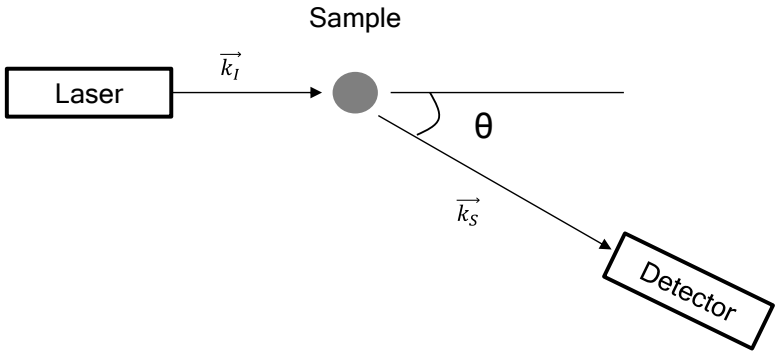

Figure 3-29: Schematic of a light scattering experiment redrawn from (Borkovec 2001)

Such equipment according to (Rawle 2002)use full Mie theory which completely solves equations for interaction of light with matter by assuming the volume of the particle once the refractive indices of the material and medium is specified as well as the absorption part of the refractive index.

The sample, schematically shown in Figure 3-29 is illuminated by an incident beam of wave vector $\overrightarrow{k_I}$ from a laser and the scattered light with wave vector $\overrightarrow{k_S}$ is monitored at a known scattering angle θ by a detector – as the scattering angle is varied, constructive and destructive interferences of the scattered light occurs and the angular dependence contains information about particle size and shape (Borkovec 2001).

[103] I.e. light, X-ray or neutrons
[104] 0.001 μm – 1 μm
[105] Mastersizer 2000 particle size analyser (Malvern Instruments, Malvern, UK)
[106] Intense light of a fixed wavelength He-Ne gas lasers λ = 0.632 μm are the most common

3.5 Characterisation Techniques (Experimental)

This Section describes the various scientific protocol employed in characterising all the samples produced within this text – details of the protocols used are not discussed as they are commercially sensitive.

3.5.1 Rheology

Controlled Strain Shear Rheometer - Oscillatory Shear Measurement

Oscillatory shear measurements were performed with the ARES-G2 (TA Instruments, USA) using parallel plate geometries. In this text, oscillatory shear experiments are used to assess the response of structured fluids in the linear viscoelastic region (LVR). The device also outputs plots of elastic stress as function strain amplitude making it possible to quantify sample yield stress as demonstrated by (Yoshimura & Prud'homme 1987).

Sample is loaded in a systematic way - material is placed between two parallel plates. The lower plate applies a sinusoidal deformation to samples via oscillating at a set fixed frequency and the response torque is recorded – a response, which is as a result of the stress transmitted through the sample.

Controlled Strain Shear Viscometer - Brookfield Viscosity Measurements

Brookfield viscosity measurements were conducted using a Brookfield DV-II+ Pro Viscometer (Brookfield Engineering Laboratories, USA) to obtain T-bar viscosities as T-bars (B or E) shown in (Figure 3-22) is rotated at a fixed speed.

The viscosity range of T-bar E is larger than T-bar B (Table 3-4) – this was used for the thicker (more concentrated) samples due to its range.

Table 3-4: Table showing T-bar geometry dimensions and viscosity measurement range.

Spindle	T-bar (cross bar) length, mm	Maximum Viscosity Measureable, Pa.s
T-B	36.4	800
T-E	15.3	10000

The T-bar geometry cuts through the sample – measuring viscosity of the fluid (i.e. Hair Conditioner) in the sample container at a fixed rotation speed as the spindle (T-bar geometry) is

being immersed by the action of the Helipath stand. The Brookfield Helipath Stand is designed to slowly lower (approx. 0.5 mm/s) or raise the Brookfield viscometer so that fresh material is available for measurement.

Transient Viscosity Measurements

Experimental protocol is commercially sensitive and cannot be discussed.

3.5.2 Microscopy

Optical (Light) Microscopy

For optical light microscopy analysis, samples were examined using an Olympus BX50 Phase POL Darkfield microscope (Olympus, US) light microscope in two modes namely – cross polarised and bright field illumination. This was used to examine birefringent entities within the underlying microstructure of samples. A range of objective lenses (10X, 20X, 40X, and 100X) were also available.

For sample analysis, a small droplet of the sample was placed onto a microscope slide and a coverslip placed carefully on top and pressed on lightly - Images of the samples microstructure are taken using a digital camera connected to the microscope. The digital camera is also connected to the desktop computer.

Optical (Light) Hot Stage Microscopy

Thermal transitions of samples were monitored using a second light microscope – Zeiss AxioVision Polarising microscope (Carl Zeiss MicroImaging, Germany). The microscope is fitted with a Linkam heated stage capable of controlling the temperature in the range of -20 to 120 °C with an accuracy of ±0.1 °C.

For sample analysis, a small droplet of the sample was placed onto a microscope slide and a coverslip placed carefully on top and pressed on lightly. The sample is subjected to a temperature ramp at a set rate of change (in °C/min) up to a maximum and then back down - Images of the changes to samples microstructure at different temperatures are captured using a digital camera connected to the microscope. The digital camera is also connected to the desktop computer.

3.5.3 Scattering I

X-Ray Scattering

SAXS measurements were performed on the I22 beamline at the Diamond Light Source synchrotron (Didcot, UK) by Cesar Mendoza[107]. The beamline operated at energy of 12.4 keV and a wavelength of 1 Å. The SAXS detector was placed at a set distance from the sample. Further details on beam line characteristics can be found in (Diamond 2014; Gurun et al. 2011; Gurun, Thio & Bucknall 2009).

Samples were subjected to quantitative analysis at the Diamond Light Source - samples are loaded into individual cells via 10ml syringe using a needle cut down to 1mm length to limit further post processing of the sample.

3.5.4 Thermal Transition

Differential Scanning Calorimetry (DSC)

DSC characterisation was performed to study the thermal behaviour of the samples using the Discovery DSC (TA Instruments, USA). Samples weighed (mg) using a microbalance and placed in a hermetically sealed pan - were placed in an automated sample holder carousel[108] -

A single heat and cool cycle up to a set maximum temperature at set rate in (°C/min) thus enabling phase transition to be assessed – heating/cooling cycles is conducted at set rate up to a maximum temperature with respect to an empty steel pan as reference (Figure 3-26). Analysis on the DSC curve is performed using the in-built analytical software.

3.5.5 Scattering II

Laser Light Scattering

A Mastersizer 2000 particle size analyser (Malvern Instruments, Malvern, UK) was used to measure the droplet size distributions of emulsion samples - resulting patterns are used to generate droplet size distribution presented as discrete volume distribution

The analysis model selected was a general purpose model able to measure droplet classes[109] within the size range of 0.020 to 2000 μm. The sized distribution calculations are based on Mie

[107] Unilever Staff
[108] Up to 50 samples can be loaded

theory alongside the standard software applied to the instrument. Relative refractive indices used were 1.469 for the sunflower oil dispersed phase and 1.330 for the continuous water phase with an imaginary component of the Sun Flower Oil (SFO) adsorption index of 0.001 were the required input for the operating procedure set up using the Malvern analysis software.

A typical size distribution (volume based) report from the Malvern outputs droplet diameter corresponding to cumulative volume fractions of D (v, 0.5), D (v, 0.1) and D (v, 0.9) for which D (v, 0.5) is the size of the particle at which 50% of the sample is smaller than and 50 % is larger than this size while D (v, 0.1) and D (v, 0.9) gives the size of the particles for which 10 % and 90 % of the sample is below this size respectively. Volume distribution in each class is reported and values such as D [4,3] & D [3,2] which are the volume mean diameter & surface area mean diameter respectively are calculated. For this work, only the D [4,3] data is used for emulsion analysis.

[109] The drops are classed using diameter in 100 geometrically spaced classes spanning the size range above (0.020 to 2000 μm).

3.6 References

- Arnold, H. (1966) 'Heat Capacity and Enthalpy of Transition of Aromatic Liquid Crystals', *Molecular Crystals and Liquid Crystals*, vol. 2, no. 1 - 2, p. 63.
- Balzer, D., Varwig, S. & Weihrauch, M. (1995) 'Viscoelasticity of Personal Care Products', *Colloids and Surfaces A: Physicochemical and Engineering Aspects*, vol. 99, pp. 233 - 246.
- Barnes, H.A. (2000) *A Handbook of Elementary Rheology*, Institute of Non--Newtonian Fluid Mechanics University of Wales, Aberystwyth, Wales.
- Barrall, E.M. & Johnson, J.F. (1974) Thermal Properties of Liquid Crystals, in G.W. Gray & P.A. Winsor (eds), *Liquid Crystals and Plastic Crystals*, John Wiley and Sons, London.
- Birkholz, M. (2005) *Thin Film Analysis by X-Ray Scattering*, Wiley-VCH, Weinheim.
- Bohlin, I. (1994) *A Basic Introduction To Rheology*, Britain
- Bongers, P.M.M., Egan, M.J. & Irving, G.N. (2013) *Method For Production Of Structured Liquid And Structured Liquid*, Great Britain.
- Borkovec, M. (2001) Measuring Particle Size by Light Scattering, in K. Holberg, D.O. Shah & M.J. Schwuger (eds), *Handbook of Applied Surface and Colloid Chemistry Volumes 1 - 2: Part V. Analysis and Characterization in Surface Chemistry*, John Wiley & Sons, Ltd, England.
- Brookfield (2000) *More Solutions To Sticky Problems: A Guide To Getting More From Your Brookfield Viscometer*, Brookfield Engineering Labs., Inc., United Kingdom.
- Brown, G.H. & Shaw, W.G. (1957) 'The Mesomorphic State - Liquid Crystals', *Chemical Reviews*, vol. 57, no. 6, pp. 1049 - 1157.
- Cruickshank, D.W.J., Juretschke, H.J. & Kato, N. (1992) *P.P. Ewald and his Dynamical Theory of X-ray Diffraction*, Oxford University Press,, USA.
- Davidson, M.W. & Abramowitz, M. (2002) *Encyclopedia of Imaging Science and Technology*, John Wiley & Sons, Inc.
- Demus, D., Goodby, J.W., Gray, G.W., Spiess, H.-W. & Vill, V. (1997) *Handbook of Liquid Crystals*, Wiley, New York.
- Diamond (2014) *Welcome To I22: Small Angle Scattering & Diffraction* [Online], Diamond, Available from: http://www.diamond.ac.uk/Beamlines/Soft-Condensed-Matter/small-angle/I22.html (Accessed).

- Eastoe, J. (2002) Scattering Techniques, in T. Cosgrove (ed.), *Colloid Science: Principles, Methods and Applications*, Blackwell Publishing, England.
- Figueiredo Neto, A.M. & Salinas, S.R.A. (2005) *The Physics of Lyotropic Liquid Crystals: Phase Transitions and Structural Properties*, Oxford University Press.
- Gary, G.W. & Goodby, J.W. (1984) *Smetic Liquid Crystals, Textures and Structures*, Leonard Hill, Philadelphia.
- Gennes de, P.G. & Prost, J. (1974) *The Physics of Liquid Crystals*, Oxford University Press, London.
- Gurun, B., Bucknall, D.G., Thio, Y.S., Teoh, C.C. & Harkin-Jones, E. (2011) 'Multiaxial Deformation of Polyethylene and Polyethylene/Clay Nanocomposites: In Situ Synchrotron Small Angle and Wide Angle X-Ray Scattering Study', *Journal of Polymer Science Part B: Polymer Physics*, vol. 49, no. 669 - 677.
- Gurun, B., Thio, Y.S. & Bucknall, D.G. (2009) 'Combined Multiaxial Deformation of Polymers With In Situ Small Angle and Wide Angle X-ray Scattering Techniques', *Review of Scientific Instruments*, vol. 80, no. 123906, pp. 123906-123901 - 123906-123906.
- Hartshorne, N.H. (1974a) *The Microscopy of Liquid Crystals*, Microscope Publication Ltd, London.
- Hartshorne, N.H. (1974b) Optical Properties of Liquid Crystals, in G.W. Winsor & W.P. A. (eds), *Liquid Crystal and Plastic Crystals*, John Wiley and Sons, London.
- Herbert, A.J. (1967) 'Transition Temperatures and Transition Energies of The P-N-Alkoxy Benzoic Acids, from N-Propyl to N-Octadecyl', *Transactions of the Faraday Society*, vol. 63, pp. 555 - 560.
- Hohne, G., Hemminger, W.F. & Flammersheim, H.J. (2003) *Differential Scanning Caloriemetry*, 2nd edn, Springer.
- Holberg, K., Shah, D.O. & Schwuger, M.J. (2002) Identification of Lyotropic Liquid Crystalline Mesophases, in S.T. Hyde (ed.), *Handbook Of Applied Surface And Colloid Chemistry Volume 1 - 2*, John Wiley & Sons Ltd,, England, pp. 299 - 321.
- Hubbell, J.H. & Overbo, I. (1979) 'Relativistic Atomic Form Factors and Photon Coherent Scattering Cross Sections', *The Journal of Physical Chemistry*, no. 8, pp. 69 - 105.
- Hubbell, J.H., Veigele, J.W., Briggs, E.A., Brown, R.T., Cromer, D.T. & Howerton, R.J. (1975) 'Atomic Form Factors, Incoherent Scattering Functions, and Photon Scattering Cross Sections', *The Journal of Physical Chemistry*, no. 4, pp. 471 - 538.

- Kumar, S. (2001a) Caloriemetric Studies, in C.W. Garland (ed.), *Experimental Study of Physical Properties and Phase Transitions*, Cambridge University Press, New York.
- Kumar, S. (2001b) *Liquid Crystals: Experimental Study of Physical Properties and Phase Transitions*, University Press, Cambridge, United Kingdom.
- Luzzati, V. (1968) *In Biological Membranes*, Chapman, Academic Press, New York.
- Luzzati, V., Mustacchi, A., Skoulious, A. & Husson, F. (1957), *Nature*, vol. 180, p. 600.
- Luzzati, V., Mustacchi, A., Skoulious, A. & Husson, F. (1960) 'La structure des colloïdes d'association. I. Les phases liquide-cristallines des systèmes amphiphile-eau', *Acta Crystallographica*, vol. 13, pp. 660 - 667.
- McCabe, W.L., Smith, J.C. & Harriot, P. (1993) *Unit Operations of Chemical Engineering*, 5th ed edn, Mc Graw-Hill.
- Meiser, J.H. & Laidler, K.J. (1982) *Physical Chemistry*, The Benjamin/Cummings Publishing Company, California.
- Rawle, A. (2002) 'The Importance Of Particle Sizing To The Coatings Industry Part 1: Particle Size Measurement', *Advances In Colour Science and Technology*, vol. 5, no. 1, pp. 1 - 12.
- Robinson, P.C. & Bradbury, S. (1992) *Qualitative Polarized-Light Microscopy*, Oxford Science Publications, New York.
- Schnablegger, H. & Singh, Y. (2011) *The SAXS Guide Getting Acquainted with The Principles*, Anton Paar GmbH, Austria.
- Stoiber, R.E. & Morse, S.A. (1994) *Crystal Identification with the Polarizing Microscope*, Chapman & Hall, New York.
- Wood, E.A. (1977) *Crystals and Light: An Introduction to Optical Crystallography*, 2nd Ed edn, Dover Publications, Inc., New York.
- Yoshimura, A.S. & Prud'homme, R.K. (1987) 'Response of An Elastic Bingham Fluid To Oscillatory Shear', *Rheologica Acta*, vol. 26, pp. 428 - 436.

Chapter 4

4 Process Design Studies; Structured liquid based on Model Hair Conditioners

Typical Hair Conditioner (H-C) formulation comprise of quaternary ammonium salts (QUAT), cationic surfactants (CS) and long chain fatty alcohol (FA) dispersed within water (Bongers, Egan & Irving 2013) - it is a dispersion of cationic surfactants and fatty alcohol in a continuous phase (water) - this forms the basic conditioning system termed lamellar gel. The lamellar aggregate structure is responsible for the bulk viscosity of the Hair Conditioner product alongside other minor ingredients such as polymer, thickener, etc. which also contribute to Hair Conditioner bulk viscosity. Equally bulk viscosity of Hair Conditioners will be highly dependent on process history and/or process routes i.e., the nature in which the process ingredients have been brought together as well as the equipment used.

Presently, not much is known (in the open literature) about the effect of process variables on the underlying microstructure of the lamellar phases formed by mixed QUAT/CS/FA/Water formulation mixtures which comprise the backbone of many commercial Hair Conditioners formulations. A better understanding of the links between processing equipment and the underlying microstructure for a particular system will be beneficial in the design/manufacture of Hair Conditioners that deliver enhanced benefits for the consumer and more importantly the environment.

The studies reported in this Chapter are performed against the backdrop of a "benchmark process" currently used in the manufacture of some commercial Hair Conditioners based on the QUAT/CS/FA/Water system which has been extracted from the patent literature (Bongers, Egan & Irving 2013). The specifics of the manufacture of the said benchmark is commercially sensitive so a full detailed manufacturing route is not discussed here but the effect of post processing this formulation and the effect of process temperature is discussed via a systemic evaluation.

A combination of analytical techniques are used to achieve the aims of this Chapter - Brookfield viscometer and control stress rheometer measurements presented a means to assess the rheology of the samples produced in relation to microstructure, light microscopy presented a more

detailed representation of the qualitative nature of the microstructure in helping identify the various components of the underlying microstructure thus complimenting all rheological (viscometry and rheometry) measurements. Microscopic techniques such as bright field/cross polarised illumination as well as hot stage microscopy were used. DSC and SAXS analysis further complimented all analysis performed in helping identify phase transition temperatures and detect (quantitatively)/assess changes to lamellar d-spacing respectively.

4.1 Benchmark System: Model Hair Conditioner based on QUAT/CS/FA/Water

In order to understand the complex interaction of a model QUAT/CS/FA/Water system, it was first necessary to develop a simplified processing route to explore the variables of processing speed[110] and temperature on the underlying microstructure and viscosity.

A simplified batch process has been developed (Figure 4-1), which allows the manufacture of a hot dispersion of the QUAT/CS/FA/Water and actives to create a bulk sample of 'crude' Hair Conditioner emulsion[111] (Unilever confidential report) which can then be passed via an inline high shear dispersion unit.

The formulation / batch process employed here was set up to allow a close approximation of pilot plant benchmark products discussed in the patent literature (Bongers, Egan & Irving 2013) for which Brookfield T-bar B viscosity[112] was 200 Pa.s.

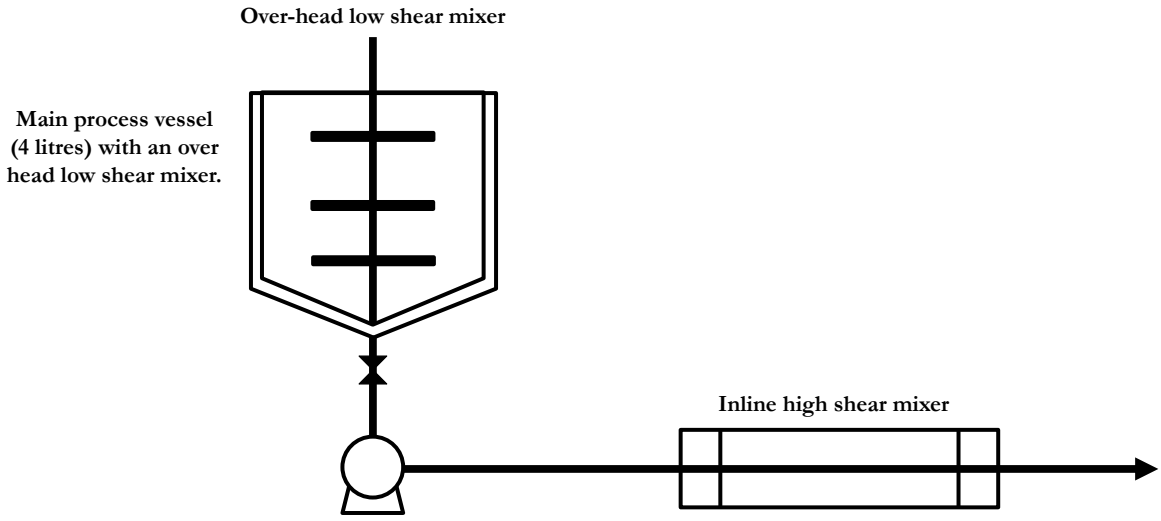

Figure 4-1: Schematic showing a conventional batch process set-up.

The main ingredients in the system in question include QUAT/CS/FA. The materials are all used as supplied without further modification and typically required melting at elevated temperatures to aid solubilisation (typically at the melting temperature of the cationic CS/FA.

[110] I.e. mixing intensity
[111] Hot premix (emulsion)
[112] Brookfield T-bar Spindle operated at 0.5 rpm

The crude HC lamellar gel was prepared utilising a proprietary methodology (Unilever confidential report) detailed in Appendix A and discussed briefly in (Bongers, Egan & Irving 2013) which involved melting the FA in a 4 litre batch mixer equipped with anchor stirrer and turbine (Figure 3-16), to which was added the QUAT/CS, and water to form a lamellar dispersion. The cationic surfactants alone form a micellar solution - the addition of the fatty alcohol generates the lamellar gel due to changes in the packing parameter of the surfactants. Process temperature = 'T4 °C'. At this point the concentration of the lamellar dispersion is 'AA % QUAT/CS/FA/Water'.

The remaining minor ingredients are then blended into the system under low shear thereby diluting the concentrated lamellar dispersion to predetermined solids loading (the standard product [1.0H-C[113]]). This is followed by a single pass discharge via an inline high shear mixer. At this point the concentration of the lamellar dispersion is 'BB % QUAT/CS/FA/Water' - this concentration is also the same concentration of the final product which will be used interchangeably as 1.0H-C in this Thesis.

The aim of the single pass discharge through the high shear mixer is to boost the product viscosity in the formulation.

4.1.1 Benchmark System – Manufacture

Actual process temperatures (T4 °C) during manufacture were within a tolerance of ± 2 °C as noticed on the temperature probe inserted in the process vessel.

4.1.2 Benchmark System – Analysis

Results and discussion of experiments aimed at reproducing the bench mark product after the work published by (Bongers, Egan & Irving 2013) for Hair Conditioners based on the 1.0H-C formulation – in this patent the viscosity of the manufactured benchmark was determined by a Brookfield viscometer (Brookfield Engineering Laboratories, USA) fitted with a T-bar B spindle and operated at a fixed rotational speed. The benchmark material had a starting viscosity of 200 Pa.s after the material has been allowed to equilibrate[114].

4.1.2.1 Rheology

Brookfield T-bar B Viscosity

[113] Fully formulated Hair Conditioner product
[114] Approximately 24 hours after manufacture

Brookfield T-Bar B viscosity as a function of inline high shear mixer rotational speed for the 1.0H-C Hair Conditioner indicate that the model system is reproducible in current device set-up when the process ingredients is discharged through the inline high shear mixing head at approximately 7500 rpm as shown in Figure 4-2.

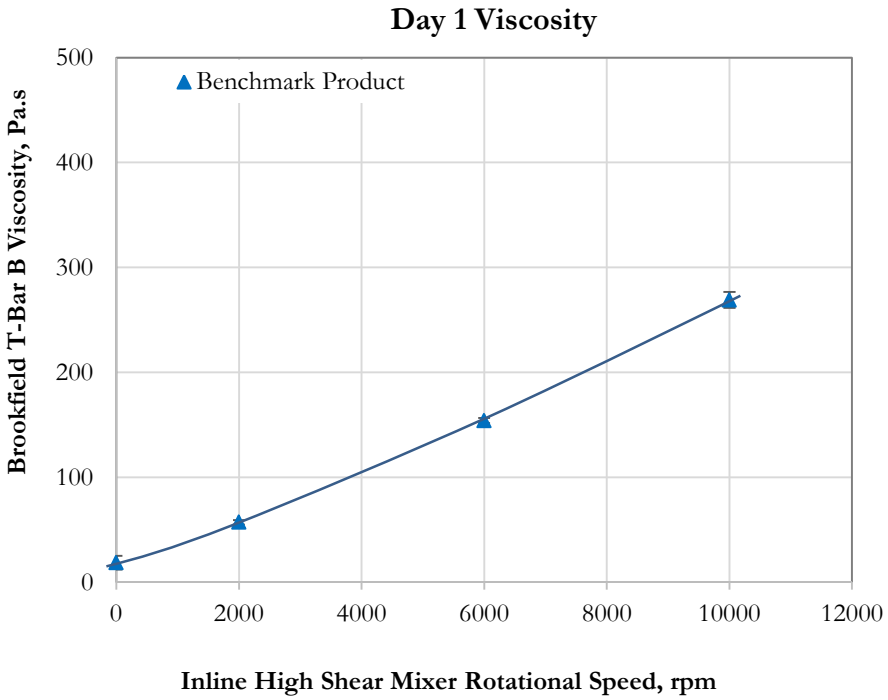

Figure 4-2: Brookfield T-Bar B viscosity as a function of inline high shear mixer rotational speed for 1.0H-C Hair for the benchmark system – process temperature = T4 °C

Figure 0-1 and Figure 0-2 in Appendix A shows the micrographs obtained from the 'AA % QUAT/CS/FA/Water' during manufacturing and Hair Conditioner products after single pass discharge through the high shear mixer respectively – although no mention has been made to the nature of the underlying microstructure in the patent, a review of the micrograph show that the underlying microstructure is a combination of [1] 'QUAT/CS' rich L_{β} microstructure and [2] 'FA' rich L_{β} microstructure – which has been formed in different proportions.

The notion of "QUAT/CS'/'FA' rich L_{β} microstructure formed in different proportion' will become clear to the reader at the end of this Chapter.

4.2 Process Design Studies - QUAT, CS, LA and FA and Water System (Solids Only)

The work discussed in this Section is based on an experimental program (Figure 4-3), designed to assess the effect of process variables on the lamellar dispersion produced (solids only) by the system in question (only QUAT/CS/LA/FA/Water) thereby testing a hypothesis. Solids only refers to just a dispersion of the QUAT/CS/LA/FA/Water – no minor ingredients included in the mixture. This dispersion is manufactured at AA %.

The hypothesis is based on the fact that microstructures are formed on a nano scale via the control of macro-scale parameters (process history) i.e. temperature, mixing intensity, process flow-rate etc., and formulation – investigating the effects of these controllable aspects of liquid-liquid mixing on the system would help elucidate the effect of process variables on the formulation (raw materials) – understanding this link, presents opportunity for process optimisation, new product opportunities etc.

4.2.1 Experimental Program

A schematic of the factors considered in the experimental programme as well as the responses measured can be seen in Figure 4-3. The objective of the experimental design was to screen for the influence and magnitude of various process parameters on the underlying microstructure of the lamellar dispersion formed with the aim of building on and improving current knowledge base for such factors - in effect such knowledge would also enable optimisation studies to be conducted on the system.

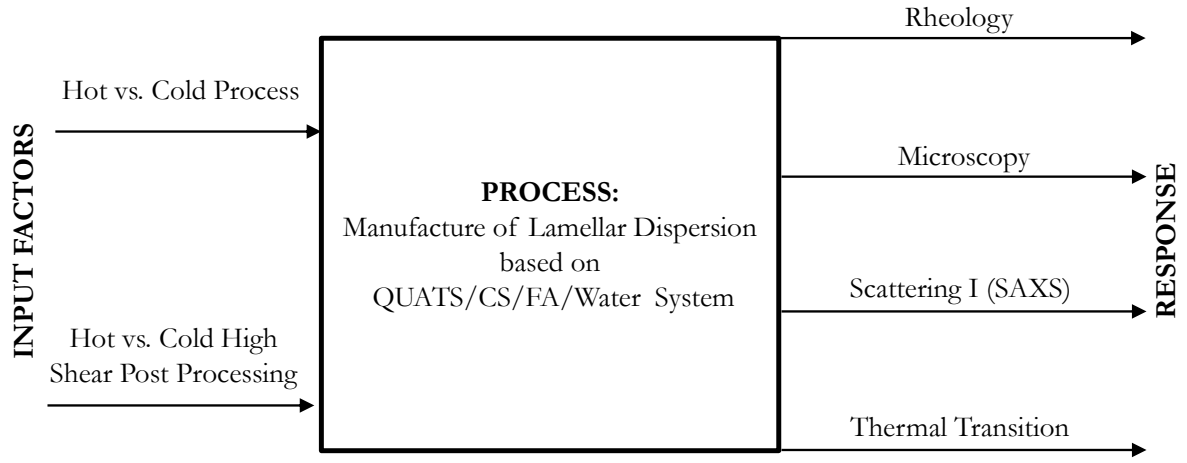

Figure 4-3: Schematic of experimental design for the manufacture of lamellar dispersion based on QUAT/CS/FA/Water System.

The experimental trials conducted assessed three input factors and subsequently measured the responses using a range of analytical tools to characterise and elucidate the effect of equipment and process variables on the underlying microstructure of QUAT/CS/FA/Water[115] system. The input factors considered included process temperature[116], route to manufacture of the lamellar system (hot vs. cold process)[117] and the impact of a high shear post processing operation[118]. The techniques used for microstructure assessment were rheology (rheometer and viscometer), optical microscopy, SAXS and DSC.

4.2.1.1 Experimental Matrix (Sample Preparation)

In order to access the impact process temperature and high shear post processing operation at [1] process temperature (Hot High shear post processing) and [2] at ambient temperature (Cold High shear post processing) on the system, the experimental matrix (Figure 4-4) was developed. The variables examined consisted of three temperatures alongside three high shear mixer rotational speeds. Samples were initially manufactured at low shear using the overhead low shear impeller – samples are then post processed at either process temperature (termed hot high shear post processing) or ambient temperature (termed cold high shear post processing) at approximately 'Ambient °C' following jacket cooling of the contents in the process vessel.

[115] Hair conditioner base (solids only)
[116] Temperature at which the lamellar system is produced
[117] Temperature at which produced lamellar is sampled i.e. [1] at process temperature – 'hot process' and [2] at ambient temperature when lamellar is actively cooled to ambient temperature in the process vessel – 'cold process'
[118] Lamellar samples obtained from either the cold and hot process are subject to further processing (post process operation) through a high shear mixer

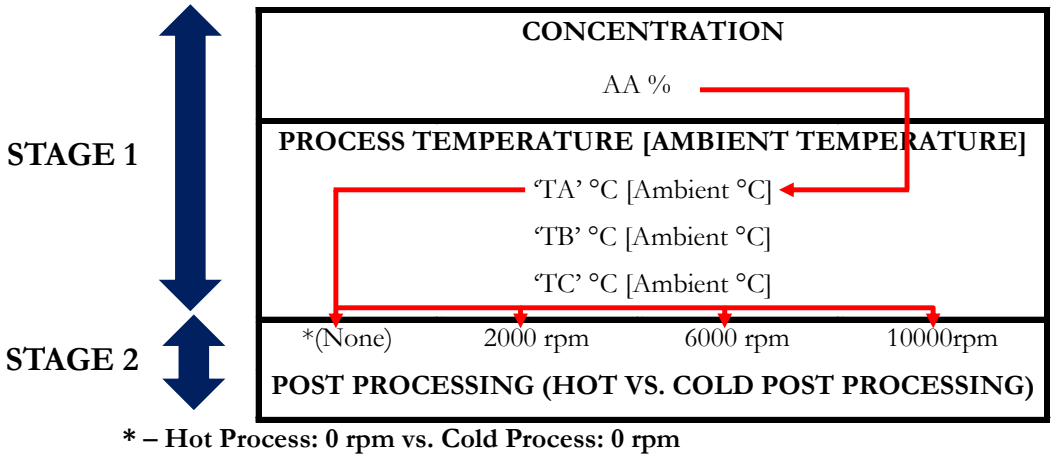

Figure 4-4: Image indicating the set of process variables considered within the experimental design and the nature of experiments conducted.

A typical experimental trial can be broken down into two stages [**STAGE 1**] lamellar dispersion manufacture [**STAGE 2**] hot/cold post processing, involving a range of shear rates. All of which occur within a timescale of approximately T = 240 minutes for a set process temperature.

STAGE 1 (LAMELLA MANUFACTURE)

A typical experimental formulation at a **CONCENTRATION** (i.e. AA % ['AA % QUAT/CS/FA/Water']) is manufactured in the 4L rig (Figure 3-16) at a specified **PROCESS TEMPERATURE** (i.e. 'T1 °C') – set temperature is maintained by the heated jacket. The mixture is processed for up to time **T = 60 minutes** with the low shear impeller Mixer-3 operating at **200 rpm**. At **T = 60 minutes,** the impeller speed is increased to **300 rpm**[119]**,** and processing is continued up until **T = 120 minutes.**

STAGE 2 HOT (HIGH SHEAR POST) PROCESSING

At this point the first sample is obtained directly from the process vessel via the peristaltic pump **None** (**NO HOT HIGH SHEAR POST PROCESSING**[120]). This is then followed by **HOT HIGH SHEAR POST PROCESSING**[121] of samples i.e. single pass discharge through the inline high shear mixer at specified mixer rotational speed (**2000 rpm, 6000 rpm and 10000 rpm**). At this stage there are 4 samples to be cooled quiescently. After the collection of the final

[119] To enhance homogeneity
[120] 'AA % QUAT/CS/FA/Water' sample is obtained hot at process temperature but not through the inline high shear mixer
[121] 'AA % QUAT/CS/FA/Water' sample is obtained hot at process temperature through the inline high shear mixer at a range of speeds

post processed hot sample the water heater/chiller is set to 'Ambient °C' – to actively cool the remaining content of the process vessel with the low shear impeller Mixer-3 still operational. Cooling to Ambient °C would usually take approximately 120 minutes.

STAGE 2 COLD (HIGH SHEAR POST) PROCESSING

At **T = 240 minutes** the sample would usually be at ambient temperature. A sample is obtained via the peristaltic pump **None (NO COLD HIGH SHEAR POST PROCESSING**[122]). This is followed by **COLD HIGH SHEAR POST PROCESSING**[123] of samples i.e. single pass discharge through the inline high shear mixer at specified mixer rotational speed (**2000 rpm, 6000 rpm and 10000 rpm**) – 4 more samples are obtained at this stage marking the end of the experimental trial.

4.2.2 Effect of Process Temperature – Hot vs Cold Processing

Results and discussion of experiments examining the effect of process temperature – hot vs cold processing on the underlying microstructure of AA % QUAT/CS/FA/Water system is conferred within this Section – for the first set of samples, process temperatures reviewed include 'T1 °C', 'T2 °C' and 'T3 °C' (set on the water heater/chiller) – actual process temperatures were within a tolerance of ± 2 °C as noticed on the temperature probe inserted in the process vessel – other samples were cooled from aforementioned process temperatures to ambient (set on the water heater/chiller) for cold processing.

4.2.2.1 Rheology

Brookfield T-bar E Viscosity

The effect of process temperature on the Brookfield T-bar E viscosity for AA % QUAT/CS/FA/Water samples manufactured via the [1] hot and [2] cold process route is shown in Figure 4-5 – no sample was obtained for cold process at 'T3 °C' due to the fact that the process material was too viscous to be mixed after it was cooled down to ambient temperature from process temperature – viscosity was high enough to prevent the operation of the overhead low shear mixer.

[122] 'AA % QUAT/CS/FA/Water' sample is obtained cold at ambient temperature but not through the inline high shear mixer

[123] 'AA % QUAT/CS/FA/Water' sample is obtained cold at ambient temperature through the inline high shear mixer at a range of speeds

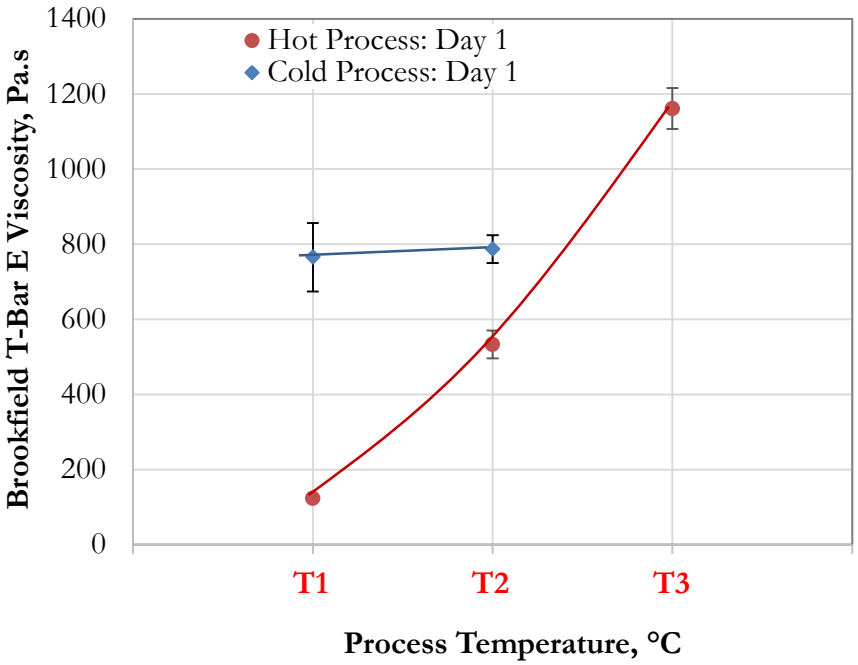

Figure 4-5: Brookfield T-Bar E viscosity as a function of process temperature for AA % QUAT/CS/FA/Water samples manufactured via both hot and cold process.

It can be seen that irrespective of processing route[124], as the process temperature is increased the viscosity of samples varied thus; "T1 °C' < 'T2 °C' < 'T3 °C" with the cold process Brookfield viscosity profile lying above the hot process – all of which obviously is as a direct result of the nature of the underlying microstructure. This suggests that the samples made at 'T3 °C' might be a more highly connected/better structured dispersion when compared to the samples made at 'T1 °C' based on the Brookfield viscosity measurement above – this notion is also complimented by rheometry[125] measurements further down shown in Figure 4-6.

It can be seen that for samples obtained from the cold process, the extra mixing time coupled with the active cooling step of the lamellar dispersion via the water heater/chiller made a huge difference in regards to the bulk viscosity of the samples manufactured at 'T1 °C' and T2 °C indicating that extending the mixing time/actively cooling the system to the L_{β}[126] at ambient temperature from L_{α} (emulsion stage) results in a better/highly connected and rigid structures. It can be inferred that that cold process promotes the formation of an increasingly rigid gel phase system as opposed to a system with decreased rigidity thus presenting lower viscosity profiles for

[124] Hot or cold process
[125] Oscillatory shear measurement
[126] Identified by SAXS measurements in Section 4.2.3.4

the samples obtained. On this basis, it can also be said that the cold process promotes the tendency of any L_1[127] present within the system into being incorporated/form the L_β phase. Likewise cooling these samples quiescently would result in it possessing a varied process history[128] as they are cooled from 'process temperature' without homogenisation - causing the sample to have varied cooling thus resulting in a poorly structured/loosely connected[129].

Further analysis[130] performed on the samples are reported in upcoming sections and should shed more light on the results in question - more importantly see Section 4.2.3 for extended inferences on the effect of either mode of processing on the behaviour of the system.

Oscillatory Shear

Earlier[131], this text introduced bulk viscosity measurements using a Brookfield viscometer and mentioned that they would be complimented with measurements obtained from rheometric analysis - in an attempt to present an underlying explanation to the effect of process temperature on the AA % QUAT/CS/FA/Water samples manufactured via the hot and cold process route. In addressing the question, one would have to also consider the micrographs of these samples displayed in Figure 4-13 alongside the oscillatory shear data obtained.

Figure 4-6 shows the plot of loss modulus[132] (left) and elastic stress[133] (right) as a function of strain amplitude thus enabling further characterisation of the effect process temperature[134] and the manufacturing process route[135] on the AA % QUAT/CS/FA/Water samples produced. It can be seen that both sets of results displayed in Figure 4-6 compliment the Brookfield viscometer data in that – increasing process temperature, results in increasing measured rheological properties[136].

[127] Small globular micelles as identified by SAXS measurements in Section 4.2.3.4
[128] I.e. cooling begins from the material closest to the body of the container in which it is stored
[129] Less rigid gel phase system (See Section 4.2.3.4 for more on 'less rigid' gel phase system)
[130] Oscillatory shear, optical microscopy, thermal transitions and small angle x-ray scattering
[131] See Figure 4-5
[132] Viscous loss modulus (G") – which is also a measure of the materials viscosity (Balzer, Varwig & Weihrauch 1995)
[133] Related to a measure of material's yield stress
[134] 'T1 °C', 'T2 °C' and 'T3 °C'
[135] Hot vs. cold process
[136] Loss modulus and elastic stress

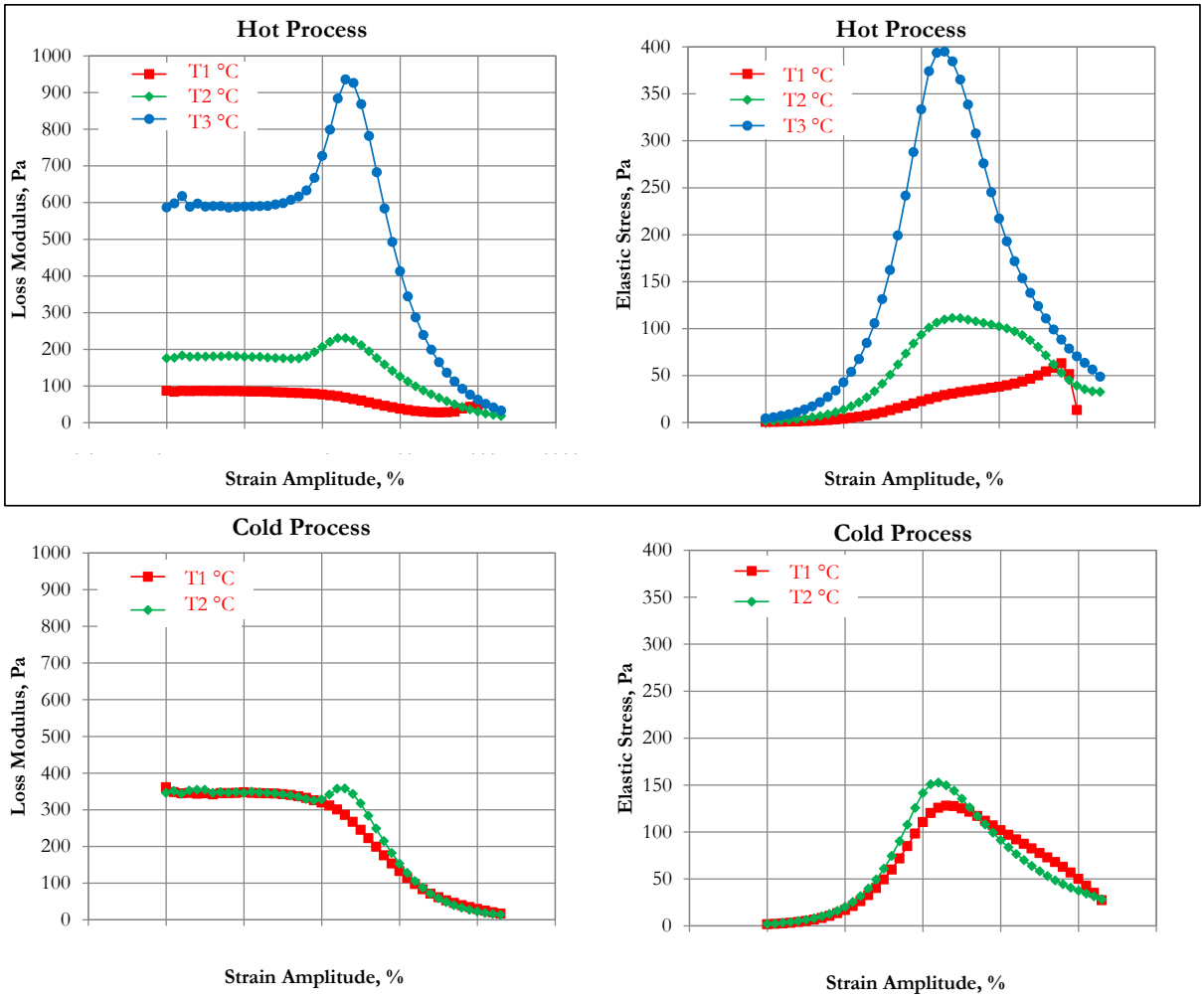

Figure 4-6: Oscillatory rheology tests results - loss modulus [left] and elastic stress [right] performed on AA % QUAT/CS/FA/Water samples as a function of strain amplitude for samples obtained different process temperatures.

In the case of the loss modulus - in general for samples obtained at 'T1 °C', the G" of the material displays a profile which initially is independent of the applied strain up to a critical strain level beyond which it begins to decrease – this behaviour is independent of process route[137]. The same is true for samples obtained at 'T2 °C' and 'T3 °C' - however at a critical strain there is an inflection in the loss modulus profile - which is more profound inflection spotted in the data obtained for samples manufactured at 'T3 °C'. This response is in line with the type III, weak strain overshoot classification according to (Kyu et al. 2002) in which G" increases before decreasing. This effect has also been referred to in literature as the 'Payne' (Payne 1962) or the 'Fletcher-Gent effect' (Fletcher & Gent 1953) – observed for a natural rubber filled with carbon black particles

[137] Hot or cold process

According to (Franck 2004b) as structured liquid is subjected to stress their rheological response is dictated by the interaction of its composition[138]. Thus such responses would be governed by the interaction between the dispersed phase components which is often dependent on i.e. particle shape, size, volume fraction etc. and its interaction with the continuous phase in which they are suspended. With this in mind, the intensity of the overshoot can therefore be associated with the volume fraction of the very bright spots[139] on the micrographs displayed in Figure 4-13 – it can see that as one tends to the right of the image[140], visually an increase in the amount (volume fraction) of these bright spots can be seen within the underlying microstructure. It can therefore be inferred that this weak strain over shoot in the data displayed in Figure 4-6 is due to the presence of structures such as these increasing amount of 'FA' rich L_{β} microstructure which results in resistance to strain deformation up to a certain strain (peak of the G" overshoot) – after which the lamellar gel network is destroyed with increasing deformation at which point the material begins to flow and the G" decreases (sample decreasing in viscosity).

The elastic stress profile increases linearly with increasing strain up to a critical point (a peak) before it begins to decrease – indicating that samples increase in viscosity with the application of strain is due to the samples elasticity to applied stresses, within the systems' yield stress. It can be seen that as the applied strain is increased, a critical point is reached in which the yield stress is exceeded[141] and the material begins to flow. For all samples obtained, the elastic profiles obtained compliments other discussed measured rheological properties[142] in that the peak value of elastic stress (yield stress) of the measured samples increase with increasing process temperature. It can therefore be said that close packing from the increasing volume fraction of the 'FA' rich L_{β} microstructure is responsible for the increasing bulk viscosity of the samples produced at the various process temperatures.

One thing that can be noticed on the elastic stress profiles of the samples produced from the hot process at both 'T1 °C' and 'T2 °C' is the unusual nature of the profiles when compared to the other profiles[143] displayed in Figure 4-6. It is as though the other samples display clear well defined profiles (similar to a Gaussian function) with respect to strain amplitude – which is not the case with those manufactured at hot process at 'T1 °C'/'T2 °C'. it is thought that these other

[138] Underlying microstructure
[139] Later identified/confirmed to be 'FA' rich L_{β} microstructure by hot stage microscopy in Section 4.2.2.2
[140] Increasing process temperature; 'T1 °C', 'T2 °C' and 'T3 °C'
[141] Lamellar gel network destroyed
[142] Brookfield T-bar E viscosity and viscous loss modulus
[143] All other samples except hot process at 'T1 °C' and 'T2 °C'

samples exhibit this probably due to the fact that they are dominated by either 'FA' rich L_β microstructure or 'QUAT/CS'[144] rich lamellar hence the clear bell shaped curve – the ones manufactured at 'T1 °C' and 'T2 °C' are probably not dominated by either i.e. they are contain a range of structures i.e. globular micelles (L_1), 'QUAT/CS' rich L_β microstructure, 'FA' rich L_β microstructure, vesicles (L_V), free 'QUAT/CS', free FA etc. – however one would need to characterise these samples using SAXS to confirm this inference.

4.2.2.2 Microscopy

Bright Field and Cross Polarised Illuminated Micrograph

Micrographs (Figure 4-7 - Figure 4-13 and Figure 4-14) obtained from the work conducted on the system in question[145] has helped identified the various components of the underlying microstructure at the assessed process temperatures.

Micrographs[146] shown in Figure 4-14 indicate that as process temperature is increased, the underlying microstructure varied from a predominantly single microstructure of [1] 'QUAT/CS' rich L_β microstructure at 'T1 °C' to one of mixed microstructure possessing both the 'QUAT/CS' rich L_β microstructure alongside a [2] 'FA' rich L_β microstructure[147] as the process temperature is increased. The micrographs (Figure 4-7 - Figure 4-13) illustrate the evolution of the microstructure of the AA % QUAT/CS/FA/Water system with respect to process time[148]. It can be seen that as time increases, the size domain of the FA droplets decrease with respect to time (see schematic in Figure 4-12) prior to it being constant at approximately 20 μm[149] as seen under the microscope for all the process temperatures considered.

From the micrographs[150], the effects of process temperatures[151] on the evolution[152] of the underlying microstructure for the manufactured lamellar dispersions is displayed under cross polarised and bright field illumination – from these, the following can be inferred in regards to the nature of the process; the concentration at which the 'QUAT/CS'[153] is dissolved in hot

[144] See section 4.2.2.2
[145] AA % QUAT/CS/FA/Water
[146] Compliment rheology data (Brookfield T-bar E viscosity and oscillatory shear)
[147] See Figure 4-14 for hot stage microscopy micrograph for investigation in 'FA' rich L_β microstructure
[148] From T = 0 minutes to T = 120 minutes and T = 240 minutes
[149] For T = 120 minutes to T = 240 minutes
[150] Figure 4-7 - Figure 4-13
[151] 'T1 °C', 'T2 °C' and 'T3 °C'
[152] From T = 0 minutes to T = 120 minutes
[153] QUAT/CS

water, they form a hot isotropic micellar solution[154] - the introduction (dispersion) of the molten FA initiates the formation of the liquid crystalline lamellar phase.

Process at T = 5 minutes

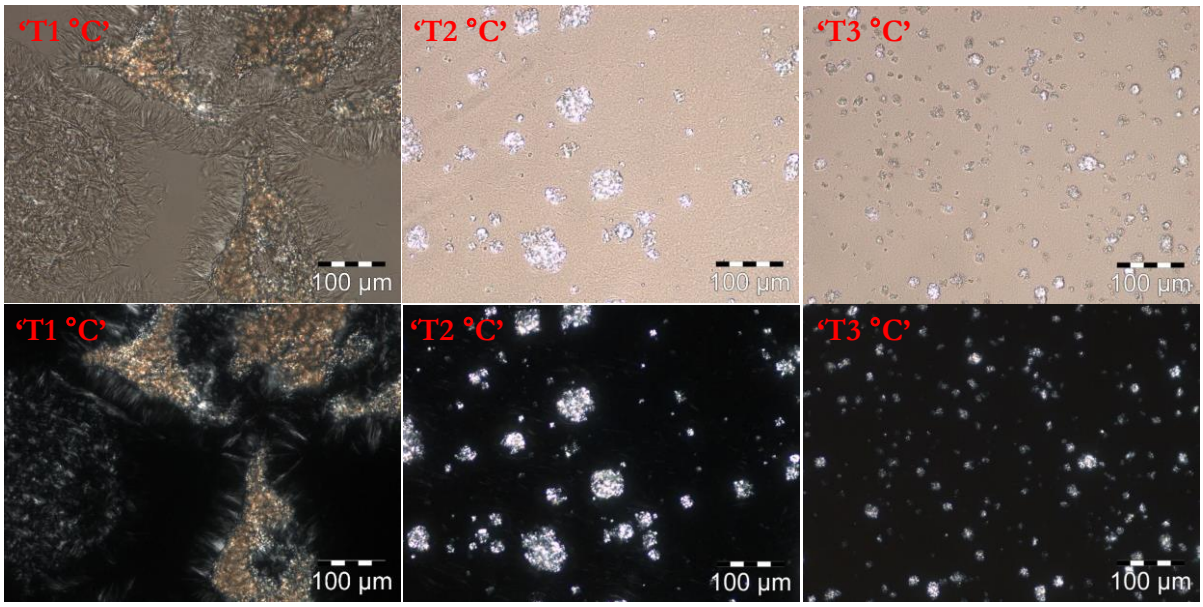

Figure 4-7: Bright field (top) and cross polarised (bottom) illuminated micrographs for AA % QUAT/CS/FA/Water samples obtained at T = 5 minutes during processing for different process temperatures.

As the molten FA is dispersed into the hot isotropic mixture, large domains of FA droplets form in the isotropic solution i.e. see micrograph at T = 5 minutes[155] - The 'QUAT/CS' rich L_β microstructure can be seen to form as breakaway structures from around the FA droplets interface with increasing time/dispersion under low shear mixing action. At the FA droplet interfaces, the 'QUAT/CS' and the FA droplets interact to form 'QUAT/CS' rich L_β microstructure and/or 'FA' rich L_β microstructure.

[154] Visual observation of the process
[155] Figure 4-7

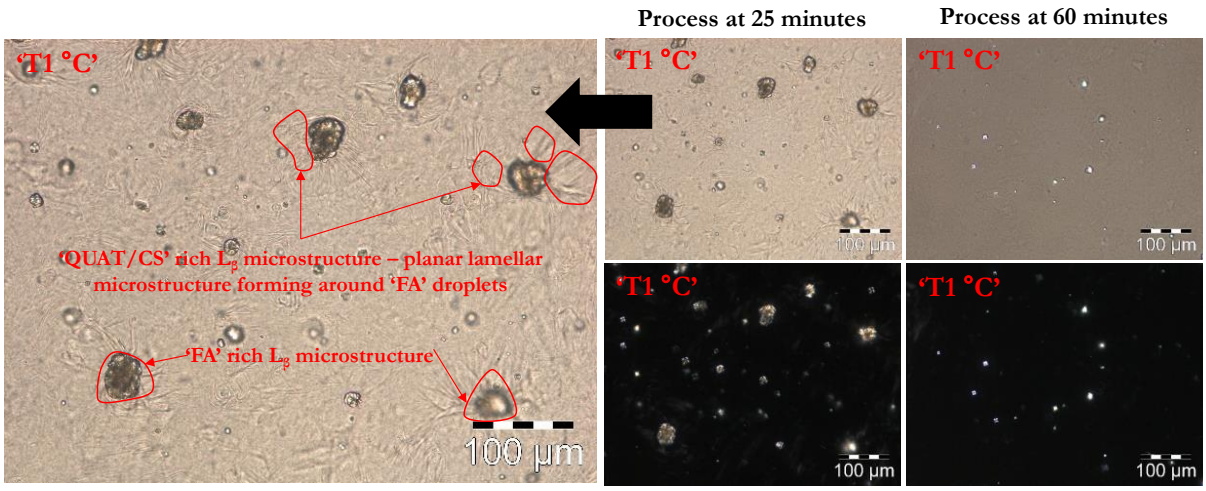

Figure 4-8: Bright field and cross polarised illuminated micrographs for AA % QUAT/CS/FA/Water samples at T = 25 and 60 minutes during processing (process temperature = 'T1 °C') – enlarged annotated image of bright field image obtained at T = 25 minutes is shown on the far left highlighting the nature of the underling microstructure.

As the lamellae form, core shrinkage of the FA droplet occurs with respect to time - schematically illustrated in Figure 4-12. At T = 120 minutes, it could be said that the process is at equilibrium and core shrinkage of the FA droplets is no longer occurring thus [1] 'QUAT/CS' rich L_β microstructure and [2] 'FA' rich L_β microstructure has been formed in different proportions – presumably other microstructures not visible at this length scale[156] are also formed.

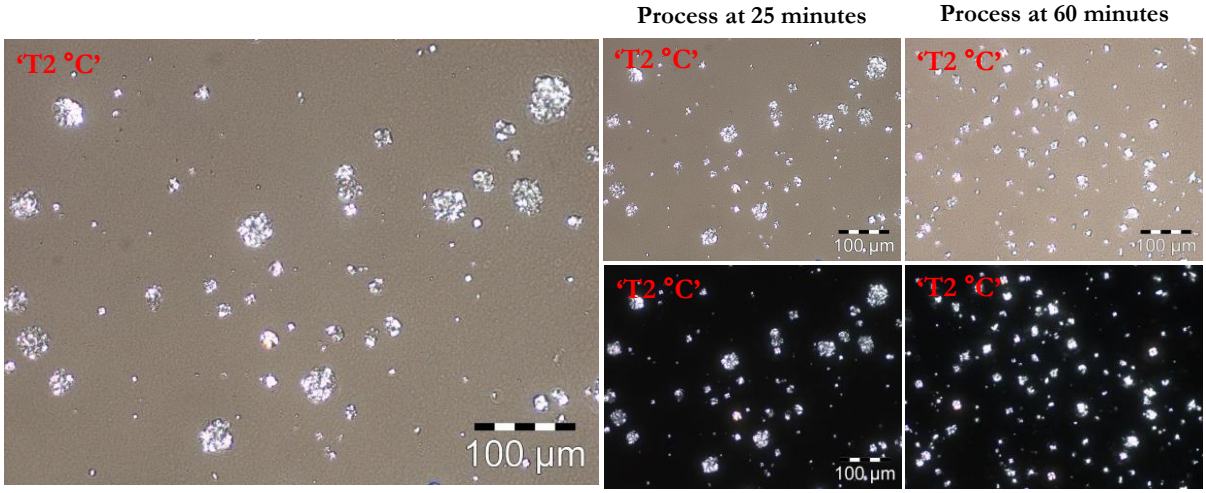

Figure 4-9: Bright field and cross polarised illuminated micrographs for QUAT/CS/FA/Water samples at T = 25 and 60 minutes during processing (process temperature = 'T2 °C') – enlarged image of bright field image obtained at T = 25 minutes is shown on the far left.

[156] Microscope - micrometer (µm), one millionth of 1 meter (limit to wavelength of light).

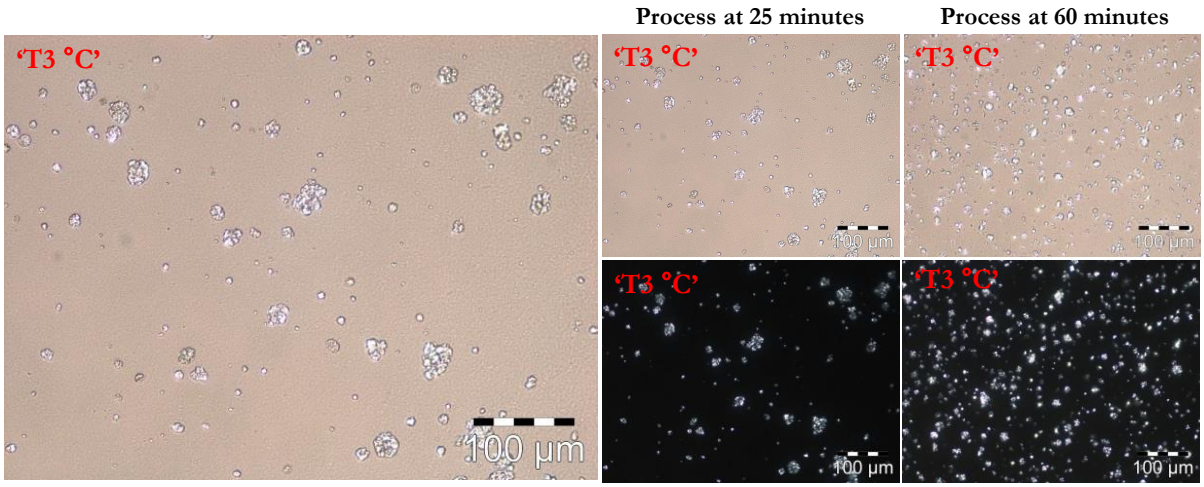

Figure 4-10: Bright field and cross polarised illuminated micrographs for AA % QUAT/CS/FA/Water samples at T = 25 and 60 minutes during processing (process temperature = 'T3 °C') – enlarged image of bright field image obtained at T = 25 minutes is shown on the far left.

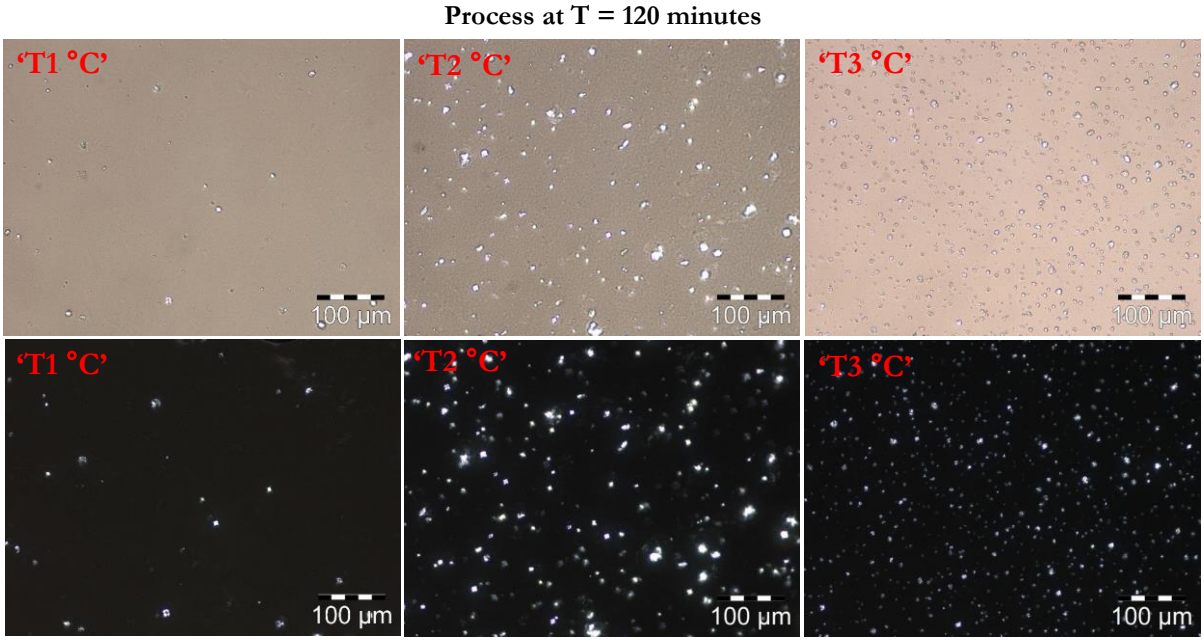

Figure 4-11: Bright field (top) and cross polarised (bottom) illuminated micrographs for AA % QUAT/CS/FA/Water samples obtained at T = 120 minutes during processing - process temperatures = 'T1 °C', 'T2 °C' and 'T3 °C'.

Mentioned earlier is the effect of process temperature on the domain size of the dispersed FA droplets - from the micrographs and the schematic in Figure 4-12, it can be inferred that that the reason the FA domains are largest at 'T1 °C' is probably because at this temperature, the system is closer to the frozen L_{β} - L_{α} phase transition temperature for the system as opposed to the other temperatures assessed ('T2 °C' & 'T3 °C') hence the amount of energy applied to the

former sample during manufacture would have less impact in breaking up these dispersed FA domains.

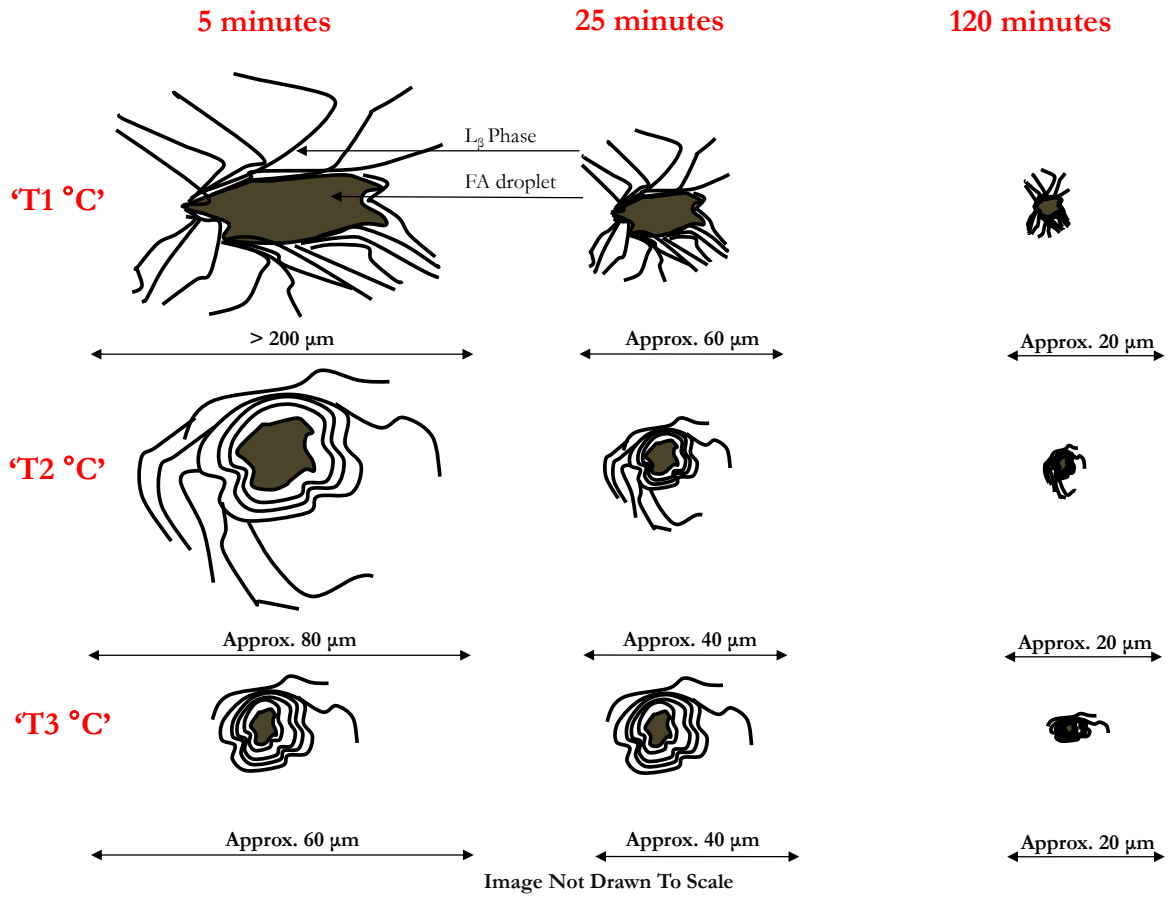

Figure 4-12: Schematic diagram of the 'FA' rich lamellae microstructure observed in the micrographs obtained for AA % QUAT/CS/FA/Water samples illustrating its approximate size distribution at various process temperatures and process times.

This offers insight to why these domain are larger than 200 µm after 5 minutes for samples manufactured at 'T1 °C'[157] in comparison to the remaining samples however at 120 minutes it is evident that these FA domains are all of similar domain size distribution after the system is given enough time to enable dispersion/homogenisation occur.

Figure 4-13 shows the micrographs of all the samples at the end of the manufacturing process for both the hot (T = 120 minutes) and the cold process (T = 240 minutes). As has been discussed earlier, at T = 120 minutes, a cross examination of the micrographs shows an increasing amount of 'FA' rich L_β microstructure with respect to process temperature and vice

[157] See Figure 4-7

versa i.e. decreasing amount of 'QUAT/CS' rich L_β microstructure with increasing process temperature.

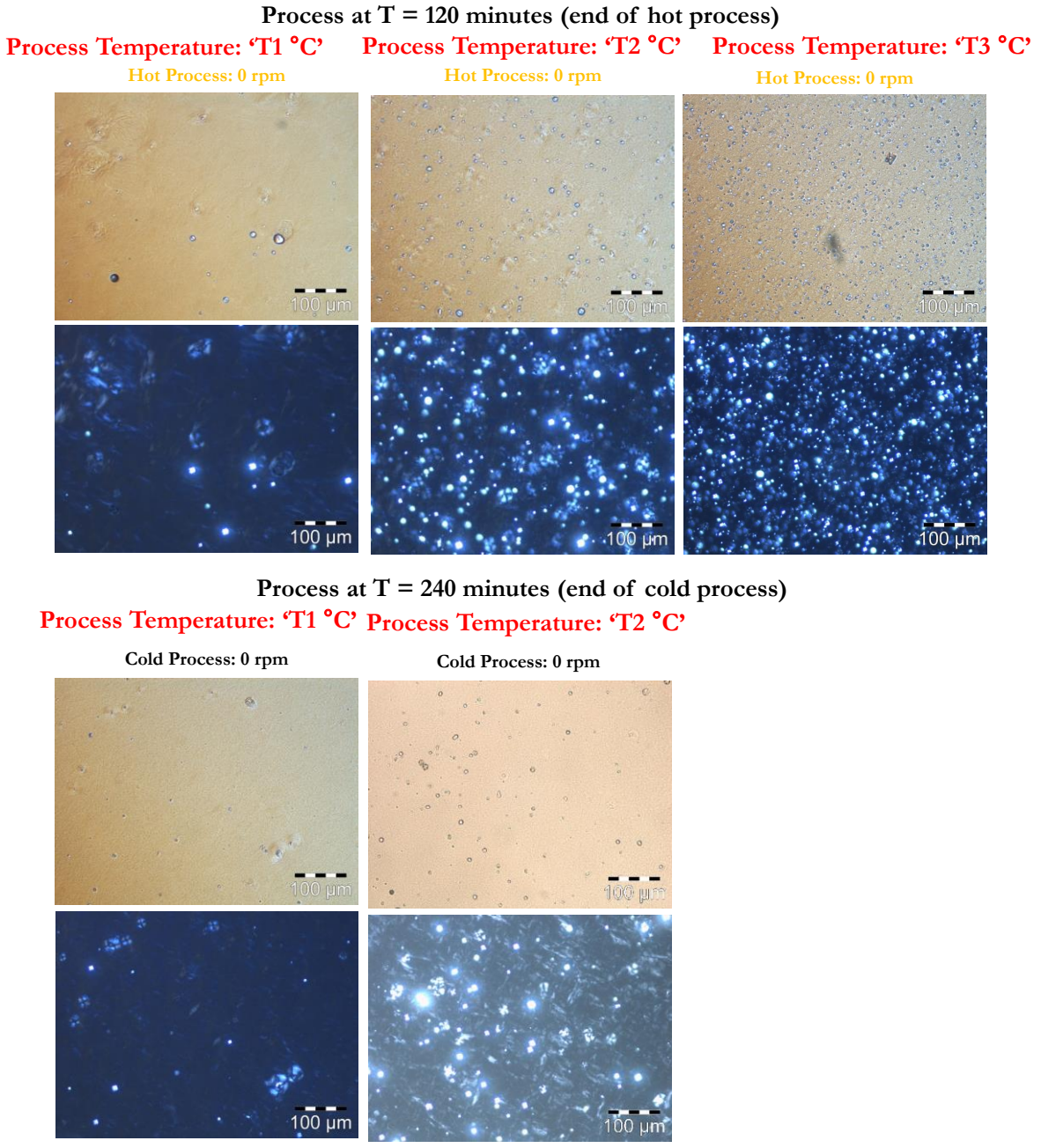

Figure 4-13: Bright field and cross polarised illuminated micrographs for AA % QUAT/CS/FA/Water samples obtained from the hot process (top half) and cold process (bottom half).

From a thermodynamic point of view, the increasing formation of 'FA' rich L_β microstructure with respect to increasing process temperature can be attributed to the effect of increasing/

(elevated) temperature[158] on the stability of the hot lamellar dispersion[159]. Presumably the elevated temperatures increases the thermal energy of the droplets i.e. increase in thermal energy of FA droplets results in an increase in the frequency of drop collision (Jones, Neustadter & Whittingham 1978) - the FA droplets would therefore combine (coalesce) quicker than they can be broken by the low shear within the process. Likewise at these elevated temperatures, the FA molecules possess more thermal energy hence as soon as it is out of the shear zone, its coalescence rate is higher at elevated temperatures ('T2 °C' and 'T3 °C') as opposed to 'T1 °C', where the coalescence rate is lower thus allowing them to be incorporated as a 'QUAT/CS' rich L_{β} microstructure that much more easily.

Hot Stage Microscopy (Cross Polarised Illuminated Micrograph)

In Section 4.2.2.2, the idea of 'FA' rich lamellar microstructure was introduced – here a hot stage microscope is used to elucidate the structural characteristics of this microstructure thereby confirming that it is indeed 'FA' rich as suggested.

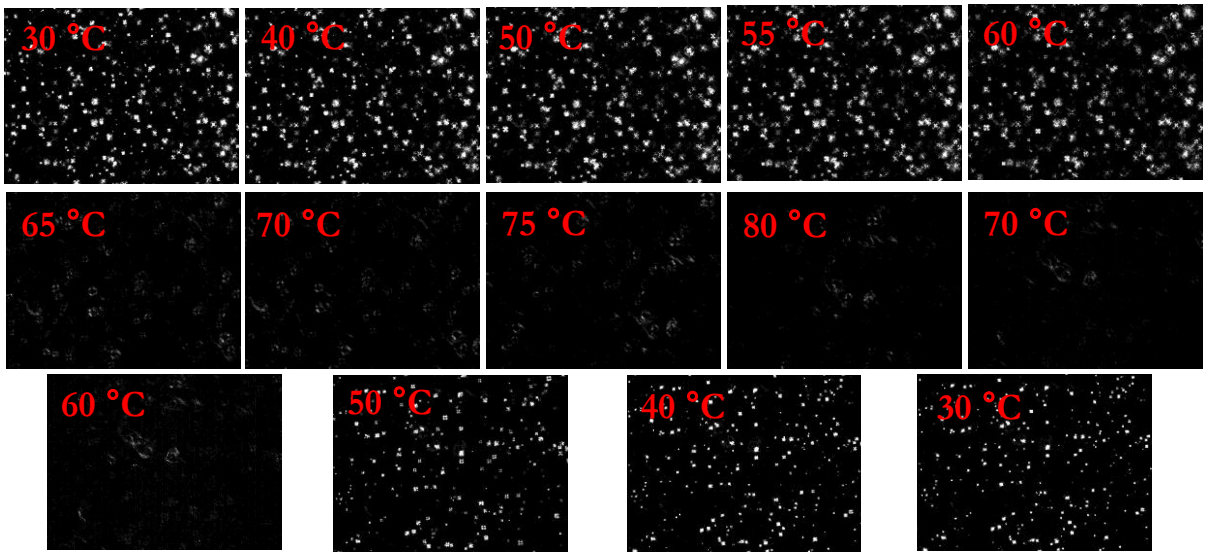

Figure 4-14: Cross polarised illuminated micrographs for AA % QUAT/CS/FA/Water samples obtained from the Linkam hot-stage microscope for sample obtained at 'T2 °C' following a temperature heat/cool cycle.

These 'FA' rich lamellar microstructure, as seen under the light microscope are irregularly shaped FA crystals - around these crystals, one can see the growth of some structure – which is believed are lamellar structure (i.e. see Figure 4-8) on the edge of the FA crystal at 25 minutes – they can

[158] Elevated temperatures - in reference to 'T1 °C'
[159] AA % QUAT/CS/FA/Water system in the L_{α} (emulsion stage)

also be seen at 120 minutes though more difficult to make out from the micrograph in Figure 4-11 with the 20X objective lens.

Visualisation of the samples under crosses polarised illumination (Figure 4-14) show the "FA' rich L_{β} microstructure' exhibit birefringent properties at ambient temperature – as the stage temperature is increased, there is activity from approximately 60 °C - far lower than the melting temperature of the surfactants[160] which is approximate 'T2 °C'. To further buttress the notion is the fact that, if these structures were pure undispersed FA crystals they would have begun melting at approximately 50 °C as the melting point of the FA used is between 48 – 52 °C. Therefore based on this slightly higher melting point, it was inferred that these structures are 'FA' rich lamellar structures hence the name "FA' rich lamellar microstructures'.

4.2.2.3 Thermal Transition

DSC

Figure 4-15 shows DSC traces for the AA % QUAT/CS/FA system manufactured via various process routes[161]. On both occasions i.e. irrespective of the route to manufacture, the heat cycle curve has a single peak, while the cool cycle curve shows multiple peaks for [1] hot process at 'T1 °C' and cold process at 'T1 °C' and 'T2 °C' and [2] a single broad peak at hot process at 'T2 °C' and 'T3 °C'. Summaries of the variables of the DSC curves i.e. enthalpy, onset temperature and peak temperature are summarised in Table 4-1.

[160] QUAT/CS
[161] Hot and cold process

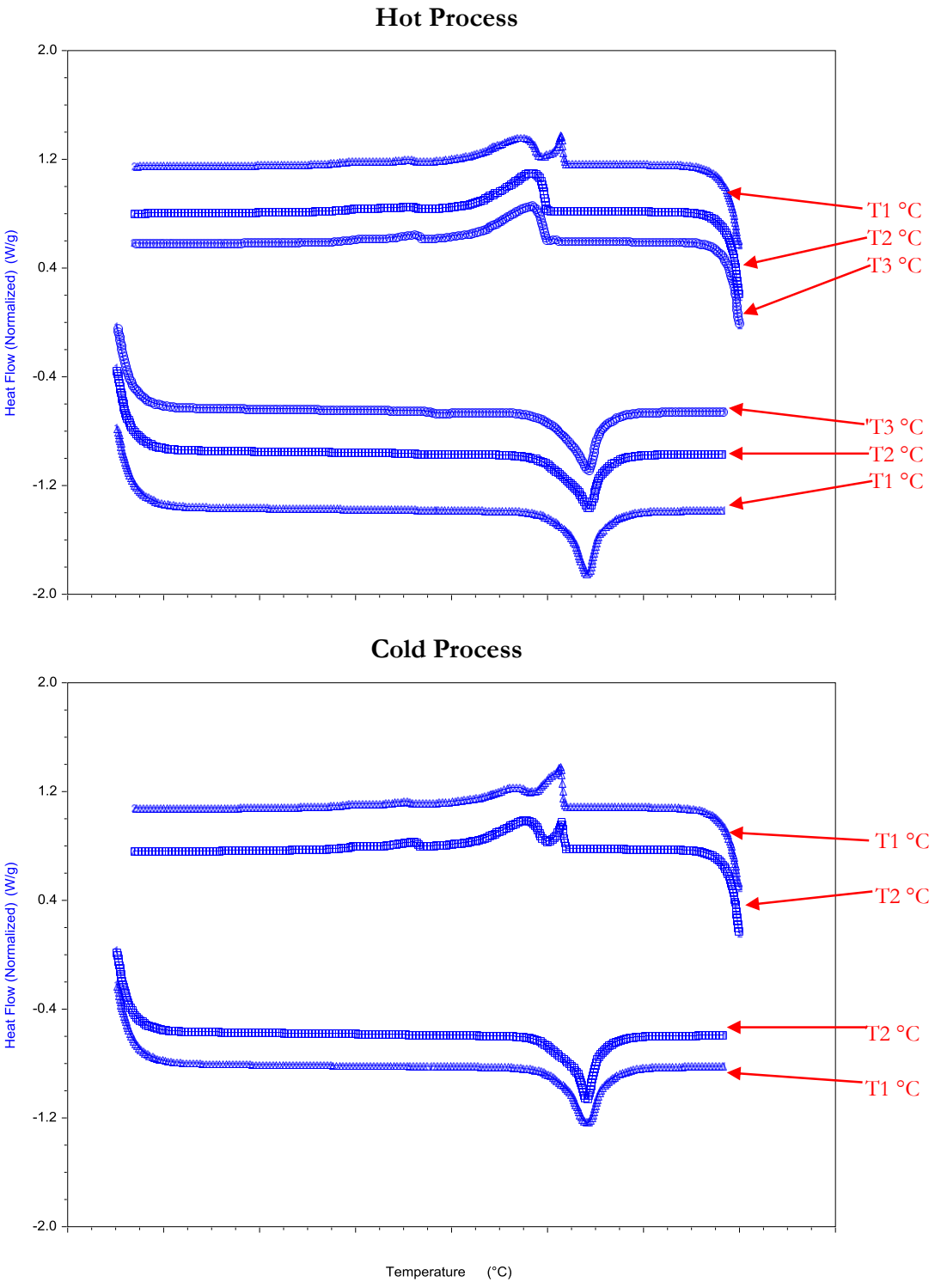

Figure 4-15: Differential scanning calorimetry trace (heat and cool cycles) of AA % QUAT/CS/FA/Water samples manufactured via the hot process (top) and cold process (bottom) at different process temperatures – for cycles with multiple peaks i.e. cooling peaks peak #1 is identified as the first peak on the curve as one moves from right to left of the Figure.

Table 4-1: Table indicating a summaries of DSC data variables i.e. enthalpy, onset temperature and peak temperature from the set of DSC curves above for hot (left) and cold (right) process.

	Hot Process									
	Heat Cycle			Cool Cycle						
	Peak(s)			Peak #2			Peak #1			
Process Temperature (°C)	Enthalpy (J/g)	Onset Temperature (°C)	Peak Temperature (°C)	Enthalpy (J/g)	Onset Temperature (°C)	Peak Temperature (°C)	Enthalpy (J/g)	Onset Temperature (°C)	Peak Temperature (°C)
T1	9.1160	71.9240	74.1200	2.9441	69.0250	67.2920	0.7519	71.6790	71.3740
T2	9.3497	71.4230	74.2420	8.1132	69.8600	68.3990	-	-	-
T3	9.2724	71.0600	74.1460	7.5699	69.7670	68.2680	-	-	-

	Cold Process								
	Heat Cycle			Cool Cycle					
	Peak(s)			Peak #2			Peak #1		
Process Temperature	Enthalpy	Onset Temperature	Peak Temperature	Enthalpy	Onset Temperature	Peak Temperature	Enthalpy	Onset Temperature	Peak Temperature
T1	9.1123	71.4780	74.0940	0.8781	67.9580	66.8000	2.6446	71.6450	71.3030
T2	9.2501	72.2830	74.0610	3.9565	69.4430	67.6200	0.8680	71.8140	71.4110
T3	n/a	n/a	n/a	n/a	n/a	n/a	n/a	n/a	n/a

For the heat cycles[162], as the DSC equipment heat flow (function of temperature) is increased – a broad transition peak can be seen for all curves with similar enthalpies, onset temperatures and peak temperatures – for which the following has been obtained; [1] Average onset temperature = 71.4690 °C[163] with a standard deviation of ±0.4338 – (hot process) and [2] Average onset temperature = 71.8805 °C[164] with a standard deviation of ±0.56922 – (cold process). From these, it can be inferred that although the micrographs (Figure 4-13) indicates that there are two sets of underlying microstructures[165], all the solids[166] which make up the manufactured lamellar (L_β) system begins to melt at these temperatures[167] (L_β forms L_α) hence, the large enthalpy values of 9.2460 J/g ±0.1191 and 9.1812 J/g ±0.0974 for both the hot and cold process respectively.

For the cool cycles[168], as the DSC equipment heat flow (function of temperature) is decreased – [1] multiple peaks can be seen for hot and cold process at 'T1 °C' and cold process 'T2 °C' and [2] a single broad peak can be seen for hot process at 'T2 °C' and 'T3 °C'. These two effects can be attributed to manufacturing above and below/close to - the lamellar system transition temperature as discussed in Table 4-2 and Table 4-3 in which the enthalpies of crystallisation for the multiple and single peaks are compared/discussed respectively.

Secondly, in discussing the cooling curves, as one moves from right to left of the image - [peak 1] can be associated with 'QUAT/CS' rich L_β microstructure while [peak 2], associated with the 'FA' rich L_β microstructure; this rationale is based on the peak/onset temperatures of both inflections - in that [peak 1] is higher than [peak 2] consistently - which can be attributed to the fact that the 'QUAT/CS' rich L_β microstructure possesses more 'QUAT/CS' than FA in terms

[162] Hot and cold process
[163] With a peak temperature at 74.1693 °C ±0.0642
[164] With a peak temperature at 74.0775 °C ±0.0233
[165] 'QUAT/CS' rich and 'FA' rich L_β microstructure
[166] AA % QUAT/CS/FA and water
[167] Phase transition temperature
[168] Hot and cold process

of ratio/ as seen under the microscope (Figure 4-13) and the 'FA' rich L_{β} microstructure possesses more FA than 'QUAT/CS' in terms of ratio hence the lower melting point and vice versa.

Table 4-2: Table explaining the characteristics of the cooling DSC curves obtained for AA % QUAT/CS/FA/Water system manufactured via [1] hot process at 'T1 °C' [2] cold process at 'T1 °C' [3] cold process at 'T2 °C' [4] hot process at 'T2 °C' and [5] hot process at 'T3 °C'.

<table>
<tr>
<td rowspan="3">It could be assumed that these experiments are performed either very close/below the transition temperature of the AA % QUAT/CS/FA/Water system</td>
<td>'T1 °C': hot process (multiple peaks)

[manufactured close to the transition temperature of the system]</td>
<td>
<table>
<tr><td colspan="2">Enthalpy of crystallisation [Onset Temperature]</td></tr>
<tr><td>peak #2</td><td>peak #1</td></tr>
<tr><td>2.9441 J/g [69.0250 °C]</td><td>0.75189 J/g [71.6790 °C]</td></tr>
</table>

Enthalpy of crystallisation associated with peak #2 is higher than peak #1 indicative of a higher amount of 'FA' rich L_{β} microstructure relative to 'QUAT/CS' rich L_{β} microstructure.
</td>
</tr>
<tr>
<td>'T1 °C': cold process (multiple peaks)

[manufactured below the transition temperature of the system]</td>
<td>
<table>
<tr><td colspan="2">Enthalpy of crystallisation [Onset Temperature]</td></tr>
<tr><td>peak #2</td><td>peak #1</td></tr>
<tr><td>0.8781 J/g [67.9580 °C]</td><td>2.6446 J/g [71.6450 °C]</td></tr>
</table>

Enthalpy of crystallisation associated with peak #1 is higher than peak #2 indicative of a higher amount of 'QUAT/CS' rich L_{β} microstructure in comparison to 'FA' rich L_{β} microstructure.
</td>
</tr>
<tr>
<td>'T2 °C': cold process (multiple peaks)

[manufactured below the transition temperature of the system]</td>
<td>
<table>
<tr><td colspan="2">Enthalpy of crystallisation [Onset Temperature]</td></tr>
<tr><td>peak #2</td><td>peak #1</td></tr>
<tr><td>3.9565J/g [69.4430 °C]</td><td>0.8680 J/g [71.8140 °C]</td></tr>
</table>

Enthalpy of crystallisation associated with peak #2 is higher than peak #1 indicative of a higher amount of 'FA' rich L_{β} microstructure in comparison to 'QUAT/CS' rich L_{β} microstructure.
</td>
</tr>
</table>

From Table 4-2, for samples manufactured at "T1 °C' hot process' which has been cooled quiescently - it can said that the manufacturing of the sample close to the transition temperature of the system promoted the formation of the 'FA' rich L_β microstructure.

On the other hand samples manufactured at "T1 °C' cold process' - it can be inferred that the extended mixing time[169] - in which process material was cooled to ambient temperature promoted the redistribution of FA thereby promoting the formation of more 'QUAT/CS' rich L_β microstructure alongside the already existing 'QUAT/CS' rich L_β microstructure in the system.

However in the case of the "T2 °C' cold process', although an extended mixing time is involved – the fact that two sets of microstructures have been formed while the dispersion was at an elevated temperature – cooling the material while mixing under low shear can only do so much in promoting the formation of more 'QUAT/CS' rich L_β microstructure. Only a prolonged mixing[170] session or an intense mixing action[171] can promote the formation 'QUAT/CS' rich L_β microstructure or conversion of the 'FA' rich L_β microstructure to 'QUAT/CS' rich L_β microstructure.

Table 4-3: Table explaining the characteristics of the cooling DSC curves obtained for AA % QUAT/CS/FA/Water system manufactured via [1] hot process at 'T2 °C' and [2] hot process at 'T3 °C'

<table>
<tr><td colspan="2">It could be assumed that these experiments were performed above the transition temperature of the AA % QUAT/CS/FA/Water system</td></tr>
<tr><td>'T2 °C': hot process (single broad peak)</td><td>'T3 °C': hot process (single broad peak)</td></tr>
<tr><td colspan="2">
<table>
<tr><td>'T2 °C': hot process (single broad peak)</td><td>'T3 °C': hot process (single broad peak)</td></tr>
<tr><td colspan="2">Enthalpy of crystallisation [Onset Temperature]</td></tr>
<tr><td>Peak #2</td><td>Peak #2</td></tr>
<tr><td>8.1132 J/g [69.8600 °C]</td><td>7.5699 J/g [69.7670 °C]</td></tr>
</table>
Enthalpy of crystallisation associated with peak #2 is very high when compared to typical values displayed in Table 4-2 indicative of a very high amount of 'FA' rich L_β microstructure within the sample.
</td></tr>
</table>

[169] Where mixing time was extended by 120 minutes
[170] Several hours
[171] High shear process operation

From Table 4-3, one can see that based on the fact that these samples have all been manufactured well above the transition temperature of the system – they are predominantly made up of 'FA' rich L_β microstructure hence the really high enthalpy value shown.

4.2.3 Effect of High Shear Post Processing Operation - Hot vs Cold Processing

The results discussed in this Section are an extension of the work reported in Section 4.2.2 in that the experiments examines the effect of a high shear post processing operation[172] on the lamellar dispersion (AA % QUAT/CS/FA/Water) formed.

From literature, it is known that lamellar states (L_α & L_β) can be interchanged via heating and cooling respectively (Sadtler et al. 2004; Tiddy, Hassan & Rowe 2001) – with this in mind, it could be said that 'this work therefore examined the impact of applying high shear to the lamellar dispersion formed at these two phases namely [1] L_α phase[173] at set process temperature and the [2] L_β phase[174], following active cooling of the lamellar dispersion from process temperature to ambient temperature' in the hope that new learnings about the system can be earned. High shear rotational speeds considered were 2000, 6000 and 10000 rpm.

4.2.3.1 Rheology

Brookfield T-bar E Viscosity

The effect of high shear post processing operation on the Brookfield T-bar E viscosity of the samples[175] obtained from both [1] hot high shear post processing[176] and [2] cold high shear post processing[177] is shown in Figure 4-6 – as was mentioned earlier[178] – no sample was obtained for cold process at 'T3 °C' due to the fact that the process material was too viscous to be mixed after it was cooled down to ambient temperature from process temperature hence no cold high shear post processing datasets.

[172] Single pass discharge of process material through the inline high shear mixer
[173] Hot process ('T1 °C', 'T2 °C' and 'T3 °C') – when the lamellar dispersion is in the hot emulsion stage
[174] Cold process ('Ambient °C')
[175] AA % QUAT/CS/FA/Water
[176] Stage 2 – hot high shear post processing (2000, 6000 and 10000 rpm)
[177] Stage 2 – cold high shear post processing (2000, 6000 and 10000 rpm)
[178] Section 4.2.2

For the hot high shear post processing[179], the impact of increasing inline high shear mixer rotational speed on Brookfield T-bar E viscosity varied thus; [1] for samples manufactured at 'T1 °C', increasing high shear post processing speed results in increasing Brookfield T-bar E viscosity up till 6000 rpm and then collapses as mixer rotational speed is further increased[180] [2] for samples manufactured at 'T2 °C', the trend is fairly similar to that which was observed for samples manufactured at 'T1 °C' and [3] for samples manufactured at 'T3 °C', increasing inline mixer rotational speed results in decreasing Brookfield T-bar E viscosity. Secondly the hot high shear post process Brookfield T-bar E viscosity profiles for process temperatures considered[181] varied thus "T1 °C' < 'T2 °C' < 'T3 °C" i.e. all the samples obtained at 'T3 °C' presented the highest set of viscosity.

On the other hand for the cold high shear post processing, the impact of increasing inline high shear mixer rotational speed results in increasing Brookfield T-bar E viscosity for samples manufactured at both 'T1 °C' and 'T2 °C' - both viscosity profiles are similar for all samples (Figure 4-16).

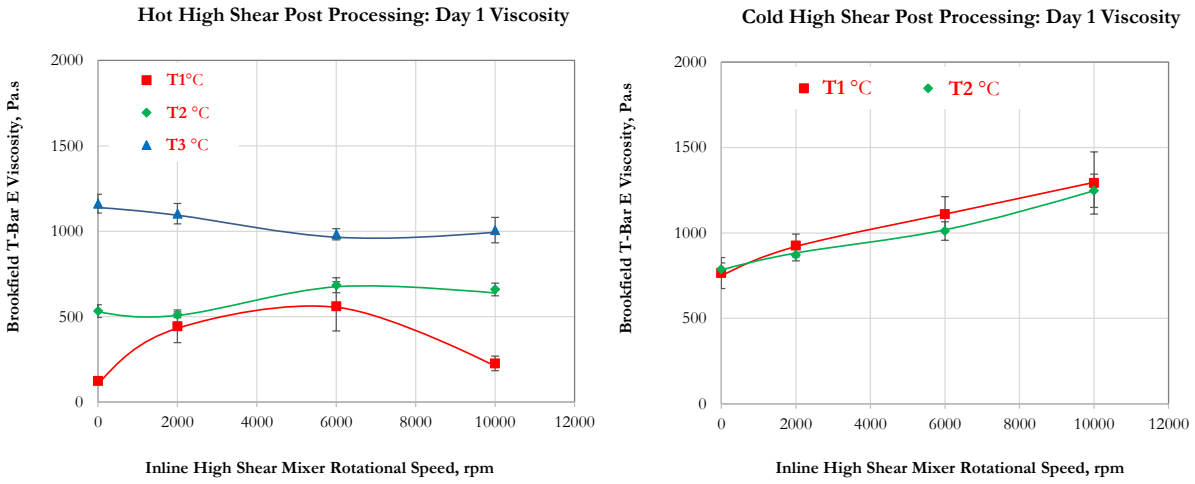

Figure 4-16: Brookfield T-Bar E viscosity as a function of inline high shear mixer rotational speed for AA % QUAT/CS/FA/Water samples prepared via hot high shear post processing (left) and cold high shear post processing (right) at various temperatures – samples not post processed through the high shear mixer head (0 rpm) have been included for the purpose of comparison.

For this system[182], in manufacturing of the lamellar dispersion under low shear[183] at a specified process temperature - the lamellar structures is in the form of long range lamellar

[179] Figure 4-16
[180] To 10000 rpm
[181] 'T1 °C', 'T2 °C' and 'T3 °C'
[182] AA % QUAT/CS/FA/Water (hot emulsion - L_α phase)
[183] Using low shear overhead Mixer-3

microstructures composed of 'QUAT/CS' rich lamellar planar sheets microstructure and/or 'FA' rich lamellar microstructure in different ratios depending on the process temperature alongside other structures such as globular micelles (Figure 4-17) – all of which contribute to the structural properties of the gel phase network. Likewise at this stage, it could be said that the system is in the L_α phase in which the alkyl chains are in a liquid like state thereby allowing each flat layer to slide past each other hence the usual low viscosity of this phase according to (Tiddy, Hassan & Rowe 2001). Secondly the molecules of the raw materials are also susceptible to mechanical stresses from the low shear mixer.

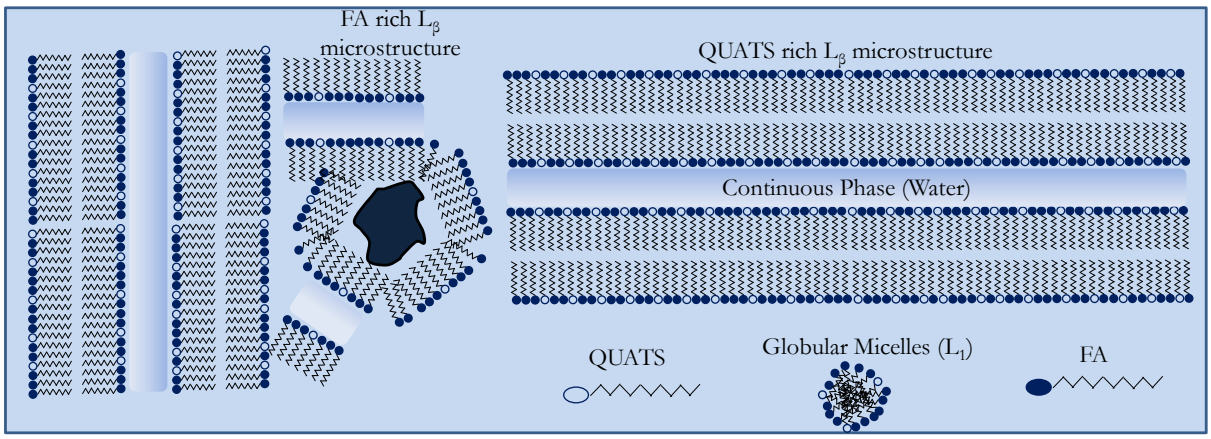

Figure 4-17: Schematic representation of the nature of the underlying microstructure formed by the AA % QUAT/CS/FA/Water system.

The effect hot high shear post processing on all the samples is therefore a simple case rearranging/restructuring a L_α system in which its alkyl chains are in a liquid like state albeit at a higher mechanical stresses[184] which is no different to what the low shear overhead Mixer-3 is doing. One could contend that the sample obtained at 'T1 °C' had the opportunity of cooling down to L_β gel phase in the pipeline as it was being pumped before being post processed – hence the initial positive gradient[185] and at 10 000rpm, the less rigid lamellar gel is broken down by the high mechanical stresses hence the collapse in viscosity of the system.

For the cold process in which the system is actively cooled from 'process temperature', one could infer that as the system is cooled and homogenised, the system will begin to freeze and lock up as it tends into the L_β - the alkyl chains become rigid. In this case the system temperature is evenly distributed due to the mixing operation performed alongside cooling thus promoting a system with improved structuring due to the extra mixing time in reference to one which has

[184] High shear rate
[185] Bulk viscosity as a function of mixer rotational speed at 2000 & 4000 rpm

been quiescently cooled. The effect of high shear post processing operation on the lamellar microstructure obtained from the cold process can therefore be thought of as one, in which frozen long range 'QUAT/CS' rich L_β microstructure and/or 'FA' rich L_β microstructure are fragmented. This[186] can be thought of as a reduction in 'QUAT/CS' rich L_β microstructure and 'FA' rich L_β microstructure particle size – in the case of the 'FA' rich L_β microstructure, it could be said that following a reduction in its particle size, more FA is incorporated in existing 'QUAT/CS' rich L_β microstructure as would be demonstrated further down this text using a range of analytical techniques. Increasing the intensity of high shear post processing operation, results in increased fragmentation[187] of underlying lamellar microstructure thus increasing the systems' bulk viscosity.

It was noticed that the outlet temperatures of actively cooled[188] material would rise in temperature (viscous heating) with increasing high shear post processing rotational speed. To combat this, it was ensured that process outlet temperature did not exceed 50 °C by waiting for high shear head to cool down before performing high shear post processing operation - in some cases when the 50 °C mark was exceeded deliberately, low viscosity product was obtained. From this one can infer that viscous heating during high shear post processing resulted in the material going back into the L_α – effectively turning the cold high shear post process back into hot high shear post process hence the low viscosity values which were comparable to the hot high shear post process values.

Further analysis[189] on the effect of high shear post processing on the underlining microstructure are reported in upcoming sections and should shed more light on the changes to the morphology/support inferences made in regards to the system during high shear post processing operation.

[186] Fragmentation
[187] Reduction in lamellar particle size
[188] Cold process
[189] Oscillatory/transient shear, optical microscopy, thermal transitions and small angle x-ray scattering

Oscillatory Shear

Oscillatory shear measurements offered more insight into the effects of hot/cold high shear post processing operation on the underlying microstructure of the AA % QUAT/CS/FA/Water samples manufactured at various process temperatures[190] - alongside these dataset, one should also consider the micrographs of the samples displayed in Figure 4-20 - Figure 4-22.

Figure 4-18 shows the plot of loss modulus (left) and elastic stress (right) as a function of strain amplitude thus enabling further characterisation of the effect hot/cold high shear post processing operation on the AA % QUAT/CS/FA/Water samples produced. The new datasets[191] have been displayed alongside previous datasets discussed in Section 4.2.2.1[192] for the purpose of comparison – so only the new datasets would be discussed.

[190] 'T1 °C', 'T2 °C' and 'T3 °C'
[191] Hot/cold high shear post processing
[192] None post processed samples

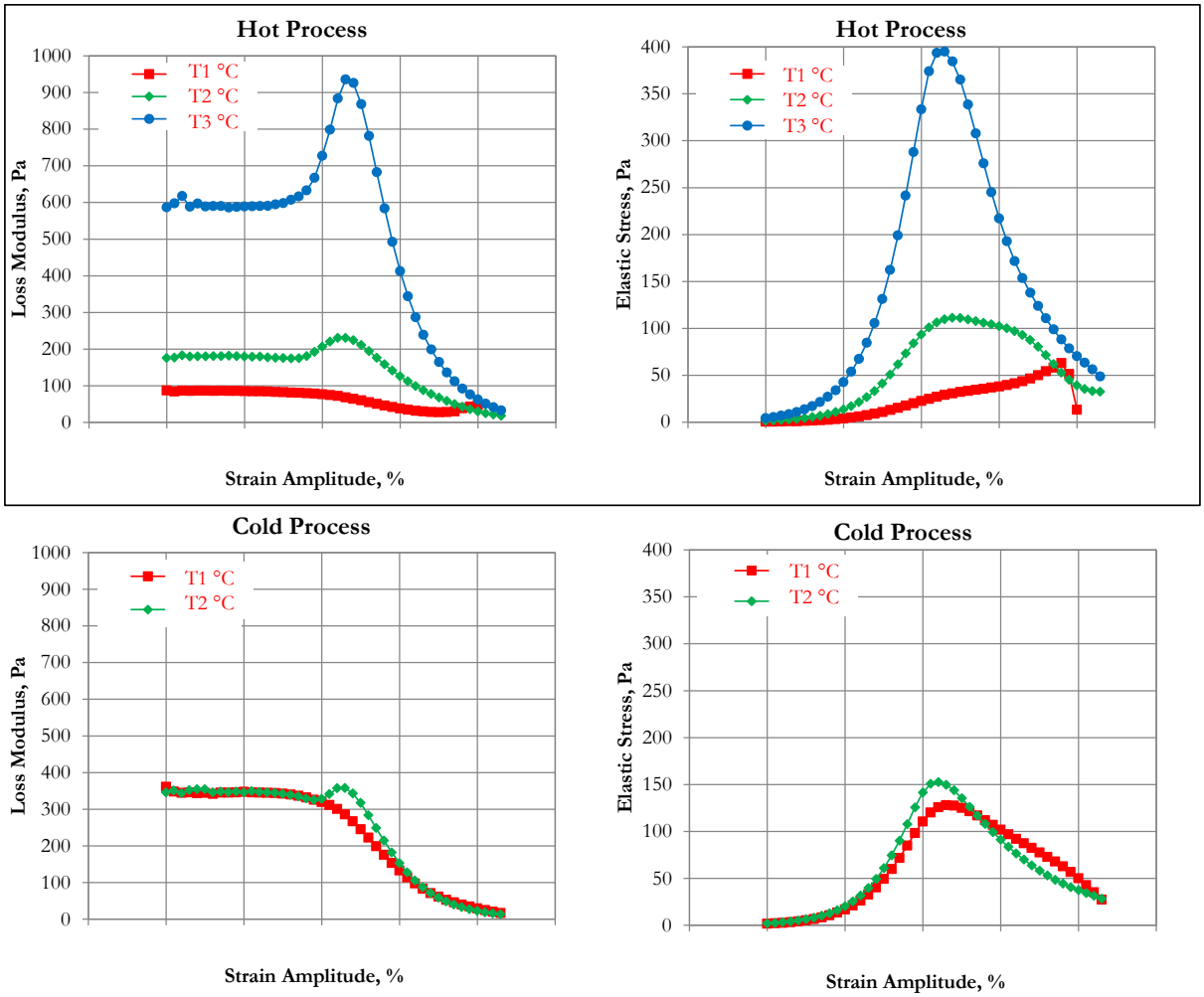

Figure 4-18: Oscillatory rheology tests loss modulus [left] and elastic stress [right]) results performed on AA % QUAT/CS/FA/Water samples obtained after hot high shear post processing [top] and cold high shear post processing [bottom] as a function of strain amplitude - for lamellar dispersions manufactured at 'T1 °C', 'T2 °C' and 'T3 °C' - None post processed (0 rpm) data included for comparison.

In general the loss modulus profiles displayed for all the samples obtained from hot post processing operation exhibit the 'Payne effect' (Payne 1962) as was described in Section 4.2.2.1 - this is expected, as the effect of hot high shear post processing on the underlying microstructure is no different from the impact the low shear overhead Mixer-3 had on the underlying microstructure of the system albeit at higher mechanical stress as has been discussed in Section 4.2.3.1[193] - the impact is basically restructuring/reduction in size of the already formed microstructure (FA/'QUAT/CS' rich) in an L_{α} phase. Both the loss modulus and the elastic

[193] Brookfield T-bar E viscosity Section above

stress compliment the Brookfield T-bar E viscosity data displayed in Figure 4-16 and micrographs displayed in Figure 4-20 - Figure 4-22 for hot high shear post processing[194].

The interesting observation about Figure 4-18 is the complete disappearance of the 'Payne effect' from the loss modulus profile of the cold high shear post processed data obtained for samples manufactured at 'T2 °C' – indicative that the cold high shear post processing operation had gotten rid of the FA L_β microstructure.

If one takes a look at the micrograph of the sample in Figure 4-21[195], one could argue that these FA L_β microstructure still exist i.e. the bright spots are still visible on the image and conclude that the effect of the cold high shear post processing merely results in size reduction of these FA L_β microstructure – and that the oscillatory shear technique is unable to detect these microstructure and the protocol would require modification i.e. adjust the gap size between the rheometer plates - this is plausible.

However if one considers Figure 4-19[196], the mean transient viscosity profile of the cold high shear post processed sample has increased significantly (bottom right of figure) when compared to none post processed counterpart (bottom left of Figure). Likewise this cold post processed profile is comparable to the sample obtained at cold high shear post processed material for material obtained at 'T1 °C' which is predominantly a 'QUAT/CS' rich L_β microstructure.

Combining these three sets of results (Figure 4-18[197], Figure 4-19[198] and Figure 4-21[199]), one can infer that the effect of cold high shear post processing on the underlying microstructure of AA % QUAT/CS/FA/Water system irrespective of process temperature includes [1] size reduction of the L_β microstructure (FA/'QUAT/CS' rich) particle size which has been also referred to as 'fragmentation' in this text and [2] restructuring of the 'QUAT/CS' rich L_β microstructure via the incorporation of fragments of FA thereby enhancing the systems homogeneity - both of which contributes to increase in the volume fraction of the 'QUAT/CS' rich L_β microstructure, hence an increase in the system viscosity. Thermal transition work discussed in Section 4.2.3.3 is also used to support this inference.

---

[194] Left half of the displayed micrograph
[195] Micrograph on the extreme left titled 'cold post processing: 10000 rpm
[196] Bottom two figures
[197] Oscillatory shear measurement
[198] Mean transient shear measurement on the graph titled 'Cold Process – None Post Processed Samples vs. Cold Process – Post Processed Samples' for samples manufactured at 'T2 °C' (bottom half of the figure)
[199] Micrograph

Transient Shear

It is proposed that the investigation of the swelling behaviour (Eccleston et al. 1988; Hauser 1984; Rydhag & Gabran 1982) of the AA % QUAT/CS/FA/Water system via transient viscosity measurement could help support the 'increase in volume fraction through fragmentation' inference introduced in previous Section.

The working hypothesis is - if the cold high shear post processing does cause fragmentation of the underlying L_β microstructure, then systems with highest amount of the 'QUAT/CS' rich L_β microstructure i.e. high volume fraction system (higher viscosity) should swell more when diluted[200] i.e. higher swelling rates for cold high shear post processed samples in comparison to none post processed samples.

Figure 4-19 shows the effect of high shear post processing operation on the transient stress growth (viscosity build) as a function of time for [1] none post processed samples and [2] samples obtained from cold high shear post processing[201]. Plots show mean measurement of up to ten repeat experiments.

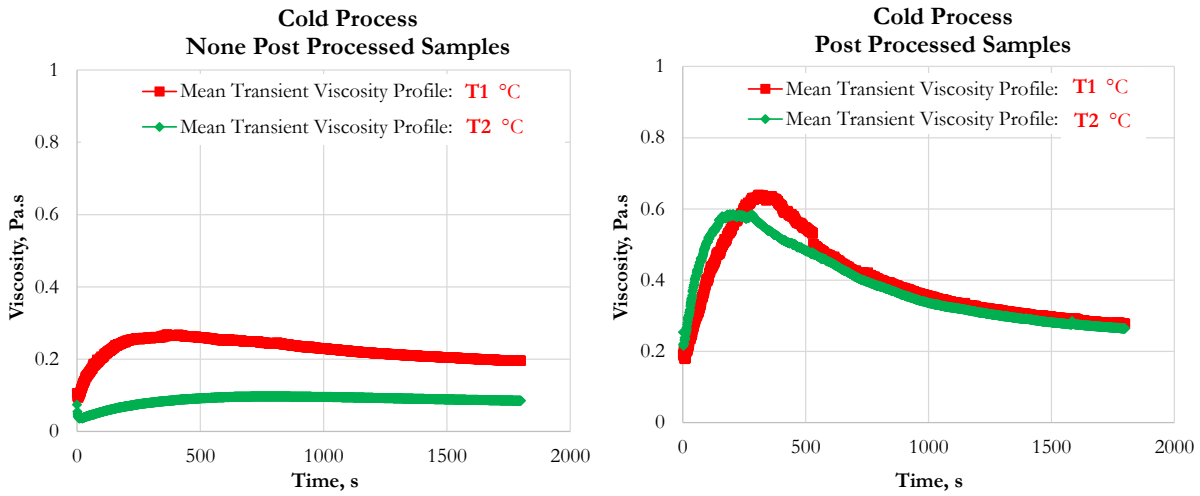

Figure 4-19: Transient viscosity tests showing viscosity as a function of time for AA % QUAT/CS/FA samples manufactured via cold process at process temperatures of 'T1 °C' and 'T2 °C' .

In general, for all the profiles displayed, the transient viscosity of the samples initially starts off quite low (system stabilising) and then with time - the viscosity begins to rise up to a peak before decreasing and levelling off presumably due to the lamellar phase orientation in the direction of

[200] When manufactured samples are brought in contact with water
[201] Data shown only for materials post processed at 10000 rpm

the shear field resulting in decreasing viscosity due to the low resistance to flow (Berghausen et al. 1998; Diat, Roux & Nallet 1993a; Oswald & Allain 1988; Partial et al. 2001).

It is expected that systems that possess more 'FA' rich L_β microstructure will swell the least in comparison to systems with predominantly 'QUAT/CS' rich L_β microstructure – one of such system is the sample manufactured at 'T2 °C' (none post processed sample) – it possess the lowest viscosity profile with respect to time.

Secondly data indicate that samples subjected to high shear high shear post processing swell more rapidly (higher rate) to a higher peak than ones that have not been subjected to cold high shear post processing - This can be used to support the increase in volume fraction of lamellar inference. In this case, it can be inferred that the introduction of cold high shear high shear post processing, results in fragmentation/restructuring of the underlying microstructure (FA/'QUAT/CS' rich)[202] resulting in a more homogeneous system of fragmented 'QUAT/CS' rich L_β microstructure thereby increasing the surface area available for water penetration i.e. making it easier and quicker for water (dilution water) to penetrate into the bilayer.

4.2.3.2 Microscopy

Bright Field and Cross Polarised Illuminated Micrograph

Series of micrographs (Figure 4-20 - Figure 4-22) obtained from a range of samples has helped identified the impact of high shear post processing on the underlining microstructure – this current Section is written to compliment what has been discussed previously in Section 4.2.3.1 and what will be discussed in subsequent Sections (Section 4.2.3.3 and 4.2.3.4)

[202] Discussed earlier

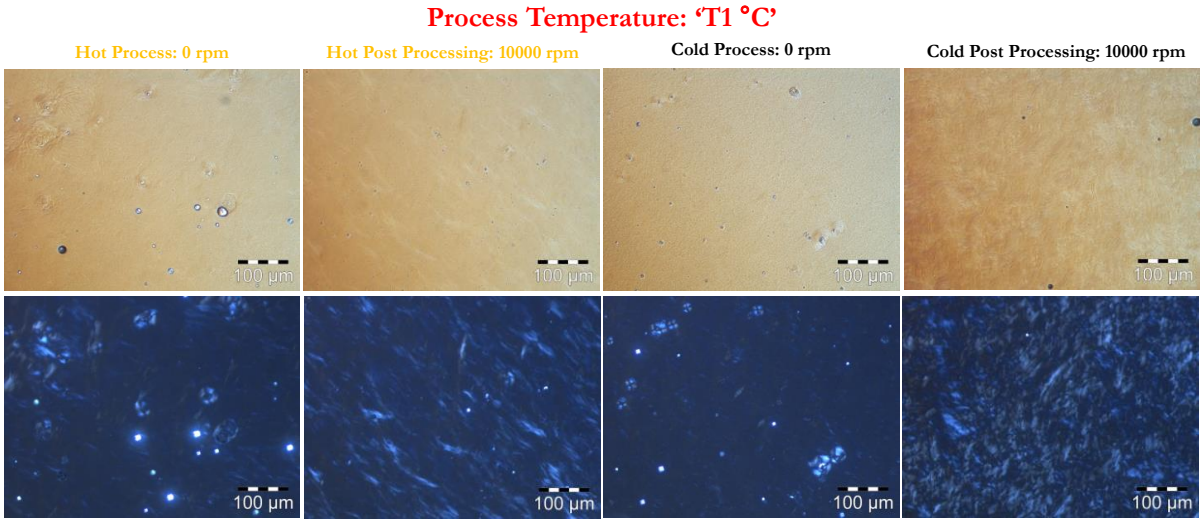

Figure 4-20: Bright field (top) and cross polarised (bottom) illuminated micrographs for AA % QUAT/CS/FA/Water samples obtained following hot and cold high shear post processing operation at 'T1 °C' – None post processed samples included for comparison.

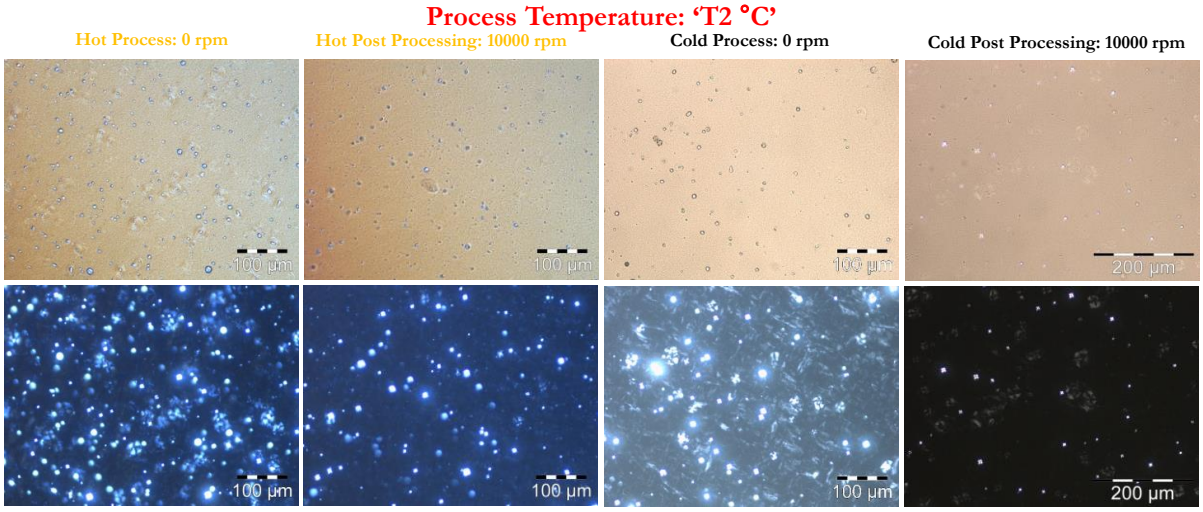

Figure 4-21: Bright field (top) and cross polarised (bottom) illuminated micrographs for AA % QUAT/CS/FA/Water samples obtained following hot and cold high shear post processing operation at 'T2 °C' – None post processed samples included for comparison.

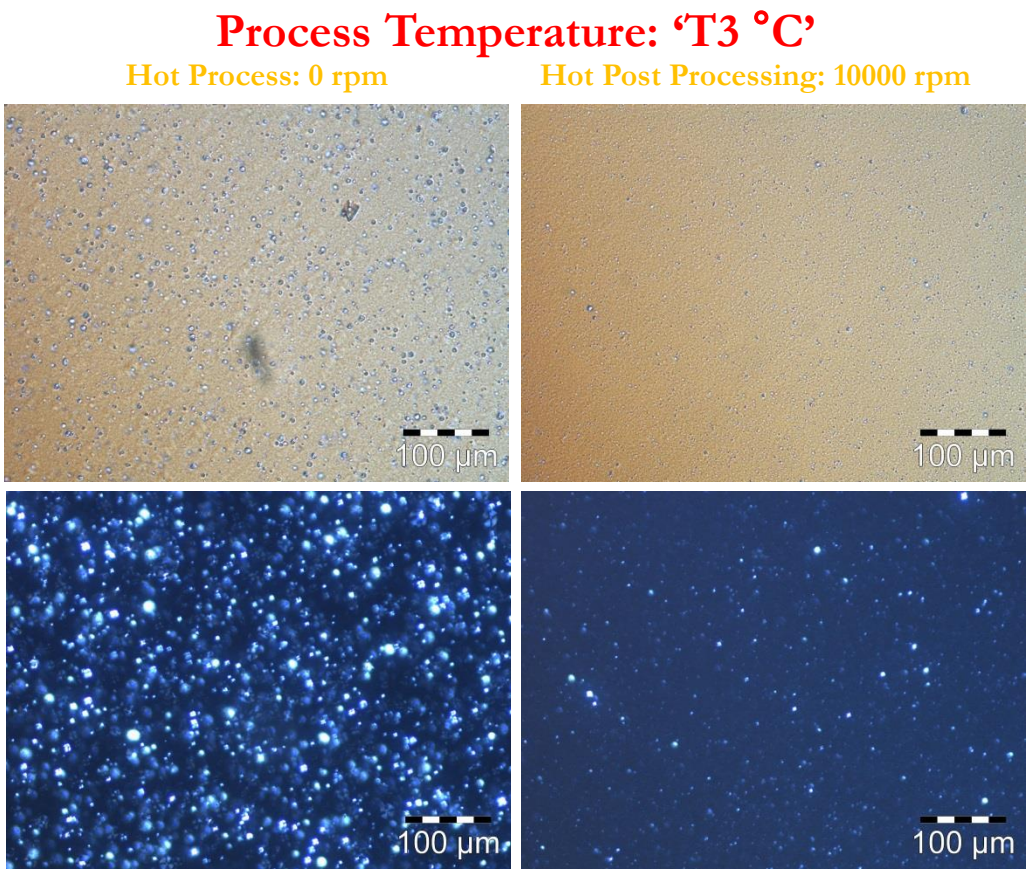

Figure 4-22: Bright field (top) and cross polarised (bottom) illuminated micrographs for AA % QUAT/CS/FA/Water samples obtained following hot high shear post processing operation at 'T3 °C' – None post processed samples included for comparison.

Figure 4-23 schematically shows the impact of cold high shear post processing on the 'FA' rich L_{β} microstructure.

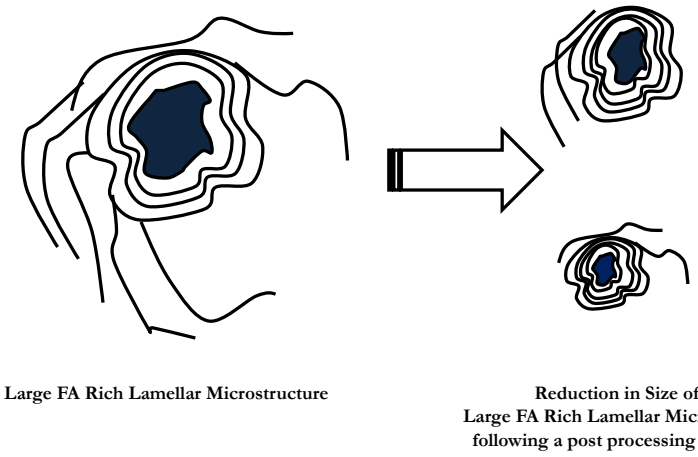

Figure 4-23: Schematic diagram of the 'FA' rich lamellae microstructure observed in the micrographs obtained for AA % QUAT/CS/FA/Water samples following high shear post processing operation.

It could be said that cold/hot high shear post processing operation help create a more homogeneous systems

4.2.3.3 Thermal Transition

DSC

Figure 4-24 - Figure 4-26 shows DSC traces for the AA % QUAT/CS/FA system which have been post processed[203] via the inline high shear mixer at 10 000 rpm – results obtained from cold/ hot process (already discussed in Section 4.2.2.3) are included for the purpose of comparison.

The trends noticed for the new dataset are not different from the trends reported in Section 4.2.2.3. It can be seen that irrespective of the nature of high shear post processing operation, the heat cycle shows a single peak, while the cool cycle shows multiple peaks for [1] hot high shear post process at 'T1 °C' and cold high shear post process at 'T1 °C' and 'T2 °C' and [2] a single broad peak at hot high shear post process at 'T2 °C' and 'T3 °C' - Summaries of the variables of the DSC curves i.e. enthalpy, onset temperature and peak temperature are summarised in Table 4-4.

.

[203] Cold/hot post processing

Table 4-4: Table indicating a summary of DSC data variables i.e. enthalpy, onset temperature and peak temperature from the set of DSC curves above for hot (left) and cold (right) post process [bottom table] – data for hot and cold process have also been displayed for the purpose of comparison [top table].

	Hot Process								
	Heat Cycle			Cool Cycle					
	Peak(s)			Peak #2			Peak #1		
Process Temperature (°C)	Enthalpy (J/g)	Onset Temperature (°C)	Peak Temperature (°C)	Enthalpy (J/g)	Onset Temperature (°C)	Peak Temperature (°C)	Enthalpy (J/g)	Onset Temperature (°C)	Peak Temperature (°C)
T1	9.1160	71.9240	74.1200	2.9441	69.0250	67.2920	0.7519	71.6790	71.3740
T2	9.3497	71.4230	74.2420	8.1132	69.8600	68.3990	-	-	-
T3	9.2724	71.0600	74.1460	7.5699	69.7670	68.2680	-	-	-

	Cold Process								
	Heat Cycle			Cool Cycle					
	Peak(s)			Peak #2			Peak #1		
Process Temperature	Enthalpy	Onset Temperature	Peak Temperature	Enthalpy	Onset Temperature	Peak Temperature	Enthalpy	Onset Temperature	Peak Temperature
T1	9.1123	71.4780	74.0940	0.8781	67.9580	66.8000	2.6446	71.6450	71.3030
T2	9.2501	72.2830	74.0610	3.9565	69.4430	67.6200	0.8680	71.8140	71.4110
T3	n/a	n/a	n/a	n/a	n/a	n/a	n/a	n/a	n/a

	Hot Post Process [10 000 rpm]								
	Heat Cycle			Cool Cycle					
	Peak(s)			Peak #2			Peak #1		
Process Temperature	Enthalpy	Onset Temperature	Peak Temperature	Enthalpy	Onset Temperature	Peak Temperature	Enthalpy	Onset Temperature	Peak Temperature
T1	10.0430	71.8030	74.1470	2.7368	71.8480	71.5390	1.1182	68.3920	67.2130
T2	9.3709	70.9910	74.6890	8.6123	69.5820	67.9370			
T3	8.7885	70.6110	74.3480	8.0953	69.6830	68.1690			

	Cold Post Process [10 000 rpm]								
	Heat Cycle			Cool Cycle					
	Peak(s)			Peak #2			Peak #1		
Process Temperature	Enthalpy	Onset Temperature	Peak Temperature	Enthalpy	Onset Temperature	Peak Temperature	Enthalpy	Onset Temperature	Peak Temperature
T1	8.7007	71.9720	74.2470	1.1681	67.5310	65.9700	2.9216	71.6540	71.2530
T2	9.2251	71.9130	74.1610	1.9944	68.2250	66.4910	2.3915	71.8570	71.5080
T3									

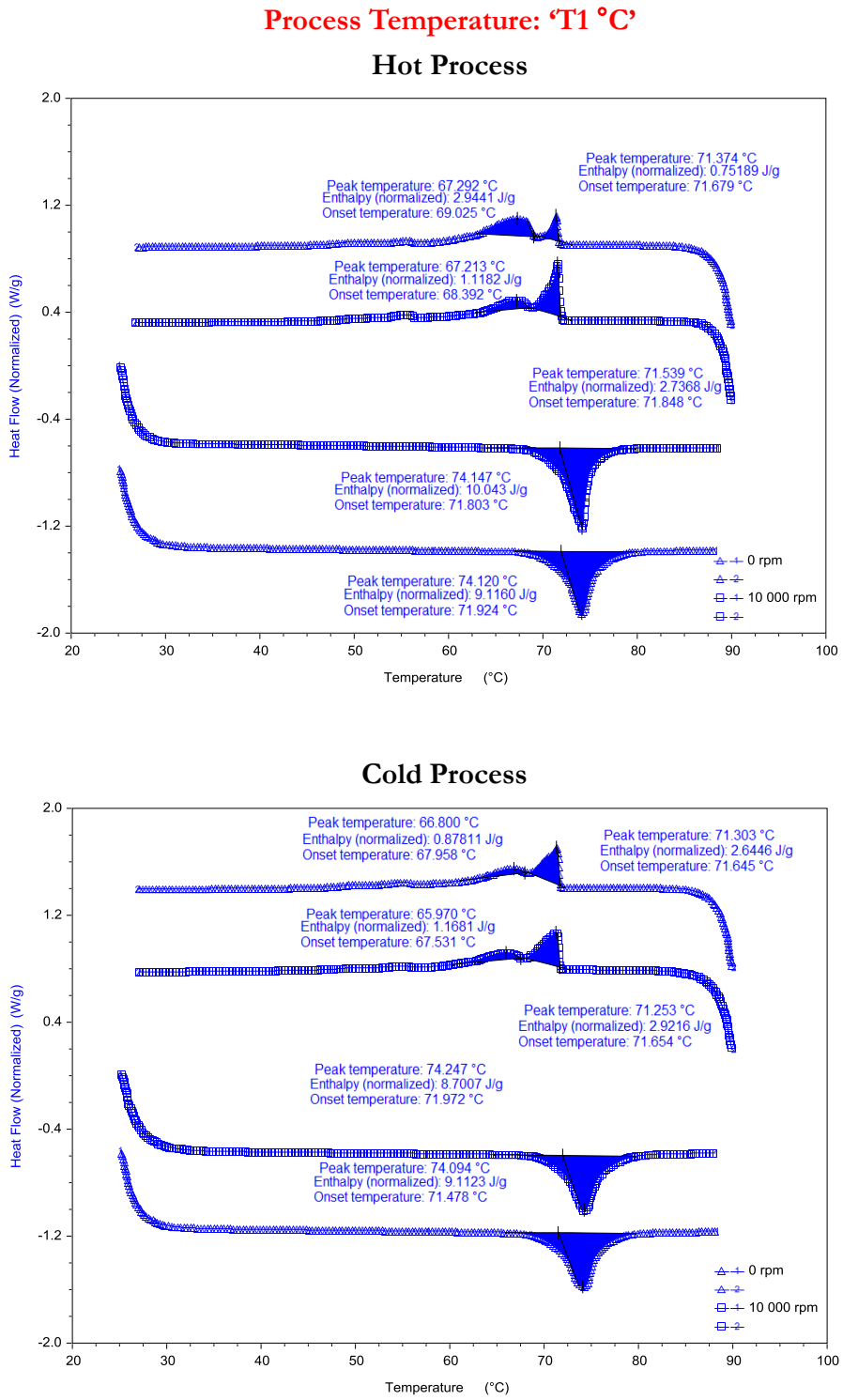

Figure 4-24: Differential scanning calorimetry trace (heat and cool cycles) for AA % QUAT/CS/FA/Water samples manufactured via the hot process (top) and cold process (bottom) - at process temperatures ('T1 °C') - displayed alongside is high shear post processed samples profile (hot and cold) at 10000 rpm.

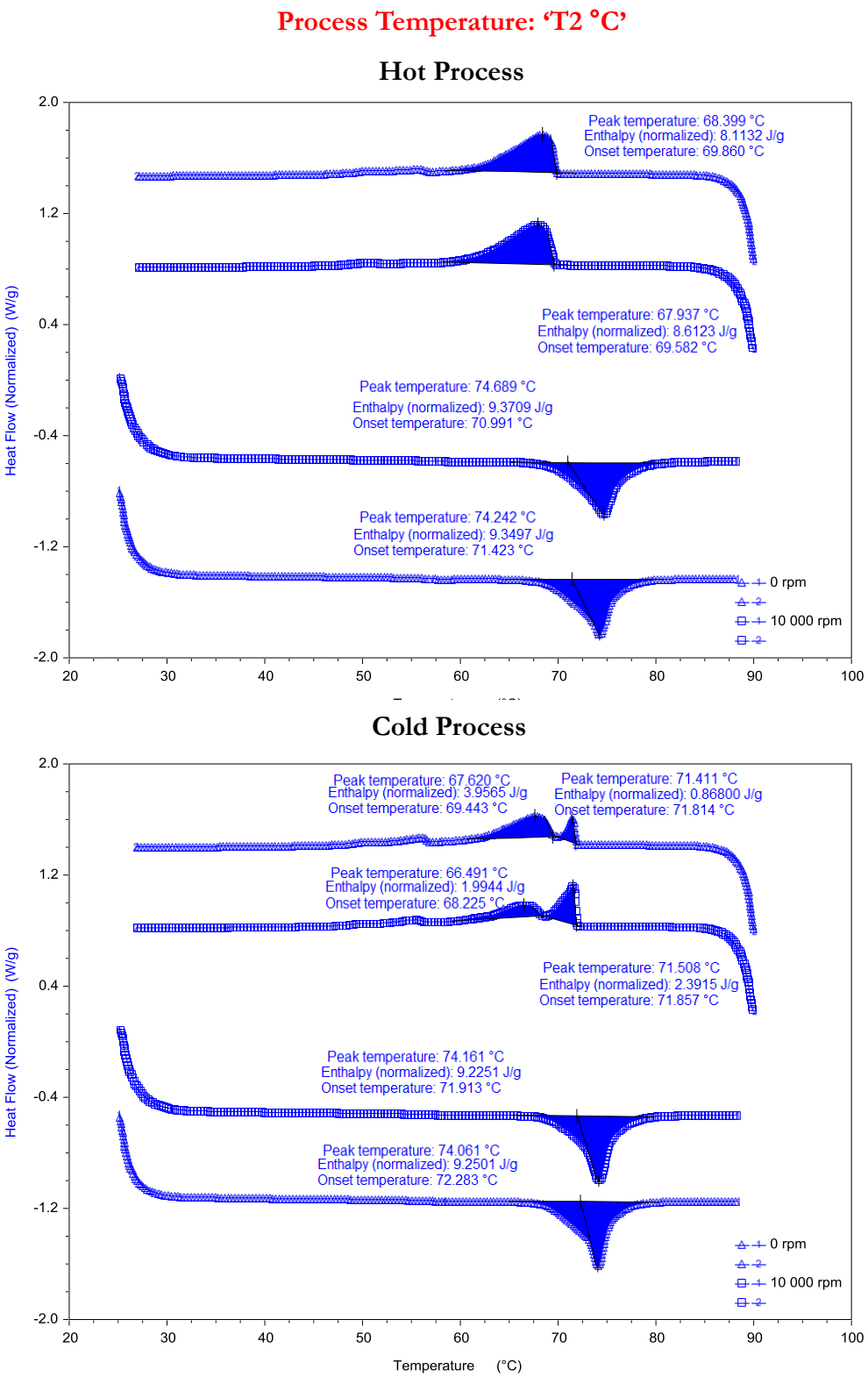

Figure 4-25: Differential scanning calorimetry trace (heat and cool cycles) for AA % QUAT/CS/FA/Water samples manufactured via the hot process (top) and cold process (bottom) - at process temperatures ('T2 °C') - displayed alongside is high shear post processed samples profile (hot and cold) at 10000 rpm.

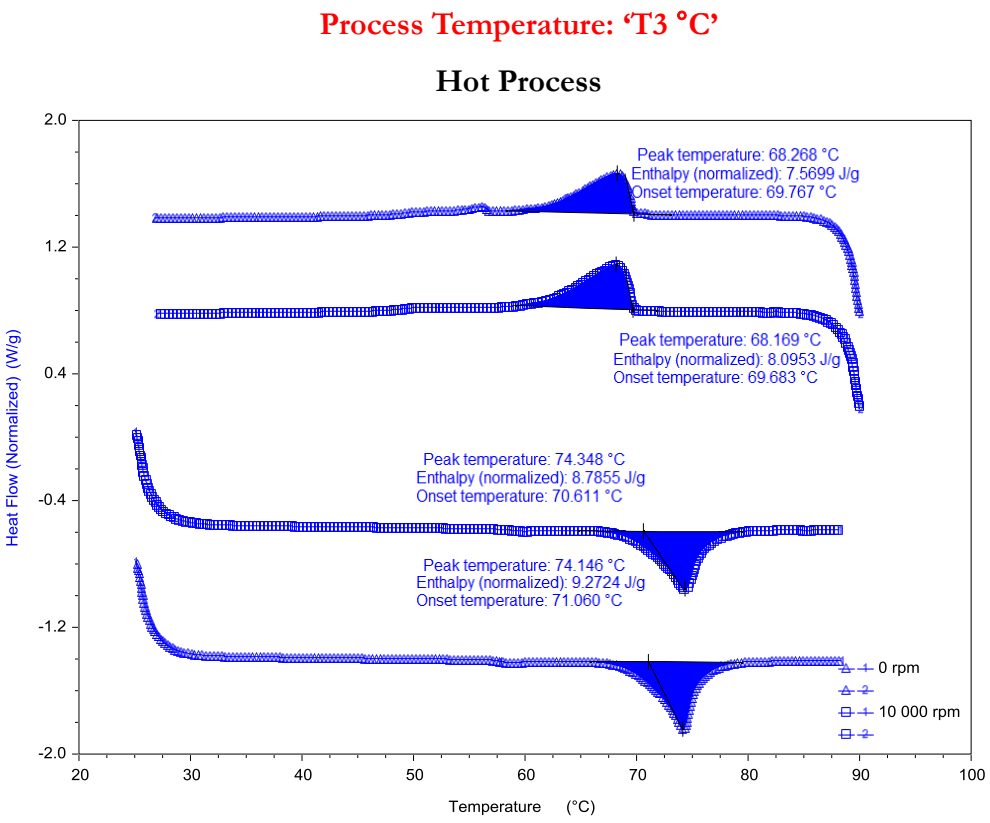

Figure 4-26: Differential scanning calorimetry trace (heat and cool cycles) for AA % QUAT/CS/FA/Water samples manufactured via the hot process - at process temperatures ('T3 °C') - displayed alongside is high shear post processed samples profile (hot and cold) at 10000 rpm.

For the heat cycles[204], as the DSC equipment heat flow (function of temperature) is increased – a broad transition peak can be seen for all curves with similar enthalpies, onset temperatures and peak temperatures all of which have been displayed in Table 4-4.

The following have been obtained – [1] an average onset temperature = 71.1350 °C ±0.6089|71.9452 °C ±0.0417, [2] average peak temperature = 74.3947 °C ±0.274|74.2040 °C ±0.061, and [3] average enthalpy = 9.4008 J/g ±0.6278|8.9629 J/g ±0.371 for hot high shear post processing | cold high shear post processing operation respectively – all of which can be attributed to the system transition temperature[205] as alluded to earlier[206].

As was the case in Section 4.2.2.3, both of these observations i.e. multiple and single peaks are observed due to the fact that high shear post processing operation are performed on the AA % QUAT/CS/FA/Water system at below and above the systems transition temperatures

[204] Hot and cold process
[205] Temperature at which the L_β forms L_α i.e. melting of the alkyl chain from frozen L_β phase to fluid like phase L_α
[206] Section 4.2.2.3

respectively. For cooling curves exhibiting multiple peaks, [peak 1] is associated with 'QUAT/CS' rich lamellar microstructure while [peak 2], is associated with the 'FA' rich lamellar microstructure.

A general trend that was noticed for materials subjected to high shear post process operation below the transition temperature of the system[207] for which multiple peaks were observed in the cool cycles – are the changes to the enthalpy values associated with Peak #1[208] and Peak #2[209] - data displayed in Table 4-4. In all cases except for the cooling curve obtained for high shear cold post processing operation at 'T1 °C'[210], all the enthalpies of crystallisation associated with Peak #1 increased with high shear post processing operation likewise all the enthalpies of crystallisation associated with Peak #2 reduced with high shear post processing operation. This supports the size reduction/restructuring[211] argument mentioned earlier in Section 4.2.3.1.

4.2.3.4 Scattering: Small Angle X-ray Scattering

Qualitative analysis performed[212], using SAXS on selected samples[213] - the analysis[214] performed on the samples does support the results discussed within this Section 4.2 - however the d-spacing data used to generate the findings are unavailable due to issues with the raw data.

The samples selected for SAXS analysis includes [1] 'T1 °C': cold process, [2] 'T1 °C': cold high shear post process at 10000 rpm, [3] 'T2 °C': cold process and [4] 'T2 °C': cold high shear post process at 10000 rpm.

Figure 4-27 shows the SAXS data for selected systems and the analysis[215] displayed on Table 4-5.

[207] Samples – cold process and cold high shear post process samples
[208] Peak associated with 'QUAT/CS' rich lamellar microstructure
[209] Peak associated with 'FA' rich lamellar microstructure
[210] Presumably due to the fact that the bilayer was already uniform and fragmentation does not really make much difference to this peak
[211] Promoting system homogeneity
[212] Performed by Cesar Mendoza
[213] Cold process and cold high shear post process samples manufactured at 'T1 °C' and 'T2 °C'
[214] Performed by Jeff Penfold
[215] Structural comments

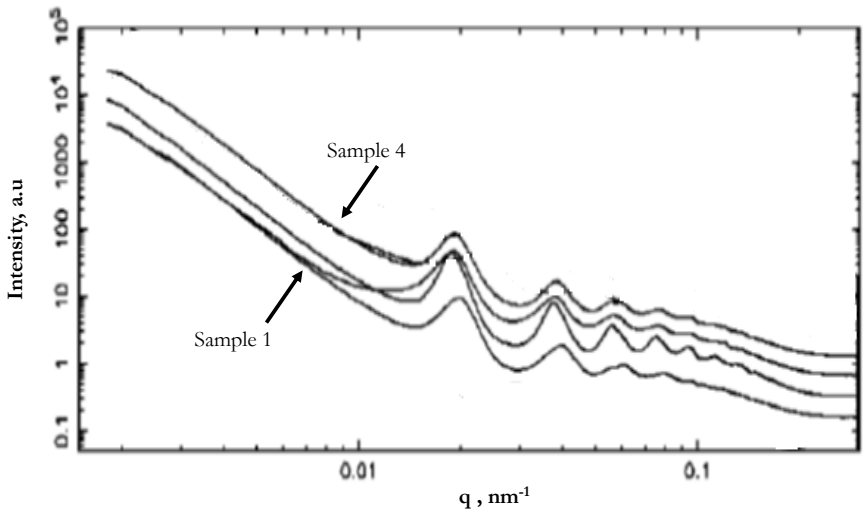

Figure 4-27: SAXS data for AA % QUAT/CS/FA/Water system manufactured via various processing routes; from top to bottom [1] cold process manufactured 'T1 °C' [2] cold high shear post process manufactured at 'T1 °C' [3] cold process manufactured 'T2 °C' and [4] cold high shear post process manufactured at 'T2 °C' – each curve is shifted vertically by a factor x2.

Table 4-5: Structure assignment for selected samples for SAX data curve /plot in Figure 4-27 (from bottom to top) (Penfold 2014)

Sample Reference	Route to Manufacture		Structure/Comments
	Process Temperature, °C	Process Details	
1	'T1 °C'	Cold process [none post processed]	[216]L_β/L_1, more rigid membrane
2	'T1 °C'	Cold high shear post process	L_β/L_1, most rigid
3	'T2 °C'	Cold process [None post processed]	L_β/L_1, similar to sample 1
4	'T2 °C'	Cold high shear post process	L_β/L_1, similar to sample 3

A review of the SAXS curves displayed Figure 4-27 - all the samples tested seem to have identical structure and very similar scattering profiles indicative of similar d-spacing – it could therefore be said that based on this evidence, there is no effect of high shear post processing operation on the d - spacing of the underlying microstructure.

From the analysis conducted (Table 4-5), it can be seen that all samples contain a mixture of phases (L_β/L_1) - where L_β (lamella gel) and L_1 (globular micelles) for which L_β is the predominant structure. SAXS measurement has detected the presence of globular micelles – although these were seen in the micrographs in this Section, it was difficult to tell it apart from very small FA L_β

[216] Coexistence of phases in which L_β is the predominant structure

microstructure – presumably large 'FA' rich L_β microstructure evolve to form these globular micelles. Secondly the introduction of high shear post processing operation seems to promotes promote more rigid L_β structures.

A quote from Penfold's report on the structures[217] can be read below:

> "where visibility/definition of the Bragg peaks decreases, we have described this in terms of a more labile/flexible membrane and vice-versa about increased rigidity when the structure is more pronounced. This can also be strongly coupled with a change in N, the number of bilayers per fragment; and it is difficult from this data to distinguish between the two. Indeed both factors are often at play (Penfold 2014)".

From literature (Brotons, Dubois & Belloni 2005; Emanuel 2011; Yang et al. 2001), membrane rigidity can be associated to fluctuations which is often characterised by Caillé parameter - a low Caillé parameter, is as a result of a rigid system with weak membrane fluctuations while a high Caillé parameter, is as a result of a less rigid system (soft system) presenting strong fluctuations with a rather high amplitude. One could therefore infer that cold high shear post processing operation decreases the Caillé number[218] of the lamellar system thus making it a more pronounced structure likewise it increases the number (N) of the lamellar bilayer - 'QUAT/CS' rich L_β microstructure which can be related to volume fraction as alluded to earlier.

[217] Table 4-5
[218] Decrease membrane fluctuations

4.3 Benchmark System: Process Improvement

The work discussed in this Section is performed against the backdrop of the work discussed in Section 4.1[219], in which the benchmark product was manufactured - however the process temperature has been adjusted in light of the new learnings obtained thus far in regards to the QUAT/CS/FA/Water system.

4.3.1 Benchmark System Manufacture

Hair Conditioner Manufacture: similar to the manufacturing step described in Section 4.1.1, however the concentrate has been manufactured at a significantly lower temperature of approx. 'T1 °C'.

4.3.2 Benchmark System Analysis

Results and discussion of experiments aimed at reproducing the benchmark 1.0H-C Hair Conditioner at a revised process temperature is conferred within this section.

4.3.2.1 Rheology

Brookfield T-Bar B Viscosity

Figure 4-28 illustrates the Brookfield T-Bar B viscosity as a function of inline high shear mixer rotational speed for the revised 1.0H-C Hair Conditioner benchmark manufactured at process temperature of approx. 'T1 °C' – displayed alongside this, is the dataset obtained from the benchmark 1.0H-C Hair Conditioner manufacture at process temperature of T4 °C – data which was initially disseminated in Section 4.1.2.

[219] The manufacture of the benchmark

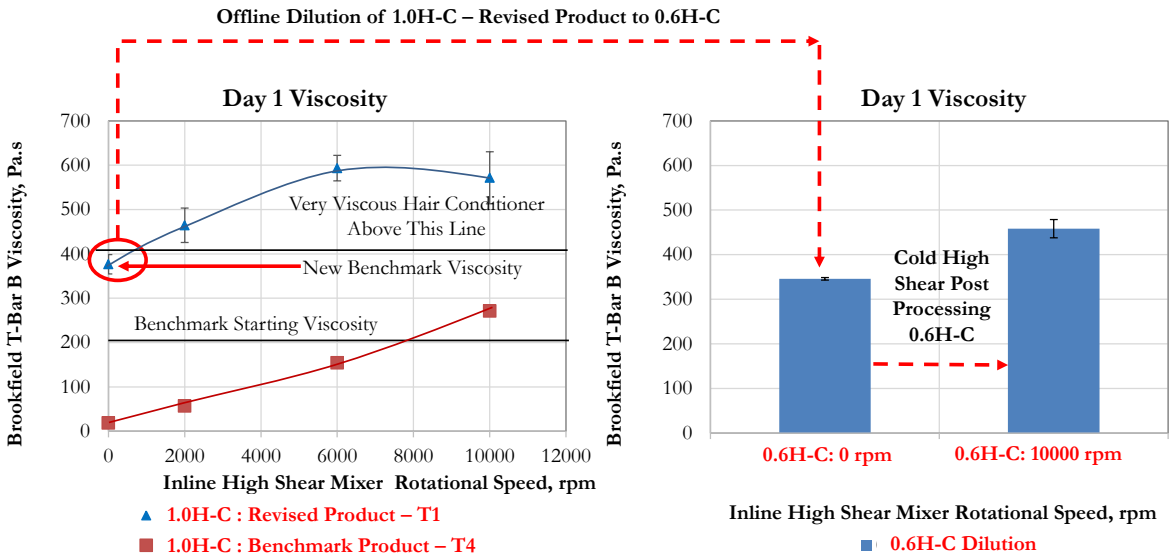

Figure 4-28: Brookfield T-bar B viscosity as a function of inline high shear mixer rotational speed for 1.0H-C Hair for the benchmark system – process temperature = 'T1 °C', benchmark Hair Conditioner data produced at process temperature = T4 °C has been included for the purpose of comparison and Brookfield T-bar B viscosity for a diluted product (1.0H-C dilution to 0.6H-C) alongside 0.6H-C material which has been subjected to high shear cold processing via the inline high shear mixer at 10000 rpm (right).

It can be seen that the viscosity profile obtained for the products manufactured at process temperature of 'T1 °C' lies above the products manufactured at process temperature of T4 °C – with distinctly different viscosities for every inline high shear mixer rotational speed considered – this result is expected in the light of what has been learnt about AA % QUAT/CS/FA/Water system – likewise offline dilution[220] from 1.0H-C to 0.6H-C) shows an increase in viscosity (circa of 400 Pa.s[221]) – comparable to the new benchmark's consistency following a post processing operation via the inline high shear mixer at 10000 rpm – effectively showing that raw material concentrations in product can be below current formulation without loss in consistency following a cold[222] high shear post processing operation.

Secondly a review of the underlying microstructure (Figure 0-4) for the Hair Conditioner products manufactured at process temperature of 'T1 °C' is seen to be predominantly 'QUAT/CS' rich L_{β} microstructure which is also expected. More work is done on the manufacturing of 1.0H-C Hair Conditioner in Chapter 5.

[220] Performed by adding required amount of water to a set amount of process material
[221] Brookfield T-Bar B Viscosity measurement
[222] Ambient temperature

As the material is passed through the inline high shear mixer at various rotational speeds, it was noticed that the process material becomes very viscous and the peristaltic pump struggled to move the material to ensure efficient cold high shear post processing.

Based on the work conferred here, a new benchmark viscosity value (400 Pa.s) is set – this will form the backdrop against the work disseminated in Chapter 5 is performed against as the aims of the Thesis is achieved.

4.4 Summary

Rheology, microscopy, scattering (SAXS) and thermal transition investigations, disseminated in this Chapter have been used to elucidate the effect of various process variables on the underlying microstructure of AA % QUAT/CS/FA/Water system – subsequently Hair Conditioners based on this system manufactured via the benchmark process.

In manufacturing this system under low shear, it was found out that the underlying principal L_β microstructure formed is either [1] 'QUAT/CS' rich, or [2] 'FA' rich – both of which are formed in different proportions depending on the systems process temperature. SAXS measurements also detected the presence of globular micelles (L_1) which presumably can be associated with 'FA' rich L_β microstructure - all these various microstructure contribute to the structural properties exhibited by the formed gel phase network.

Manufacturing the system at elevated temperatures (above systems' transition) encourages the formation of increased amount of 'FA' rich L_β microstructure by volume fraction.

Prolonged mixing coupled with cooling the system down from elevated temperatures towards ambient temperature can promote the formation 'QUAT/CS' rich L_β microstructure or conversion of the existing 'FA' rich L_β microstructure to 'QUAT/CS' rich L_β microstructure. This is also true for intense mixing action[223] at elevated temperatures of the already formed lamellar microstructure otherwise referred to in this text as hot high shear post processing.

High shear post processing at ambient temperature induces a number of changes to the morphology of the lamellar system [1] size reduction of the L_β microstructure (FA/'QUAT/CS' rich) particle size which has been also referred to as 'fragmentation' in this text and [2] restructuring of the 'QUAT/CS' rich L_β microstructure via the incorporation of fragments of FA thereby enhancing the systems homogeneity. Both, contributes to increasing the volume fraction of the 'QUAT/CS' rich L_β microstructure, thus resulting in a significant increase in the system viscosity – which decreases lamellar membrane fluctuation effectively promoting membrane rigidity as was revealed by SAXS results.

The new knowledge gained from carrying out these empirical studies prompted the revision of the process temperature at which the benchmark material is made – i.e. from approx. 'T4 °C' to 'T1 °C' thus allowing the optimisation of batch benchmark process for higher rheology and

[223] High shear mixing

better microstructural properties. This culminated to setting a new benchmark viscosity value of 400 Pa.s which forms the backdrop for the work conducted and disseminated in Chapter 5.

4.5 References

- Balzer, D., Varwig, S. & Weihrauch, M. (1995) 'Viscoelasticity of Personal Care Products', Colloids and Surfaces A: Physicochemical and Engineering Aspects, vol. 99, pp. 233 - 246.
- Berghausen, J., Zipfel, J., Lindner, P. & Richtering, W. (1998) 'Shear-induced Orientations In A Lyotropic Defective Lamellar Phase', Europhysics Letters, vol. 43, no. 6, pp. 683 - 689.
- Bongers, P.M.M., Egan, M.J. & Irving, G.N. (2013) Method For Production Of Structured Liquid And Structured Liquid, Great Britain.
- Brotons, G., Dubois, M. & Belloni, L. (2005) 'The Role of Counterions On The Elasticity of Highly Charged Lamellar Phases: A Small-Angle X-ray and Neutron-Scattering Determination', The Journal of Chemical Physics, vol. 123, pp. 024704-024701 - 024704-024718.
- Diat, O., Roux, D. & Nallet, F. (1993) 'Effect Of Shear On A Lyotropic Lamellar Phase', Journal de Physique. II, vol. 3, no. 9, pp. 1427 - 1452.
- Eccleston, G.M., Behan, M.K., Jones, G.R. & Towns-Andrews, E. (1988) 'Swelling Properties of Emulsifying Wax/Water Gel Phases', Journal of Pharmacy and Pharmacology, pp. 1 - 39.
- Emanuel, S. (2011) Generic and Specific Roles of Saccharides at Cell and Bacteria Surfaces - Revealed by Specular and Off-Specular X-Ray and Neutron Scattering, Springer, Berlin Heidelberg.
- Fletcher, W.P. & Gent, A.N. (1953) 'Non-linearity in the Dynamic Properties of Vulcanized Rubber Compounds', Transactions of the Institution of the Rubber Industry, vol. 29, pp. 266 - 280.
- Franck, A.J. (2004) Understanding Rheology of Structured Fluids, United States
- Hauser, H. (1984) 'Some Aspects of The Phase Behaviour of Charged Lipids', Biochimica et Biophysica Acta, vol. 772, pp. 37 - 50.
- Jones, T.J., Neustadter, E.L. & Whittingham, K.P. (1978) 'Water-In-Crude Oil Emulsion Stability And Emulsion Destabilization By Chemical Demulsifiers', Journal of Canadian Petroleum Technology, vol. 17, no. 02, pp. 1 - 10.

- Kyu, H., Sook, H.K., Kyung, H.A. & Seung, J.L. (2002) 'Large Amplitude Oscillatory Shear as Away To Classify The Complex Fluids.', Journal of Non-Newtonian Fluid Mechanics, vol. 107, no. 1 - 3, pp. 51 - 65.
- Oswald, P. & Allain, M. (1988) 'Rheology and Structural Defects In a Lyotropic Lamellar Phase', Journal of Colloid and Interface Science, vol. 126, no. 1, pp. 45 - 53.
- Partial, P., Kowalski, A.J., Machin, D., Kiratzis, N., Berni, M.G. & Lawrence, C.J. (2001) 'Rheology and Microstructural Transitions in the Lamellar Phase of a Cationic Surfactant', Langmuir, vol. 17, pp. 1131 - 1337.
- Payne, A.R. (1962) 'The Dynamic Properties of Carbon Black Loaded Natural Rubber Vulcanizates. Part II', Journal of Applied Polymer Science, vol. 6, no. 21, pp. 368 - 372.
- Penfold, J. (2014) Analysis of Hair Conditioner and Shampoo Formulation X-ray Data,
- Rydhag, L. & Gabran, T. (1982) 'Phase Equilibria In The System Dimyristoyl Phosphatidyl Choline/Hexadecyl Trimethylammonium Bromide/Water at 30 °C. Swelling Behaviour of The Lamellar Phase With Different Electrolyte Solutions', Chemistry and Physics of Lipids, vol. 30, pp. 309 - 324.
- Sadtler, V.M., Guely, M., Marchal, P. & Choplin, L. (2004) 'Shear-induced Phase Transitions in Sucrose Ester Surfactant', Journal of Colloid and Interface Science vol. 270, no. 2, pp. 270 - 275.
- Tiddy, G.J.T., Hassan, S. & Rowe, W. (2001) Surfactant Liquid Crystals and Surfactant Chemical Structure, in K. Holmberg, D.O. Shah & M.J. Schwuger (eds), Handbook of Applied Surface and Colloid Chemistry, vol. 1 - 2, John Wiley & Sons Ltd, Chichester.
- Yang, B., Jyotsana, L., Richetti, P., Marques, C.M., Russel, W.B. & Prud'homme, R.K. (2001) 'Interaction of Hydrophobically Modified Polymers and Surfcatant Lamellar Phase', Langmuir, vol. 17, pp. 5834 - 5841.

Chapter 5

5 Process Design Studies; Processing of Model Hair Conditioner Using CDDM Technology

The work disseminated in this Chapter was conducted in parallel with that discussed in Chapter 4 - in which the effect of process variables on the manufacturing of H-C based Hair Conditioners was reviewed.

5.1 Pilot Plant Studies - Manufacturing of Hair Conditioners Based on the QUAT/CS/FA/Water System

The work discussed in this Section builds on the foundation laid - from the work discussed in Chapter 4 - in that it investigates the effect of temperature on the manufacture of H-C based concentrated lamellar dispersions albeit in a different equipment[224]. The new equipment set-up allowed for a closer control of process temperatures – for which temperature accuracy were within (± 0.1 °C) of measured temperature which was not possible in the equipment set-up used in Section 4.2.

More importantly the work is performed against the back drop of the work discussed in Section 4.3.2 – in which a Brookfield T-bar B viscosity value of 400 Pa.s[225] was obtained from the batch benchmark process for a fully formulated 1.0H-C Hair Conditioner.

Another feature of this work was that - a fully formulated Hair Conditioner was manufactured alongside these temperature tests as a continuous process i.e. as the AA % QUAT/CS/FA/Water system is made; it is combined with other minor ingredients to form a fully formulated Hair Conditioner (1.0H-C = BB % concentration) – viscosity of which would be compared to the aforementioned day 1 Brookfield T-bar B of 400 Pa.s.

Effectively, the work considered the development of a continuous manufacturing process route for the manufacture of an optimum Hair Conditioner (solids and minor)[226].

[224] CDSM-1 (Figure 3-12) and CDSM-2 (Figure 3-13)
[225] Measured at approximately 24 hours after manufacturing (day 1 viscosity) – See Figure 4-28
[226] In parity/surpassing results obtained from the work discussed in Section 4.3.2 in terms of rheology and underlying microstructure.

The experiments are conducted using a purpose built static[227] variant of CDDM technology (CDSM); (CDSM-1[Figure 3-12] and CDSM-2 [Figure 3-13])[228] - via experimental program described in Figure 5-1. Continuous process would present benefits such as manufacturing of Hair Conditioner with consistent characteristics as well as increased rate of production.

5.1.1 Experimental Program

A schematic of the factors considered in the experimental program as well as the responses measured can be seen in Figure 5-1. The objective of the experimental design was to investigate an optimum process route (in terms of equipment setup and process variables) for the continuous manufacture of Hair Conditioners via the CDSM technology.

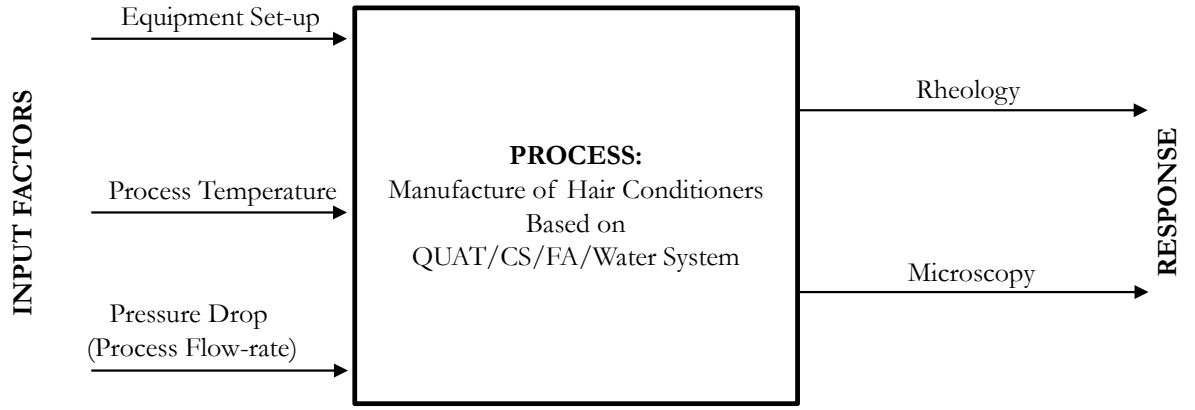

Figure 5-1: Schematic of experimental design for the manufacture of Hair Conditioners based on QUAT/CS/FA/Water System.

The experimental trials conducted assessed the effect of several process variables on the underlying microstructure of the lamellar dispersion produced - subsequently the resulting Hair Conditioner (solids and minors). The input factors considered during the experimental trials conducted include; equipment set-up[229], process temperature[230], and process flow-rate[231] – analytical techniques used for microstructure assessment were rheology and optical microscopy.

[227] The absence of moving parts results in a lower operational/maintenance costs as well as inherently safe.
[228] A high shear rotor-stator static device
[229] The way in which process streams containing raw materials are combined in the CDSM device
[230] Temperature at which concentrated lamellar dispersion (AA %) is manufactured – new set-up offers better accuracy
[231] Flow-rates at which the various streams are combined together - also comparable to pressure drop within the system

5.1.1.1 Experimental Matrix (Sample Preparation)[232]

The continuous process route utilised mirrored the batch process (Section 4.1.1) in which the FA and the 'QUAT/CS' are initially mixed to form a concentrated lamellar dispersion ('AA % QUAT/CS/FA/Water')[233] before the addition of minors. The process stream containing the dispersion of AA % QUAT/CS/FA/Water can also be referred to as 'molten ingredients or molten ingredient stream'

The continuous process is carried out in two stages (Figure 5-2) namely; the formation of a 'AA % QUAT/CS/FA/Water' which is combined with the minors downstream as well as diluted – stream components are disclosed in Table 5-1.

The first stage is the formation of a concentrated (AA %) lamellar dispersion at different process temperatures[234] - temperature control was achieved via an energy balance on the input stream (Figure 5-2).

Figure 5-2: Schematic illustration of 2 stage production of 1.0H-C Hair Conditioners.

[232] Pilot plant technician (John Naughton) help set-up these experiments as I am not a trained to use any of the equipment in the pilot plant
[233] Molten ingredients
[234] This is achieved via the bleed of cold demineralised water as illustrated in Figure 5-2

Table 5-1: Table indicating process streams and its components.

Stream	Stream Descriptor	Stream Component	Stream Temperature °C
S1	Confidential	Confidential	Confidential
S2	Confidential	Confidential	Confidential
S3	Confidential	Confidential	Confidential
S4	Confidential	Confidential	Confidential

The energy balance calculations are performed to overestimate required process temperature and then corrected by manually adjusting the needle valve until target temperature is reached - real time feedback of stream temperature is monitored on the connected data logging software (Figure 5-2) – when a required process temperature is reached in real time, a sample is obtained.

In the second stage, the concentrate (AA % lamellar dispersion) is diluted to standard product formulation (1.0H-C) via the introduction of S4 – stream of water at ambient temperature. Components of the various streams disclosed in Table 5-1.

In order to assess the effectiveness of the CDSM technology for the manufacturing of H-C based Hair Conditioners, a series of process (trials) strategies was reviewed (see below) - experimental trials conducted have been grouped under two different categories namely [1] TU21 – 22: **CDSM-2**, and [2] TU25: **CDSM-2 – CDSM-1** – the set-ups were based on the nature/make-up of the equipment in question – refer to Section 3.3.2 for equipment details. Process flow diagrams for experimental set-up are shown in Figure 5-3 and Figure 5-4 respectively.

Experimental Trial: TU21 – 22: CDSM-2

TU21 and TU22 assessed the effectiveness of the CDSM-2 device for the manufacturing of lamellar dispersion based products. For Stage 1, a temperature scan ('T#1 °C – T#11 °C') was conducted in the device followed by cooling/dilution by S4.

Actual temperature at which lamellar concentrates were made is shown in Table 5-2 - for both experiments. TU21 and TU22 reviewed two different process setups using CDSM Mk II - illustrated in Figure 5-3.

Figure 5-3: Schematic process flow diagram of pilot plant equipment set-up during experimental trials – TU21 (left) and TU22 (right).

Table 5-2: Table indicating the estimated process temperatures at which lamellar dispersion ('AA % QUAT/CS/FA/Water') was formed for both TU 21 and TU 22 experimental trials.

	Lamellar Dispersion Temperature ('AA % QUAT/CS/FA/Water') T, °C										
Sample	**#1**	**#2**	**#3**	**#4**	**#5**	**#6**	**#7**	**#8**	**#9**	**#10**	**#11**
TU 21	**Low**					**Med**				**High**	
TU 22											

For TU21, the molten ingredient stream is injected via the central shaft i.e. along the static rotor with the Aqueous and Hot water streams were introduced via the outer ports. For TU22, the molten ingredient stream was fed into the process to the outer port and aqueous stream fed centrally alongside the Hot water stream. The cool stream was fed into the process via the top port.

Pressure drop of approx. 30 bar_g was anticipated for flow-rate of 0.300 kg/s (molten ingredient stream at 0.150 kg/s and cool at 0.150 kg/s)[235]. Actual flow-rate and pressure drop are displayed in Table 5-4.

Experimental Trial: TU25: CDSM-2 – CDSM-1

These experimental trials assessed the performance of the combination of the CDSM-2 and CDSM-1in series (Figure 5-4) for the manufacture of lamellar dispersion based product alongside the effect of the temperature and pressure at which the L_α phase is formed.

[235] 0° angular offset and 2.4 mm spacer shift - mixer mechanical setup

Figure 5-4: Schematic process flow diagram of pilot plant equipment set-up during experimental trials – TU 25.

For TU25, a temperature scan from 'T#1 °C – T#11 °C' (Table 5-3) was conducted using the hot water stream/cold water bleed as a temperature modifier on the 'AA % QUAT/CS/FA/Water' prepared in CDSM Mk II device followed by cooling by chilled water blend in the CDSM-1 device.

Table 5-3: Table indicating the estimated process temperatures at which lamellar dispersion ('AA % QUAT/CS/FA/Water') was formed for both TU 21 and TU 22 experimental trials.

	Lamellar Dispersion Temperature ('AA % QUAT/CS/FA/Water') T, °C										
Sample	**#1**	**#2**	**#3**	**#4**	**#5**	**#6**	**#7**	**#8**	**#9**	**#10**	**#11**
TU25	**Low**				**Med**					**High**	

Hot water and aqueous premix streams are fed into the outer ports to merge with molten ingredient stream entering via central shaft in the CDSM-2 followed by pressure drop down to atmospheric pressure in the CDSM-1device.

Stage 1 of TU25 was set for a low pressure operation approx. 30 - 23 bar (**ΔP approx.7 bar_g**) in CDSM-2 and ΔP approx. 23 bar_g to atmospheric across CDSM-1 was (**ΔP approx. 23 bar_g**). Flow-rates values were set at 7 kg/min for both stages; actual process variables are recorded in Table 5-5.

High pressure drop[236] trials were performed however due to leaks in the system – the results have been reported in Appendix A as TU24 experiments

[236] Higher pressure drop at Stage 1 (ΔP approx. 23 bar_g) of the process in comparison to Stage 2 (ΔP approx.7 bar_g)

Table 5-4: Table indicating actual process variables recorded during experimental trials – TU21, TU22, and TU25.

	Process Flow-rates								
Trial #	S1	S2	S3	S4	Concentrate	Product	Pressure drops		
	Pump Flow-rate, kg/s						CDSM-2	CDSM-1	Total
							bar_g		
TU21									
TU22									
TU25									

5.1.2 Effect of Process Variables: Temperature and Pressure

The results discussed in this Section are of the experimental trials, which consider a range of process variables[237] in the continuous manufacturing of a fully formulated[238] Hair Conditioner via the purpose built static CDSM. For the Stage 1 (Figure 5-2) of the manufacturing process – the 'AA % QUAT/CS/FA/Water' is manufactured at a range of process temperatures ('T#1 °C – T#11 °C') – these temperatures were accurate to within ± 0.1 °C as has been already mentioned followed by the addition of cool water and minor ingredient in Stage 2.

5.1.2.1 Rheology

Brookfield T-bar B Viscosity

The effect of process temperature on the Brookfield T-bar B viscosity for 1.0H-C Hair Conditioner product manufacture via a range of process route[239] is shown in Figure 5-5 – data is displayed for Brookfield T-bar B viscosity measured on day 0[240], 1, 7 and 28.

[237] Process temperature, pressure drop (process flow-rate), Equipment set-up
[238] QUAT/CS/FA/Minor Ingredients/Water
[239] TU 21, 22, 24 and 25
[240] Brookfield T-bar B viscosity measured with one hour of manufacture

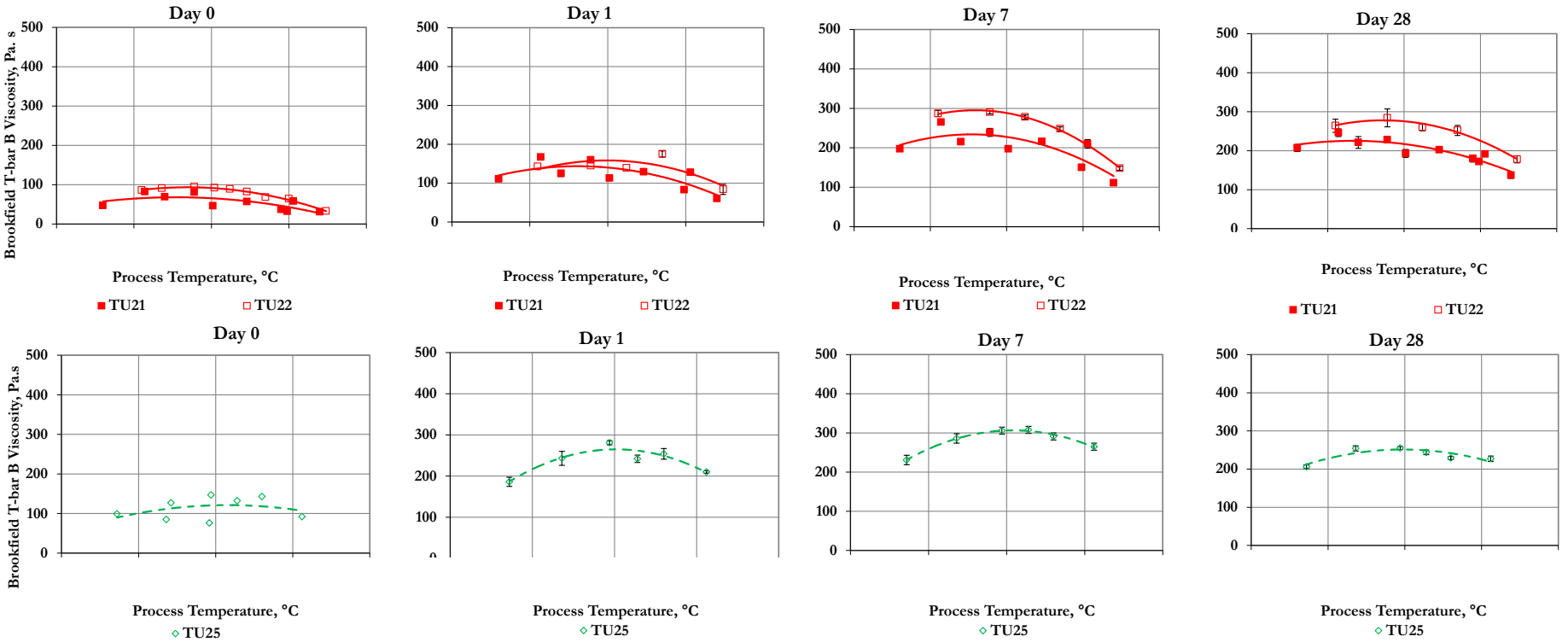

Figure 5-5: Brookfield T-bar B viscosity as a function of process temperatures ('T#1 °C – T#11 °C') for Hair Conditioners based on the 1.0H-C formulation – Brookfield T-bar B viscosity is also shown as a function of product age (fresh viscosity [left], day 28 viscosity [right]) for experimental trials TU21, TU22 and TU24.

In general it can be seen that as the process temperature at which the 'AA % QUAT/CS/FA/Water' lamellar dispersion is manufactured[241] is increased, the viscosity of the Hair Conditioner product increases up to a maximum peak at approximately 'T-optimum °C' at which point it begins to descend. This temperature ('T-optimum °C') would be referred to as 'optimum T[242]' in the context of these new set of experiments[243] – which is presumably, the temperature at which the underlying microstructure of the Hair Conditioner product is predominantly 'QUAT/CS' rich L_β microstructure with the least amount of 'FA' rich L_β microstructure.

So far we already know from the work discussed in Chapter 4, more importantly Section 4.2.3.1, that when a AA % QUAT/CS/FA/Water ('QUAT/CS' rich L_β microstructure) system is diluted[244], the system swells – effectively increasing systems' bulk viscosity, and that the manufacture of a predominantly 'QUAT/CS' rich L_β microstructure is preferably at approximately 'T1 °C' – with this in mind, a reference to an optimum temperature being 'T-optimum °C' against the backdrop of current work is a plausible assumption.

Secondly, assuming the minor ingredient have no effect or similar effects[245] on the underlining microstructure, one can infer that the dilution of the concentrate at 'Stage 2' of the manufacturing process i.e. adding cool water, causes the underlying L_β microstructure[246] to swell – hence samples manufactured at the 'optimum T' would possess the highest viscosity when compared to other samples - as they will swell better than their counterparts.

Schematic in Figure 5-6 is used to explain the inferred underlining microstructural differences between manufactured samples with respect to process temperature - both of which are responsible for the Brookfield T-bar B viscosity profile data reported in Figure 5-5 – obviously route to manufacture (equipment set up) would also affect the system bulk viscosity when inter-samples[247] are compared but not when intra-samples[248] are compared.

---

[241] Stage 1
[242] Temperature at which the underlying microstructure is predominantly 'QUAT/CS' rich L_β microstructure
[243] Experiments reported in current Section 5.1.2
[244] Which is no different to what occurs when a 'AA % QUAT/CS/FA/Water' is diluted to a BB % concentration alongside the addition of minor ingredients to form a 1.0H-C Hair Conditioner.
[245] Across all the experimental trial conducted
[246] Available 'QUAT/CS' rich - (see micrographs in Section 5.1.2.2 for nature of the underlying microstructure of the Hair Conditioner products
[247] I.e. comparing experimental trials - TU21 vs. TU22
[248] I.e. comparing samples manufactured at different process temperatures within the same experimental trials – TU21

From the datasets obtained, it can be inferred that - at 'optimum T', 'AA % QUAT/CS/FA/Water' possess the most 'QUAT/CS' rich L_β microstructure than any other temperature examined hence the higher viscosity following its dilution and the addition of minor ingredients when intra-samples are compared.

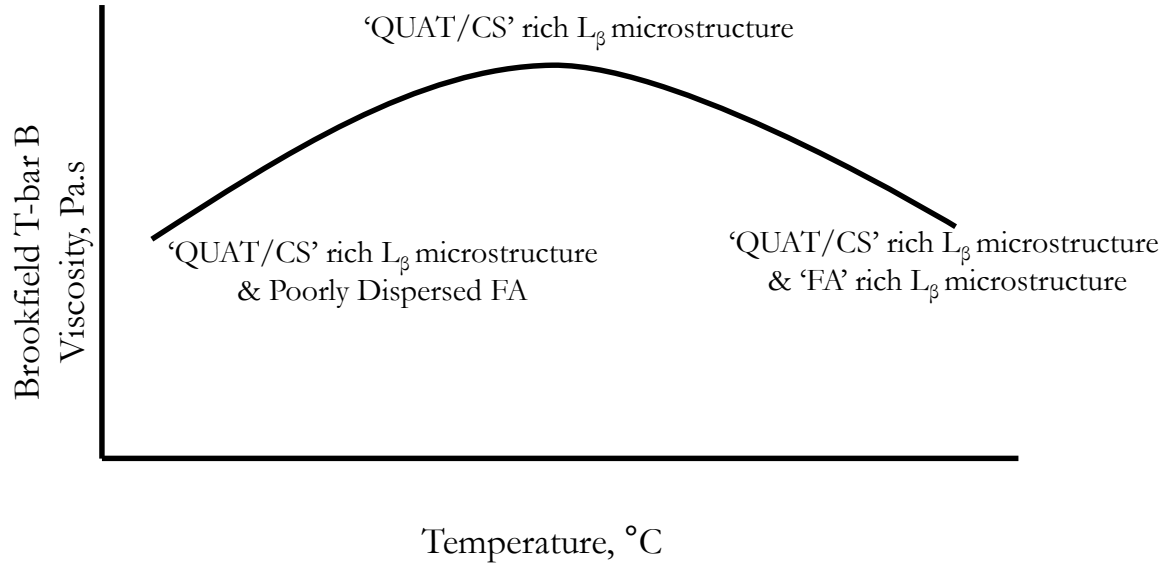

Figure 5-6: Schematic illustrating the effect of process temperature on the nature of the underlying lamella microstructure formed in H-C based Hair Conditioners

For samples obtained left to the 'optimum T', it can be inferred that as the process temperature is decreased, the system temperature approaches the set temperature of the molten ingredients at which point it becomes increasingly difficult to disperse as molten process ingredients will begin to set making homogeneous mixing more difficult to achieve - this action thus results in a poor state of dispersion of the concentrate (see Figure 5-7) - a coarse dispersion is thus assumed to result in a poorly structured lamellar concentrate hence the low viscosity of subsequent products.

Conversely, as process temperature is increased past the optimum T, the system temperature approaches temperatures increasingly favourable to a system dominated by 'FA' rich L_β microstructure alongside 'QUAT/CS' rich L_β microstructure hence a lamellar system that is less prone to swelling on dilution[249] - resulting in poor properties of subsequent products in this case low viscosity.

[249] And minor addition

Only at 'optimum T' is the best state of dispersion (see micrographs Figure 5-7, Figure 0-7[250] and Figure 0-10[251]) obtained for which microstructure is fully a 'QUAT/CS' rich L_β microstructure - further analysis on the samples obtained, is conducted using cross polarised illuminated micrographs (Figure 5-7).

All in all, inter trial (i.e. TU 21 – 22 vs. TU25) viscosity curve profiles comparison shows that the product viscosity increases according to TU 21 < TU 22 < TU25 as seen in Figure 5-5 i.e. the viscosity of the samples obtained from TU25 are the highest – largest day 1 viscosity obtained from TU25 is 281 Pa.s at a process temperature of X °C. All the viscosity obtained from the experimental trial is lower than the Benchmark viscosity set in Figure 4-28.

Following a review of all the results[252], a take home message from this work is - the continuous manufacturing of Hair Conditioners based on 1.0H-C, is best conducted in two steps as originally introduced from preceding Sections. These one stage experiments have been performed because the CDSM-2 allowed for multiple stream combinations.

Secondly the ineffectiveness of the static CDDM technology (CDSM-1 and CDSM-2) in ensuring a good state of dispersion for the 'AA % QUAT/CS/FA/Water' in the Stage 1 of the process[253] is the underlying reason for the poor product - with respect to viscosity.

This is evident if all the micrographs (Figure 5-7, Figure 0-7[254] and Figure 0-10[255]) and the Brookfield T-bar B viscosity data (Figure 5-5, Figure 0-6[256], and Figure 0-9[257]) obtained are compared[258] - micrographs (Figure 0-7 and Figure 0-10) obtained for the Mixer-1 experiment (please see Appendix A) show that the products in general have good state of dispersion and maximum day 1 viscosities profiles were very close to the 400 Pa.s mark – it is worth mentioning that the high pressure trials conducted for the Mixer-1 – CDSM-2 set also had a leak as well – hence why it has not been reported in this Chapter.

---

[250] Micrograph of TU 24 in Appendix A
[251] Micrograph of TU26 and TU27 – experiments utilised the Mixer-1 and CDSM-1 in series. TU26 experimental set-up – Mixer-1 (high ΔP) – CDSM-1 (low ΔP)
TU27 experimental set-up – Mixer-1 (low ΔP) – CDSM-1 (high ΔP)
[252] TU21, TU22, TU24, TU25 and the results reported in Appendix A for TU26 and TU27
[253] Continuous manufacturing of 1.0H-C Hair Conditioner
[254] Micrograph of TU24 in Appendix A
[255] Micrograph of TU26 and TU27 in Appendix A
[256] Brookfield T-bar B viscosity profile for TU24
[257] Brookfield T-bar B viscosity profiles for TU26 and TU27
[258] Micrograph of TU26 and TU27 – experiments utilised the Mixer-1 and CDSM-1 in series.

Brookfield T-bar B viscosity analysis carried out on evolved products at time scales 1 day, 7 days and 28 days is shown in Figure 5-5. The evolution of Brookfield T-bar B viscosity with time shows product viscosity increases from point of sample collection time T = 0 to T = 24 as it ages. It can be inferred that this thickening effect is due to the lamellar microstructure taking in more water from the continuous phase thus leading into the swelling of the bilayer (a slow process) - no data (i.e. SAXS data) has been collected to support this as it is beyond the scope of this report – presumably this is occurring as the system tends towards stability.

A final thought is the impact of operating pressure (flow rate) on the viscosity profile – from which it can be deduced that increasing pressure drop results in increase in Brookfield T-bar B viscosity. It is thought that increasing the system pressure results in better state of dispersion of the molten ingredients - upcoming Section 5.1.2.2 sheds more light on this.

5.1.2.2 Microscopy

Micrograph (Figure 5-7) obtained from the experimental trials conducted has helped identified the effect of process variables on the nature of the underlying microstructure for TU21, TU22 and TU25.

A review of trial micrographs indicates a finer dispersion was obtained with TU22 set-up as opposed to TU21 indicating TU21 is a poorly dispersed system possessing domains of > 200 – 300 μm of undispersed molten ingredients presumably due to the point at which Stream 3 was introduced however since no data was collected to support this, lower viscosity will be attributed to the state of dispersion as seen under the microscope.

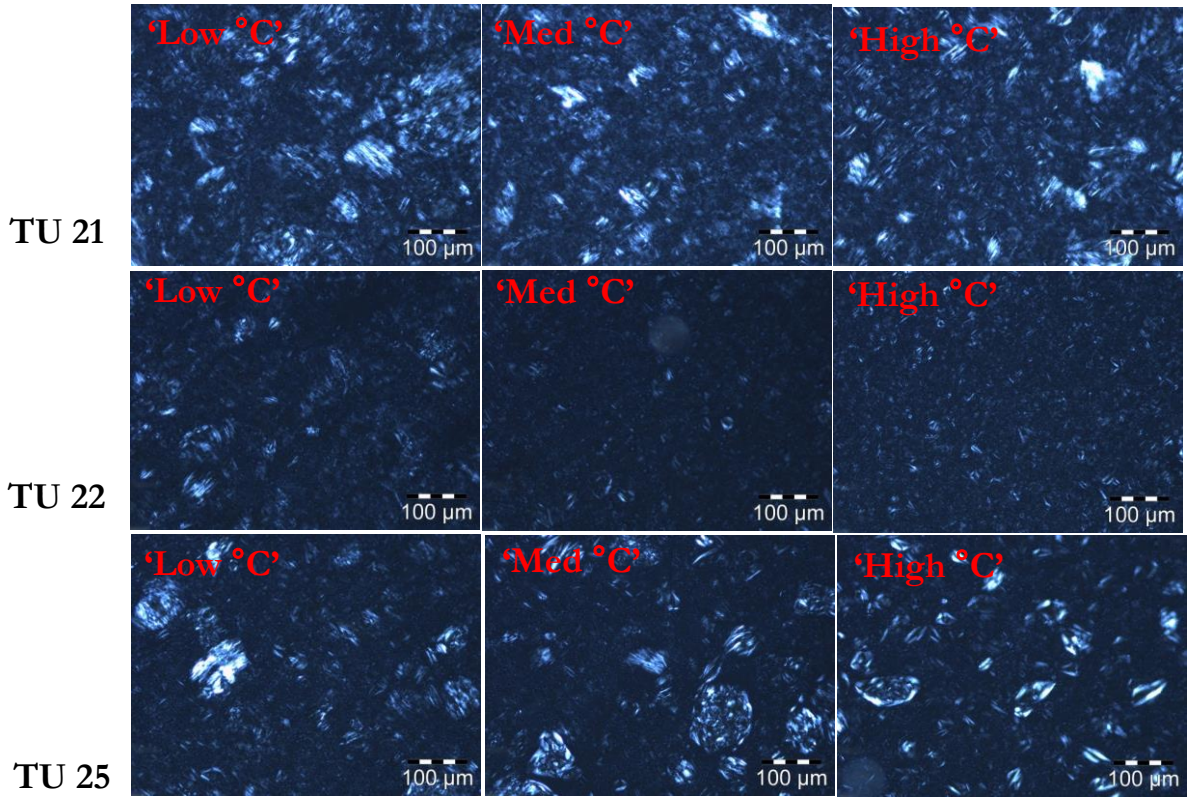

Figure 5-7: Cross polarised illuminated micrographs for 1.0H-C Hair Conditioners obtained at a range of process temperatures (low, medium and high) for Hair Conditioners manufactured via different routes (TU21, TU22, and TU 25) based on the 1.0H-C formulation.

TU25 shows that dispersion of the molten ingredients under low pressure gave products with coarse dispersions possessing larger domains - presumably higher pressures would give products with smaller domains and in effect higher product viscosity – this is the case if micrograph in Figure 0-7 (see Appendix A) is compared however the leak at high pressure experiments delivered product starved of molten ingredients hence the low viscosity.

In general – For the high temperature experiments, No 'FA' rich L_{β} microstructure was seen under the microscope – presumably this is probably due to a combination of two factors [1] the fact that either the samples are too dilute or the [2] 'FA' rich L_{β} microstructure had been completely incorporated into the lamellar microstructure in Stage 2 of the experiment due to the nature of the experimental set-up. The lack of 'FA' rich L_{β} microstructure was confirmed as there was no inflection in the loss modulus profiles - see Figure 0-5 in Appendix A for loss modulus of selected samples.

5.2 Cold High Shear Post Processing Of Hair Conditioners based on QUATS/CS/FA/Water System (Product Structuring)

The work discussed in this Section investigates the question of product (1.0H-C) structuring in reference to raw material efficiency thus addressing the issue of efficient use of resources via the dematerialisation approach. The basis/hypothesis for the work follows on from the experiments/conclusions obtained previously in preceding Sections more importantly Section 4.2.3, in that - increasing high shear deformation can induce changes to a pre-existing 'QUAT/CS' rich lamellar gel microstructure of Hair Conditioners based on the QUAT/CS/FA/Water system - resulting in an increasing bulk viscosity of such system through fragmentation. This Chapter further develops the concept of dematerialisation and the various factors that could affect it with respect to implementation of such concept within Unilever factories.

5.2.1 Experimental Program

A schematic of the factors considered in the experimental program as well as the responses measured can be seen in Figure 5-8. The objective of the experimental design was to further address the question of cold high shear post processing of Hair Conditioners based on the QUAT/CS/FA/Water system - by looking into ways in which it can be exploited i.e. the various factors that could affect the deployment of cold high shear post processing of Hair Conditioners within Unilever factories.

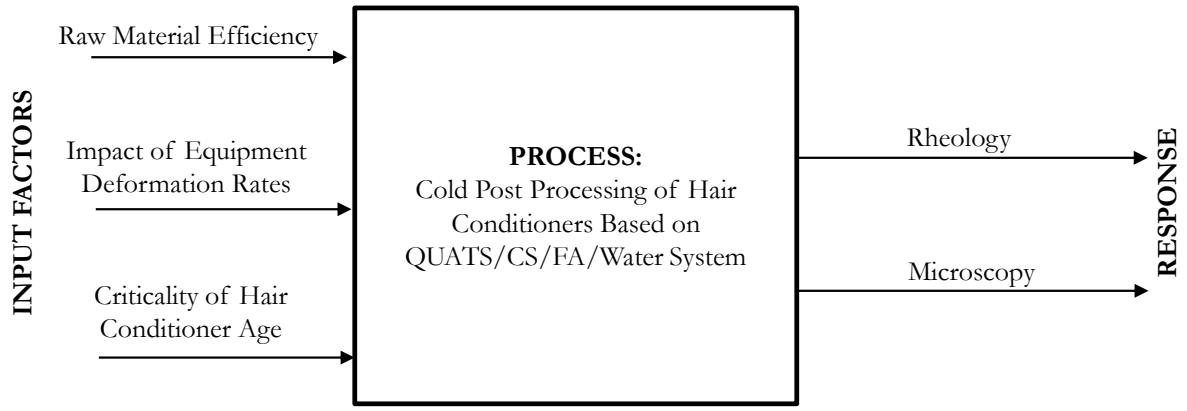

Figure 5-8: Schematic of experimental design for the cold high shear post processing of Hair Conditioners based on QUAT/CS/FA/Water System.

The experimental trials assessed a number of variables that at the time was thought could impact the extent of viscosity build of this Hair Conditioner – the most important of these variables

being the impact of age of Hair Conditioner[259]. Other variables assessed include the extent of dematerialisation[260], and finally the performance[261] of alternative technologies with reference to the question of cold high shear post processing of Hair Conditioners. With regards to analysis conducted – predominantly, Brookfield viscosity measurement is used to assess the bulk rheology measurements in relation to microstructure and occasionally oscillatory rheology and light microscopy are used to support Brookfield viscosity data.

5.2.1.1 Experimental Matrix (Sample Preparation)

In conducting the various experiments in this Section, three process equipment were utilised - the first two, are commercially available technology - the Mixer-1 (Figure 3-14) and the Mixer-2 (Figure 3-15) - refer to Section 3.3.2 for experimental setup details.

The third is the CDDM-1 (Figure 3-2) located at the University of Liverpool – refer to Section 3.3.1 for experimental set-up details.

All the experimental materials used in this Section used were manufactured at the pilot plant on a scale of approximately (0.300 kg/s [total flow-rate]) - process details are not discussed in this report as they are commercially sensitive. Henceforth this process used to manufacture this material would be referred to as 'Process X'.

Rheological properties of the material i.e. Brookfield T-bar b viscosity with respect to age/optical properties and oscillatory shear of the material can be seen in Figure 5-9, and Figure 0-12 respectively.

[259]Is there a correlation between the age of the product and the extent to which viscosity can be built
[260] The scope for raw material savings for Hair Conditioners based on 1.0H-C formulation
[261] Performance with respect to viscosity build

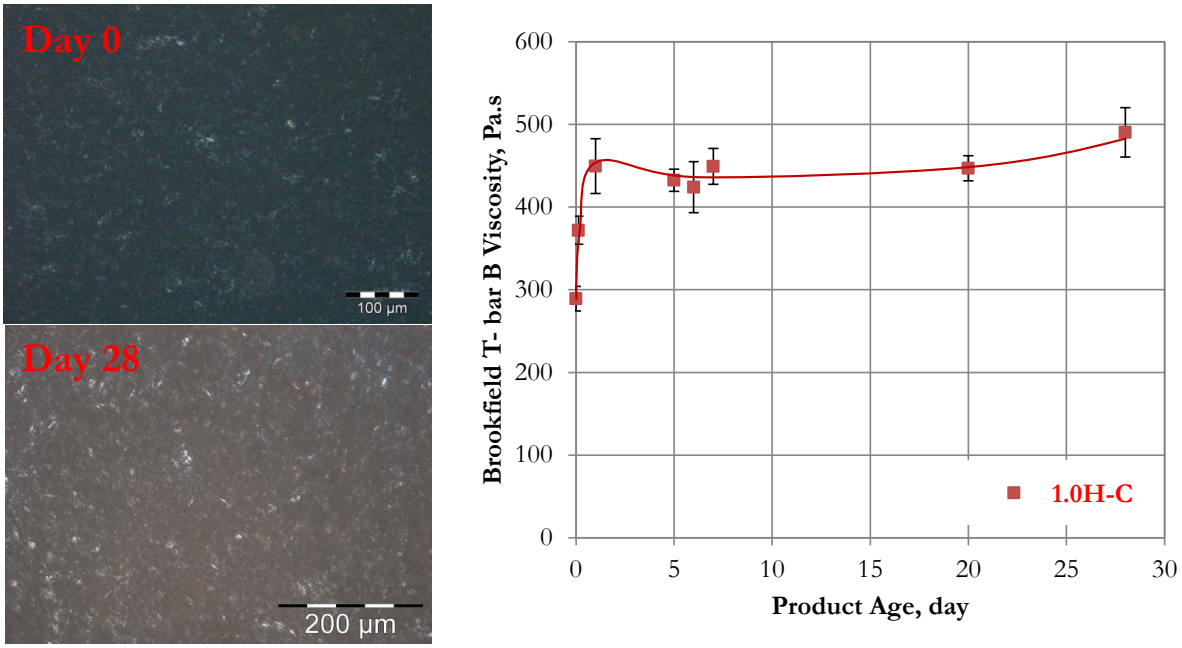

Figure 5-9: Cross polarised illuminated micrograph with respect to age (left) and Brookfield T-bar B viscosity as a function of Hair Conditioner product age for premix material supplied from Unilever Port Sunlight pilot plant

One can see that the underlying microstructure for the Hair Conditioner premix is predominantly 'QUAT/CS' rich lamellar microstructure which remains unchanged as the product is aged – no evidence of 'FA' rich lamellar microstructure was found.

From Figure 5-9, it can be seen that the lamellar Sheet Formulation (1.0H-C) viscosity increases with age i.e. from time T = 0 (point of discharge) where it has a Brookfield T-bar b viscosity of approximately 289 Pa.s[262] and had increased to approximately 430 Pa.s[263] on day 1 at which point the Brookfield T-bar b viscosity remained constant as the Hair conditioner aged.

It could be inferred that its viscosity is initially a function of temperature as opposed to time - however as the core temperature of the product tends towards ambient – the system tends towards a semisolid gel network phase. Initial insights to this inference was gained from the work discussed in Section 4.2.2 - in which AA % lamellar dispersion samples which were obtained from the vessel at both ambient[264] and process temperature[265] - samples obtained at ambient temperature after it had been actively cooled by the chiller/heater showed no further increase in viscosity with respect to time immediately after manufacture and samples which had been

[262] Measured within 15 minutes of discharge
[263] Measured approximately 24 hours after discharge
[264] Cold process - samples obtained cold at ambient temperature but not through the inline high shear mixer.
[265] Hot process - samples obtained hot at process temperature but not through the inline high shear mixer.

obtained at elevated temperatures presented increasing viscosity as they began to cool down to ambient temperature with respect to time.

Prior to any experimental trials conducted in the Section (see below), the 1.0H-C premix material manufactured from 'Process X' would usually be manufactured at Unilever Port Sunlight and then transported via road in 25 kg drums – experimental trials would usually commence after the material has been allowed to age.

Experimental Trials: Raw Material Efficiency - Results Discussed within Section 5.2.2

These experimental trials were performed to investigate the extent to which raw materials could be saved via dematerialisation/cold high shear post processing operation in the CDDM technology. This was only performed under static conditions (CDDM operating at 0 rpm: 0.08 kg/s) as sighting experiments to see what was possible. Samples were obtained for analysis.

In performing these experiments, different dilutions (0.2, 0.4, 0.5, 0.6 and 0.75) of the 1.0 H-C Hair Conditioner were manufactured at Port Sunlight[266] via Process X and shipped to the University of Liverpool to be cold post processed via the CDDM-1 at 0 nip position. These dilutions (i.e. 0.4H-C, 0.6H-C, 0.7H-C) are shown with numerical descriptors (i.e. 0.4, 0.6, 0.7 etc.) which indicate the level of solids in the formulation relative to the fully formulated 1.0H-C Hair Conditioner – in essence 0.4H-C or 0.8H-C indicate a dilution of 1.0H-C.

Post processing operation was performed at a range of process flow-rates and mixer rotational speeds according to the experimental methodology described in Section 3.3.1.

Experimental Trials: Criticality of product Age[267] - Results Discussed within Section 5.2.3

Prior to experimental trials, the material would usually be manufactured at Unilever Port Sunlight[268] and then transported via road in 25 kg drums. It was deemed that the time between manufacturing and cold high shear post processing might be critical.

Experimental trials were designed and performed to assess the impact of age time of Hair Conditioners on viscosity build achieved via cold high shear post processing. This work follows on from the work conducted on raw material efficiency in which 0.6H-C proved to possess very

[266] The manufacturing process for this Hair Conditioner would be referred to as 'Process X' from here on
[267] Experimental trials was performed using 0.6H-C Hair Conditioner
[268] Process X

similar (viscosity) rheology to the fully formulated 1.0H-C after cold high shear post processing through CDDM-1.

Experimental cycle commenced as soon as the material (0.6H-C) was manufactured at Unilever Port Sunlight pilot plant and transported to the University of Liverpool. Experiment were conducted on day 0 (after 2 hours of transport time), day 1, 5 and 6 after the material was manufactured. On each day, material was post processed cold through the CDDM-1 at 0 nip under static condition (0 rpm) at 0.08 kg/s and samples were obtained for analysis.

Post processing operation was performed at a range of process flow-rates and mixer rotational speeds according to the experimental methodology described in Section 3.3.1.

Experimental Trials: Cold High Shear Post Processing Equipment Comparison[269] - Results Discussed within Section 5.2.4

Experimental trials were designed and performed to investigate and compare the extent to which the various technologies tested, are able to build the viscosity of a 0.6H-C Hair Conditioner which has been manufactured via 'Process X'.

The experimental data are obtained by cold processing the 0.6H-C material with the device through the range of equipment variables accessible within each device setup. The various devices in question include are listed in Table 5-5 alongside the process/equipment variables considered. Results obtained would be compared to the viscosity of a fully formulated 1.0H-C viscosity.

Data obtained from technologies such as the Mixer-1 (Figure 3-14) and Mixer-2 (Figure 3-15) are also crudely compared to the CDDM-1 (Figure 3-2) operating at static and dynamic conditions respectively.

[269] Experimental trials was performed using 0.6H-C Hair Conditioner

Table 5-5: Table indicating the various process equipment and variables reviewed for the cold high shear post processing of 0.6H-C experiments.

Device	Nominal ΔP, psi	Approx. Q, kg/s	ΔP, bar	Mixer Speed, rpm [Tip Speed, m/s]			
Mixer-1	Confidential	Confidential	Confidential				
	Confidential	Confidential	Confidential				
	Confidential	Confidential	Confidential				
CDDM-1		Confidential	Confidential				
		Confidential	Confidential				
		Confidential	Confidential				
		Confidential	Confidential				
Mixer-2		Confidential		Confidential	Confidential	Confidential	-
		Confidential		-	-	Confidential	-
		Confidential		-	-	Confidential	-
CDDM-1		Confidential	Confidential	Confidential	Confidential	Confidential	Confidential

The Mixer-1 is compared to static operation of CDDM-1 with respect to pressure drop while the Mixer-2 is compared to the dynamic operation of the CDDM with respect to tip speed.

For the Mixer-1, three different pressures (P1, P1 and P3 psi) were reviewed by varying the process flow-rate for Mixer-1 process flow rate was also varied in the CDDM-1 set at 0 nip position to achieve the different pressure drops listed in Table 5-5 thus allowing comparison as was stated earlier.

For the Mixer-2, a range of process flow-rates were reviewed alongside tip speeds - for the CDDM-1, a range of different tip speeds are reviewed for a single process flow-rate for mixer operating at 0 nip position.

The 0 nip position was selected based on historical experimental trials – from which it has been realised that pressure drops, comparable to ones recorded from varying process flow-rate through Mixer-1 can be achieved. Analysis for cold post processed products was conducted using a Brookfield viscometer to which a T-bar B spindle was attached.

The above work was then extended to investigate the effect of the CDDM-1 set-up[270] on the viscosity build of a 0.6H-C Hair Conditioner – as has been described in Section 3.3.1 positive displacement pump operation/sample collection can be in one of two modes – this prompted an investigation to examine the effect this has on the process material.

[270] See Section 3.3.1

5.2.2 Raw Material Efficiency

Results and discussion of the experimental trials investigating the extent to which raw material within the 1.0H-C Hair Conditioner formulation could be saved via dematerialisation and cold high shear post processing through the CDDM-1 operating at 0 rpm: 0.08 kg/s is discussed within this Section. The Hair Conditioner premixes[271] used have been manufactured via 'Process X' as earlier mentioned in footnote [266] above and then transported to the University of Liverpool for cold high shear post processing operation to be conducted.

5.2.2.1 Rheology

Brookfield T-bar B Viscosity

The effect of dematerialisation (reduction in solids content) on the Brookfield T-bar B viscosity of 1.0H-C Hair Conditioner following a cold high shear post processing operation[272] through the CDDM-1 is shown in Figure 5-10 – on this Figure, control samples are also displayed alongside cold high shear post processed samples to quantify the extent to which viscosity has been increased via fragmentation.

[271] 0.2, 0.4, 0.5, 0.6 and 0.75H-C
[272] 1 pass using the positive displacement pump at approx. 0.08 kg/s : 0 rpm

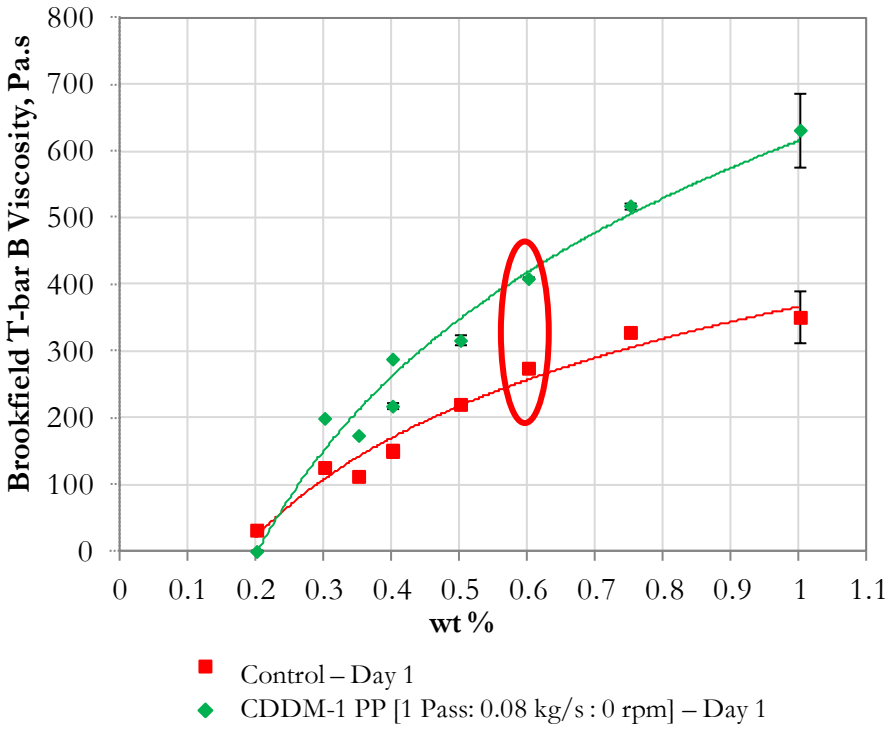

Figure 5-10: Brookfield T-bar B viscosity as a function varying w/w % (solids only) for Hair Conditioners (1.0H-C) following cold high shear post processing operation in the CDDM-1 – control samples has been included as reference points.

From this, it can be seen that in all cases[273], Brookfield T-bar B viscosity is increased to different extents via fragmentation of the underlying 'QUAT/CS' rich L_{β} microstructure following a single pass discharge[274] through the CDDM-1 mixer. Highlighted in 'red circle' is the viscosity of 0.6H-C before and after cold high shear post processing through the CDDM-1. This has been highlighted because it is the only formulation that is in parity with the benchmark 400 Pa.s values realised in Section 4.3.2 (Figure 4-28). Further work conducted on the 0.6H-C system is displayed below in Figure 5-11.

Figure 5-11 shows three different product age profiles for the 0.6H-C formulation; [1] 0.6H-C, control formulation as delivered from the Unilever pilot plant with respect to product age, [2] 0.6H-C delivered from the Unilever pilot plant which has been subjected to cold high shear post processing operation via the CDDM-1[275] with respect to product age and [3] 0.6H-C delivered

[273] For each formulation
[274] Cold high shear post processing operation using the positive displacement pump
[275] At 0.08 kg/s : 0 rpm (similar to the dataset disseminated in Figure 5-10

from the Unilever pilot plant which has been subjected to cold high shear post processing operation via the CDDM-1[276] - with respect to product age.

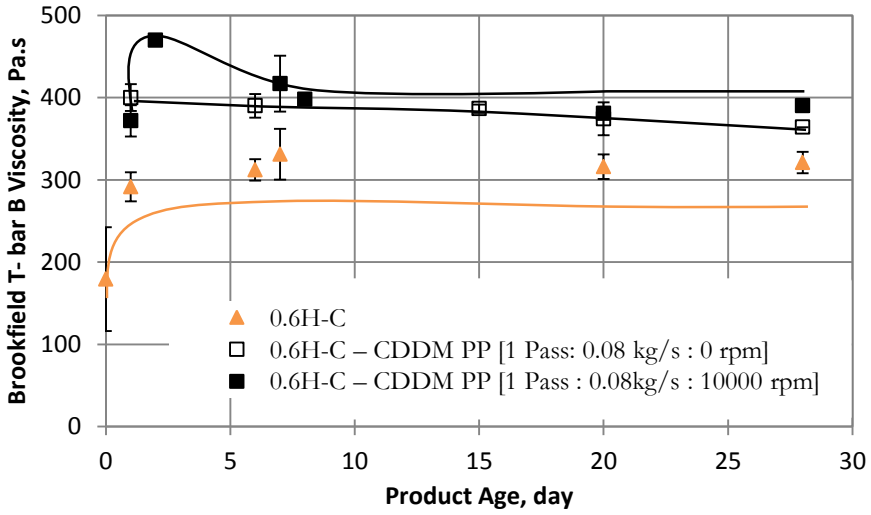

Figure 5-11: Brookfield T-bar B viscosity as a function Hair Conditioner product age for [1] 0.6H-C, [2] 0.6H-C cold processed through CDDM-1 at (0.08 kg/s : 0 rpm) and [3] 0.6H-C cold processed through CDDM-1 at (0.08 kg/s : 10000 rpm)

Thus far[277], it is known that the extent to which fragmentation can occur can be a function of mechanical stress[278] for a set formulation – this is evident in Figure 5-11. For the 0.6H-C formulation, it can be seen that, after the cold high shear post processing operation via the CDDM-1 under different conditions namely [1] 1 pass using the positive displacement pump at approx. 0.08 kg/s: 0 rpm and [2] 1 pass using the positive displacement pump at approx. 0.08 kg/s : 10000 rpm – the day 1[279] present different viscosity profiles – with the single pass through the dynamic mixer[280] being significantly higher than the 400 Pa.s benchmark mark and the single pass through the static mixer[281] sitting very close to the 400 Pa.s mark.

Secondly a review of the day 28 viscosities after the material has been left to age and stabilised, the Brookfield T-bar B viscosity profile for the dynamic operation still sits above the static operation and the viscosity of the product obtained under static condition has slightly drop to a value of approximately 360 Pa.s.

[276] At 0.08 kg/s : 10000 rpm
[277] See Section 4.2.3
[278] Deformation rate
[279] And product age viscosity profile
[280] 10000 rpm
[281] 0 rpm

Evidently it can be deduced that the formulation is highly sensitive to certain process variables i.e. process flow-rate and mixer rotational speed both of which can be directly associated to extensional and rotational shear rates available within the CDDM-1 mixer, and that the higher the mechanical stresses the high the chance of producing a rigid 'QUAT/CS' rich L_{β} system.

5.2.3 Criticality of Product Age on Cold High Shear Post Processing Viscosity Build

Results and discussions of the experimental trials investigating the impact of age time of Hair Conditioners, on the extent of viscosity build achievable after a cold high shear post processing operation is conferred within this Section – for this work, a 0.6H-C Hair Conditioner[282] is supplied to the University of Liverpool where it is aged before it is cold post processed through the CDDM-1 operating at 0 rpm: 0.08 kg/s.

5.2.3.1 Rheology

Brookfield T-Bar B Viscosity

The effect of product age before conducting cold high shear post processing experiment is displayed in Figure 5-12 - straightway it can be seen that product age has no impact - as product viscosity is seen to be independent of product age.

[282] Manufactured via 'Process X'

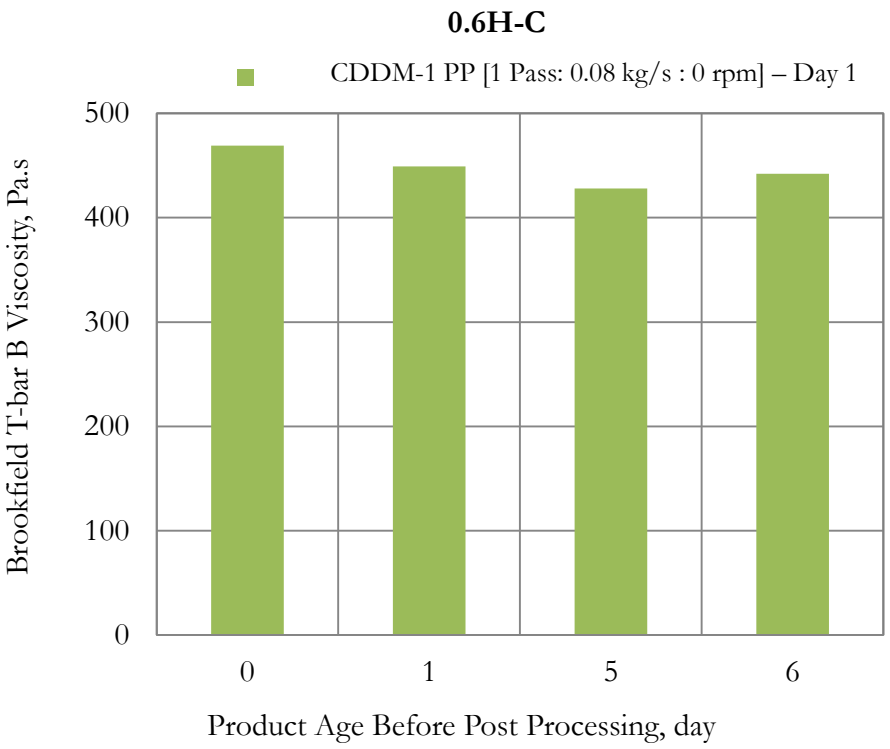

Figure 5-12: Brookfield T-bar B viscosity as a function of aged cold post processed Hair Conditioner (0.6H-C) through the CDDM-1.

This indicates that the extent of viscosity build is mainly a direct consequence of the state of the lamellar microstructure[283] (i.e. L_α & L_β) before a high shear post processing operation as alluded in Section 4.2.2 and secondly it would not be wrong to include that the systems nearness to stability would also have an impact on this viscosity effect although very little, and nowhere near the impact that the lamellar states as suggested.

5.2.4 High Shear Post Processing Equipment Comparison

Results and discussions of the experimental trials comparing the extent to which various high shear technologies[284], - are able to build the viscosity during a cold high shear post processing operation is conferred within this Section - for this work, a 0.6H-C Hair Conditioner[285] is used - process variables reviewed for the various equipment are shown in Table 5-5.

.

[283] 'QUAT/CS' rich lamellar microstructure
[284] Mixer-1, CDDM-1 and Mixer-2
[285] Manufactured via 'Process X'

5.2.4.1 Rheology

Brookfield T-Bar B Viscosity

In the Mixer-2, based on (Cooke, Rodgers & Kowalski 2012) the rotation of the rotor would cause some pumping action which will be proportional to rotor speed however it is very likely this effect will be trumped by the flow generated by the pump in our case.

From the results displayed in Figure 5-13, It can be inferred that as process fluid enters the Mixer-2 due to the action of the pump[286] at a constant flow rate (i.e. 0.075 kg/s) and tip speed (i.e. 8.3 m/s) – change in bulk viscosity (277 Pa.s ±6) of the starting material is as a result of fragmentation of the 'QUAT/CS' rich L_β microstructure is due to extensional and shear flow from the action of the pump and the spinning rotor pushing the process fluid through the holes in the screen and within the high shear gap.

Shearing forces[287] can be related to the velocity gradient - tip speed can be related to the amount of shear process fluid experiences in the mixer - hence increasing tip speed (i.e. 8.3 – 25.0 m/s) at a constant flow-rate (0.075 kg/s), the fluid undergoes increasing shear as it is impelled though the holes in the stator and the shear gap thereby resulting in increased fragmentation and thus increasing bulk viscosity.

At constant tip speed (25.0 m/s) - as process flow-rate is increased there is not much change in bulk viscosity of the material indicating the dominant effect of the shear rate from rotation of the rotor and that no further fragmentation occurs with increasing flow-rate which is indicative of either very low/no extensional flow in the Mixer-2 .

[286] Progressive cavity pump
[287] Mechanical stress

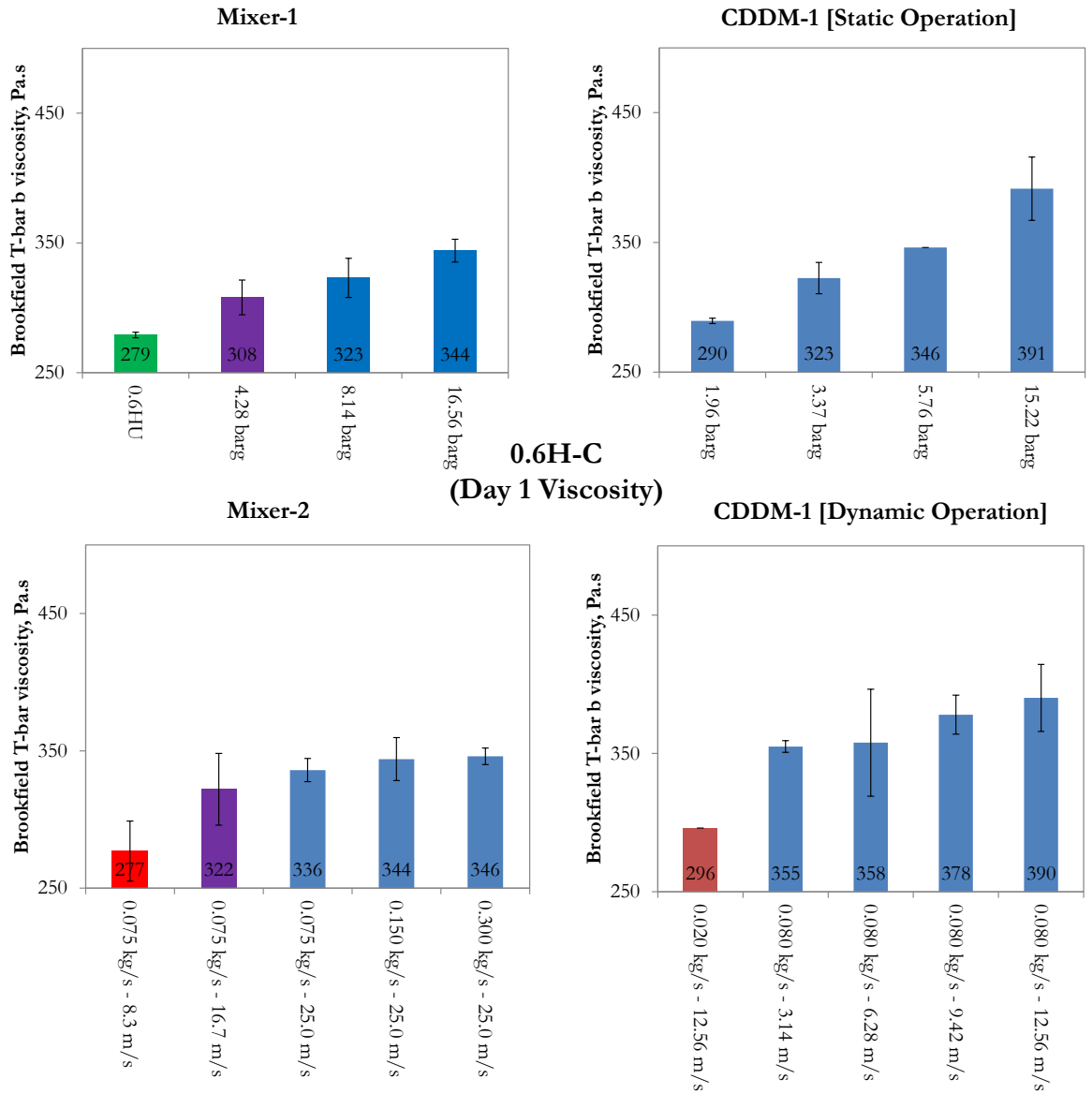

Figure 5-13: Brookfield T-bar B viscosity as a function various process histories (cold high shear post processing) for Hair Conditioners (0.6H-C) – varying process history accessed via different commercially available mixing technologies.

Mixer-1: In the Mixer-1, process fluid enters through the narrow orifice of the Mixer-1 under the action of the pump[288]. From the result displayed in Figure 5-13, it can be inferred that as the flow-rate (pressure) is increased, the fluid velocity through the orifice is also increased thus changing the shear characteristics. As the fluid passes through the orifice, it encounters increasing extensional flow - increasing bulk viscosity (290 – 391 Pa.s) of the material is thus due

[288] Progressive cavity pump

to increasing fragmentation intensity of the 'QUAT/CS' rich Lβ microstructure due to increasing extensional rates from the action of the pump.

CDDM-1: With the CDDM, one can see the effectiveness of both extensional flow due to increasing flow-rate and shear flow due to increasing rotational speed in affecting increasing fragmentation of the 'QUAT/CS' rich L_{β} microstructure.

For static operation, it can be inferred from the results displayed in Figure 5-13, that increasing pressure drop, a direct consequence of increasing process flow-rate for a set CDDM axial position[289] results in increasing viscosity of the Hair Conditioner. It can be inferred that fragmentation of the lamellar microstructure occurs as it passes through the small gaps created at 0 nip position thereby increasing the systems bulk viscosity.

From the results displayed Figure 5-13, one can infer that during processing in the dynamic operation of the CDDM, as process fluid enters into the mixer due to the action of the pump, it is subjected to both extension rates due to set flow-rate i.e. 0.020 kg/s and rotational shear rates due to the rotor speed as it passes through the small gaps created at 0 nip position thereby increasing the systems bulk viscosity (296 Pa.s) as fragmentation of the lamellar occurs. At a set process flow-rate i.e. 0.080 kg/s, increasing shear flow due to increasing rotational speed i.e. 2500 – 10000, rpm dominates increasing fragmentation intensity as the bulk viscosity of the Hair Conditioner increases.

In summary – dataset collected up till this point has demonstrated that underlining microstructure of structured liquids i.e. Hair Conditioner can be fragmented i.e. reduction in particle size by increasing shear and extensional deformation rates for a set formulation. The extent to which fragmentation can occur with respect to deformation rates based on pump flow-rate and mixer rotational speed is investigated using available mixing technologies thus allowing for a crude comparison. Estimates of these values (deformation rates) have not been discussed for both the Mixer-1 and the Mixer-2 as it is beyond the scope of this work - however Chapter 6 (Table 6-4 and Figure 6-13) introduces/discusses the nature of deformation rates values within the CDDM technology in general.

It can be said that these mixers (Mixer-1, Mixer-2 and CDDM) all generate shear and/or extensional flow to different degrees and that the work discussed here has helped highlight

[289] 0 nip

opportunities to improve current technology - It can also be said that though the data points out that the rotational speed of the rotor and the connected pumps are important in determining the deformation rates available within the mixers, deformation rates is more a function of the geometry of the mixing head.

The effect of CDDM-1 operating mode (batch vs. pseudo continuous) on the Brookfield T-bar b viscosity is shown in Figure 5-14 i.e. Single-shot and Multi-shot mode, there is no significant difference as data points obtained are within the error limits however multi shot sample collected in 200 ml pot at 0.08 kg/s possess a slightly higher viscosity when compared to samples collected in larger pot.

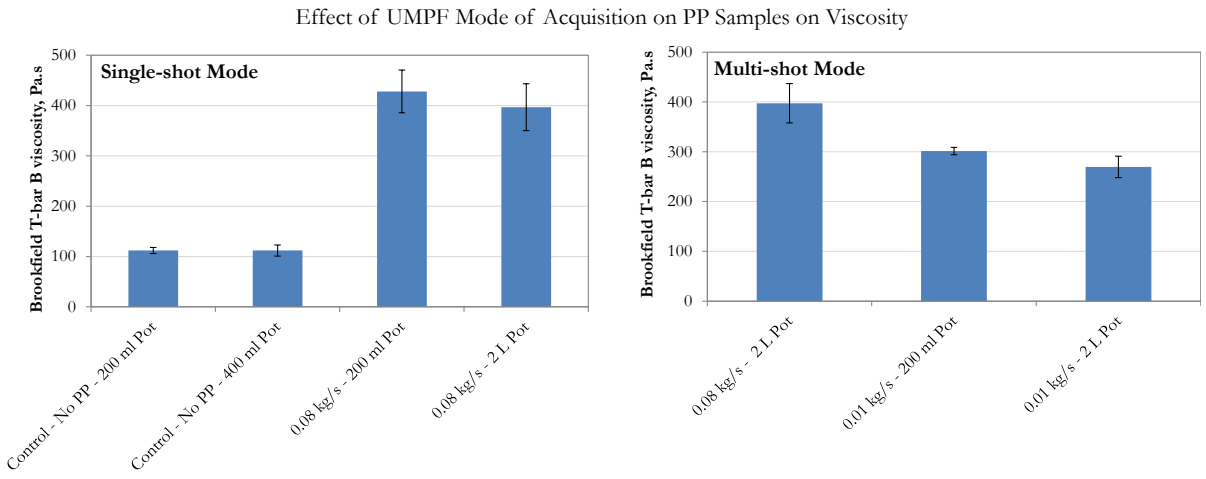

Figure 5-14: Brookfield T-bar B viscosity as a function of Hair Conditioners (0.6H-C) possessing various process histories (cold high shear post processing) in the CDDM-1 for varied UMPF acquisition mode.

One can infer that the reason for this could lie in the fact that samples collected in the 200 ml pots are done with a single LIP pump stroke as opposed to samples collected in larger pots. For larger pots; multiple strokes were required to fill pots up i.e. combination of up to 10 individual shots with about 2 minutes apart to allow for pump priming. Lower viscosity may arise from the fact that layers are created between individual shots which could trap air resulting in individual layer which do not anneal with each other. Data obtained also indicate that there is no significant difference with respect to product viscosity when pots of various sizes (i.e. 200 ml and 2 L) are used for sampling

5.3 Summary

Rheology and microscopy investigations, disseminated in this Chapter have been used to elucidate the effect of various process variables on the underlying microstructure of Hair Conditioners[290] based on QUATS/CS/FA/Water system – this work was performed against the backdrop of rheological[291] and microstructural[292] specification set from the revised benchmark product.

Initially the work began by developing a continuous process for the manufacturing of 1.0H-C Hair Conditioner which is in parity with the rheological/microstructural properties set by the revised benchmark process – this work continued investigating the key process parameters relevant to the process[293] which began in Chapter 4.

It is concluded that the production of this system[294] is best performed as a two staged process. [Stage 1] the manufacture of a concentrated lamellar dispersion[295] forming the gel phase network which serves as the structuring component to the Hair Conditioner, and [Stage 2] the cool/dilution and the addition of minor ingredients.

Two key process parameters for Stage 1 of the process are the pressure and temperature at which the lamellar concentrate is manufactured - manufacturing the lamellar concentrate at approx. T-optimum °C ensures that the underlying microstructure formed is predominantly 'QUAT/CS' rich L_{β} microstructure thus making the system susceptible to the optimum rheology on dilution/minors addition at Stage 2. Secondly the pressure drop of this Stage influences the systems state of dispersion as see under the microscope. A high pressure[296] at the concentrate production stage is recommended, as it results in a fine state of dispersion of the product intermediate which can be directly related to higher rheology[297] and product morphology.

Second aspect to the work began by establishing the extent to which raw material (solids) could be reduced to achieve resource efficiency with respect to building Hair Conditioner rheology via cold high shear post processing operation. It is concluded that a minimum of 60 % w/w of the

[290] I.e. various manufactured and cold high shear post processed Hair Conditioners.
[291] Minimum of approx. 400 Pa.s (Brookfield T-bar B viscosity)
[292] Predominantly 'QUAT/CS' rich L_{β} microstructure
[293] Continuous production of H-C based Hair Conditioners
[294] Manufacturing of Hair Conditioners based on the QUAT/CS/FA/Water mixture
[295] Approx. AA % QUAT/CS/FA/Water
[296] Pressure within manufacturing plant safety regulations
[297] Quantities

total amount of solids contents[298] is required to ensure the rheology of the cold post processed Hair Conditioner is in parity with specification set by the revised benchmark process. In principle, a 0.6H-C is manufactured via a continuous process under afore discussed process parameters. This[299] is the cold post processed at high deformation rates[300] in the CDDM technology as it was found out that the - Hair Conditioner viscosity build is most sensitive to the rotational speeds and the flow-rates in the CDDM technology (CDDM-1).

Finally experimental studies conducted to assess the criticality of product age before post processing operation showed that there is no effect of age on the extent of viscosity build for the time scale conducted[301] and with respect to product stabilisation, viscosity build appears to stabilise within the first week after the 0.6H-C material has been cold post processed.

[298] Major ingredients
[299] 0.6H-C Hair Conditioner
[300] High extensional (pump flow-rate) and shear flow (high rotational speed) - increasing deformation rates results in increasing fragmentation rates
[301] Minimum timescale reviewed was with 1 hour of manufacturing of 0.6H-C Hair Conditioner

5.4 References

- Cooke, M., Rodgers, T.L. & Kowalski, A.J. (2012) 'Power Consumption Characteristics of An In-line Silverson High Shear Mixer', *American Institute of Chemical Engineers*, vol. 58, no. 6, pp. 1683 - 1692.

Chapter 6

6 CDDM Technology Testing and Optimisation

This Chapter is focused on extensive testing of the CDDM technology but more specifically optimising its operation as well as developing insights into scale-up correlations.

Testing and optimisation studies are performed on variants of this technology namely; [1] CDDM-1 (Figure 3-2), [2] Bench Top CDDM (Figure 3-7), and [3] CDDM-2 (Figure 3-3) as introduced in Chapter 3 – the latter two were designed, constructed and commissioned during the duration of the project.

The aims of the Chapter were all achieved through empirical means using two sets of raw materials namely; 1.0H-C formulation relevant to the personal care category and coarse (premix) 50%, w/w SFO emulsion relevant to the food category – details of which can be found in Section 3.2. The 1.0H-C premix has been manufactured through Process X[302] while the steps taken in manufacturing the coarse 50%, w/w SFO emulsion is discussed in Section 6.2.1.1.

Insights into scale up correlations were performed using two semi-geometrically similar CDDM technologies namely Bench Top CDDM [303] & CDDM-2[304] using only the coarse 50%, w/w SFO emulsion.

The Chapter is divided into two Sections – Section 6.1 discusses the work conducted using the 1.0H-C and Section 6.2 discusses the work conducted using the SFO emulsion - analysis for experiments conducted using 1.0H-C formulation and SFO emulsion was performed using the Brookfield DV-II+ Pro Viscometer (Brookfield Engineering Laboratories, U.S.) and Mastersizer 2000 (Malvern Instruments Ltd, Worcestershire, UK) respectively.

[302] As was introduced in Section 5.2.1.1
[303] Figure 3-7
[304] Figure 3-3

6.1 CDDM Technology Testing and Optimisation (H-C Hair Conditioner)

Thus far it has been demonstrated that the characteristics of process fluid and its subsequent product are dependent on equipment and process variables (Chapters 4 and 5) and often, a process and/or a formulation would require optimisation for a particular equipment type or vice versa.

For the work reported in this Section, the latter is chosen in that the work disseminated here was aimed at optimising the CDDM technology for a process and/or formulation - in this case optimising the technology for cold high shear post processing of H-C based Hair Conditioner.

6.1.1 Experimental Program

A schematic of the factors considered in the experimental program as well as the response measured can be seen in Figure 6-1. The objective of the experimental design was to assess the effect of process conditions/equipment design as a function of extent of increase in viscosity of a control 1.0H-C premix following a cold high shear post processing operation – thereby aiding optimisation studies of the CDDM technology.

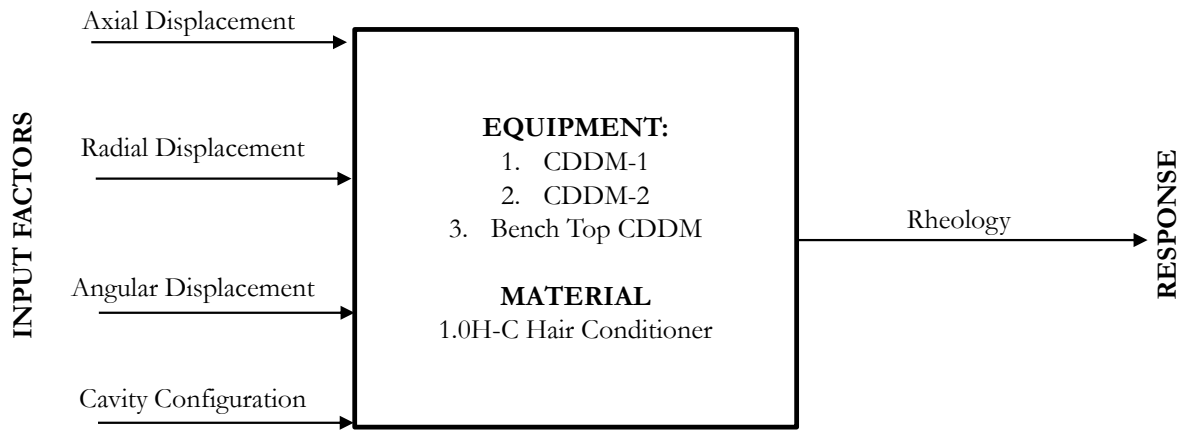

Figure 6-1: Schematic of experimental design for the CDDM technology testing and optimisation using 1.0H-C Hair Conditioner.

The experimental trials conducted assessed various input factors relevant to the optimisation of the design of the CDDM technology in ensuring an optimised operation following a cold high shear post processing operation. The input factors considered included; CDDM [1] mixer axial displacement[305],

[305] Changing mixer axial position – previously only 0 nip has been considered (see Sections 5.2.2, 5.2.3 and 5.2.4)

[2] mixer radial displacement[306], [3] mixer angular displacement and, [4] mixer cavity configuration[307]. The technique used for rheology assessment was viscometer[308] only.

6.1.1.1 Experimental Matrix (Sample Preparation)

The premix (1.0H-C) used in this section is the same as the one used in Section 5.2.1.1 prepared at Unilever Port Sunlight via 'Process X'. The material was delivered in large batches - over 300 Litres worth in variety of containers[309] on different occasions[310] to the University of Liverpool to be post processed at single pass discharge through the [1] CDDM-1, [2] CDDM-2 at a range of processing conditions available in the UMPF setup (see Section 3.3.1) and [3] Bench Top CDDM at a range of processing conditions available in the Bench Top CDDM setup (see Section 3.3.1).

Initially the work began by investigating the optimum cavity configuration for confronting CDDM surfaces (rotor and stator), with respect to [1] optimum relative axial position of these surfaces, [2] optimum relative angular position and [3] the relative radial set-ups and, [4] the effect of the number of cavities on either surface is also considered. It is fair to assume that changes to the parameters listed would have a direct impact on the mixer flow patterns thereby affecting the mixing properties[311].

Experimental trials occurred over several weeks - a typical day would commence by obtaining a control sample[312] – a control sample is a sample taken from the hopper (Figure 3-1 and Figure 3-5) after the Hair Conditioner material has been loaded from the large barrels in which they have been supplied in.

It was noticed throughout the duration of the experimental trials the Brookfield T-bar B viscosity value obtained for 1.0H-C control samples would vary below the 400 Pa.s mark as shown in Figure 6-2 – this figure shows a few of the control samples measured during the experimental campaign – from this it can be seen that, after a control sample had been obtained, the measured Brookfield T-bar b viscosity value fluctuates – this led to obtaining an average value of 342 (± 38), Pa.s for the control viscosity for a range of control samples collected.

[306] Changing mixer radial clearance
[307] Number of cavities on the surface of the rotor and stator i.e. even vs odd number of cavities
[308] Brookfield T-bar B viscosity measurement
[309] 15 and 25 L drums
[310] As required
[311] I.e. - the extent of distributive and/or dispersive mixing properties of the mixer.
[312] Reference sample

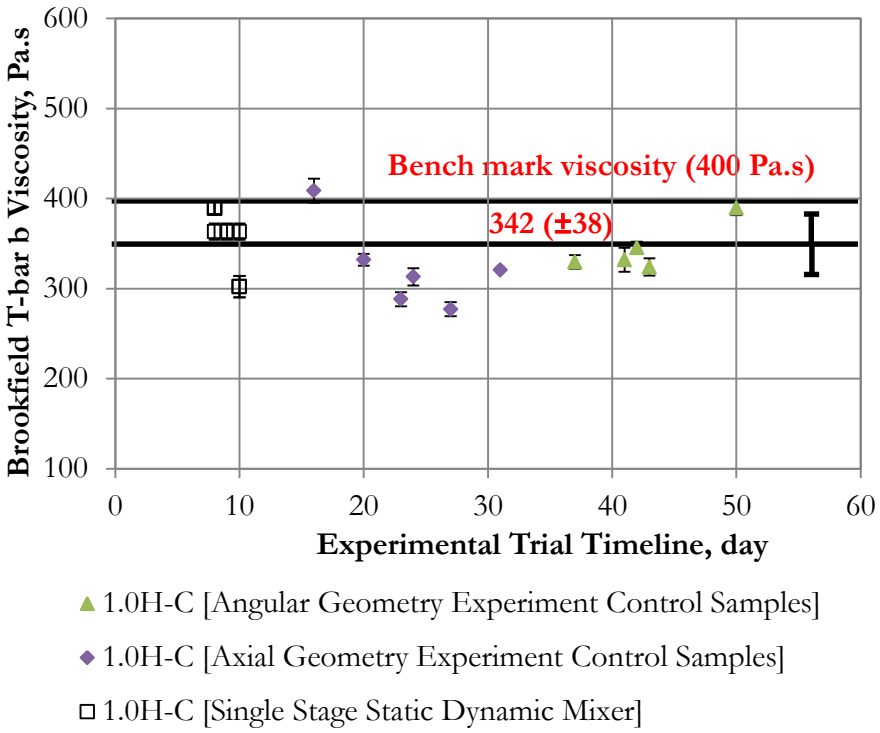

Figure 6-2: Brookfield T-bar B viscosity as a function of experimental trial timeline for a number of control samples

If one considers Figure 6-2 and Figure 0-14[313], it is hypothesised that the reason for the lower viscosity relative to the 400 Pa.s benchmark viscosity value can be can be attributed to the effect of shear induced re-alignment on the lamellar gel network during sampling.

During the course of the experimental campaign, hydrodynamics data (i.e. pressure drop and flow rate) was recorded for each individual post processing experiments via the automatic data logger for all experimental trials- see Section 3.3.1 for location of sensors.

It is worth mentioning at this point that any references made to 'CDDM-2' refers to the dynamic section (top section of the mixer) unless stated otherwise i.e. "otherwise" would refer to bottom static section of the mixer (See Figure 3-3).

Experimental Trials: Effects of Axial Displacement (Radial Displacement) – Results Discussed Within Section 6.1.2

The CDDM-1 and CDDM-2 (dynamic section) allowed the investigation of the impact of axial and radial clearances on the performance of the CDDM technology – this is based on the fact

[313] Appendix C

that both devices allowed for axial adjustments as well as possess different nominal radial clearances - XX and YY μm respectively (XX > YY) thus aiding the assessment of the impact of radial clearance on the performance of both mixers. The two mixers had 12-14 cavity configuration set i.e. 12 cavities on the rotor and 14 cavities on the stator.

The experimental trials were performed to determine the optimal specification i.e. relative position of surfaces and process conditions for a 12–14 cavity configuration mixer using the 1.0H-C premix system - thereby allowing nip positions listed in Table 6-1 with reference to Figure 6-3

Table 6-1: Table showing relative nip positions examined for 1.0H-C experimental trials for the (1) CDDM-1, and (2) CDDM-2.

CDDM-1, mm	CDDM-2 (Dynamic Section), mm
- 0.55	- 0.30
- 0.29	- 0.25
- 0.10	0.00
0.00	+ 0.25
+ 0.10	+ 1.25
+ 0.40	+ 1.75
+ 1.52	+ 2.75
+ 2.97	+ 3.00

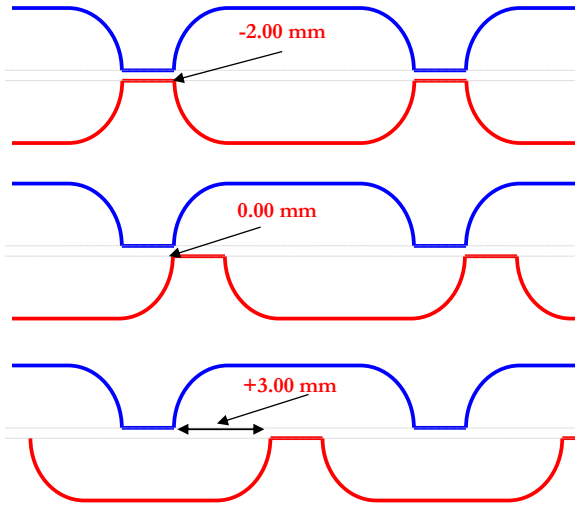

Figure 6-3: Schematic representation of three extreme axial positions in the CDDM technology setup.

For each axial position, a full experimental matrix (Table 3-2) was performed - where the Hair Conditioner premix was pumped into the installed mixer[314] via the LIP. For experiments involving the CDDM-2, process material is injected directly into the dynamic section of the mixer (see Figure 3-2).

Post processing operation was performed at a range of process flow-rates and mixer rotational speeds according to the experimental methodology described in Section 3.3.1 for each nip position listed in Table 6-1

Experimental Trials: Effects Of Angular Displacement (Cavity Configuration 12:14 Vs 11:11) – Results Discussed Within Section 6.1.3

This section considers the effect of changing the cavity configuration as well as angular displacement (see Figure 3-4). The CDDM-2 was purposely built for this experiment in that the upper dynamic section has a 12:14 cavity configuration set-up while the bottom static section has an 11:11 cavity configuration set-up (See Figure 3-2).

This static section of the CDDM-2 therefore enabled the investigation of the effect of angular position (see Figure 3-4 and Figure 0-15 in Appendix C) alongside the impact of cavity configuration (11:11 vs. 12:14) on mixer performance with respect to Hair Conditioner premix viscosity build – all the angular positions in Figure 3-4 were reviewed.

Data obtained from these experiments is then compared to data obtained from experiments conducted on the mixers with 12:14 cavity configuration (Section 6.1.2) more importantly the CDDM-2 as this is the newer mixer hence the radial clearance is larger.

For each axial position (Table 6-2), a full experimental matrix (Table 3-2) was conducted for various angular positions (Figure 3-4) where the Hair Conditioner premix was pumped into the mixer via the LIP directly into the static section of the CDDM-2 (see Figure 3-2).

Table 6-2: Table showing relative axial nip positions examined for 1.0H-C experimental trials for the (1) CDDM-2 (static section).

CDDM-2 (Static Section), mm				
+ 1.00	+ 1.25	+ 1.75	+ 2.00	+ 2.25

[314] Either the [1] CDDM-1, [2] CDDM-2

Post processing operation was performed at a range of process flow-rates and mixer rotational speeds according to the experimental methodology described in Section 3.3.1 for each nip position listed in Table 6-2.

6.1.2 Effects of Axial Displacement (Radial Displacement)

Results and discussion of the experimental trials investigating the effects of axial displacement (radial displacement) on the viscosity of post processed Hair Conditioner premix (1.0H-C) through the [1] CDDM-1 and [2] CDDM-2 mixer (dynamic section) at a range of process variables (Table 3-2) is conferred within this Section – both mixer are 12:14 cavity configuration set-up. Brookfield T-bar B viscosity and hydrodynamics data is discussed as well.

6.1.2.1 Rheology

Brookfield T-bar B Viscosity

The effect of axial displacement (nip position) on the Brookfield T-bar B viscosity (day 1) of post processed 1.0H-C Hair Conditioner premix for the CDDM-1 and CDDM-2 mixer (dynamic section) is shown in Figure 6-4 – data is also plotted with rotor speed and process flow-rate. Datasets displayed are for a single pass discharge of process material

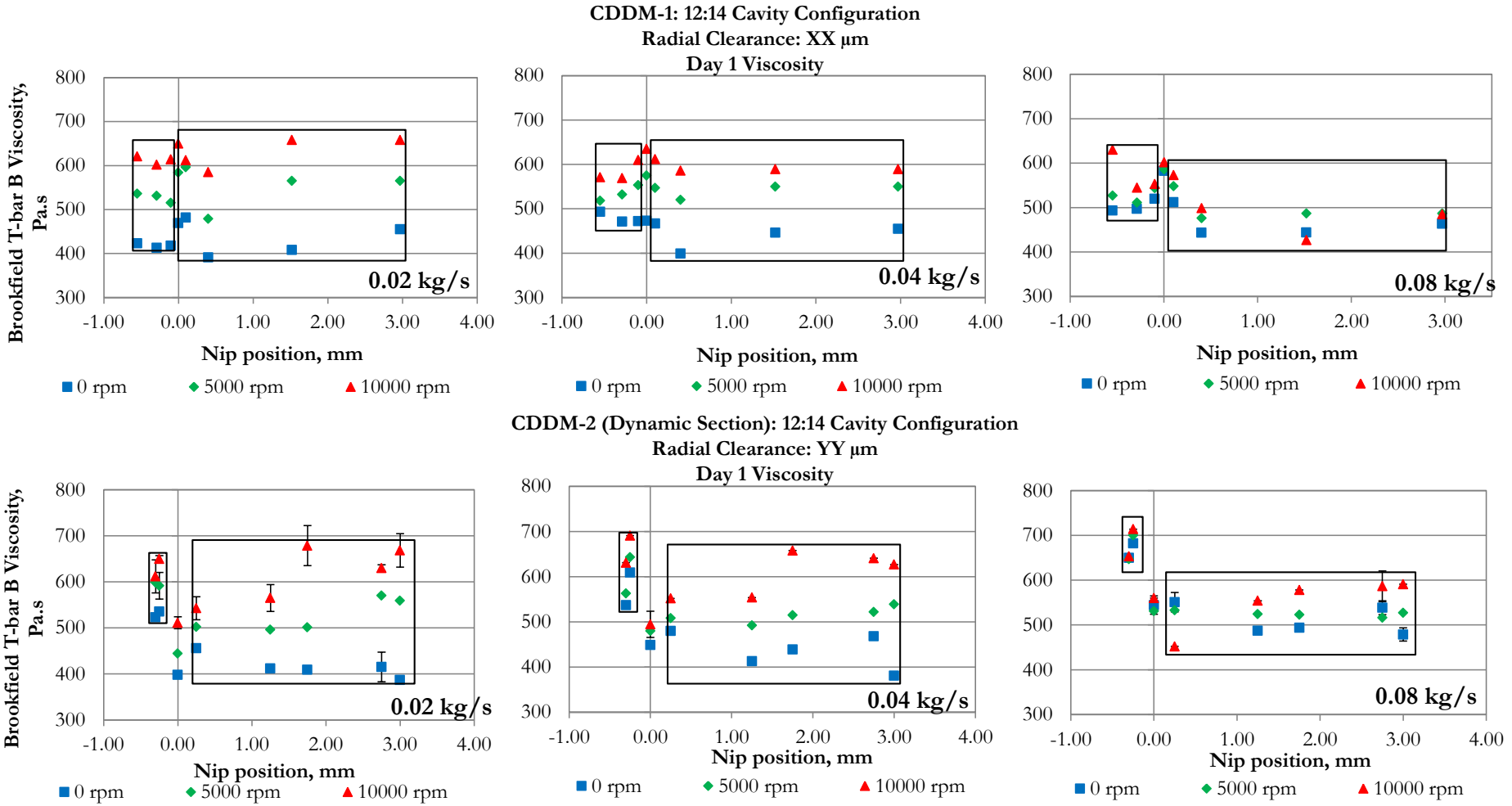

Figure 6-4: Brookfield T-bar B viscosity (day 1) as a function of mixer nip position for both the CDDM-1 (top), nominal radial clearance = XX µm and the CDDM-2 (bottom), nominal radial clearance = YY µm operating at different process flow-rates - for 1.0H-C Hair Conditioner material.

It can be seen that for both mixers, there is no clear trend between changing nip position and Brookfield T-bar b viscosity – this is indicative of bulk viscosity insensitivity to changing mixer axial displacement. Secondly, the measured viscosity of the samples show sensitivity to dynamic[315] operation i.e. as mixer rotational speed is increased (static[316], 5000 and 1000 rpm), sample viscosity is seen to increase irrespective of nip position.

Rationally, one can see a general trend for the effect of axial position - if position groups and process flow-rates are considered i.e. all –ve, 0, and +ve positions with respect to either mixer. As the process flow-rate is increased (0.02 – 0.08 kg/s), the viscosity of samples decreases for both the static and dynamic datasets at +ve positions and increase for the –ve positions in both mixers - it can also be said that the behaviour at 0 nip position is similar to the behaviour at –ve positions.

The above can then be explained in terms of deformation rates experienced by the process fluid at the nip group position configuration[317] - It can be said[318] that for the data presented in Figure 6-4 increasing rotational shear and extensional shear presents increasing viscosity build for a set mixer position – both of which vary to different extents at a specified axial position (-0.30, 0.00, +0.55, +2.75 etc.).

Considering Figure 6-13 - which schematically shows the inferred effect of change in axial positions, (+ve, 0 and –ve) on the nature of deformation encountered by the process fluid - it can be said that the formation of nips (-ve positions) results in fluid experiencing increased extensional shear with increasing process flow-rate at static operation (0 rpm). Under dynamic conditions, the afore-described is complemented with increasing shear due to the action of increasing mixer rotational speed.

For the +ve positions as process flow rate is increased, the decrease in sample viscosity can be attributed to the length of time (residence time) the process fluid is exposed to low deformation at these positions – although this is complemented by dynamic operation – the rates of deformation present at these +ve positions is low when compared to the -ve positions as described in Figure 6-13. At these positions, to obtaining increased fragmentation would require

[315] 5000 & 10000 rpm
[316] 0 rpm
[317] –ve, 0, and +ve positions
[318] Based on the conclusions from Chapters 4 and 5

long residence times (low process flow-rates) which is impractical in a manufacturing environment.

It is worth mentioning that there is also no correlation between pressure drop data (Figure 6-5) and viscosity values (Figure 6-4) for both mixers.

6.1.2.2 Hydrodynamics

Pressure Drop

The effect of axial displacement (nip position) on the pressure drop characteristics of the CDDM-1 and CDDM-2 mixer (dynamic section) is shown Figure 6-5 for the post processing of 1.0H-C Hair Conditioner at a range of process flow-rates.

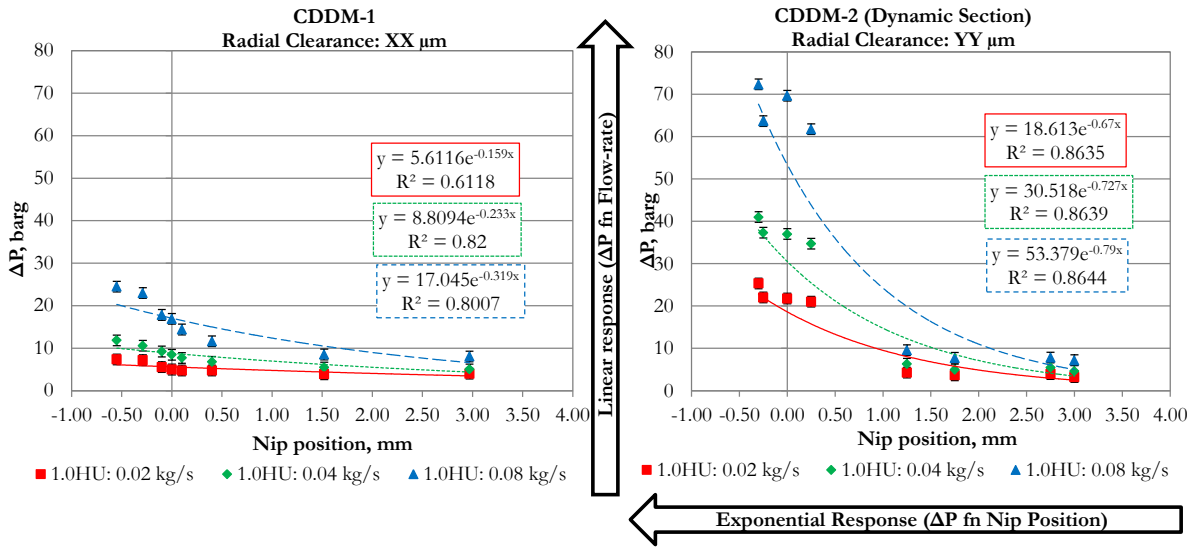

Figure 6-5: Average pressure drop as a function of nip position for the CDDM-1, nominal radial clearance = XX µm (left) and the CDDM-2, nominal radial clearance = YY µm (right) operating at different process flow-rates - for 1.0H-C Hair Conditioner material.

In general it can be seen that the average pressure drop values obtained for the CDDM-2 are higher than those obtained for the CDDM-1. Secondly, as the mixer position moves from +ve to –ve positions, the pressure drop in the mixer increases for a set process flow-rate. Likewise, an increase in process flow-rate, for a set nip position results in increase in system pressure drop.

For this work, it was discovered that there is no impact of mixer rotational speed on the pressure drop data so – an average pressure drop has been obtained for the dataset recorded at a set flow-

rate and nip position for varying mixer rotational speed[319] with a standard deviation obtained and plotted as error bars. This observation is based on pressure probe accuracy expressed as a combined NL&H: ± 0.25% of span [1.25 bar_g] i.e. the variation in the pressure drop readings for 0, 5000 and 10000 rpm for a set axial position were within this specified error limit hence indistinguishable from each other.

The theoretical response of flow-rate and nip position with respect to pressure drop is linear and 2nd order polynomial respectively as shown in Figure 0-16 and Figure 6-14 with increasing pressure drops recorded as the axial position tends towards the –ve nip positions. A comparison of the pressure drop data for both mixers indicates that – lower pressure drop values were obtained for CDDM-1 presumably due to changes in radial clearance. Maximum pressure drop readings are lower for CDDM-1 mixer (i.e. 25 bar) compared to CDDM-2 (i.e. 80 bar) which is due to the size of the radial clearance for both mixers - XX μm for the CDDM-1 vs. YY μm for the CDDM-2 of the 2 stage mixer – (XX > YY)

Secondly, both mixers reviewed[320] have similar cavity shape, size and ratio (12:14) on both the rotor and stator however the number of annular rings vary (6 on the CDDM-1 and 5 on the CDDM-2) and the CDDM-1 is approximately twice the length of the CDDM-2 thus making a direct hydrodynamic comparison very nigh impossible – however a working hypothesis could be that the value of pressure drop is more sensitive to the specified mixer radial clearance. An extended inference on the hydrodynamics of the CDDM mixers is discussed in Section 6.2.2.

6.1.3 Effects of Angular Displacement (Cavity Configuration 12:14 vs 11:11)

Results and discussion of the experimental trials investigating the effects of angular displacement on the viscosity of post processed Hair Conditioner premix (1.0H-C) through the CDDM-2 mixer (static section) at a range of process variables (Table 3-2) is conferred within this Section – mixer has an 11:11 cavity configuration set-up. Brookfield T-bar B viscosity and hydrodynamics data are discussed as well.

[319] i.e. 0, 5000 and 10000 rpm
[320] CDDM-1 and CDDM-2

6.1.3.1 Rheology

Brookfield T-Bar B Viscosity

The effect of angular displacement (angular position) on the Brookfield T-bar B viscosity (day 1) of post processed 1.0H-C Hair Conditioner premix for the CDDM-2 mixer (static section) is shown in Figure 0-16 – data is also plotted with rotor speed and process flow-rate.

As was recognised in Section 6.1.2.1 – there is no correlation/clear trend between viscosity (Figure 0-16) and pressure drop (Figure 6-6) with respect to changing angular position index likewise mixer axial position - similar conclusions as was discussed in Section 6.1.2.1 can be drawn.

6.1.3.2 Hydrodynamics

Pressure Drop

The effect of angular displacement (angular position index) on the pressure drop characteristics of the CDDM-2 (static section) is shown in Figure 6-6 for the post processing of 1.0H-C Hair Conditioner at a range of process flow-rates. As has been noticed earlier - increasing process flow-rate results in increase in pressure drop.

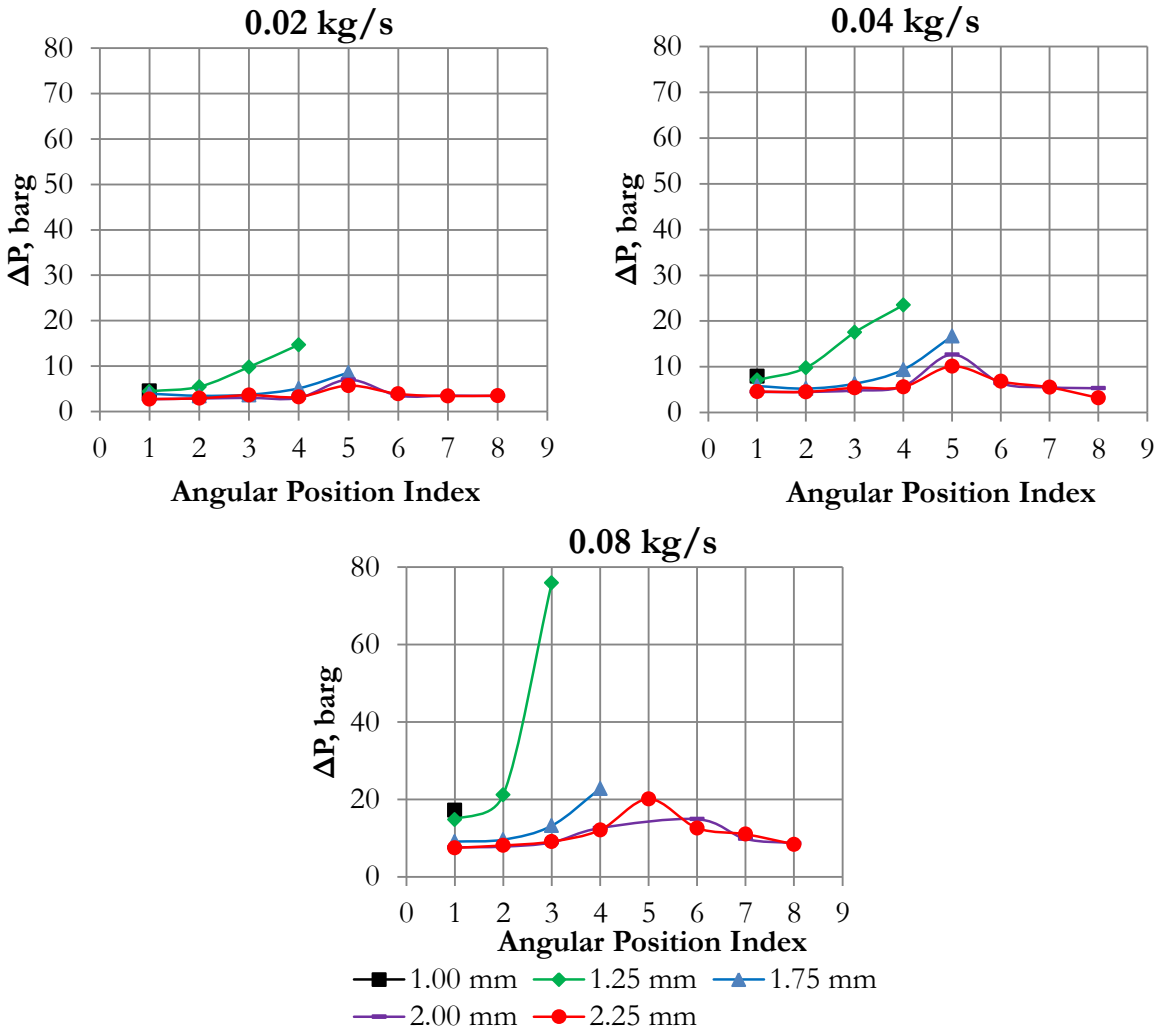

Figure 6-6: Pressure drop as a function of angular position for the CDDM-2 (static section) operating at various process flow-rates – 1.0H-C Hair Conditioner cold post processing.

For the axial positions reviewed - in general the pressure drop in the mixer is generally low (approx. 5 -10 bar_g) for the larger +ve positions (i.e. 2.25 mm) at certain angular positions index (i.e. 1, 2, 6, 7 and 8). However pressure drop is seen to spike (peak) at angular index position index 5 - this trend is seen again at other axial positions reviewed (2.00, 1.75, 1.25 and 1.00 mm) - in that the pressure drop begins to rise exponentially as the angular position index is changed (1 – 8) and then peaks out at angular index position 5.

In the case of axial position 1.75 and 1.25 mm the spike in pressure drop resulted in a ruptured bursting disc in the LIP process line.

From the results displayed in Figure 6-6, it can be inferred that in the 11:11 cavity set-up as angular position index is changed (i.e. 1 – 8) for a set axial position (i.e. 2.00 mm CTM, 2.25 mm

CTM) the flow paths begin to close up - with the most constrict flow path at 'Angular Position 5°' resulting in very high pressures and then begins to open up as one begins to approach 'Angular Position 8°' hence a pressure profile that starts off relatively low and reaches a peak at "Angular Position 5°' before reducing.

For other axial positions[321] (i.e. 1.75, 1.25 and 1.00 mm) - as the angular position is changed (i.e. 1 – 8), the flow paths begin to close up – at these axial positions, the flow path gets even more constricted as one encroaches on "Angular Position 5°' thereby leading to a failure of a bursting disk due to very high pressure (approx.. 7500 bar_g) - flow path schematics in Figure 6-7 aids the explanation.

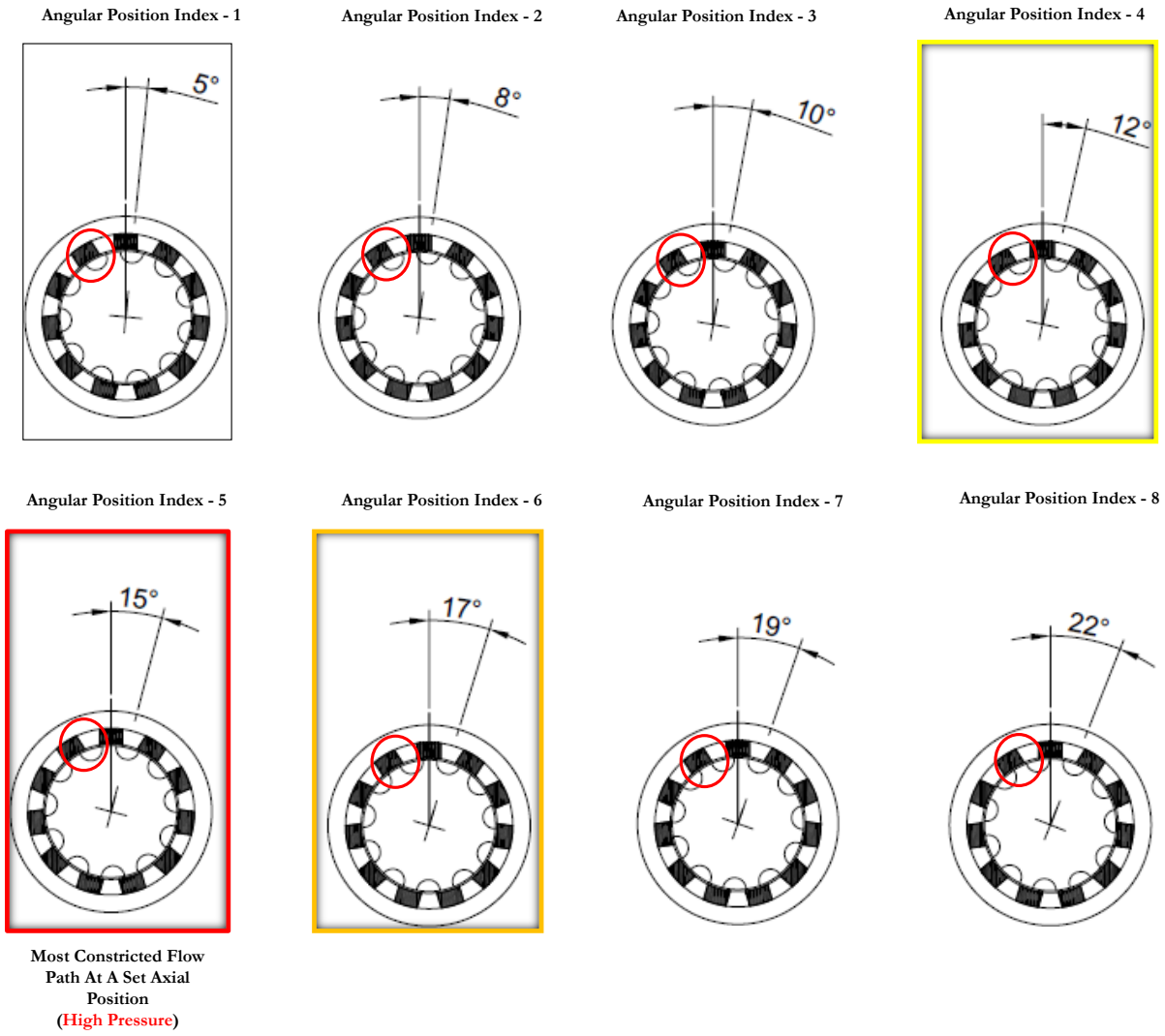

Figure 6-7: Schematic cavity overlaps for both the rotor (not shaded) and the stator (shaded) for the 11:11 cavity configuration set-up for various angular positions.

[321] As the position tends towards the –ve positions (refer to Figure 6-13)

Considering the schematic shown in Figure 6-7 for the 11:11 cavity set-up, one can see that as the angular position is changed (5° - 22°), process fluid flow path within the mixer changes. Due to the nature of the cavity set up on both the rotor and stator in relation to change in axial position.

At a set axial position (i.e. full +ve), pressure will always be highest at angular position "15°" if intra-trial[322] experimental pressure drops are compared - as this is the angular position with most constrict flow path . A comparison of inter-trial[323] experiments - as the axial position is moved from i.e. +ve to –ve position, the flow path becomes even more constricted as the mixer nips hence increasing pressure. This explains the pressure spike at +1.25 and +1.75 mm resulting in a burst disc likewise the system failure at +1.00 mm.

A comparison between the 11:11 and the 12:14 cavity configuration, one can see (Figure 6-8) that for any angular position, there will always be fluid paths open offering safer mixer operation at both static and dynamic modes.

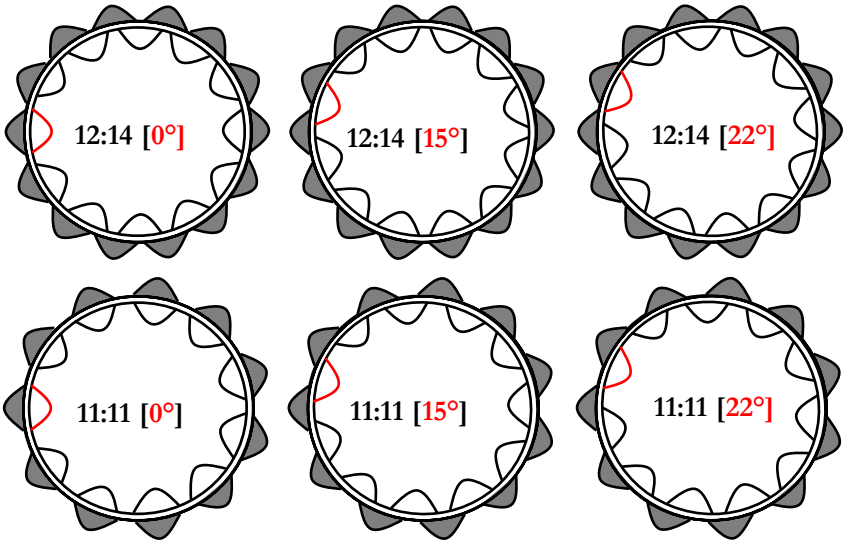

Figure 6-8: Schematic showing cavity overlap comparison for a 12:14 (top) and the 11:11 (bottom) cavity configuration for various angular positions.

In general a comparison of the fluid flow path of the 11:11 and the 12:14 cavity configuration shows (Figure 6-8) that the flow path in the 11:11 is more restricted - this highlights the importance of cavity configuration (i.e. number of cavities/ratio on the rotor and stator) on within the mixer.

[322] Intra-trial – Experiments conducted at set axial position for different angular position (5° - 22°)
[323] Inter-trial – Experiments conducted at different axial position for a set angular position

6.2 CDDM Technology Testing and Optimisation (50 % w/w O/W SFO Emulsion)

This work follows on from the work conducted in Section 6.1 as a means to test the CDDM mixing technology performance however a model coarse emulsion premix manufactured in a batch process is used to assess the performance characteristics of the CDDM mixers as opposed to lamellar premix used earlier – lamellar premix tested at various process/equipment variables exhibited no recognisable pattern thus making optimisation studies impossible.

This model emulsion system has dispersed oil phase fractions ϕ = 50 % w/w and a fixed dispersed phase - continuous phase[324] in which a surfactant[325] was dissolved in the ratio of 10:1 (oil: surfactant).

6.2.1 Experimental Program

A schematic of the factors considered in the experimental program as well as the response measured can be seen in Figure 6-9. The objective of the experimental design was to assess the effect of process conditions/equipment design as a function of coarse emulsion droplet size reduction following a high post processing operation thereby aiding mixer performance assessment alongside optimisation study.

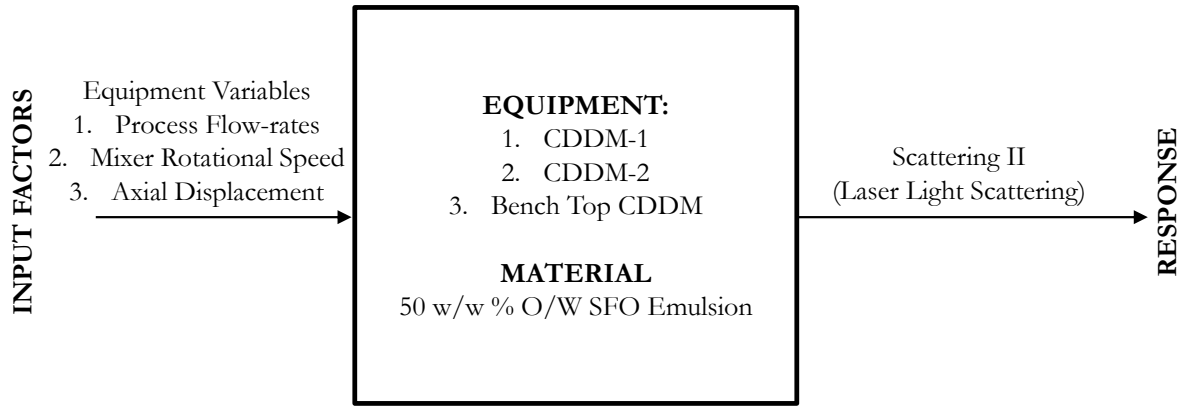

Figure 6-9: Schematic of experimental design for the CDDM technology testing and optimisation using 50 % w/w O/W SFO emulsion

The experimental trials conducted assessed various input factors deemed relevant to the optimisation of the performance of the CDDM technology in ensuring an optimised operation. The input factors considered included; CDDM [1] mixer axial displacement, [2] mixer rotational

[324] Demineralised water
[325] Pluronic F68

speed, and [3] process flow-rates – the techniques used for emulsion droplet size assessment was the light scattering device - Mastersizer 2000 (Malvern Instruments Ltd, Worcestershire, UK).

6.2.1.1 Experimental Matrix (Sample Preparation)

Initially a continuous aqueous phase is prepared by dissolving the required amount[326] of Pluronic-F68 (CMS Chemicals, UK) non-ionic surfactant in deionised water. A large magnetic stirrer was used to aid the solubilisation of the surfactant in solution.

The coarse emulsion is manufactured using the FDM (Maelstrom Advanced Process Technology GB) (Figure 3-9) - the FDM rotor speed is initially set at 1800 rpm to enable oil addition into the aqueous phase (continuous phase) in the first minute of processing.

The mixer speed is then further increased to 3000, rpm for 9 minutes. Coarse emulsion drop size distribution as measured using a Mastersizer 2000 particle size analyser (Malvern Instruments, Malvern, UK) – it has a volume weighted mean size D [4, 3] of approximately 20 μm.

Experimental trials occurred over several weeks and a typical day of experiment would begin by manufacturing multiple 8 litres coarse emulsion batches i.e. up to 50 litres.

Emulsion premix is then transferred into the holding hoppers of selected CDDM mixer prior to the start of an experimental matrix – coarse emulsion is also agitated on several occasions to avoid emulsion creaming. Experimental trials were then conducted at a range of process variables available for the selected CDDM technology[327].

Experimental Trials: Relationship between Process/Equipment Variables and Emulsion Droplet Size – Results Discussed Within Section 6.2.2

The optimum relative axial position was investigated for a 12–14 cavity configuration CDDM mixers. The mixers tested were [1] CDDM-1, [2] CDDM-2 and [3] Bench Top CDDM – the experimental trials conducted assessed the emulsification performance of the mixers operating at a range of equipment/process variables.

The experimental trials were performed to assess mixer performance as the extent of reduction in emulsion droplet size relative to a premix of starting D[4, 3] size of approximately 23 μm

[326] For an 8 litre scale
[327] [1] Single CDDM, [2] CDDM-2 (dynamic section) and [3] Bench Top CDDM

measured using a Mastersizer 2000 (Malvern Instruments Ltd, Worcestershire, UK) – a range of axial positions (Table 6-1) were tested – refer to Figure 6-3.

Table 6-3: Table showing relative nip positions examined for SFO experimental trials for the (1) CDDM-1, (2) CDDM-2 and (3) Bench Top CDDM.

CDDM Mixers Relative Nip Positions Reviewed (Nip Overlap), mm		
CDDM-1	**CDDM-2 (Dynamic Section)**	**Bench Top**
- 0.28	- 0.75	- 0.25
- 0.10	- 0.25	0.00
+ 0.05	0	+ 0.25
+ 0.48	+ 0.25	+ 0.50
+ 1.85	+ 0.75	+ 0.75
+ 2.90	+ 3.00	+ 1.00
		+ 1.35

For each axial position, a full experimental matrix (Table 3-2) was performed for the CDDM-1 and the CDDM-2 likewise for the Bench Top CDDM, a full experimental matrix (Table 3-3) was performed - Premix emulsion is pumped into the mixer[276] via the attached pumps. For experiments involving the CDDM-2, process material is injected directly into the dynamic section of the mixer (see Figure 3-3).

Post processing operation was performed at a range of process flow-rates and mixer rotational speeds according to the experimental methodology described in Section 3.3.1 for each nip position listed in Table 6-3 – similar protocol is followed for the experimental trials conducted on the Bench Top CDDM

6.2.2 Relationship between Process/Equipment Variables and Emulsion Droplet Size

Results and discussion of the experimental trials investigating the effects a range of process/equipment variables (nip position, process flow-rate and mixer rotational speed) on the droplet size (d [4, 3]) of the post processed SFO emulsion (50 % w/w) through the [1] CDDM-1, [2] CDDM-2 (dynamic section) and [3] Bench Top CDDM. Hydrodynamics data is discussed as well.

6.2.2.1 Particle Size Measurement

Emulsion Droplet Size Distribution

The effect of axial displacement (nip position) on the emulsion droplet size D [4, 3] of post processed 50 % w/w SFO emulsion premix for the [1] the CDDM-1, [2] the CDDM-2 mixer (dynamic section) and, [3] the Bench Top CDDM are shown in Figure 6-10, Figure 6-11, and Figure 6-12 respectively – data is also plotted with rotor speed and process flow-rate. Datasets displayed are for a single pass discharge of process material.

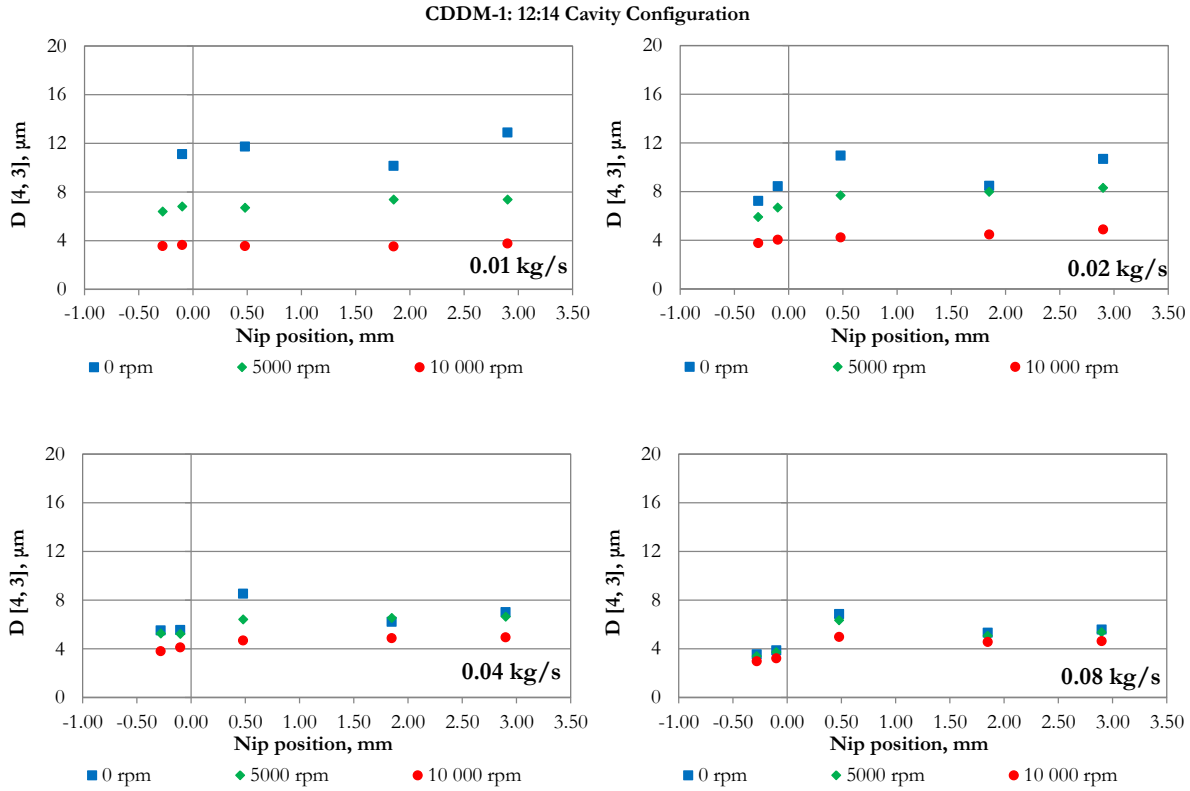

Figure 6-10: Emulsion droplet size D [4, 3] as a function of nip position for the CDDM-1 operating at various process flow-rates – 50 % w/w O/W SFO emulsion

The effects of process variables (flow rate, rotational speed and nip position) on emulsion droplet size (d [4, 3]) of emulsion is shown on these Figures - at low flow-rates, coarse emulsion droplet break-up is dominated by increasing mixer rotational speed (rotational shear flow).

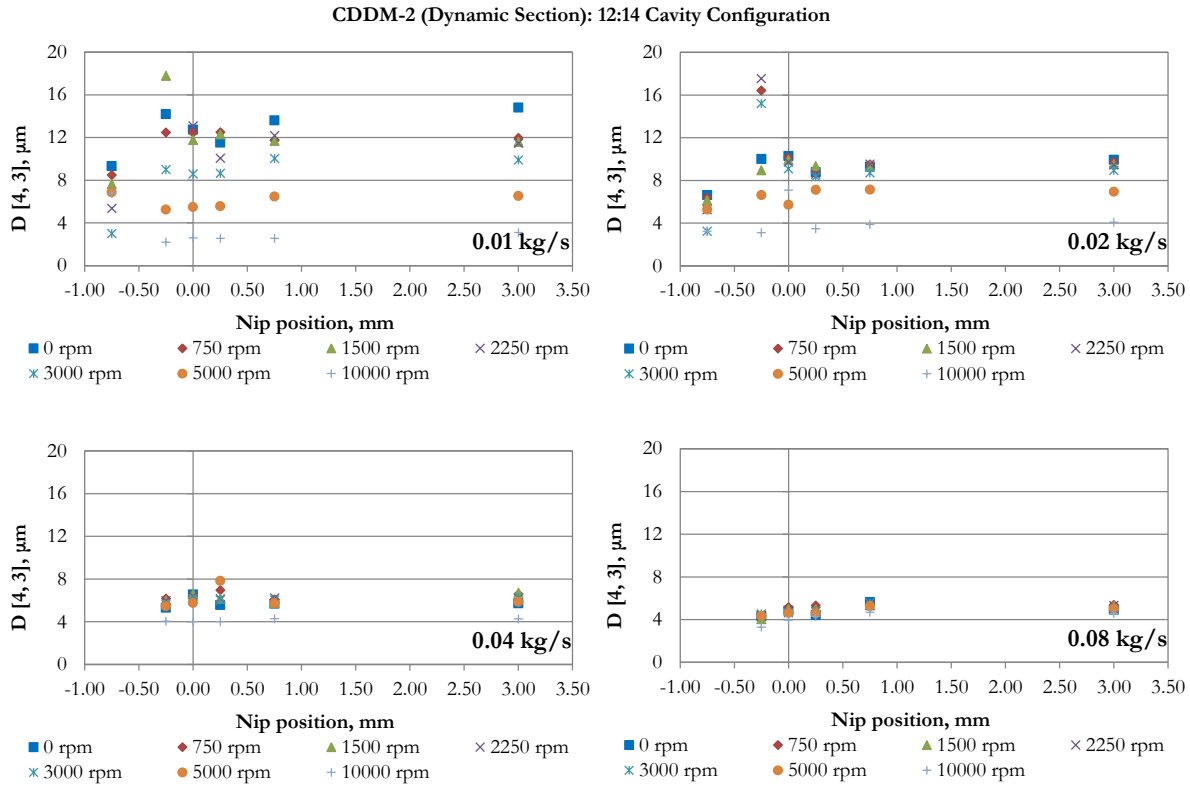

Figure 6-11: Emulsion droplet size D [4, 3] as a function of nip position for the CDDM-2 operating at various process flow-rates – 50 % w/w O/W SFO emulsion.

Likewise for a set process flow-rate and rotational speed, moving the mixer position from +ve to a –ve position results in droplet breakup – this effect is masked in the CDDM-1 and CDDM-2 but can be seen better in the Bench top CDDM dataset in Figure 6-12. It should be stated that for the dataset - it is difficult to rationalise what is going on in the CDDM technology by just considering a single variable or by looking at just one mixer.

It can be inferred from the hydrodynamics data displayed in Figure 6-14 – at points where pressure drop within the mixer is very low(est)[328] – the extensional flow component due to process flow-rate (pressure drop) within the mixer is very small and droplet break up is dominated by rotational shear (refer to Figure 6-10 - Figure 6-12).

It can be seen that for a constant low flow-rate i.e. 0.01 kg/s in the CDDM-1, CDDM-2 and 0.002 kg/s where very low pressure drop are obtained (Figure 6-14), emulsion droplets size reduction is due to increasing mixer rotational speed (rotational shear flow) as shown in Figure 6-10, Figure 6-11 and Figure 6-12 respectively.

[328] I.e. larger +ve positions and +ve positions in general relative to 0 and –ve positions

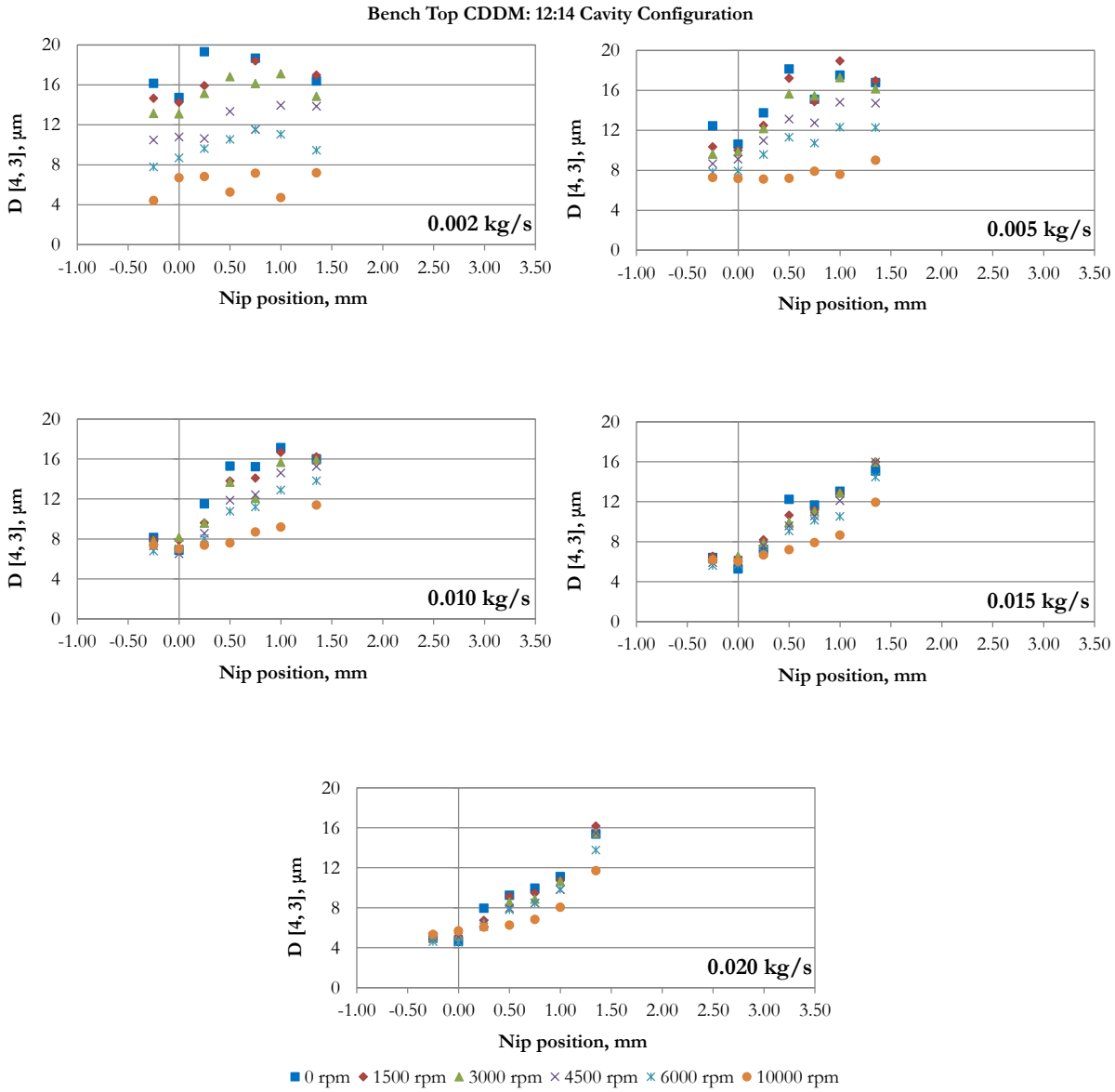

Figure 6-12: Emulsion droplet size D [4, 3] as a function of nip position for the Bench Top CDDM operating at various process flow-rates – 50 % w/w O/W SFO emulsion.

With this in mind it could be said for the post processing of 50 % w/w O/W SFO emulsion in the CDDM technology - as coarse emulsion enters the mixer (Figure 6-13), droplet break-up occurs within high shear gap due to either extensional flow only[329] or superimposed extensional and rotational shear due to dynamic operation. One can infer that the combination of these flows pulls the emulsion droplets apart thus breaking them into smaller droplets (Figure 6-13) – although no attempt has been made to describe the flow regime (droplet break up regime), as this is beyond the scope of this work.

[329] When the mixer is operating under static conditions

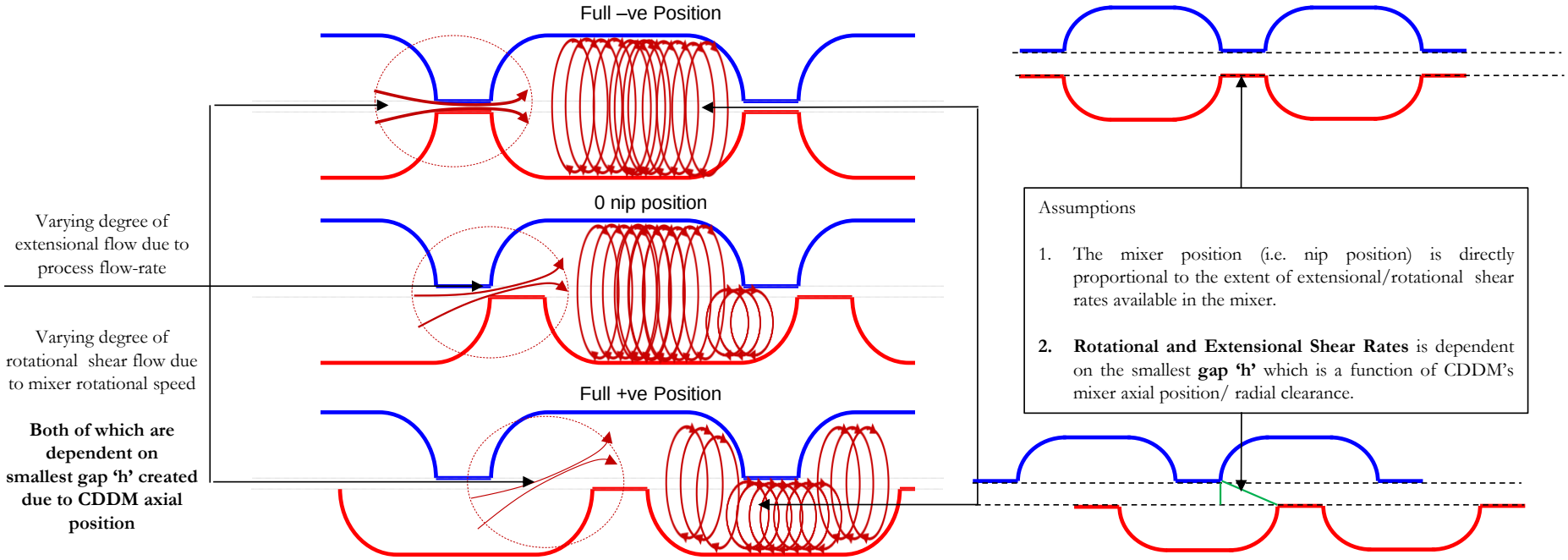

Deformation rates at any axial position i.e. +ve & -ve nip positions can be characterised by the displacement of the rotor relative to the stator i.e. L (see image on the right) and the subsequent smallest 'gap size h' it creates.

Figure 6-13: Schematic illustrating the presumed effect of change in axial positions (+ve, 0 and –ve) on the flow encountered by process fluid.

Subsequently from the results displayed in Figure 6-10, Figure 6-11 , Figure 6-12 and schematic displayed in Figure 6-13, it can be inferred that in the case when there is nip – nip overlap is formed between the rotor and stator[330] nips[331] (Figure 6-13) with a set flow gap size "h" also referred to in this text as the rotor-stator clearance. It can be said that these positions presents the maximum extensional and rotational shear rates available in the mixer as both the process flow-rates and mixer rotational speed is increased respectively thus resulting in increasingly smaller emulsion droplet sizes - the same can be said for 0 nip positions. Deformation rates[332] can be estimated using Equations displayed in Table 6-4.

Table 6-4: First approximation for rotational and extensional shear rates

<table>
<tr><th colspan="4">First Approximation For Various Mixer Nip Positions</th></tr>
<tr><th colspan="3">Extensional Shear Rate</th><th>Rotational Shear Rate</th></tr>
<tr><td colspan="3">Extensional shear rate is obtained using the expression
$$\text{Shear rate} = \frac{\dot{V}}{\pi\, r\, h^2}$$</td><td rowspan="4">$$\text{Shear rate} = \frac{\pi\, D\, N}{h}$$</td></tr>
<tr><td>$\dot{V}$</td><td>Volumetric flow-rate</td><td>m^3/s</td></tr>
<tr><td>r</td><td>rotor radius</td><td>m</td></tr>
<tr><td>h</td><td>smallest gap</td><td>m</td></tr>
</table>

At 0 nip position, the smallest gap within the mixer available for flow is no different from that which is available at the –ve positions (Figure 6-13) hence very high extensional and rotational shear is available.

For +ve positions – deformation rates at these position is reduced when compared to other negative position hence the large emulsion droplet sizes – as the mixer position tends towards the full +ve position due to the displacement of the rotor relative to the stator, the smallest flow gap "h" available within the mixer increases (Figure 6-13) from a set minimum[333] – this progressively decreases the maximum extensional and rotational shear rates available within the mixer – based on the results (Figure 6-10 - Figure 6-12), more evident in Figure 6-12.

[330] I.e. –ve positions
[331] Surface
[332] Rotational and/or extensional shear rates
[333] I.e. the in the CDDM-2 (XX μm) and in the CDDM-1 (YY μm)

6.2.2.2 Hydrodynamics

Pressure Drop

The effect of axial displacement (nip position) on the pressure drop characteristics of [1] the CDDM-1, [2] the CDDM-2 mixer (dynamic section) and [3] the Bench Top CDDM is shown in Figure 6-14 for the post processing of 50 % w/w SFO emulsion.

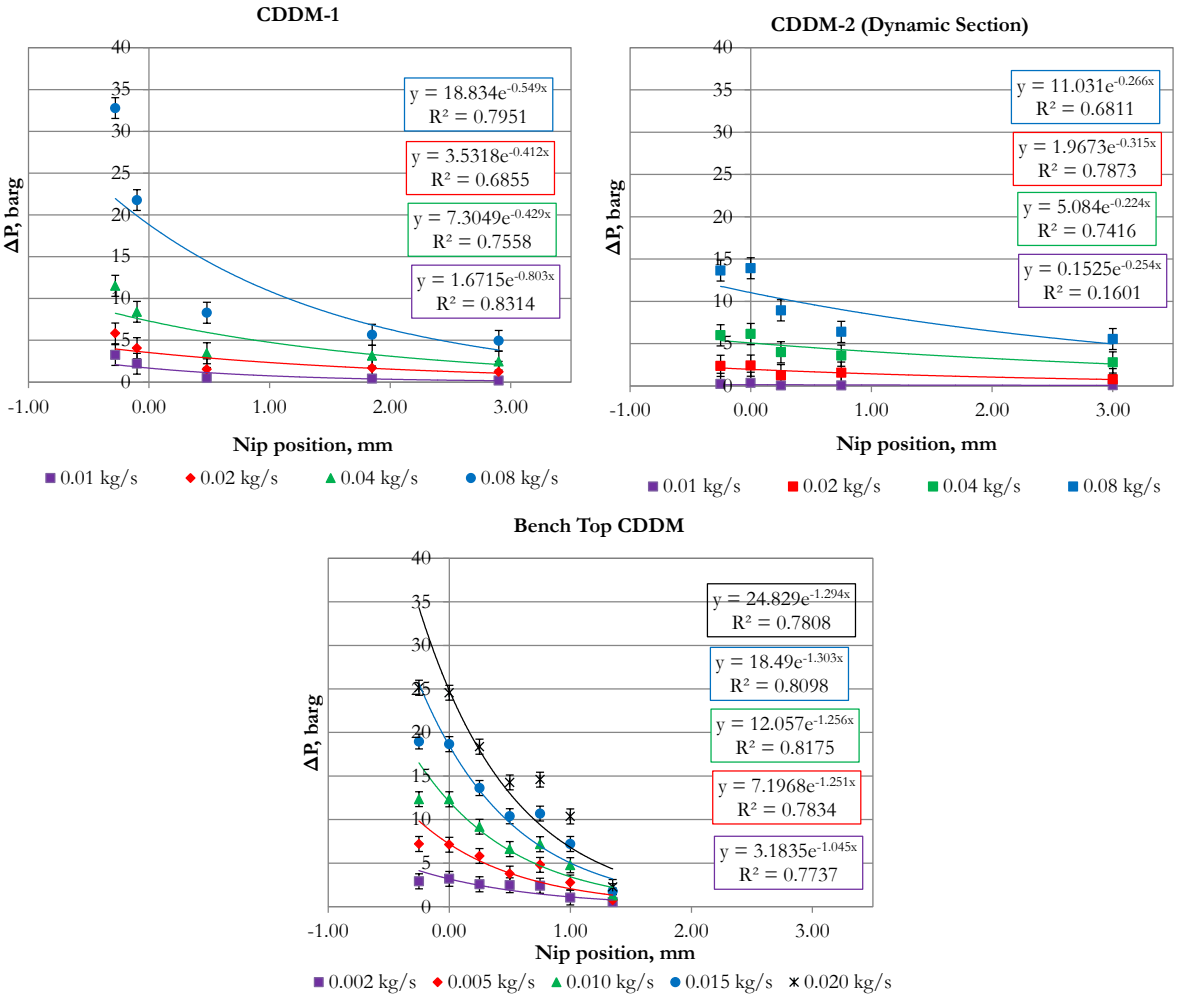

Figure 6-14: Average pressure drop as a function of nip position for the (1) CDDM-1, (2) CDDM-2 and, (3) the Bench Top CDDM operating at various process flow-rates – 50 % w/w O/W SFO emulsion.

It can be seen that as the mixer position moves from +ve to –ve positions, the pressure drop in the mixer increases for a set process flow-rate (exponential function). Likewise increasing process flow-rate results in increasing pressure drop (linear function).

For this work (as was discussed in Section 6.1.2.2), it can also be seen that there is no effect of mixer rotational speed on the pressure drop data so – an average pressure drop has been

obtained for the dataset obtained at a set flow-rate and nip position for varying mixer rotational speed with a standard deviation obtained and plotted as error bars.

From the result, it can be inferred that as the nip position tends from +ve to –ve position (lower pressure recorded) for a set flow rate, one can see an exponential rise in the pressure drop recorded – flow through the mixer at such positions (+ve positions) could be approximated as one through an orifice (Figure 6-13) with a known radius and a set length (nip position) – as the mixer position tends towards 0 nip, the increasing pressure is as a result of reduction in the cross sectional area available for process fluid flow due to the rotor nip moving towards the stator nip.

Moving past 0 nip - for positions when mixer position (i.e. rotor is moved vertically allowing for nip-nip overlap (i.e. -ve positions) - flow through the mixer could be approximated as flow through an annular geometry with a set length L determined by the nip overlap. At this position higher pressure drop is recorded. At these positions (any –ve position), the cross sectional area available for flow is at its smallest (= rotor-stator clearance). Increasing the length of the overlap further cause an exponential increase in pressure drop.

6.3 Summary

The CDDM technologies[334] have been tested for the purpose of optimising its performance with respect to increasing viscosity of the 1.0H-C lamellar[335] and droplet size reduction of a 50 % w/w SFO emulsion[336] premix. Test[337]/optimisation studies are conducted with respect to equipment variables [1] axial displacement (radial displacement) and, [2] Angular displacement (cavity configuration) for operating variables such as increasing process flow-rate and mixer rotational speed.

The following conclusions can be drawn for mixer pressure drop and performance characteristics[338]. Pressure drop is also found to be independent of mixer rotational speed. Secondly, pressure drop as a function of process flow-rate and changing axial position[339] is that of a linear and exponential function respectively. Moving from a +ve towards a –ve position in which an overlap is formed between the rotor – stator nip result in manifestation of a very small gaps 'h' available for the flow of process fluid for all technologies tested. This small gap 'h' also forms the back drop against which deformation rates can be estimated.

Deformation rates within the CDDM technology determines the mixer performance and is a function of [1] primarily mixer axial position and [2] operating conditions i.e. process flow-rates and rotational speed. Process flow-rates and mixer axial position determine the quantity of extensional deformation rates while mixer rotational speed and axial position determine the quantity of rotational deformation available within the CDDM technology.

Axial/radial specification of the CDDM technology, determines the deformation rates available to process fluids during an operation i.e. dynamic (increasing mixer rotational speed) and static (increasing process flow-rate) – increasing deformation rates results in increasing viscosity for lamellar premix and reduction in droplet size of premix emulsion.

Angular position/cavity configuration specification has a profound effect on pressure drop within the mixer when the rotor-stator cavity configuration is the same i.e. if rotor-stator ratio is = 1 in the case of the 11:11 cavity configuration, unsafe pressures would be attained within the mixer – this notion applies for both static and dynamic operation although only static conditions

[334] [1] CDDM-1, [2] CDDM-2 and, [3] Bench Top CDDM
[335] Analytical technique – Rheology (viscometry)
[336] Analytical technique – Laser
[337] Mixer hydrodynamics (pressure drop)
[338] Increasing viscosity of the 1.0H-C lamellar and 50 % w/w SFO premix
[339] From +ve to 0 to -ve

was tested. Data suggests cavity configuration of 12:14 presents safe process during both dynamic and static operation due to the fact that process fluid would always have an open path for flow.

Finally, the size of the smallest flow gaps created by adjusting any equipment variable[340] will determine the extent of the axial and rotational shear rates available within the CDDM mixer at a set flow rate and rotational speed respectively - more work needs to be done in quantifying the rates of deformation rates available at the various mixer axial position as this will be essential if any scale-up operation were to be conducted for geometrically similar mixers.

[340] [1] axial/radial specification and, [2] angular position/cavity configuration

6.4 References

None

Chapter 7

7 Conclusions and Future Work

The overall aim of the Thesis was to develop a resource efficient product and/or manufacturing process that make efficient use of raw materials. Conclusions to the various work disseminated within the Thesis (Chapters 4, 5 and 6) have been presented as summaries at the end of the respective Chapters – This intention of this Section is to attempt to bring together the various summaries and draw up an overall conclusion with respect to the Thesis aim. Future work is also discussed in Section 7.2.

7.1 Conclusions

The first part of the work investigated the effects of a range of process variables on the underlying microstructure/rheology of the intermediate of the selected model product (1.0H-C Hair Conditioner) – the various process variable investigated included process temperature, route to manufacture (cold and hot processing), high shear post processing operation (hot vs cold) with respect to batch processing of the intermediate likewise CDDM equipment setup and system pressure drop with respect to continuous processing of product intermediate, subsequently a fully formulated product. It also reviewed the CDDM technology in a continuous manufacturing context for the processing of the model fully formulated product.

The Second part reviewed the optimisation of the CDDM technology for the processing of Hair Conditioner) by examining a range of equipment variables relevant to the confronting surfaces of the rotor and stator – these include the relative axial position/radial separation and the relative angular displacement/cavity configuration of the surfaces. A second process fluid in the form of 50 % w/w SFO emulsion premix is also used for this work

7.1.1 Process Design and Equipment Optimisation Studies

Rheology, microscopy, scattering (SAXS) and thermal transition investigations, disseminated in this Thesis have been used to obtain quantitative/qualitative data for the effect of a range of process variables relevant to the continuous manufacturing of a resource efficient H-C based Hair Conditioner[341] - which is in parity with a revised benchmark specification set in Section 4.3

[341] Formulation is based on the quaternary mixture of QUAT/CS/FA/Water system (product intermediate)

in terms of rheological[342] and microstructural[343] specification for which product performance is upheld i.e. consumer perceived benefits.

It has been concluded that; the continuous manufacturing of HC based Hair Conditioners is best performed as a two staged process[344] - [Stage 1] the manufacture of a concentrated lamellar dispersion[345] forming the gel phase network which serves as the structuring component to the Hair Conditioner, and [Stage 2] the cool/dilution and the addition of minor ingredients to the concentrated lamellar dispersion to a specified Hair Conditioner formulation i.e. concentration (1.0H-C[346], 0.7H-C, 0.6 H-C etc.)[347].

With respect to achieving the aim of this Thesis[348], dilution from the concentrated lamellar dispersion should be to 0.6H-C Hair Conditioner – which is a Hair Conditioner possessing only 60 % w/w of the total amount of solids contents[349].

Empirical studies conducted (Chapters 4 and 5) highlights; the most important Stage of the manufacturing process is the nature of the 'manufactured lamellar gel[350]' at [Stage 1] - which is the structuring step - the second step[351] is merely a case of ensuring a good distribution of the minor ingredients in the continuous phase and thus a function of distributive mixing.

The important parameters which determine the nature of the structuring phase - vital to the manufacturing of a resource efficient H-C based marketable Hair Conditioner as defined by rheological and microstructural specification of Brookfield T-bar B viscosity of 400 Pa.s[352] and 'QUAT/CS' rich L_β microstructure are [1] process temperature and [2] system pressure drop;

[1] Process Temperature - from the work discussed in Section 4.2, more importantly Section 4.2.3.1, it was demonstrated that when a AA % QUAT/CS/FA/Water system is diluted, the system swells – effectively increasing systems' bulk viscosity. The extent of this increase in viscosity is directly proportional to the nature of the underlying lamellar microstructure i.e. a system with the most amount of 'QUAT/CS' rich L_β microstructure in relation to other forms of

[342] Minimum of approx. 400 Pa.s (Brookfield T-bar B viscosity)
[343] Predominantly 'QUAT/CS' rich L_β microstructure
[344] As is schematically introduced in Figure 5-2
[345] Approx. AA % QUAT/CS/FA/Water
[346] Approx. BB % QUAT/CS/FA/Water (concentration of AA % > BB %)
[347] With respect to Process X
[348] Implementation of a resource efficient process for the manufacture of H-C based Hair Conditioner
[349] Major ingredients
[350] Stage 1
[351] Stage 2 - addition of minor ingredients
[352] An Hair Conditioner of good rheology during consumer dispensing

microstructure[353] would swell more than one with the least amount of 'QUAT/CS' rich L_β microstructure. Process temperature of approximately 'T-optimum °C' is presumed to be the temperature which presents the most favourable condition for the formation of a system with predominantly 'QUAT/CS' rich L_β microstructure – this value is obtained against the backdrop of the data disseminated in Chapters 4 and 5.

[2] Pressure - pressure at which the concentrated lamellar dispersion is formed is vital as it determines the state of dispersion[354] of the product intermediate[355], subsequently the state of dispersion of the Hair Conditioner product both of which have profound effects on the rheological and morphological properties of the formed Hair Conditioner. From the work discussed in Section 5.1, the state of dispersion as seen under the microscope for a 'QUAT/CS' rich L_β microstructure is affected by systems pressure drop. Work discussed in Section 5.1 and results shown in Appendix B prove that manufacturing the lamellar concentrate under low pressures results in products with coarse dispersions states possessing larger domains in comparison to ones manufactured at higher pressures – which results in products with finer state of dispersion possessing small domains. These factors have a direct impact on the rheology/morphology of the Hair Conditioner product i.e. higher system pressure drop[356] results in product of higher rheological quantities. Based on this it could be said that this step is a function of dispersive mixing actions and high system pressure within manufacturing plant safety regulations is recommended

With regards to high shear cold post processing of the formed 0.6H-C Hair Conditioner[357] in order to boost the viscosity, dataset discussed within this Thesis (Chapters 4, 5 and 6) have proven that increasing deformation rates i.e. intensity of high shear post processing operation, results in increased fragmentation[358] of underlying 'QUAT/CS' rich L_β microstructure thus increasing the systems' bulk viscosity. The dynamic operation of the CDDM technology has been found to be the most effective in delivering the levels of deformation needed to ensure the highest viscosity build is achieved.

Increasing deformational rates in the CDDM technology is a function pump flow-rate (pressure drop) and mixer rotational speed – energy lost can be converted to heat resulting in system

[353] 'FA' rich L_β microstructure and globular micelles L_1
[354] When viewed under the microscope
[355] Approx. AA % QUAT/CS/FA/Water
[356] Pressure within manufacturing plant safety regulations
[357] 'QUAT/CS' rich L_β microstructure system
[358] Reduction in 'QUAT/CS' rich L_β microstructure particle size

temperature rise[359] during cold high shear post processing. If this temperature is significant enough to cause phase transition (L_β going back into the L_α) by heating – the effect of cold high shear post processing operation would be lost. An instance of this was seen in the work performed in Section 4.2.3.

With respect to optimised operation of a dynamic CDDM, deformation rates is a function of the smallest gap available for the flow of process fluid within the mixer - a CDDM possessing a 12:14 cavity mixer provides the safest setup – i.e. radial clearance should be set at approximately YY μm and mixer axial position should be set to 0 nip – at this point, the smallest possible gap in the mixer is achieved at the price of small pressure drop - hence very high deformational rate relative to other positions.

Finally, qualitative data obtained from product performance tests to confirm consumer liking of 0.6H-C products which have been cold post processed in the CDDM technology compared to similar test for a fully formulated 1.0H-C products which have been manufactured via Process X manufacturing. None of these results have been shown in this text due to the confidential nature of the data however the performance testing has showed positive results in overall liking – indicative of no impact of reduction is solids content on the product functionality i.e. style and conditioning benefits.

[359] Viscous heating

7.2 Future Work

Work disseminated in this Thesis has proven that the nature of the quaternary mixture of QUAT/CS/FA/Water system is affected by a range of process conditions - more importantly increasing deformation rates results in increasing fragmentation effectively leading to the increase in bulk viscosity of this intermediate subsequently the resulted Hair Conditioner.

Firstly, repeat and/or elaborate on the work disseminated in Section 4.2.3.4 [360] - the aims of current thesis is still applicable.

Secondly, a rigorous experimental protocol could be conducted to quantify the particle size and/or particle size distribution of the quaternary system before and after a cold post processing operation – this work should be used to complement current work disseminated within this Thesis/develop new insights.

Light scattering equipment - Malvern 2000[361] and Zetasizer nano ZS[362] particle analyser (Malvern Instruments, Malvern, UK) can be used to asses particle size distribution for the AA % QUAT/CS/FA/Water before and after cold high shear post processing operation. This analysis can be used to deliver a quantitative/qualitative measure for comparison. This experiment should be repeated multiple times ensuring reproducibility for set experimental protocol.

Dataset obtained from above work should be complemented with small angle neutron scattering, x-ray scattering and cryo SEM measurements – this will help identify the various microstructural details[363] and components being assessed by the light scattering equipment.

Further empirical studies should be designed to monitor/further understand the changes to the underlying microstructure of the intermediate[364]/fully formulated Hair Conditioner with respect to process time and age i.e. to better understand lamellar gel network evolution at a range of process variable.

The CDDM technology is likely to be deployed as cold post processing equipment – trials using 'QUAT/CS' rich L_{β} microstructure Hair Conditioner should be conducted in the new (2014) pilot plant CDDM (Figure 7-1) installed at Unilever Research and Development Port Sunlight.

[360] SAX analysis
[361] Particle size range of 0.020 to 2000 μm
[362] Particle size range of 0.0003 to 10 μm
[363] I.e. size distribution
[364] Approx. AA % QUAT/CS/FA/Water

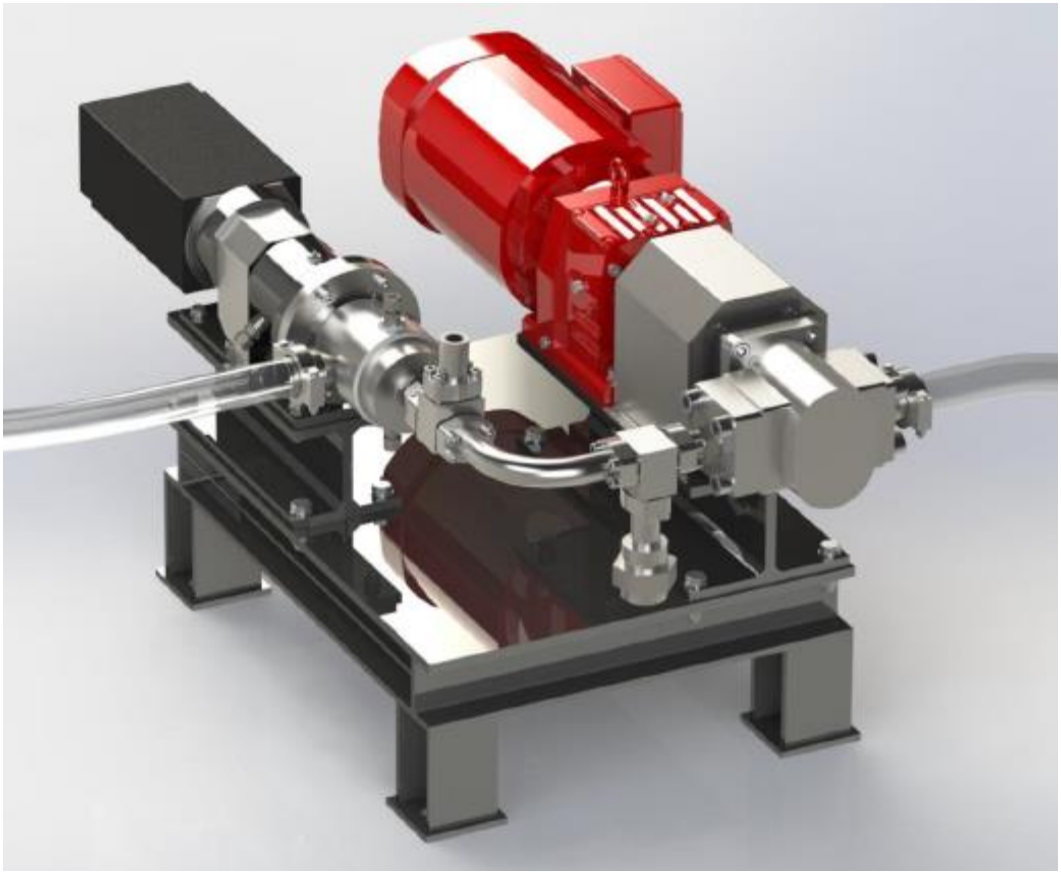

Figure 7-1: New pilot plant CDDM to be installed at Unilever Research and Development Port Sunlight (image courtesy CDDM Technology, England).

Likewise for the new pilot plant CDDM mixer, experimental trials using SFO emulsion formulation, similar the one utilised in this work should be used to assess its performance. Performance characteristics should be plotted as a function of deformational rates (rotational and extensional shear rates) or any other appropriate measure and compared to the other CDDM technology already disseminated in this Thesis for the purpose of scale-up correlations.

Computer simulations i.e. ANSYS Fluent to help solve, show and better understand the complete flow regimes experienced by process fluids within the various CDDM technology. Simulation should begin by modelling fluid flow for a steady state, laminar isothermal flow. This work can then be progressed into attempting to quantify/predict the values of shear rate for the specified fluid. This work will compliment afore proposed scale up operation.

Appendices

Appendix A

Benchmark System – Manufacture – Section 4.1.2

Experimental procedure is commercially sensitive and cannot be discussed.

Benchmark System - Analysis– Section 4.1.2

Optical Microscopy Images

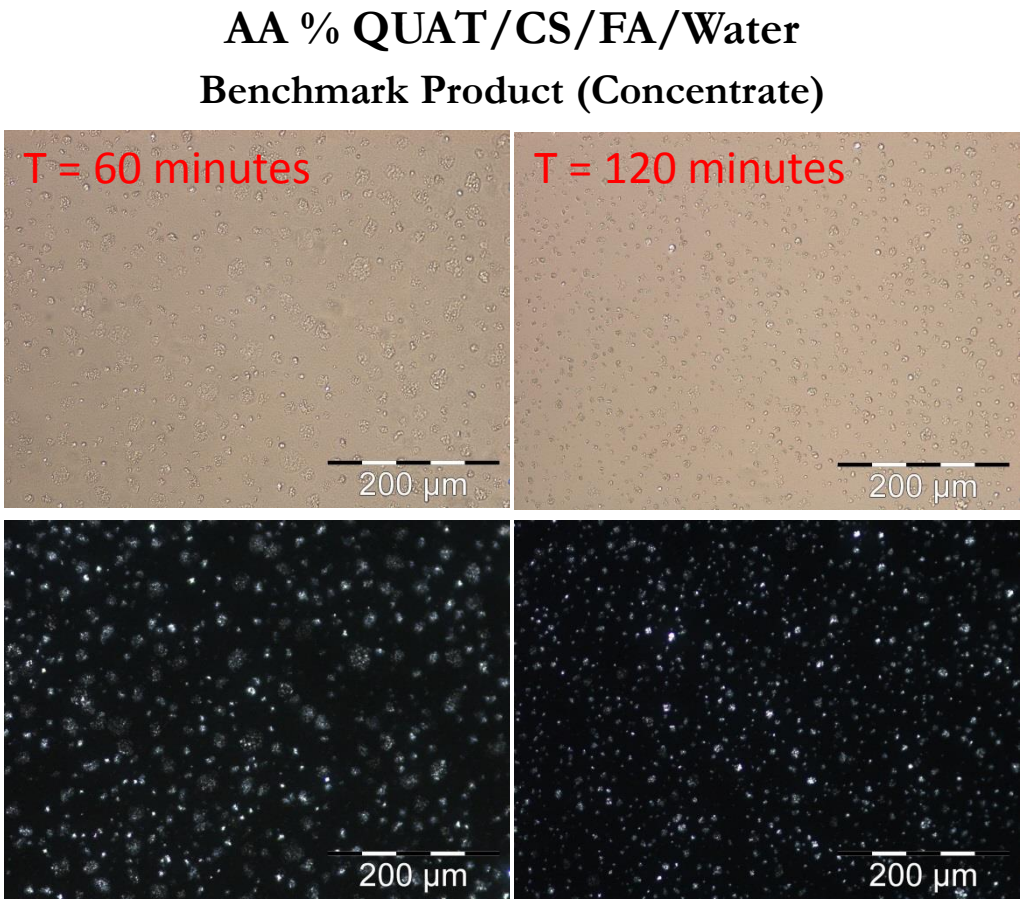

Figure 0-1: Bright field (top) and cross polarised (bottom) illuminated micrographs for approx. 'AA % QUAT/CS/FA/Water' intermediate obtained at various time T during the manufacturing of the Benchmark 1.0H-C Hair Conditioner.

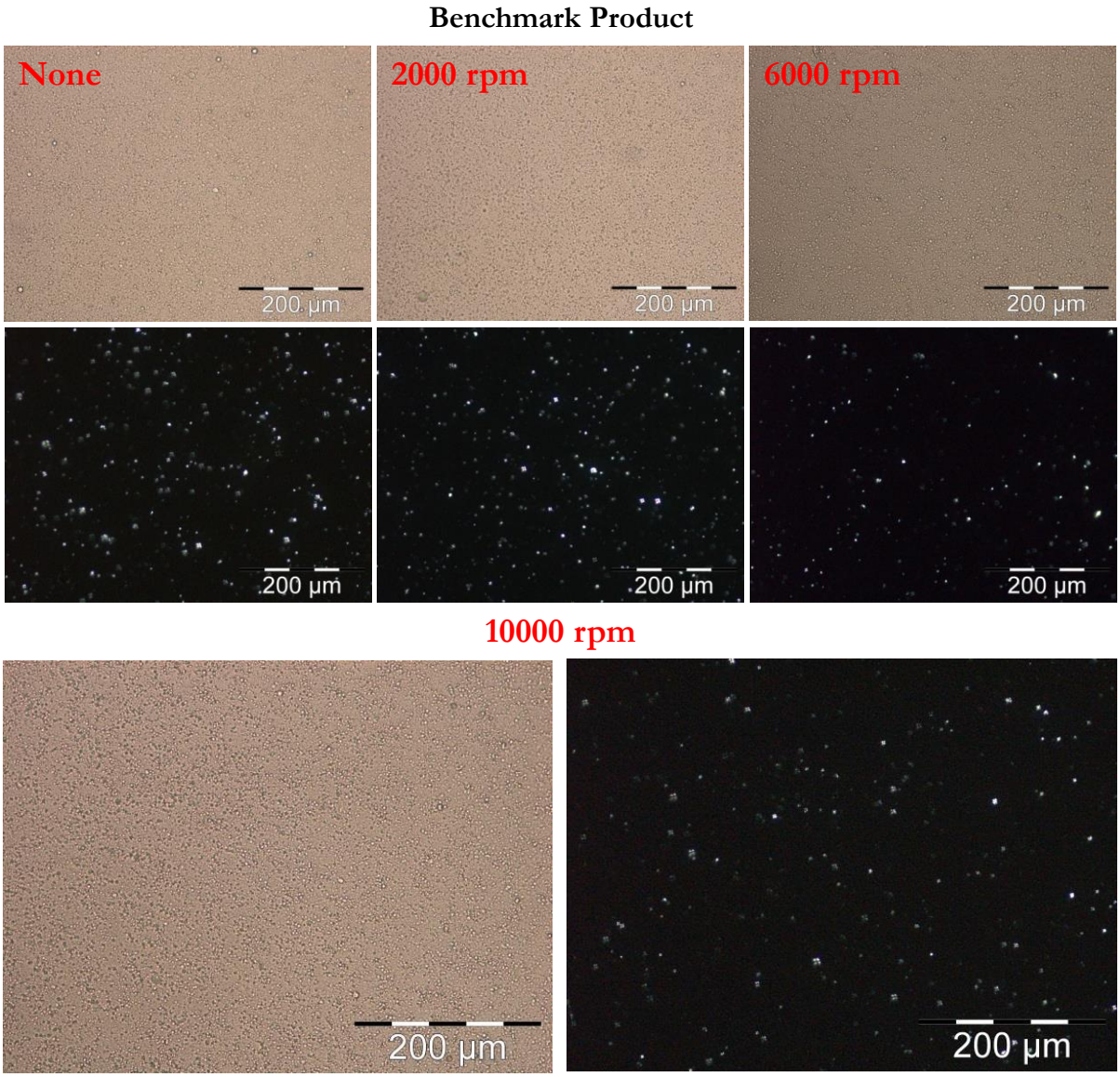

Figure 0-2: Bright field and cross polarised illuminated micrographs for benchmark 1.0H-C Hair Conditioner obtained following a single pass discharge through the inline high shear mixer.

Benchmark System - Analysis– Section 4.3.2

Brookfield T-bar B Viscosity

Hair Conditioner offline dilution involved the offline dilution of 1.0H-C to 0.6H-C – performed by adding required amount of water to a set amount of process material.

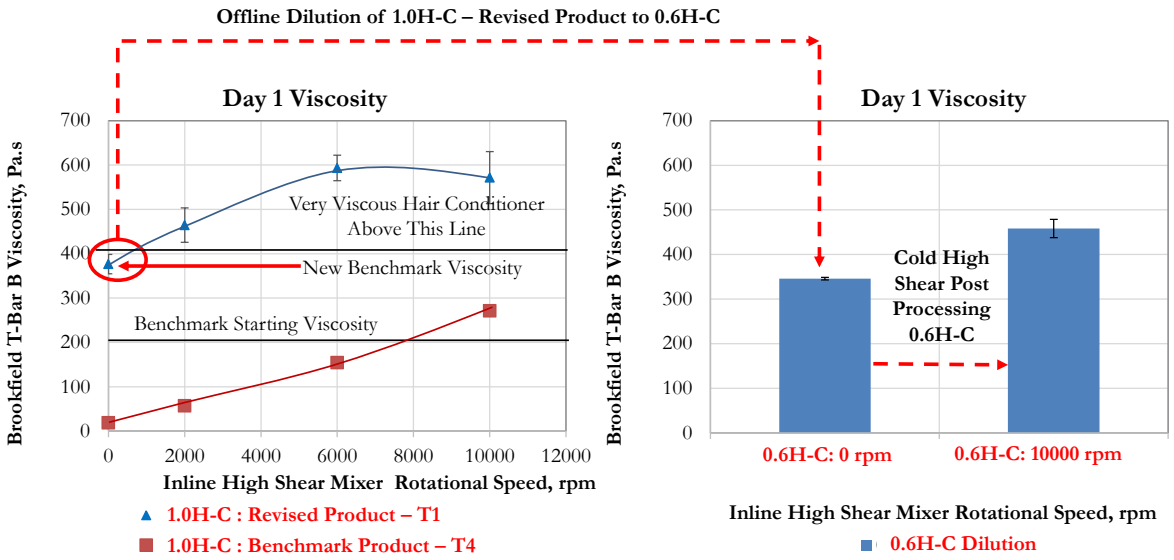

Figure 0-3: Brookfield T-Bar B viscosity as a function of inline high shear mixer rotational speed for 1.0H-C Hair for the benchmark system – process temperature = 'T1 °C', benchmark Hair Conditioner data produced at process temperature = T4 °C has been included for the purpose of comparison (left) and Brookfield T-bar B viscosity for a diluted product (1.0H-C dilution to 0.6H-C) alongside 0.6H-C material which has been subjected to high shear cold processing via the inline high shear mixer at 10000 rpm (right).

Optical Microscopy Images

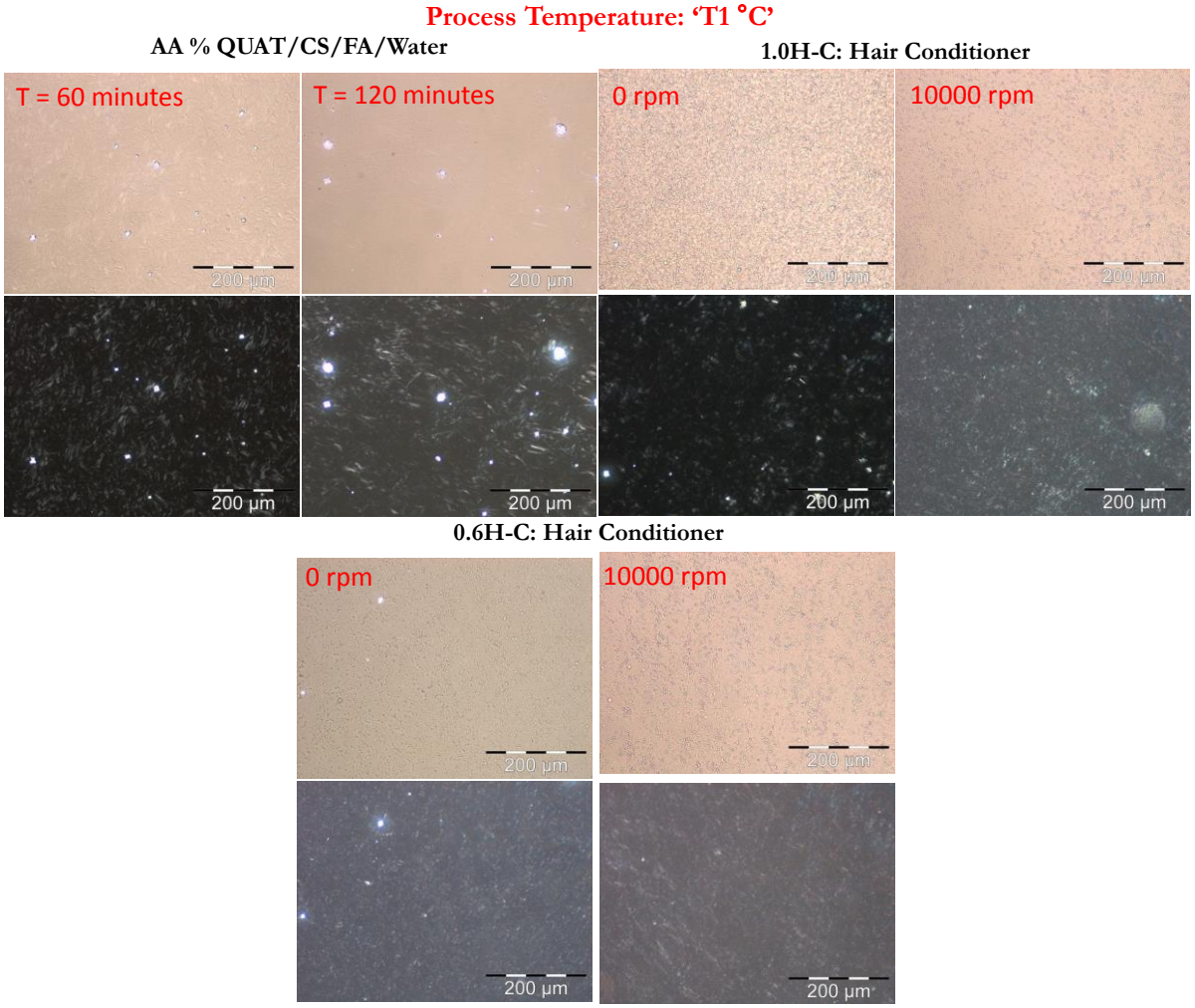

Figure 0-4: Bright field and cross polarised illuminated micrographs for revised benchmark 1.0H-C Hair Conditioner obtained following a single pass discharge through the inline high shear mixer (top half) and diluted product (1.0H-C dilution to 0.6H-C) alongside 0.6H-C material which has been subjected to high shear cold processing via the inline high shear mixer at 10000 rpm (bottom half)

Appendix B

Effect of Process Variables: Temperature and Pressure Section 5.1.2

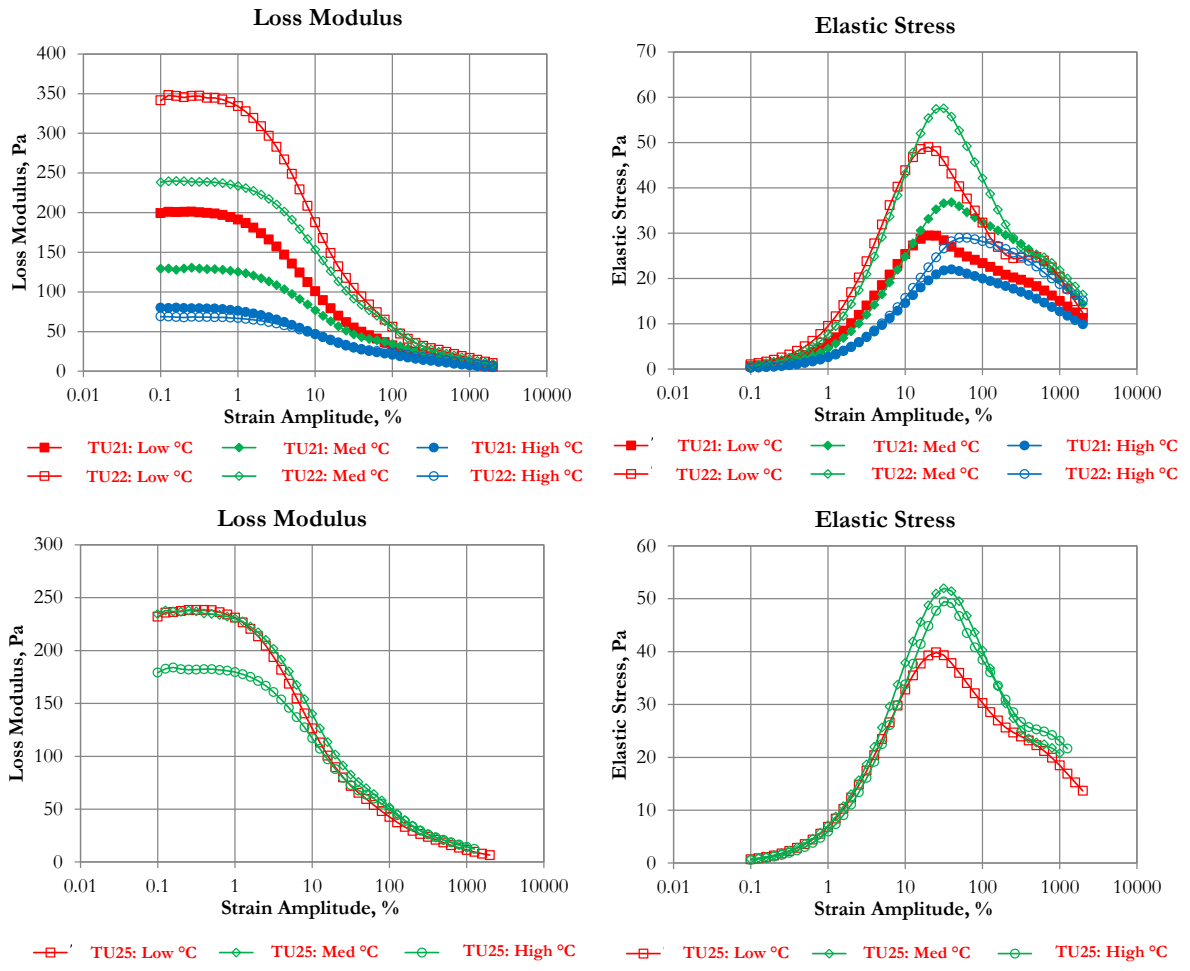

Figure 0-5: Oscillatory rheology tests (loss modulus [left] and elastic stress [right]) results performed on selected samples from experimental trials – TU21, TU22 and TU25

TU24 Experiments: CDSM-2 – CDSM-1

These experimental trials assessed the performance of the combination of the CDSM-2 and CDSM-1 in series (Figure 5-4) for the manufacture of lamellar dispersion based product alongside the effect of the temperature and pressure at which the L_α phase.

For TU24, a temperature scan from 'T#1 °C – T#11 °C' (Table 0-1) was conducted using the hot water stream/cold water bleed as a temperature modifier on the 'AA % QUAT/CS/FA/Water' prepared in CDSM-2 device followed by cooling by chilled water blend in the CDSM-1 device.

Table 0-1: Table indicating the estimated process temperatures at which lamellar dispersion ('AA % QUAT/CS/FA/Water') was formed for TU24 experimental trials.

	Lamellar Dispersion Temperature ('AA % QUAT/CS/FA/Water') T, °C										
Sample	**#1**	**#2**	**#3**	**#4**	**#5**	**#6**	**#7**	**#8**	**#9**	**#10**	**#11**
TU24	**Low**				**Med**					**High**	

Table 0-2: Table indicating actual process variables recorded during experimental trials – TU24

	Process Flow-rates						Pressure drops		
Trial #	**S1**	**S2**	**S3**	**S4**	**Concentrate**	**Product**			
	Pump Flow-rate, kg/s						**CDSM-2**	**CDSM-1**	**Total**
							bar_g		
TU24									

For this set-up, the temperature of 'AA % QUAT/CS/FA/Water' could not be measured directly due to the design of the CDSM-2 device, so it was inferred it via a simple theoretical calculation from the streams. Presumed pressure drop across CDSM-2 is **approx. 23 bar_g** and across CDSM-1 approx. 7 – atmospheric pressure is **approx. 6 bar_g**.

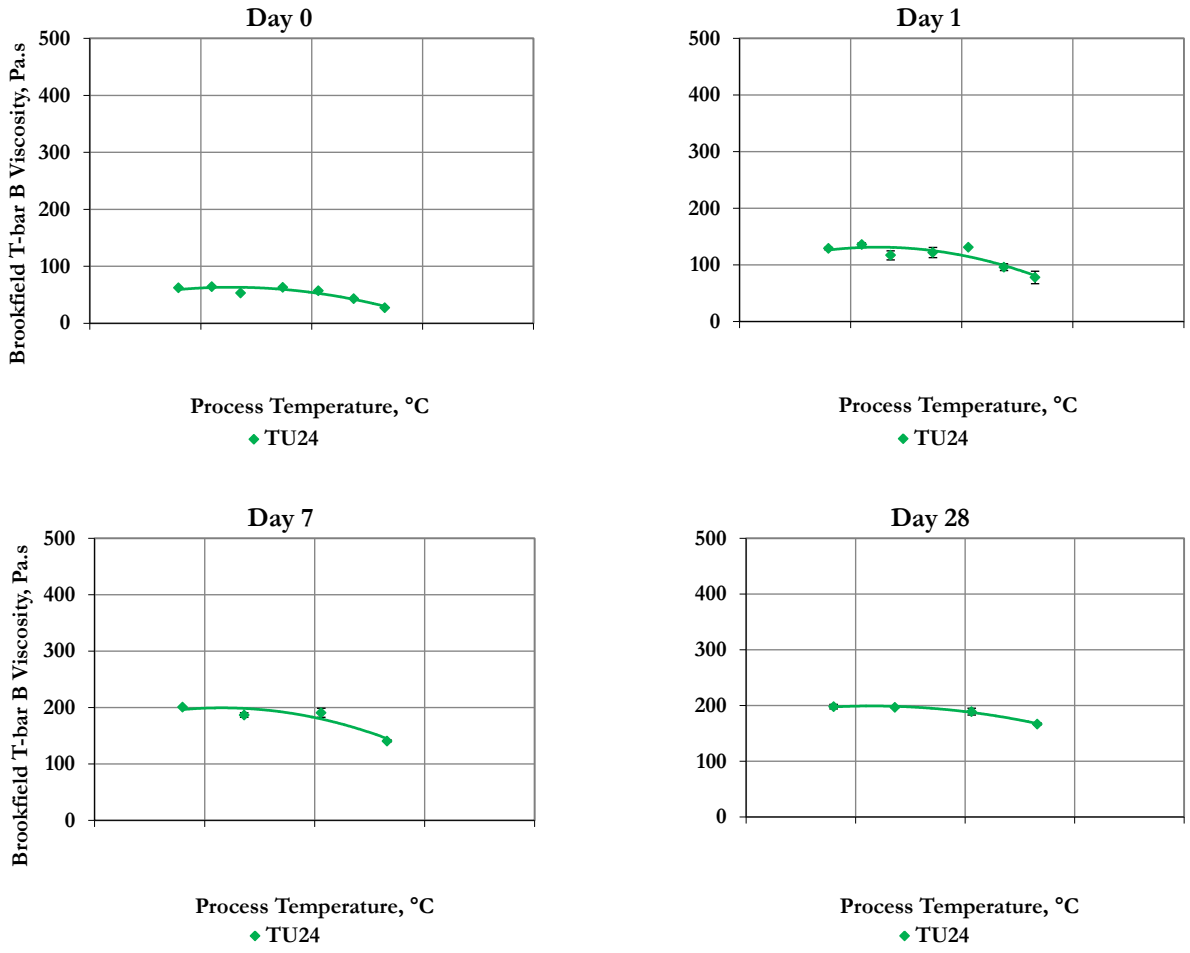

Figure 0-6: Brookfield T-bar B viscosity as a function of process temperature for Hair conditioners based on the 1.0H-C formulation – Brookfield T-bar B viscosity is also shown as a function of product age fresh (day 0), day 1, day 7 and day 28 for experimental trials TU24.

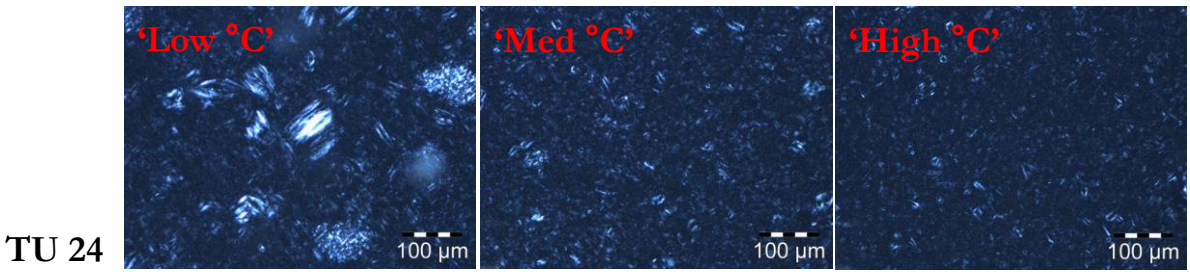

Figure 0-7: Cross polarised illuminated micrographs for 1.0H-C Hair Conditioners obtained at a range of process temperatures (low, medium and high) for Hair Conditioners manufactured via TU24 based on the 1.0H-C formulation.

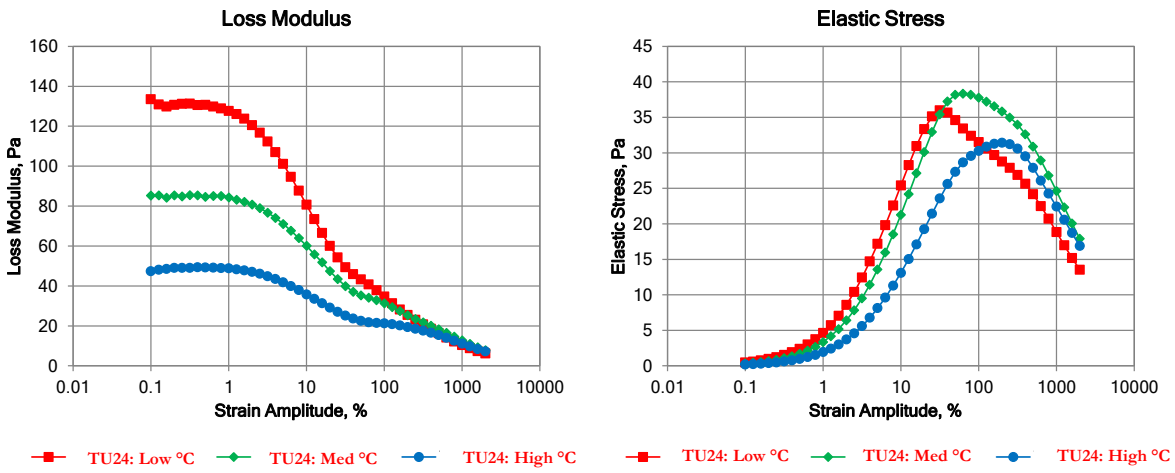

Figure 0-8: Oscillatory rheology tests (loss modulus [left] and elastic stress [right]) results performed on selected samples from experimental trials – TU24.

TU26 and TU27 Experiments: CDSM-2 – CDSM-1

These experimental trials assessed the performance of the combination of the Mixer-1 and the CDSM-1 connected in series (similar to set-up displayed in Figure 5-4) in the manufacture of lamellar dispersion based product. For trial TU26, 'AA % QUAT/CS/FA/Waters' are produced at different temperatures 'T#1 °C – T#11 °C' (Table 0-3) in steps. The 'AA % QUAT/CS/FA/Water' is formed in the Mixer-1 device which is followed by cooling/blending in the CDSM-1 device.

Table 0-3: Table indicating the estimated process temperatures at which lamellar dispersion ('AA % QUAT/CS/FA/Water') was formed for TU26 and TU27 experimental trials.

	Lamellar Dispersion Temperature ('AA % QUAT/CS/FA/Water') T, °C										
Sample	#1	#2	#3	#4	#5	#6	#7	#8	#9	#10	#11
TU26	**Low**					**Med**				**High**	
TU27											

Table 0-4: Table indicating actual process variables recorded during experimental trials – TU26 and TU27

			Process Flow-rates								
Trial #	**Mixer-1 Orifice (in^2)**	**Mixer-1 Const ($m\ s^{-1}\ bar^{-0.5}$)**	**S1**	**S2**	**S3**	**S4**	**Concentrate**	**Product**	**CDSM Gaps**	**Pressure drops**	
			Pump Flow-rate, kg/s						**CDSM-1 (mm)**	**Mixer-1 bar_g**	**CDSM-1 bar_g**	**Total bar_g**
TU26											
TU27											

For TU26, a pressure drop of approx. **22.5 bar_g** in the Mixer-1 followed by a pressure drop down to atmospheric pressure in the CDSM-1 ΔP approx. **6.5 bar_g.** This is achieved by maintaining a constant flow-rate across a Mixer-1.

A summary of settings for both devices is shown in Table 0-4 - total flow-rate in the system is approx. 21 kg/min.

For this trial, there are no rated fittings available to measure intermediate pressure between Mixer-1 and CDSM-1 therefore a theoretical pressure drop value was obtained via validated relationships from past experiments which are not discussed in this report[365].

TU27 had similar setup to TU26 however a Mixer-1 for which a **ΔP approx. 5 bar_g** followed by a pressure drop down to atmospheric pressure in the CDSM-1 (**ΔP approx. 25 bar_g**). Total

[365] Performed by John Naughton

flow-rate in the system are similar to TU26; Actual pressure drop split values and flow-rates are displayed in Table 0-4.

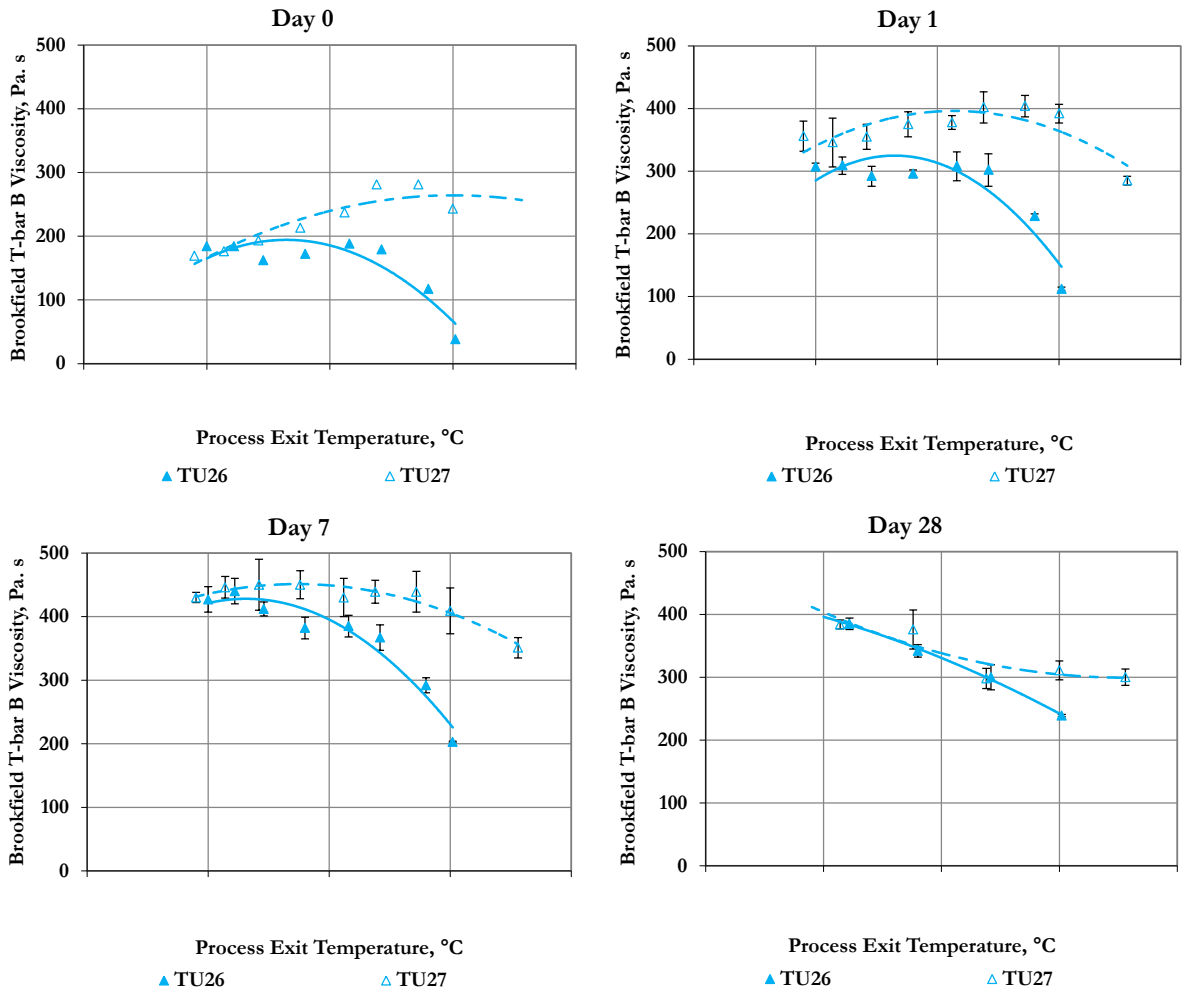

Figure 0-9: Brookfield T-bar B viscosity as a function of process temperature for Hair conditioners based on the 1.0H-C formulation – Brookfield T-bar B viscosity is also shown as a function of product age fresh (day 0), day 1, day 7 and day 28 for experimental trials TU26 and TU27

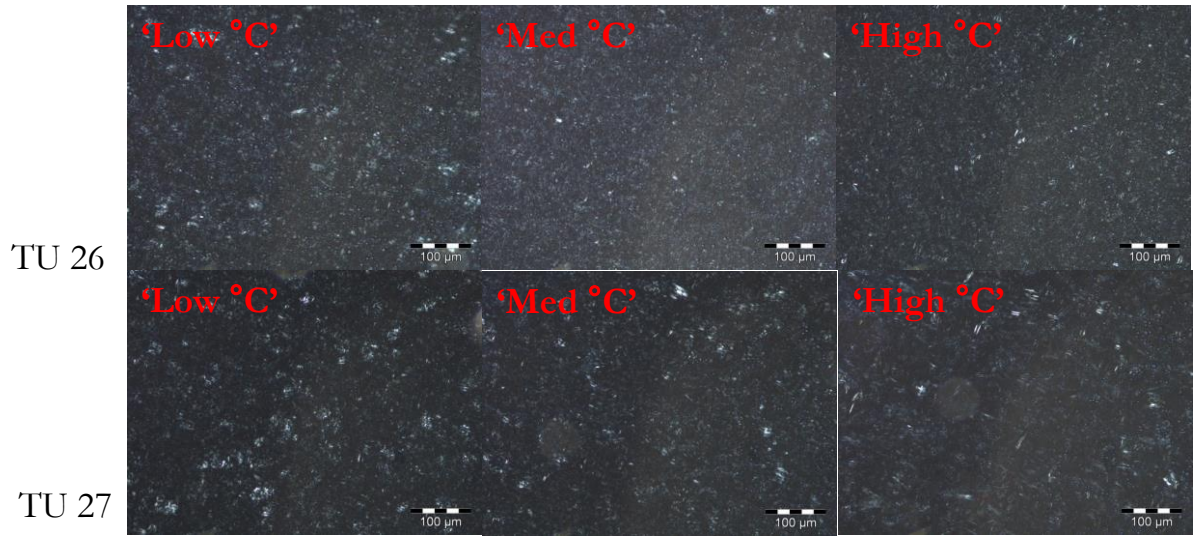

Figure 0-10: Cross polarised illuminated micrographs for 1.0H-C Hair Conditioners obtained at a range of process temperatures (low, medium and high) for Hair Conditioners manufactured via TU26 and TU27 based on the 1.0H-C formulation.

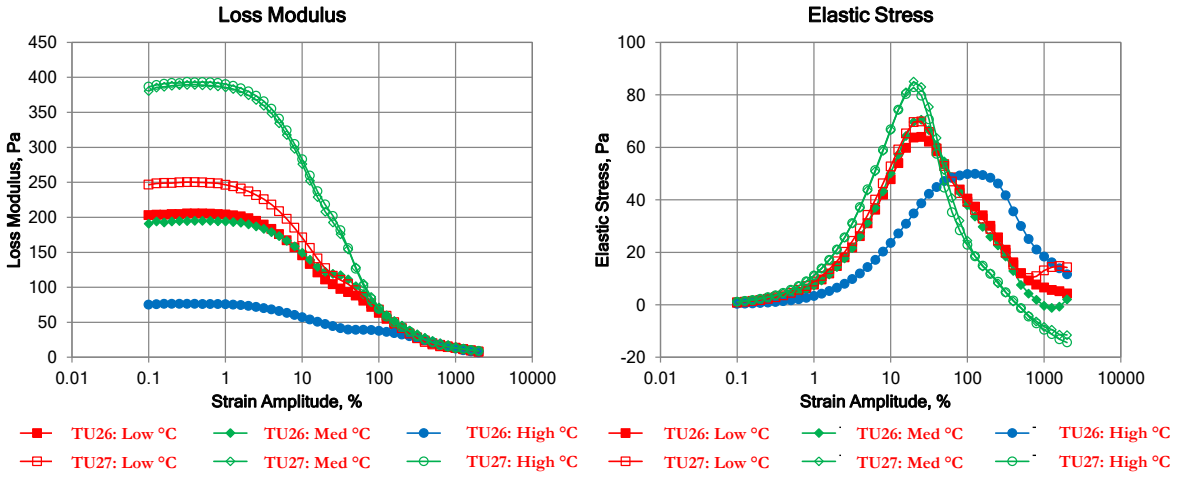

Figure 0-11: Oscillatory rheology tests (loss modulus [left] and elastic stress [right]) results performed on selected samples from experimental trials – TU26 and TU27

Raw Material Efficiency Section 5.2.2

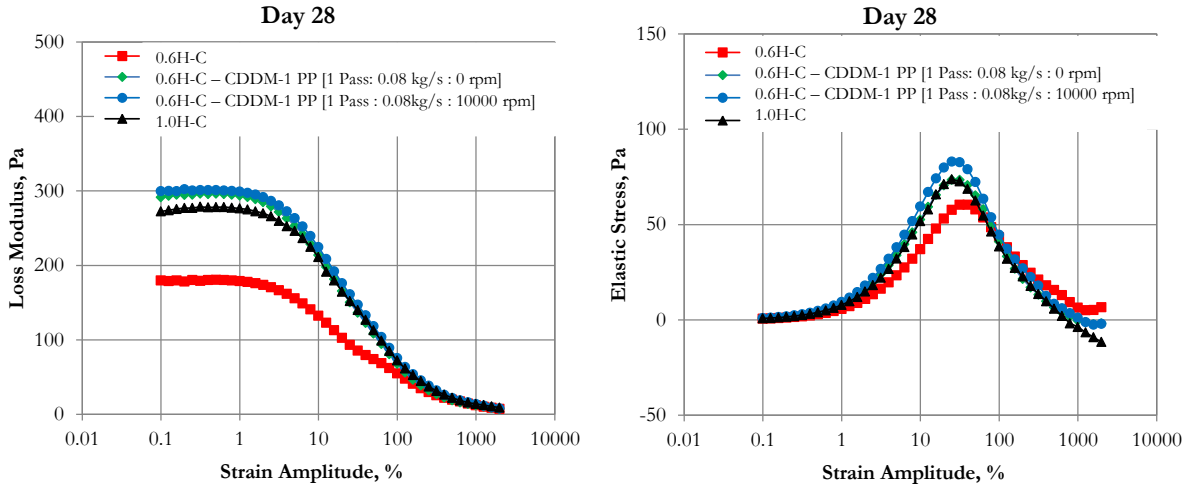

Figure 0-12: Oscillatory rheology tests loss modulus [left] and elastic stress [right]) results performed on aged Hair Conditioner - [1] 0.6H-C, [2] 0.6H-C cold processed through CDDM-1 at (0.08 kg/s : 10000 rpm), [3] 1.0H-C, and [4] 1.0H-C cold processed through CDDM-1 at (0.08 kg/s : 10000 rpm)

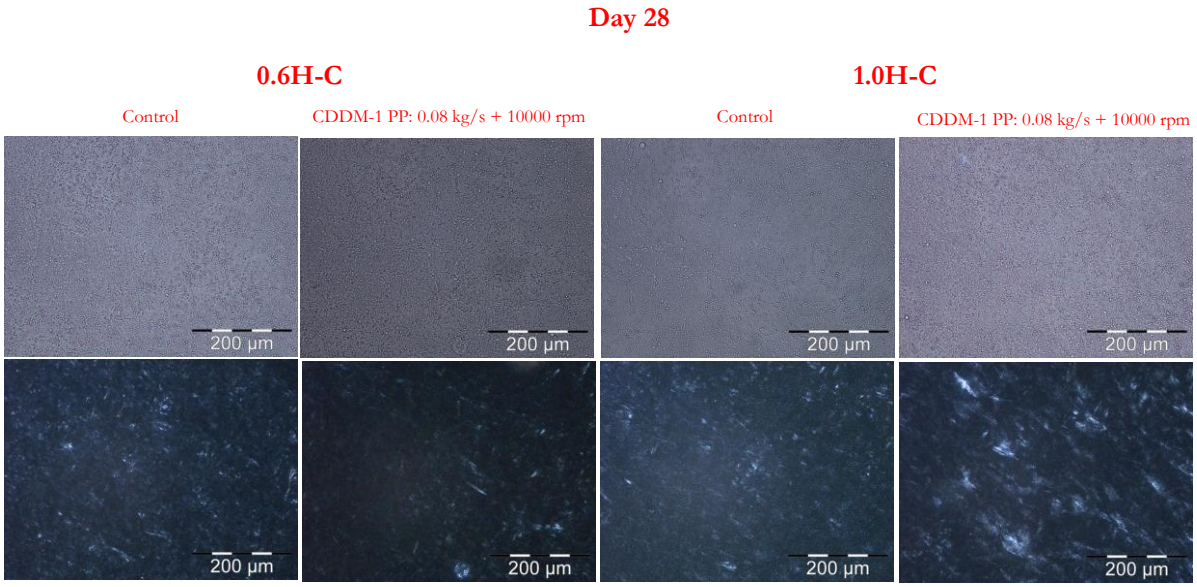

Figure 0-13: Bright field and cross polarised illuminated micrographs for day 28 Hair Conditioner product [1] 0.6H-C, [2] 0.6H-C cold processed through CDDM-1 at (0.08 kg/s : 10000 rpm), [3] 1.0H-C, and [4] 1.0H-C cold processed through CDDM-1 at (0.08 kg/s : 10000 rpm)

Appendix C

Experimental Program: Section 6.1.1

1.0H-C sample as supplied from Port Sunlight – Hair Conditioner Brookfield T-bar B viscosity measured directly from the container –
Hair Conditioner is not Pourable

1.0H-C sample as supplied from Port Sunlight and then mixed vigorously using a silicone spatula before every measurement – Hair Conditioner Brookfield T-bar B viscosity measured directly from the container –
Hair Conditioner is Pourable

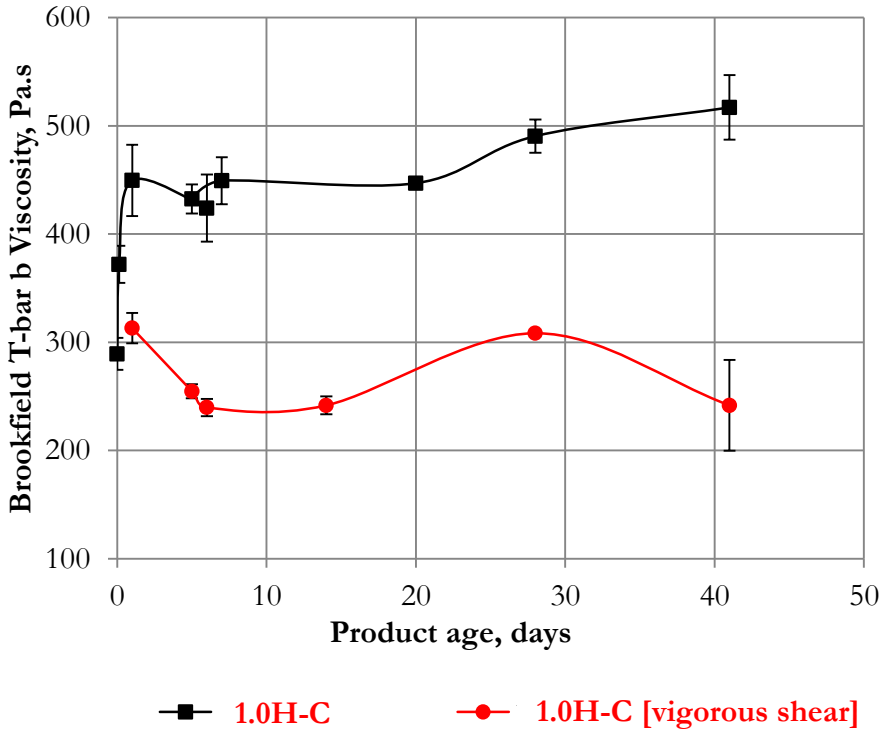

Figure 0-14: Image of Hair Conditioner 1.0H-C Hair Conditioner a supplied from Unilever Pilot Plant (top left), and after the application of vigorous shear from the action of a silicone spatula – Brookfield T-bar B viscosity as a function of product age for afore described samples.

Figure 0-15: Image (top) and schematic (bottom) showing the CDDM-2 (static section) for various angular position adjustments (bottom image courtesy Maelstrom APT Ltd, England).

Effects of Angular Displacement (Cavity Configuration 11:11) Section 6.1.3

Brookfield T-Bar B Viscosity

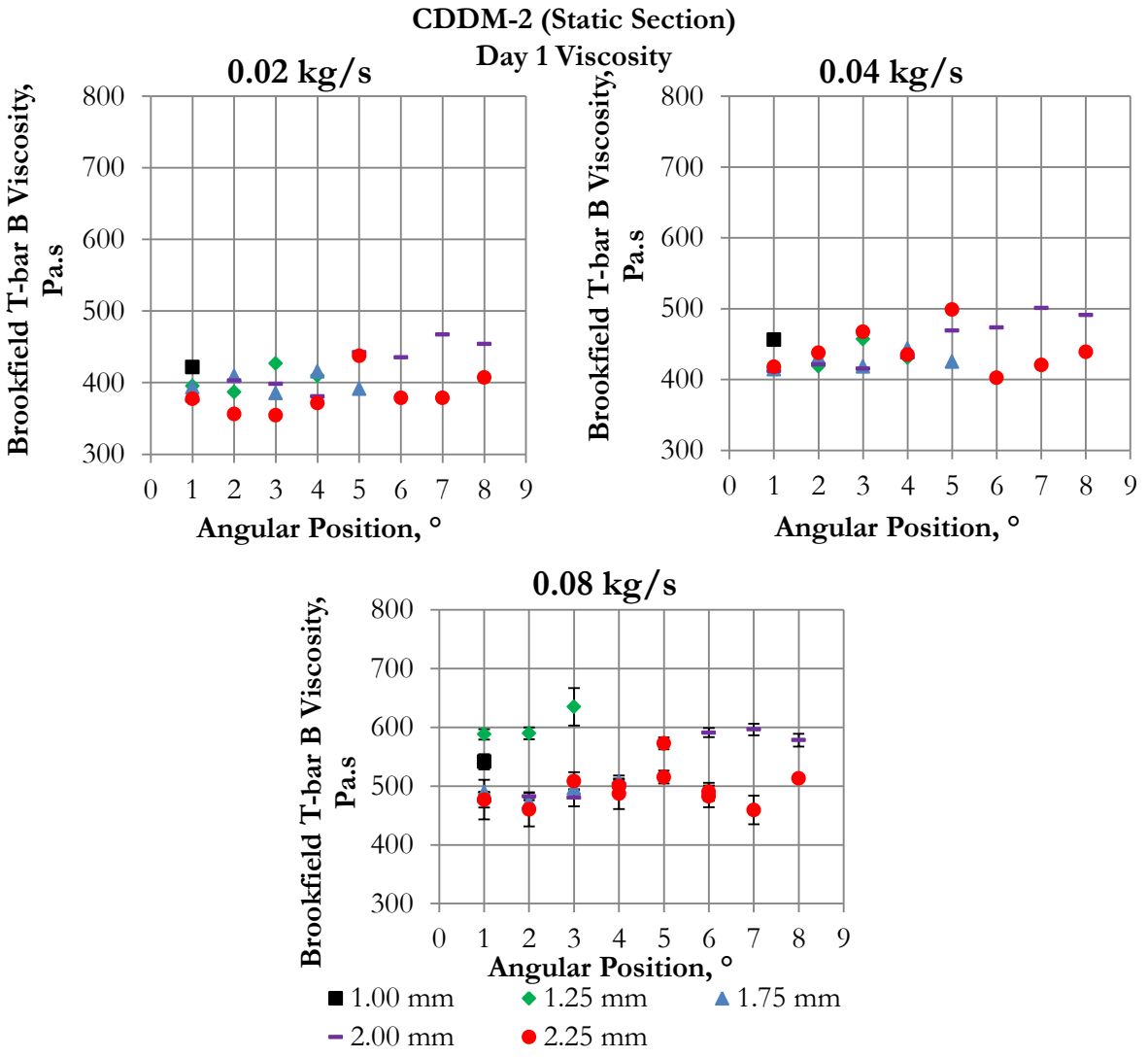

Figure 0-16: Brookfield T-bar B viscosity as a function of angular position for the CDDM-2 (static section) operating at various process flow-rates – 1.0H-C Hair Conditioner cold post processing.

Appendix D

Additional Information

The combination of the QUATS[366]/CS/FA during the manufacturing processes[367] forms the structuring components of the Hair Conditioner product – effectively its rheological properties i.e. viscosity etc. hair conditioner is prepared by dissolving QUATS/CS surfactant in hot water (above Krafft temperature) at a concentration above their CMC[368] effectively forming a hot isotropic micellar solution – prior to the addition of CSA.

In its basic form, surfactant molecules (QUATS/CS) possesses a polar hydrophilic head group and a non-polar paraffinic group (Clint 1992; Nakarapanich et al. 2001; Pincus & Witten 2004) – at sufficiently high concentrations (in our case approx. 2.66 X 10^{-2} mol/dm^3 [approx.. 9982.85 mg/L])[369], in an aqueous environment, they can form a variety of structures and phases i.e. spherical, elongated micelles, lamellae, hexagonal and cubic phases (Hoffmann 1984; Israelachvili 1994; Tiddy 1980).

Hydrophobic CSA[370] aggregates with the already dispersed hydrophilic surfactant solution - the interaction between the cationic surfactants and the molten FA give rise to the constituents of the crystalline gel phase characterised by a swollen lamellar structure of bilayers of the surfactant molecules and the FA molecules separated by layers of water (Eastoe 2002c; Mitchell et al. 1983; Nakarapanich et al. 2001).

The swelling mechanism is electrostatic in nature – the charged surfactant inserts into the α-crystals of the amphiphile and the charges created at the surface of the bilayers increases the forces of repulsion between them (Eccleston 1997). This swelling has been observed/discussed microscopically by (Eccleston 1997) in which a cationic surfactant interaction with FA in 93 w/w % water, for which interlamellar water layer spacing is approximately 500 Å – as soon as surfactant solution makes contact with alcohol crystals[371], the sharp edges of the alcohol become progressively less well defined. As the FA crystal swells, the lamellar phase spreads over the field of view, giving the appearance of a linked system (Eccleston 1977). As discussed earlier - such

[366] QUATS are protonated by an acid to form a cationic surfactant (Bongers, Egan & Irving 2013).
[367] Described within this text.
[368] Approx. 40 – 80 mg/L (Sajic & Kameshwer Rao 2000).
[369] Refer to Figure 2-6.
[370] Similar to a non-ionic surfactant - effectively capable of aggregation under the right conditions.
[371] Presumably 'or vice versa'.

systems often form highly viscoelastic gel networks when cooled[372] from elevated temperatures (typically a lamellar phase) to temperatures below their chain melting point (Barry 1975; Barry & Shotton 1967). The addition of other minor ingredients i.e. preservative, perfume, silicon emulsion etc to the above mixture makes the final Hair Conditioner product.

High shear post processing at ambient temperature induces a number of changes to the morphology of the lamellar system [1] size reduction of the L_β microstructure particle size which has been also referred to as 'fragmentation' in this text and [2] restructuring of the L_β microstructure via the incorporation of fragments of FA thereby enhancing the systems homogeneity. Both actions, contributes to increasing the volume fraction of the L_β microstructure, thus resulting in a significant increase in the system viscosity – which decreases lamellar membrane fluctuation effectively promoting membrane rigidity as was revealed by SAXS[373] results.

References

- Barry, B.W. (1975) 'Viscoelastic Properties of Concentrated Emulsions', *Advances in Colloid and Interface Science*, vol. 5, pp. 37 - 75.
- Barry, B.W. & Shotton, E. (1967), *Journal of Pharmacy and Pharmacology*, vol. 19(Suppl.), no. 110 - 120.
- Bongers, P.M.M., Egan, M.J. & Irving, G.N. (2013) *Method For Production Of Structured Liquid And Structured Liquid*, Great Britain.
- Clint, J.H. (1992) *Surfactant Aggregation*, Blackie, Glasgow.
- Eastoe, J. (2002) Surfactant Chemistry and General Phase Behaviour, in T. Cosgrove (ed.), *Colloid Science: Principles, Methods and Applications*, Blackwell Publishing, England.
- Eccleston, G.M. (1977) 'Influence of Long Chain Alcohols (or Acids) and Surfactants on The Stabilities and Consistencies of Cosmetic Lotions and Creams', *Cosmetic & Toiletries Science Applied*, vol. 92, pp. 21 - 28.
- Eccleston, G.M. (1997) 'Functions of Mixed Emulsifiers and Emulsifying Waxes In Dermatological Lotions and Creams', *Colloids and Surfaces A: Physicochemical and Engineering Aspects*, vol. 123 - 124, pp. 169 - 182.

[372] L_α & L_β can be interchanged via heating and cooling respectively (Sadtler et al. 2004; Tiddy, Hassan & Rowe 2001)
[373] Figure 4-27

- Hoffmann, H. (1984) 'From Micellar Solutions To Liquid-Crystalline Phasess', *Berichte der Bunsengesellschaft für physikalische Chemie*, vol. 88, pp. 1078 - 1093.
- Israelachvili, J.N. (1994) 'The Science and Application of Emulsions - An Overview', *Colloids and Surfaces A: Physicochemical and Engineering Aspects*, vol. 91, pp. 1 - 8.
- Mitchell, D.J., Tiddy, G.J.T., Waring, L., Bostock, T. & McDonald, M.P. (1983) 'Phase Behaviour of Polyoxyethylene Surfactants With Water. Mesophase Structures and Partial Miscibility (Cloud Points)', *Journal of the Chemical Society, Faraday Transactions*, vol. 79, no. 975 - 1000.
- Nakarapanich, J., Barameesangpet, T., Suksamranchit, S., Sirivat, A. & Jamieson, A.M. (2001) 'Rheological Properties and Structures of Cationic Surfactants and Fatty Alcohol Emulsions: Effect of Surfactant Chain Length and Concentration', *Colloid and Polymer Science*, vol. 279, pp. 671 - 677.
- Pincus, P. & Witten, T. (2004) *Structured Fluids: Polymers, Colloids, Surfactants*, Oxford University Press, New York.
- Sadtler, V.M., Guely, M., Marchal, P. & Choplin, L. (2004) 'Shear-induced Phase Transitions in Sucrose Ester Surfactant', *Journal of Colloid and Interface Science* vol. 270, no. 2, pp. 270 - 275.
- Sajic, B.L. & Kameshwer Rao, S. (2000) *Cleaning, Conditioning and Styling Hair Care Composition*, United states.
- Tiddy, G.J.T. (1980) 'Surfactant-Water Liquid Crystal Phases', *Physics Report*, vol. 57, no. 1, pp. 1 - 46.
- Tiddy, G.J.T., Hassan, S. & Rowe, W. (2001) Surfactant Liquid Crystals and Surfactant Chemical Structure, in K. Holmberg, D.O. Shah & M.J. Schwuger (eds), *Handbook of Applied Surface and Colloid Chemistry*, vol. 1 - 2, John Wiley & Sons Ltd, Chichester.